PHOTOPHYSICS OF LINEAR AND STAR-SHAPED OLIGOFLUORENES AND THEIR APPLICATION IN LASERS

Neil A. Montgomery

A Thesis Submitted for the Degree of PhD
at the
University of St Andrews

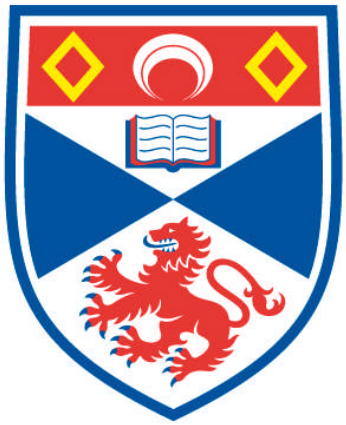

2013

Photophysics of linear and star-shaped oligofluorenes and their application in lasers

Neil Andrew Montgomery

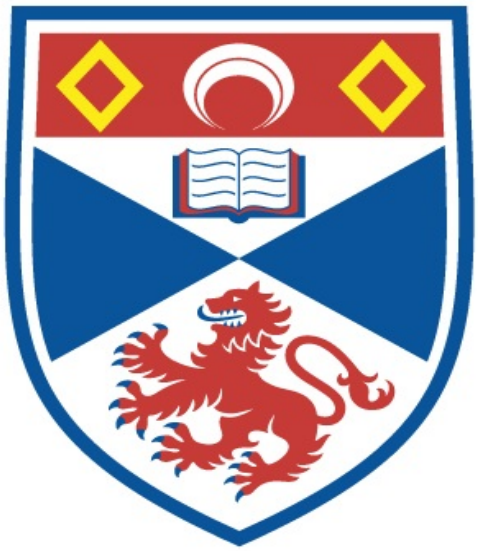

A thesis submitted for the degree of Doctor of Philosophy at the University of St Andrews

August 2012

0

Abstract

This thesis presents a study of the photophysical properties of a number of fluorene molecules used for organic semiconductor lasers. These results are then combined with lasing results to assess what the important properties in an organic semiconductor laser material are.

Photophysical measurements were performed on a family of oligofluorenes; results show a redshift in the peak absorption and emission wavelengths with increasing length. There is also an increase in the molar extinction coefficient and photoluminescence quantum yields of the molecules. Transition dipole moments also increase with length, but fluorescence scales more slowly than absorption due to self-trapping occurring at longer molecular lengths.

This study was then expanded to two families of star-shaped molecules with fluorene arms and differing cores. These molecules have three arms connected to either a central benzene unit or a larger truxene core. These star-shaped molecules show an increase in PLQY and roughly three times higher molar extinction coefficients than comparable linear oligofluorenes. The star-shaped molecules PLQY and transition dipole moments are both greater than their linear oligofluorene counterparts.

Energy transfer was then studied in the truxene-cored molecules, this showed that the symmetry of the molecule was broken due to interactions with the solvent. Energy transfer was observed on two timescales; a fast 500 fs process which is attributed to a localisation onto a single arm to emit, and a 3-10 ps second decay component, which was assigned to resonant energy transfer between the arms. Both decays were found to be wavelength dependent.

Lasing results were then obtained for the benzene-cored molecules. This showed that star-shaped molecules present improved lasing characteristics with lower ASE and lasing thresholds. These results were compared with those obtained for truxene-cored molecules whose rigid core provides them with even better lasing and ASE characteristics.

Declaration

1. Candidate's declarations:

I, Neil Montgomery, hereby certify that this thesis, which is approximately 42,000 words in length, has been written by me, that it is the record of work carried out by me and that it has not been submitted in any previous application for a higher degree.

I was admitted as a research student in October 2008 and as a candidate for the degree of Doctor of Philosophy in October 2008; the higher study for which this is a record was carried out in the University of St Andrews between 2008 and 2012.

Neil Montgomery August 2012

2. Supervisor's declaration:

I hereby certify that the candidate has fulfilled the conditions of the Resolution and Regulations appropriate for the degree of Doctor of Philosophy in the University of St Andrews and that the candidate is qualified to submit this thesis in application for that degree.

Ifor D. W. Samuel August 2012

3. Permission for electronic publication:

In submitting this thesis to the University of St Andrews I understand that I am giving permission for it to be made available for use in accordance with the regulations of the University Library for the time being in force, subject to any copyright vested in the work not being affected thereby. I also understand that the title and the abstract will be published, and that a copy of the work may be made and supplied to any bona fide library or research worker, that my thesis will be electronically accessible for personal or research use unless exempt by award of an embargo as requested below, and that the library has the right to migrate my thesis into new electronic forms as required to ensure continued access to the thesis. I have obtained any third-party copyright permissions that may be required in order to allow such access and migration, or have requested the appropriate embargo below.

The following is an agreed request by candidate and supervisor regarding the electronic publication of this thesis:

(i) Access to printed copy and electronic publication of thesis through the University of St Andrews.

Neil Montgomery August 2012

Ifor D.W. Samuel August 2012

Acknowledgments

To thank everybody who has helped me in this work would take a document almost as long as the thesis itself. I would firstly like to offer my greatest thanks to Professor Ifor Samuel and Dr Graham Turnbull, for allowing me the opportunity to study this project and for greatly assisting me along the way. Also to the postdocs of the polyopto group, thank you to Arvydas, Gordon, Ashu and Georgios, I am eternally grateful for your time and patience in helping me throughout this work. As well as those named, I would also like to thank all the other members of the polyopto group during my time here. They have helped and allowed me to thoroughly enjoy working and learning here. Also, none of this work could have been achieved without the support and assistance in repairing and setting up equipment that was provided by Steve, Calum and George.

The nature of my work has been highly collaborative and I would like to thank all the people on the HYPIX project, who have all worked hard towards achieving difficult goals, but have been very helpful along the way. Out of this team, I would like to single out the Strathclyde Chemistry team of Professor Peter Skabara, Dr Alexander Kanibolotsky and Clara Orofino for special praise; they have performed some excellent work to provide new and interesting materials, and were always on hand to offer help and advice.

The other collaboration that I worked on was in conjunction with Heriot Watt. This project has greatly helped in the production of this document and allowed me to work on some very interesting projects. My deepest thanks go to Professor Ian Galbraith, Dr Stefan Schumacher and Jean-Christophe Denis, who have worked hard to help with the understanding in this project and to go the extra distance to perform calculations, which completed the picture of understanding during the project.

Outside of work I would firstly like to thank my parents who have always supported me and pushed me to achieve my goals. As well as my parents, I would also like to thank the rest of my family for the help and guidance over the years. While I have been studying in St Andrews, I have also met some great people who have made the time outside of work highly enjoyable. Out of these I wish to thank Roberta for always being there, and my friends for all the good times shared. I hope they appreciate them as much as I did.

Table of contents

1

Introduction

In the modern world one is unable to simply categorise objects as belonging to one class or another, as many things that were once taken for granted have now been placed into more than one of their classical divisions. This work will explore one such set of materials, by investigating the photophysical properties of organic semiconductors. These materials are plastic like and should in the old classification system be labelled as insulators, because it was believed that all plastics were insulators. However, after the pioneering work of Heeger, MacDiarmid and Shirakawa it was realized that there was a new category of plastic materials which possessed semiconducting properties.[1] For this research they were awarded the Nobel Prize in Chemistry in 2000, with the citation being given as "for the discovery and development of conductive polymers".[2]

These organic materials allow for the production of so called "plastic electronics". They have the advantage that, during the last 50 years, the use of their non-conducting brethren has completely shaped the world that we live in, being used in countless commercial products. They are used in the form of simple shopping bags, housing for TVs, car parts and countless other examples. Up until the discovery and development of plastics, each of these products would have required the use of expensive natural resources, such as wood or metal, and so the development of plastics has led to a revolution which has resulted in a fall in the price of consumer goods. It is this cheap and simple fabrication of polymers that has sparked the drive to develop a lot of new organic semiconducting materials, where their versatility and ease of processing is expected to be a huge advantage over their inorganic semiconductor counterparts.[3-6]

The fact that these materials are part of the semiconductor family gives them the advantage of light emission, both through optical and electronic excitation. Electroluminescence was first discovered in small molecules in 1987[7] and then in conjugated polymers in 1990.[8] This discovery laid the way to the great development of organic light emitting diodes (OLEDs), which have since been found to be useful in both solid state lighting and as a very promising display technology: research on OLEDs has now been successfully commercialised. OLED technology had a slow initial start, due to lifetime issues with the materials, but with the development of better barrier layers the lifetimes have been dramatically increased.[9] This increase in the lifetimes of the materials has recently led to a surge in the number of organic electronic devices reaching the market. The advantage of using an OLED screen over its competitors is that they have both high contrast ratios and vivid colours, which has meant that they have recently become one of the top displays for mobile phone, and portable electronic technologies.

With this advent of a new class of electroluminescent devices, attention was then turned to producing lasers. One of the reasons for this was that lasing had been very successfully demonstrated in organic dye lasers for many years; with these becoming a very well established technology. In these lasers small conjugated dye molecules are suspended in solution and excited by an external laser source; by changing the molecule one can tune the laser over a broad range of wavelengths.[10,11] However, the fact that these materials need to be suspended in solvents makes them less than ideal for making compact laser sources. This meant that attention has turned to conjugated polymers, which differ from dyes by possessing high photoluminescence quantum yields in both film and solution.[6] The first organic semiconductor laser however was not developed until 1992; this had the polymer in solution, and so closely resembled a dye laser.[12] It was not until 1996 that the first solid state organic semiconductor laser was produced in a microcavity geometry.[13] Since then there has been a lot of research done on different laser systems, and development has led to increasing efficiencies and lower lasing thresholds.[5,6,14]

The long term goal within organic semiconductor lasers is to develop an electrically pumped version, which would have the advantage of being compact and tunable.

Electrically pumped lasers have yet to be demonstrated for a number of reasons, but the main three are: Firstly, organic materials have low carrier mobilities,[6] which makes lasing difficult to achieve. This is because they require very high currents which organic materials cannot support. Secondly, there are losses associated with the metal contacts required to drive the system; again these mean that the device needs to be pumped harder; but by pumping harder losses are increased due to exciton annihilation. Thirdly, there is a build-up polarons and of long lived triplets, whose absorption creates losses which could stop lasing.[14] High numbers of molecules in their triplet state also reduces the amount of singlet absorption within the system.

Another route to approach this problem is through indirect electrical pumping, in which high powered inorganic LEDs are used as the pump source. This type of pumping then has the possibility to be further controlled by complementary metal oxide on semiconductor (CMOS) technology. The first LED driven organic semiconductor laser was developed here in St Andrews by Yang et al in 2008.[15] This promising development led to the start of the Engineering and Physical Sciences Research Council funded HYPIX project under which the research presented in this thesis was carried out. This project set out to improve organic semiconductor lasers and to develop CMOS driven microLED pumped organic semiconductor lasers. The work in this project has been highly successful and has led to dramatic improvements in laser thresholds, which have led to microLED pumped organic lasers. As well as this it has developed compact fluorescence lifetime devices that use time correlated single photon counting,[16] and new explosive detection devices.[17] In addition to device improvement there was also an objective to develop new laser materials and to increase understanding of the key structural and photophysical properties required for good organic semiconductor laser materials.

This project also addressed one of the problems regarding organic semiconductor lasers, which is the lack of development of new materials for them. Materials are constantly being developed for OLEDs,[18-20] however, as many OLED materials emit from the triplet state, they are not suitable for lasing applications.[6] This has meant that the development of new laser materials is now far behind that of OLED materials. This means that there is an increased importance in identifying the key structural and

photophysical parameters that make for a good lasing material. This can be achieved by studying the photophysical and lasing properties of good lasing materials to identify key parameters and comparing these against values for other materials, in order to identify what is important.

This thesis focus upon addressing this issue, and aims to build a better understanding of the photophysical properties of oligofluorene based molecules, including a one dimensional oligofluorene and two dimensional star-shaped molecules. The photophysical results for these materials are then compared with their lasing results to identify the key parameters. To do this it employs a number of different experimental techniques to measure absorption and emission spectra, lifetimes, photoluminescence quantum yields and lasing. This work is supported by theoretical calculations performed at Heriot Watt University. This collaboration has led to an accurate theoretical framework being developed for calculating the properties of organic semiconductor materials. It has also led to a greater understanding of the low energy electronic absorption and emission transitions in oligofluorene based molecules. This research provides a good and timely understanding of an emerging class of important fluorescent materials.

The thesis is outlined as follows. Chapter 2 covers the theory behind the study. This combines the physics behind the materials, including both the nature of electronic conduction and the optical transitions. It then goes on to cover the theory behind the design of organic semiconductor materials, and why going to two-dimensional structures improves the performance. It finally covers the theory behind organic semiconductor lasers and the design of the cavity. Chapter 3 covers the experimental methods used in this study. It starts by describing steady state absorption and emission spectroscopy and then examines how the photoluminescence quantum yield is determined. It proceeds to discuss the time resolved fluorescence measurements employed, including streak camera measurements and fluorescence upconversion spectroscopy before discussing an application of these measurements; that of measuring the anisotropy. From here it procedes to describe the techniques used for characterising lasers, including gain, loss and ASE measurements as well as lasing and

efficiency measurements. It concludes by describing the Density functional theory and chemistry synthesis techniques used by the colaborators in this study.

Chapter 4 discloses a photophysical study of oligofluorene molecules; this uses experimental results determined by measuring absorption, emission, PLQY, and the molecules lifetime to calculate the transition dipole moments. This is then compared against the results calculated by density functional theory (DFT) and time dependent density functional theory (TD-DFT) performed at Heriot Watt University. These results show that by increasing the number of repeat fluorene units, there is a redshift in absorption and emission spectra and an increase in the absorption coefficient. There is also an increase in the PLQY and the transition dipole moments with increasing length. The results show that the absorption occurs across the molecule for up to 12 repeat fluorene units, whilst the fluorescence transition is self-trapped on approximately 5 repeat units.

In Chapter 5 these results are then compared against values obtained for a pair of promising new laser materials. These new materials are star-shaped; both consist of oligofluorene arms attached to a central core. In this case the core materials are a benzene unit and an oligofluorene truxene core. Again these molecules have been experimentally measured and the results combined with TD-DFT results to obtain an accurate picture of what is occurring within the molecules. The results for these molecules show that a significant advantage can be obtained by progressing from a linear structure to a star-shaped structure, because there is an increase in the molar absorption coefficient, PLQY, and transition dipole moments when compared against equivalent size linear oligofluorene molecules. The results also show that the star-shaped molecules present two absorption transitions, but there is then a localisation to a single arm for fluorescence.

Chapter 6 investigates intermolecular energy transfer within the star-shaped truxene cored molecules, and looks at the localisation from absorption to emission. This process is found to happen on an ultrafast timescale and is measured using fluorescence anisotropy by upconversion spectroscopy. The results show that there are two decay processes occurring; these are a fast ~500 fs decay and then a slower

second 3-10 ps component. Both decays were found to be dependent upon the excitation energy. The results show that in solution the symmetry of the molecule is already broken. Time dependent density functional theory calculations performed at Heriot Watt University present a number of different conformational disorders possible for the molecule to form in order to produce the required symmetry breaking. This disorder causes the exciton to only activate one of the two absorption transitions in the molecule.

Chapter 7 investigates the lasing performance of the benzene-cored molecules. The results for this family show that as the arm length is increased there is a redshift in the emission wavelength, an increase in the solid state PLQY, and a reduction in the pump power density for the onset of ASE. The results also show that the lasing emission is tunable from 402 - 462 nm with lasing thresholds as low as 1.1 $kWcm^{-2}$ and efficiencies as high as 6.6%. These results were then compared against the lasing results obtained for the oligofluorene truxene-cored molecules, whose photophysical results are reported in Chapter 5. This comparison shows the importance of reducing the intermolecular interactions within the film to develop a high quality organic semiconductor laser material.

Chapter 8 will present the conclusions from this research and highlight the key results. By examining all the results it shows why moving away from a simple linear molecule can be beneficial in a number of different cases. The thesis continues by evaluating future laser materials, and by proposing where this research should continue in future experiments.

1.1 References

1 Shirakawa, H., Louis, E. J., MacDiarmid, A. G., Chiang, C. K. & Heeger, A. J. Synthesis of electrically conducting organic polymers: halogen derivatives of polyacetylene, (CH). *Journal of the Chemical Society, Chemical Communications*, 578-580 (1977).

2 Nobelprize.org. *The Nobel Prize in Chemistry 2000*, <http://www.nobelprize.org/nobel_prizes/chemistry/laureates/2000>

3 Zhong, C., Duan, C., Huang, F., Wu, H. & Cao, Y. Materials and Devices toward Fully Solution Processable Organic Light-Emitting Diodes†. *Chem. Mat.* **23**, 326-340, doi:10.1021/cm101937p (2010).

4 Yamashita, Y. Organic semiconductors for organic field-effect transistors. *Science and Technology of Advanced Materials* **10**, 024313 (2009).

5 Grivas, C. & Pollnau, M. Organic solid-state integrated amplifiers and lasers. *Laser & Photonics Reviews*, n/a-n/a, doi:10.1002/lpor.201100034 (2012).

6 Samuel, I. D. W. & Turnbull, G. A. Organic semiconductor lasers. *Chem. Rev.* **107**, 1272-1295, doi:10.1021/cr050152i (2007).

7 Tang, C. W. & VanSlyke, S. A. Organic electroluminescent diodes. *Appl. Phys. Lett.* **51**, 913-915 (1987).

8 Burroughes, J. H. *et al.* Light-emitting diodes based on conjugated polymers. *Nature* **347**, 539-541 (1990).

9 Universal, Display & Corporation. *UNIVERSAL DISPLAY REPORTS RECORD RESULTS FOR WHITE PHOLED FLEXIBLE LIGHTING PANELS*, <http://www.universaldisplay.com/downloads/Press%20Releases/2012/06.06.12%20UDC%20Reports%20Record%20Results%20for%20White%20PHOLED%20Flexible%20Lighting%20Panels.pdf> (2012).

10 Schäfer, F. P. & Drexhage, K. H. (Springer, Berlin, 1990).

11 Svelto, O. *Principles of Lasers*. 4 edn, (Springer, 1998).

12 Moses, D. High quantum efficiency luminescence from a conducting polymer in solution: A novel polymer laser dye. *Appl. Phys. Lett.* **60**, 3215-3216 (1992).

13 Tessler, N., Denton, G. J. & Friend, R. H. Lasing from conjugated-polymer microcavities. *Nature* **382**, 695-697 (1996).

14 Chénais, S. & Forget, S. Recent advances in solid-state organic lasers. *Polymer International* **61**, 390-406, doi:10.1002/pi.3173 (2012).

15 Yang, Y., Turnbull, G. A. & Samuel, I. D. W. Hybrid optoelectronics: A polymer laser pumped by a nitride light-emitting diode. *Appl. Phys. Lett.* **92**, doi:16330610.1063/1.2912433 (2008).

16 Rae, B. *et al.* A CMOS Time-Resolved Fluorescence Lifetime Analysis Micro-System. *Sensors* **9**, 9255-9274 (2009).

17 Wang, Y. *et al.* Ultra-portable explosives sensor based on a CMOS fluorescence lifetime analysis micro-system. *AIP Advances* **1**, 032115 (2011).

18 Lo, S.-C. & Burn, P. L. Development of Dendrimers: Macromolecules for Use in Organic Light-Emitting Diodes and Solar Cells. *Chem. Rev.* **107**, 1097-1116, doi:10.1021/cr050136l (2007).

19 Geffroy, B., le Roy, P. & Prat, C. Organic light-emitting diode (OLED) technology: materials, devices and display technologies. *Polymer International* **55**, 572-582, doi:10.1002/pi.1974 (2006).

20 Kamtekar, K. T., Monkman, A. P. & Bryce, M. R. Recent Advances in White Organic Light-Emitting Materials and Devices (WOLEDs). *Adv. Mater.* **22**, 572-582, doi:10.1002/adma.200902148 (2010).

2

Theory of organic semiconductor molecules and lasers

2.0 Introduction

Organic materials fit into more than one category. The majority can be classed as insulators; there is, however, a small selection which fit into a second class, which is that of organic semiconductors. This chapter will present the theory that underpins the research in the subsequent chapters, with the aim of this chapter being to outline what organic semiconductors are and how the chemical nature of these molecules defines the properties both structural and electrical. It will then go on to outline the optical properties of the molecules, which will be extremely important in the rest of this thesis, and provide information on what the transitions imply about the molecules. It also presents a discussion on how changing the materials' structure can lead to improvements in their performance. This will then proceed to discuss a particular application of organic semiconductors, that of lasers. The requirements for a laser will then be explained, before relating these to organic semiconductor materials.

Section 2.1 introduces what an organic semiconductor is and discusses the importance of the electron bonding in a conjugated system. Section 2.2 explores the optical transitions, this will focus on absorption and emission, and the processes related to these. Section 2.3 discusses the difference between linear one dimensional molecules and two dimensional molecules and a particularly important emerging class of materials, that of the star-shaped molecules. Section 2.4 outlines the theory behind

lasers and then focuses on organic semiconductor lasers and the nature of the distributed feedback resonator.

2.1 Organic semiconductors

A semiconductor is a material which has a conductivity that lies between an insulator and a conductor; this is because they possess an energy gap over which the electrons must be excited to be able to conduct. The use of semiconductors has completely shaped the technological developments of the last 60 years since the invention of the transistor in 1948.[1,2] After this the use of semiconductors spread, and they are now used in lasers, photodiodes, solar cells and many other devices. These developments have led to improvements in many aspects of technology, such as efficient LED lighting[3] and photovoltaics.[4,5]

The main class of semiconductors used in these devices are inorganic. These are crystals, typically composed of either silicon or a combination of elements from groups 3 and 5 of the periodic table. They have many desirable properties such as high mobilities[6] and well defined energy band gaps. However, they are expensive to produce and process. They also have difficulties in being tuned to emit in the green region of the spectrum. A class of materials which can address these problems are organic semiconductors.

An organic semiconductor is a relatively new class of materials, on which a huge amount of effort has been undertaken to research and understand the properties. They are conjugated carbon molecules, which consist of a series of alternating double and single bonds. The most common type of systems are semiconducting polymers, which were first studied by Heeger, MacDirmid and Shirikawa in 1972, with their work on the conjugated polymer polyacetylene.[7] Their research on these systems and the development of a new class of materials led to them being awarded the Nobel Prize in Chemistry in 2000.[8]

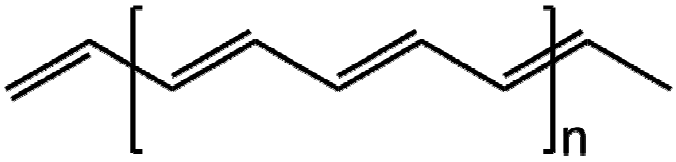

Figure 2.1: Structure of polyacetylene

In order to understand why a series alternating of double and single bonds are able to produce conduction when an ordinary polymer is an insulator, one needs to relate this to certain features of a carbon atom, and how it bonds with other atoms. A carbon atom has 6 protons and 6 neutrons within the nucleus, which is surrounded by 6 electrons. These electrons then have to fill a series of set orbitals which describe the probability of finding the electrons within a certain radius of the centre. These orbitals each lie further from the nucleus than the first, and in the case of carbon, it has a $1s^2$, $2s^2$ and $2p^2$ configuration.[9] The 1s and 2s states are spherical orbitals about the core, and can both accept two electrons, this means that these states are full. But the p orbital which can accept 6 electrons is only partially filled with the remaining 2 electrons. There are three separate p orbitals, which form lobe like structures with there being zero probability of finding the electrons in the nucleus; these orbitals lie in the x, y and z planes and are labelled p_x, p_y and p_z respectively.[9]

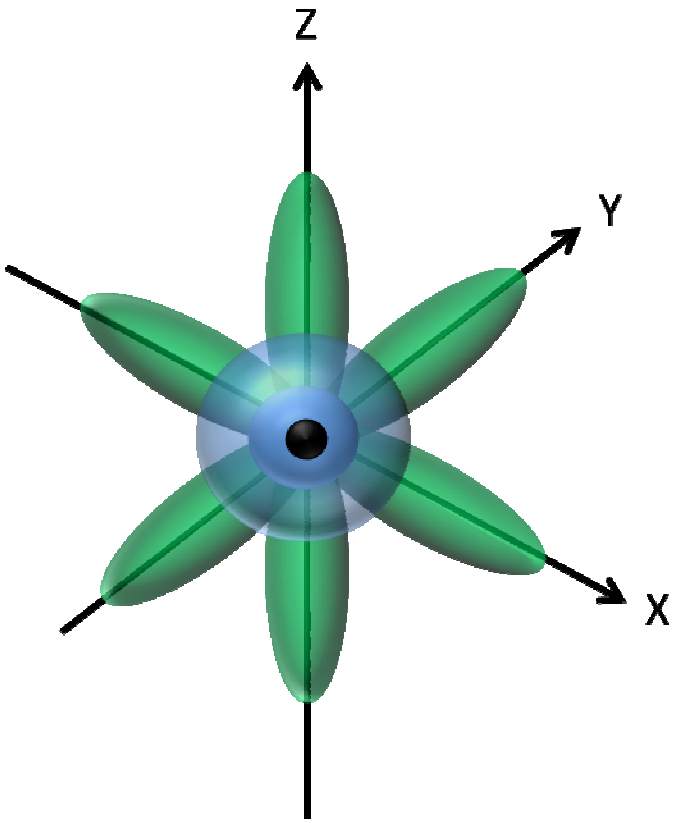

Figure 2.2: Shows the $1s^2$, $2s^2$ and 2p orbitals. The black centre circle is the nucleus, with the two s shells being the blue spheres and the p orbitals the three green lobes in the x, y and z direction.

The electrons of the carbon atom have to form bonds with other molecules in order to be stable, as is the case in methane, where each of the four outer electrons bonds with a hydrogen atom. When forming a bond, the electrons filling the orbitals are able to form hybrid orbitals, by mixing one or two electrons from one orbital with those of another. If one electron in the s orbital interacts with the electrons in the p orbital they form a sp^3 hybrid orbital. A similar process occurs in a sp^2 hybrid orbital, but one of the p electrons does not interact in the hybridisation. This is the case in double bonded carbon atoms, which have three sp^2 orbitals. If these hybrid orbitals overlap with the orbitals from neighbouring carbon atoms then they can share the electrons and form a covalent σ bond, which hold the molecule together. These σ bonds, typically bond each carbon to two other carbon atoms and one hydrogen. Each of the σ bonds sit at 120^o to each other within the plane of the molecule; this gives the molecules their geometric shapes. The one remaining electron is then responsible for the double bond

between the two carbon atoms. This electron is in the p_z orbital and sits at 90° to the plane of the molecule, and when the electron orbitals of the neighbouring carbon atoms overlap they form π bonds.[10]

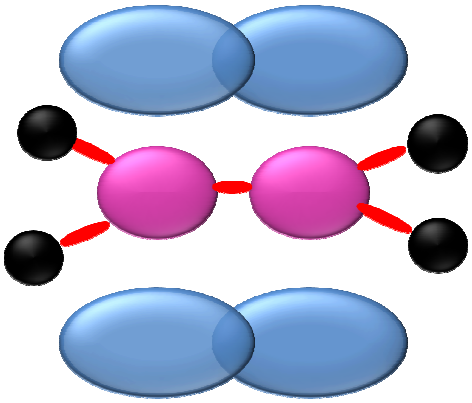

Figure 2.3: Diagram showing the bonding of an ethene molecule. The purple dots are the carbon atoms and the red bonds represent the σ bonds binding together with the black hydrogen atoms, whilst the blue represents the overlapping p_z orbitals of the π bonds.

It is these π bonds, which allow for organic semiconductors to conduct electricity. This is because they are out of the plane of the other bonds and are weakly bound to the nucleus. This increases the delocalisation, which allows them greater overlap with orbitals of the neighbouring atoms. Knowing this, if we consider a benzene ring then the reasons for conduction seem more apparent. Each carbon atom bonds to two others and a hydrogen atom via σ bonds. The remaining π bond is weakly bound and sticking up at 90° to the plane of the molecule. The sp_z electron orbitals on neighbouring atoms overlap with each other, leaving a delocalised ring of electrons above and below the benzene ring. This delocalised ring of electrons is then free to conduct electricity, as illustrated in Figure 2.4. Or, in the case of a polymer this creates a line of delocalised electrons along the backbone of the polymer chain.

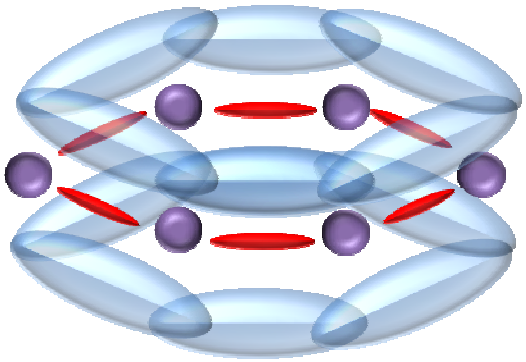

Figure 2.4: Diagram showing the electron delocalisation around a benzene molecule. The purple is the carbon atoms and the red bonds represent the σ bonds binding together, whilst the blue represents the overlap of the π bonds.

If we consider that one of the advantages of organics is the ability for their emission to be tuned across the visible spectrum, then one needs to understand how these molecules are able to form an excited state. When the molecule absorbs light, an electron is excited to a higher energy level and this breaks the π bonding and forms a π* anti-bond. When the molecule returns to the ground state, the electron is then able to drop back into the p_z orbital and the π bonding returns. The π bond is the lower energy state, and classed as the highest occupied molecular orbital (HOMO). The π* is the higher energy state, which is the lowest unoccupied molecular orbital (LUMO). The energy difference between these bond configurations causes the difference in energy levels shown in organic semiconductors; this is similar to the difference between the valence and conduction band in inorganic semiconductors. An image of these states can be seen for ethane in Figure 2.5. It is possible to form a σ to σ* transition, but this type of transition requires much more energy than the π to π* transition. This is because the π bond is much more weakly bound, and this transition does not destroy the backbone of the molecule.

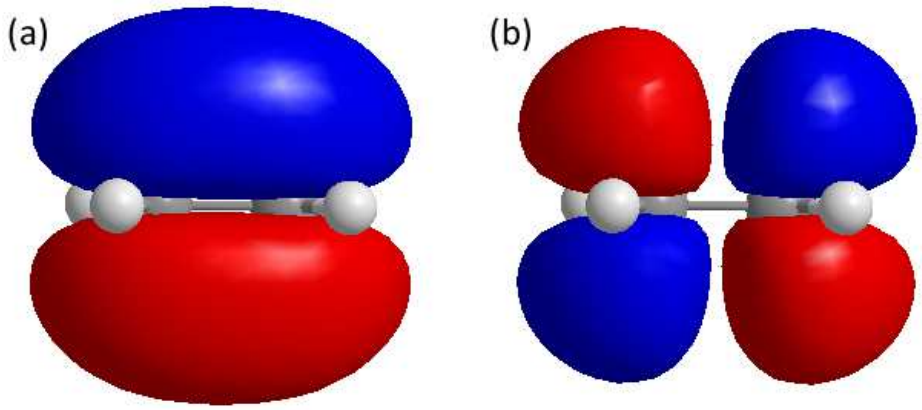

Figure 2.5: (a) HOMO orbitals for Ethene, (b) LUMO orbitals for the same molecule. Figure drawn in Chemdraw 3D.

The control of the size of this energy gap is possible by a number of methods. This can be as simple as an increase in the conjugation length, which increases the length of the delocalised excited state, and as such decreases the energy gap between the states. Another way is to add a non-carbon atom to the conjugated chain, which causes a so called substituent effect. The other atoms are usually electron accepting or donating atoms such as sulphur and nitrogen; by adding these to the chain, it either increases or decreases the delocalisation respectively.

When a molecule is excited, it forms an exciton, with the electron in a higher energy level coulombically bound to a hole in the ground energy level. As both the hole and electron are spin ½ particles, there are four possible spin states. These fall into two separate categories: a singlet state in which the total spin of the system is 0, and a triplet state which has a spin of 1. There is only one possible way of forming a singlet state, whilst there are three for forming triplets. Due to the selection rules in quantum mechanics, singlet-singlet and triplet-triplet transitions are allowed due to spin conservation, but crossovers are forbidden. As the ground state is typically a singlet, because it is a filled energy level, photophysical measurements usually excite singlet transitions. These are allowed transitions, which are able to decay back to the ground state very quickly; this typically happens on a nanosecond timescale.

2.2 Optical transitions in organic semiconductor materials

An organic semiconductor is able to undergo an optical transition when it interacts with light. To fully understand all the mechanisms behind this would be worthy of a more lengthy description than could be provided here. There are, however, several monographs written on the subject.[11,12]

At room temperature the majority of the molecules are in their lowest energy (ground) state, and to be excited they must undergo a photoinduced transition. If some incident radiation, which is of a frequency matching the absorption band of the molecule, interacts with the molecule, then there is a possibility that the molecule will absorb the incident radiation. In the absorption process the molecule gains the energy of the incoming radiation and promotes an electron to a higher energy level.

Once the molecule has been excited, it must lose this energy to return to its stable ground state. It has two decay path ways to do this; one is a radiative decay and the other is a non-radiative decay. Radiative decay occurs when the molecule in the excited state decays via the emission of a photon. Non-radiative decay occurs when the energy is lost via vibrational modes of the molecule. The energy states of the molecule are schematically shown in Figure 2.6. These transitions have different timescales on which they occur, and the measured decay rate k of the molecule is a combination of the rate of radiative emission k_R and the rate of non-radiative emission k_{NR} by the following formula:

$$k = k_R + k_{NR} \qquad (2.1)$$

As mentioned above, a particle can lose energy via two processes: one is radiative decay and the other is non-radiative decay. In the case of a radiative decay there are two possible decay mechanisms open to the molecule. The most common is that of spontaneous emission. This occurs when the molecule in the excited state decays back to the ground state with the emission of a photon with an energy equal to the energy gap. This can happen due to a fluorescence or phosphorescence transition. The fluorescence transition occurs from the lowest energy singlet state to the ground state

whilst the phosphorescence occurs from the lowest energy triplet state to the ground state. For triplet states however this downward transition is formally forbidden as the ground state is a singlet state. This means in practice that this transition is considerably slower than the fluorescence transition; this is because in order for this transition to occur there must be a spin orbit coupling process.

To measure the efficiency of a molecule we need to relate absorption with emission. This is done using the photoluminescence quantum yield (PLQY), which is a measure of the number of photons emitted by the molecule to the number of photons absorbed. This can be calculated by the following relation:

$$PLQY = \frac{number\ of\ photons\ emitted}{number\ of\ photons\ absorbed} \quad (2.2)$$

The PLQY then allows us to determine the percentage of radiative to non radiative transitions. This can also be used in conjunction with the measured lifetime of the molecule to determine the lifetime of the radiative fluorescence state, which can be calculated from the following relation:

$$\tau_R = \frac{\tau_f}{QY} \quad (2.3)$$

Where τ_R is the radiative lifetime, τ_f is the fluorescence lifetime and QY is the quantum yield.

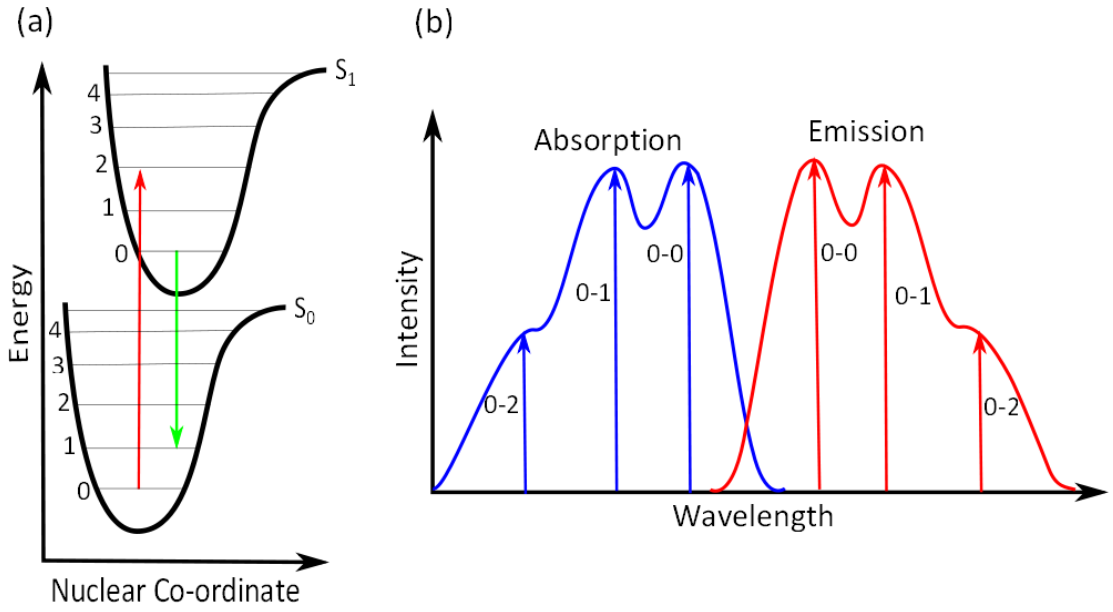

Figure 2.6: (a) Franck-Condon diagram of the absorption and emission processes for organic semiconductors. Vertical transition energies in absorption (red arrow) and emission (green arrow). (b) schematic of the typical absorption and emission from an organic semiconductor material, with the transitions marked.

Figure 2.6 is a so called Franck-Condon diagram, which represents the energy of the ground and excited state against the nuclear co-ordinates. The energy levels are represented as potential wells with a number of sub energy levels within them. These sub energy levels are vibronic states. The lower energy level represents the singlet S_0 ground state, whilst the higher level is the S_1 excited singlet state. The excited state is shown slightly displaced, to the S_0 ground state, due to the change in the nuclear coordinates caused by the excited electron. The Franck-Condon Principle states that, because nuclei are much more massive than electrons, the electronic transitions take place faster than the nuclei can respond.[13] The diagram shows the options available for each transition. When a molecule is in the ground state it can absorb a photon and be excited to a higher energy level. The excitation to the higher energy level can take place to all the vibronic levels of S_1, but is most likely to occur into a vibrational S_1 state which has the greatest wavefunction overlap with the S_0 ground state. Within the S_0 and S_1 states, it can then vibronically lose energy and move to a lower energy state. The dominant emission energy will then correspond to the gap between the S_1 minimum and an S_0 state with the greatest wavefunction overlap. The molecule will

then vibronically decay from this state, back to the bottom of the S_0 state. The direct vertical transition energies in the process are from the potential energy minima of the wells, and are indicated by the red and green arrows for absorption and emission respectively.

The different transitions within this diagram relate to the absorption and emission spectra seen in organic molecules, shown in Figure 2.6(b). At low temperatures the absorption and emission spectra have a highly structured spectrum, with the absorption typically being a mirror image of the emission. It is these vibronic peaks which correspond to the energy transitions in the Franck-Condon diagram with a 0-0 absorption transition being from the minima of the absorption well to the lowest point of the S_1 energy well; whilst a 0-1 absorption transition would be from the lowest point of the S_0 state to the first vibronic of the S_1 state, and so on for the other transitions.

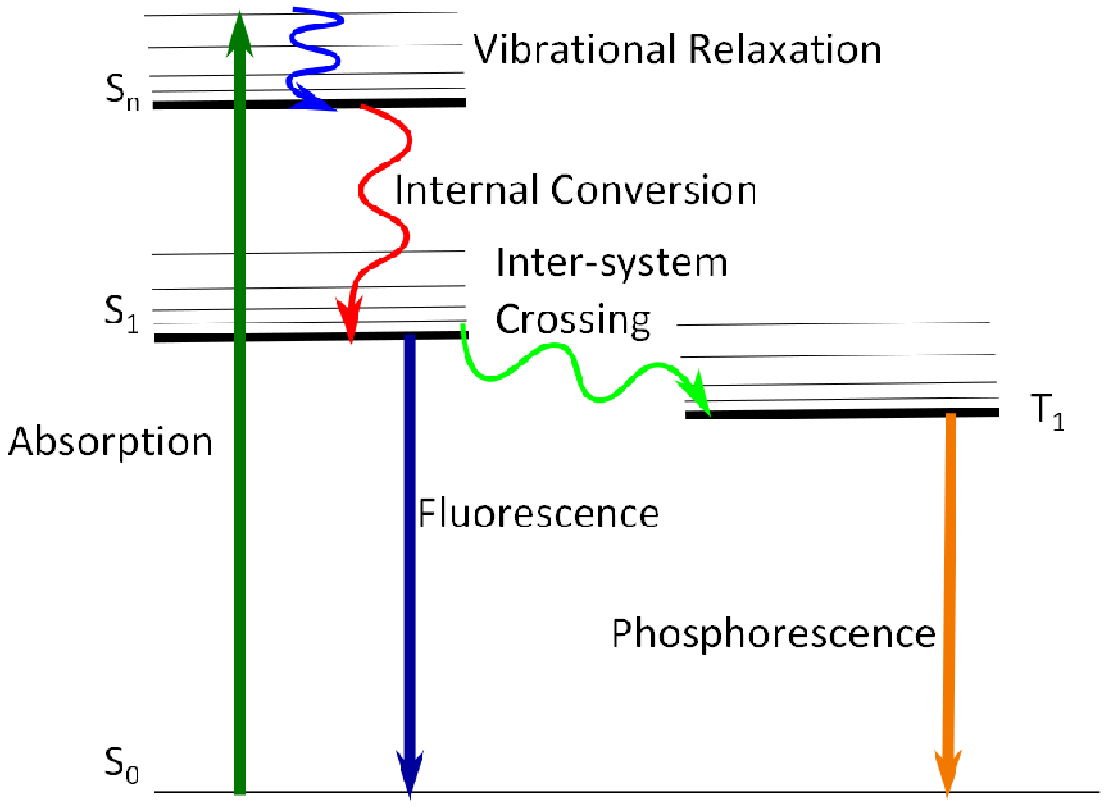

Figure 2.7: Jablonski diagram of the possible transitions open to an organic molecule.

The other radiative process is stimulated emission. Stimulated emission occurs when a molecule in an excited state is triggered to undergo an emissive transition by the

presence of a photon of the same energy as the energy gap between the ground and excited state.[14] This generates a second photon, with the same phase and momentum. If there are enough molecules in their higher energy states, then the emission of a photon by spontaneous emission in one molecule can cause stimulated emission in other molecules, as shown in Figure 2.8. This process can build up and is known as amplified spontaneous emission (ASE). This emission has a narrow spectral width and can be quite directional, but not as directional or narrow as laser emission, which will be discussed further in Section 2.4.

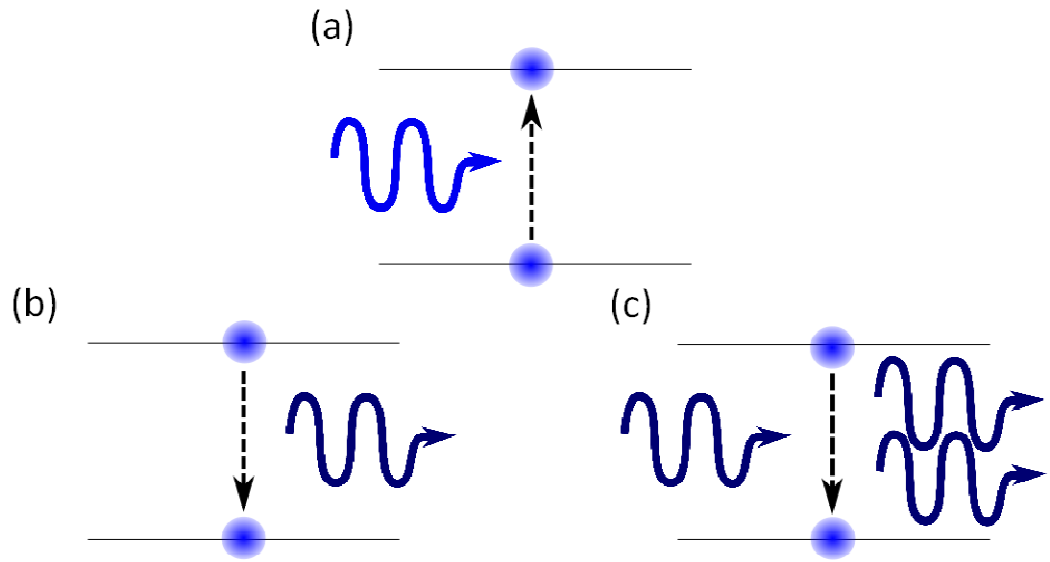

Figure 2.8: The three possible transitions for a molecule to undergo: (a) absorption, (b) spontaneous emission and (c) stimulated emission.

For a molecule to absorb or emit light it must possess an oscillating dipole at that frequency; this is caused by the resulting displacement of charges from the transition. The transition during absorption or emission is then given a transition dipole moment for this to occur; this is the dipole moment associated with the redistribution of electrons within the molecule during absorption or emission and provides information on the strength of the transition. If the molecule has a large transition dipole moment, then it means that the molecule interacts strongly with the electric field and that there is a large displacement of the electrons from their ground state positions. The formula for the absorption transition dipole is given by:

$$|d_a|^2 = 9.186 \times 10^{-3} n_0 \int [\varepsilon(\tilde{\nu})/\tilde{\nu}] d\tilde{\nu} \qquad (2.4)$$

Where d_a is the frequency integrated transition dipole moment measured in Debyes. The formula for the fluorescence transition dipole moment is given by:

$$|d_f|^2 = \frac{3\pi\varepsilon_0\hbar^4c^3\langle E^{-3}\rangle}{n_0\tau_{rad}} \quad (2.5)$$

Where $|d_f|$ is the fluorescence transition dipole moment, $\langle E^{-3}\rangle = [\int E^{-3}I(E)dE]/\int I(E)dE$ and $I(E)$ is the fluorescence intensity expressed in number of quanta, ε_0 is the vacuum dielectric constant, $\hbar = h/2\pi$ is Planck's constant, c is the speed of light in a vacuum, τ_{rad} is the natural radiative lifetime. These will be discussed in more detail in Chapter 4, where they are first used.

2.3 Star-shaped molecules

The typical organic semiconductor as outlined in section 2.1 has been largely unchanged since the early work done on polyacetylene. These consist of long chains, which have the repeat units lined up one after each other, to a range of lengths. The length can be approximately determined by the molecular weight of the fraction extracted by the chemists, and the known weight of the monomer repeat unit. These polymers have advantages of relatively simple processing and low cost production. Within these long chains, which consist of a number of repeat conjugated units, there are smaller subsections. These effective conjugation lengths are bounded by kinks or twists to the molecular structure or the length over which the exciton wavefunction localises. The effective conjugation length is different for each molecule, and can be determined experimentally by extrapolation of the photophysical properties from measurements of known length oligomers.[15-17]

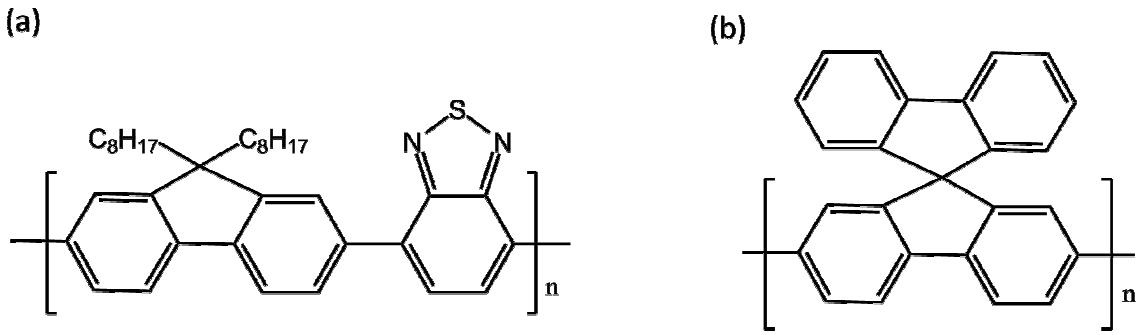

Figure 2.9: (a) Structure of F8BT, and (b) structure of a basic spirofluorene unit.

The photophysical properties of a polymer can be changed in a number of ways. One is to add different functional groups to the molecule to create a co-polymer as is the case of Poly[(9,9-di-*n*-octylfluorenyl-2,7-diyl)-*alt*-(benzo[2,1,3]thiadiazol-4,8-diyl)] F8BT; this allows for energy transfer from the higher energy fluorene (F8) to the lower energy benzothiadiazole (BT) unit to provide green emission, as shown in Figure 2.9(a).[18,19] Another way is to change the structure; this can be done by creating spiro-compounds[20] such as spirofluorene, as shown in Figure 2.9 (b),[21] which join two fluorene units across a central bridging carbon atom. This structural modification prevents the molecules from pi stacking, because the molecules sit at 90^o to each other.

One of the issues of using polymers is that the properties of a device can change for different molecular weights.[22,23] This is because different weights can have different packing structures and as such experience different intermolecular interactions. Certain processing techniques can be used to control and improve the performance of long chain polymers such as thermal[24] or solvent annealing.[25] These have been found to be beneficial mainly in blended materials for solar cells. Solvent vapour exposure has also been used to define regions of different refractive index in polyfluorene, which can form two different phases. This showed some tunability to the laser emission wavelength, depending upon the pumped region of the film.[26]

To overcome some of these issues, one can also use small molecules, because they can be monodisperse and have less conformational issues than polymers, where the longer chains can have twists and kinks and limit performance.[27-29] To date, there have been

many developments in small molecules which has been driven by the work done on phosphorescent molecules for organic light emitting diodes OLEDs.[30] The main class of material favoured for OLEDs are Iridium cored molecules with three (2-phenylpyridine) units connected to the core known as $Ir(ppy)_3$.[31] When these molecules are used in OLEDs they have been found to have internal efficiencies of nearly 100%.[32] Due to the heavy transition metal core these molecules present efficient intersystem crossing and as such emit via phosphorescent transitions.

However, for this study we are interested in developing materials for lasing and working from the triplet state for lasing is not very good, because it has a very weak emission transition and the strong excited-state absorption will overwhelm possible gain.[33] This means that other (fluorescent) molecular systems need to be investigated.

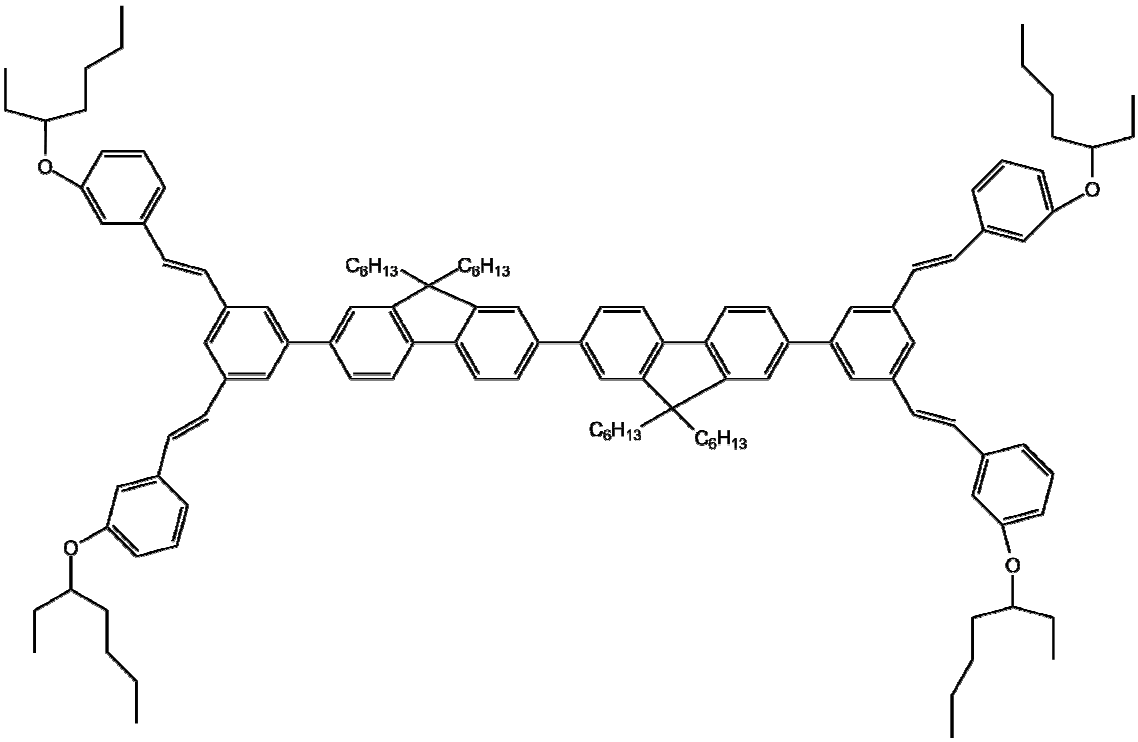

Figure 2.10: Structrure of a first generation bisfluorene dendrimer as used by Tsiminis et al. for two photon lasing. [34]

Moving to small molecules has been found to be beneficial in fluorescent materials as well; this is because small structural changes to the molecule can provide a greater photophysical change in smaller systems. As well as adding a different functional group there is also the opportunity to alter the architecture. This has been shown to be

particularly productive in dendrimers,[27,29] where the arms (dendrons) can be used to determine the absorption, and the core is used for the emission. Dendrimers are a family of large branched macromolecules, which have a central active core unit with inactive arm units attached; these can then be further branched multiple times to lead to large generational order. Surface groups can then be added to arms to functionalise the dendrimers, i.e. solubilising units, or for chemical sensing. This type of structure has the advantage of having a well-defined shape and size, with the number of successive branching points defining the generation of the dendrimers. The design of having a central emitting core with outlying dendrons offers other advantages. Firstly unlike $Ir(ppy)_3$, dendrimers are solution processable which opens up the opportunity for a number of different fabrication techniques. Secondly the different parts of the molecules have different functions, which means that there can be relatively easy optimisation of the molecular structure. This can be done by choosing arm units which absorb at a convenient wavelength for organic semiconductor lasers and then the core can be tuned to select the chosen emission wavelength. Thirdly the additions of the dendrons can affect the level of molecular packing, which can reduce the amount of intermolecular interactions, thus increasing photoluminescence quantum yields.[27]

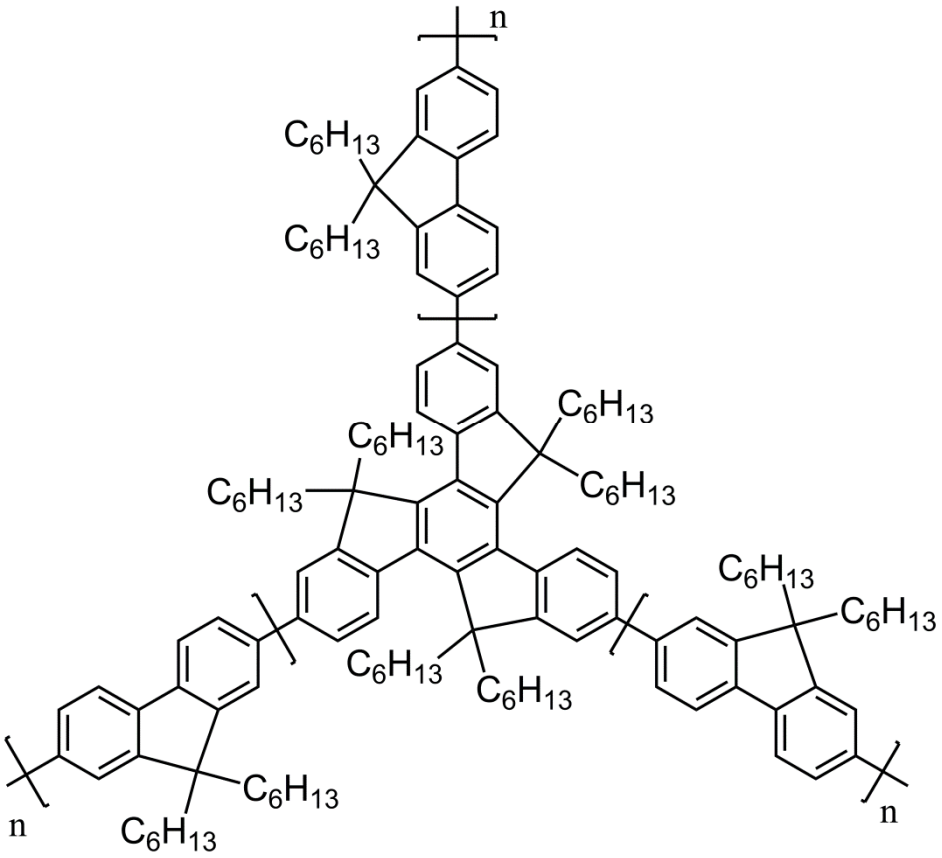

Figure 2.11: Structure of a star-shaped truxene-cored oligofluorene molecule.

Another area of growing interest is in star-shaped molecules.[28] These molecules have a number of functional arms fused to a central core, and can be either 2D propeller like structures or have a 3D tetrahedral architecture. This structure is determined by the number of arms and the nature of the core. Tuning of the desired properties can be achieved by either changing the arms or the core, with the arms typically consisting of linear oligomers. As with the polymer there is the ability to add other functional groups to the arms or the core to change performance.[35] Core units can be chosen so that they can either provide or not provide conjugation between the arms; this depends upon its structure, which can vary from single atoms to fused aromatic units. This provides the effect of controlling the increase or decrease in the conjugation length of the molecules, so that absorption and emission wavelengths can be tuned. The size and symmetry of the core has also been found to affect the interaction between the arms of star-shaped molecules.[36] This can also affect the rate of energy transfer within the molecule between the arms.

Much in the same way as with the dendrimers, the structure of the star-shaped molecules defines a number of factors, such as the solubility, packing and absorption and emission wavelengths. In the case of these molecules it is not only the arms that determine the packing as with a dendrimer, but also the core and the side-groups attached; this is discussed further in Chapter 7.

As mentioned, the core of a star shaped molecule can define the symmetry of the molecule. This is an interesting effect of the star-shaped molecules as the symmetry can impose certain constraints on the energy levels of the molecule. Depending on the choice of core there are a number of different symmetries which can be imposed. These are rotational C group symmetries or rotational and reflectional D group symmetries. In a rotational point group symmetry, if a molecule has a symmetry group of three or higher then degeneracy between energy levels will be present.

Some of the molecules studied in this thesis have a C_3 symmetric structure, an example of which is shown in Figure 2.11. These molecules each have three equal arms, which have an excitation energy E; these are coupled through the core by a coupling constant d. The Hamiltonian for this is a 3x3 matrix with E along the leading diagonal and d in the other spaces. From this it is possible to calculate the eigenvalues of the system, which produces two equal eigenvalues of E-d, and a third E+2d. Having two equal eigenvalues means that the molecule possesses two degenerate energy levels. The eigenvectors for this case are the 2D wavefunctions, on the arms of the molecule. The third eigenvalue then corresponds to a transition out of the plane of the molecule; this therefore cannot be excited, which means that this state is dark.

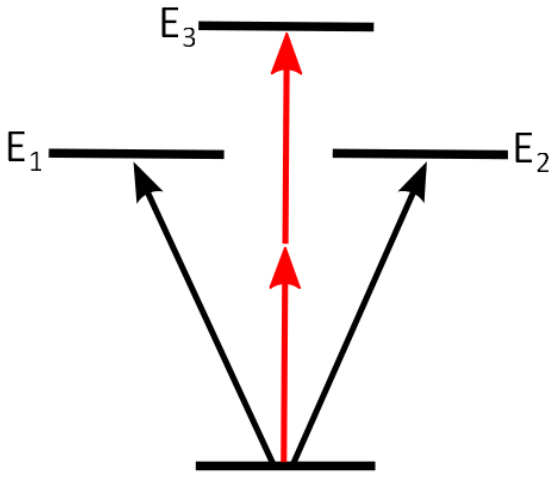

Figure 2.12: Energy level diagram for a C_3 symmetric molecule showing the two degenerate levels and the third higher excited state.

For certain C_3 symmetric molecules with two degenerate energy levels, the two degenerate transitions are found to be one photon allowed and have equal orthogonal dipoles. The higher energy dark state is allowed only for a two photon absorption process.[38] A molecule which is excited into a degenerate state cannot be stable due to the Jahn-Teller theorem.[39] In this case the molecule is not stable and must undergo a distortion of the geometry, which lifts the degeneracy of the system and lowers the energy of the system. This means that a single photon is able to excite both electronic transitions within the molecule, there is then a geometry change within the molecule which causes the energy levels to split which causes the exciton to localises on the lowest energy transition. This process will be further studied in Chapters 5 and 6.

2.4 Organic semiconductor lasers

Laser is an acronym for Light Amplification by Stimulated Emission of Radiation. This acronym accurately portrays what is happening within a laser system, where light is being amplified by stimulated emission, which was outlined in section 2.2. The concept of stimulated emission which led to the laser was first developed by Einstein in 1917;[40] who used the laws of black body radiation to describe the possible transitions for a molecule and developed coefficients to describe the three transitions in Figure 2.9. But it was not until 1960 that the first laser was developed using a Ruby crystal as the gain

material.[41] This initial development has led to a vast and changing field of technology, with a huge number of different laser types being produced.[42,43] One of the key developments within this field was the diode laser in 1962,[44] which has led to small and efficient lasers being produced. Although there has been a great amount of work carried out on organic dye lasers,[45] it was not until 1996 that the first solid state organic semiconductor laser was developed by Tessler et al..[46] To cover all the aspects of organic semiconductor lasers would be beyond the scope of this chapter, but there are several excellent review papers on the subject.[33,47,48]

In order to generate laser light there are three important requirements. Firstly, a gain medium: this is responsible for the amplification of light and is often what defines the laser's operation and gives the majority of lasers their names. Secondly, there is a cavity; this is used to provide feedback for the emitted light, and so defines the resonant modes of the device. Thirdly, one needs a pump or excitation source, which is used to excite the molecule into a higher energy level, so that they can emit and amplify light. How each of these relates to organic semiconductor lasers will be highlighted below.

2.4.1 Light amplification

As outlined in Section 2.2 there are three key transitions which a molecule can undergo when interacting with light. If an incoming photon has an energy equivalent to the energy gap between the ground and excited state, then it is possible for the light to be absorbed and an electron to be excited into a higher energy level. As the molecule is unstable in this configuration, it must then lose the energy; this can either be done radiatively or non-radiatively. In a laser system it is the radiative stimulated emission process that one is interested in; this is because the emission of one photon can then lead to the production of two identical photons.

The rate at which the system changes between energy levels is governed by the Einstein coefficients. These give the rates at which the absorption, spontaneous and stimulated emission take place, and are given by the following equations:

$$\Gamma_{absorption} = n_1 B_{12} \rho \qquad (2.6)$$

$$\Gamma_{stimulated} = n_2 B_{21} \rho \qquad (2.7)$$

$$\Gamma_{spontaneous} = n_2 A_{21} \qquad (2.8)$$

Where $\Gamma_{absorption}$ is the rate of absorption, $\Gamma_{stimulated}$is the rate of stimulated emission and the rate of spontaneous emission is given by $\Gamma_{spontaneuos}$, ρ is the photon density and A and B are the Einstein coefficients of the transitions.

During stimulated emission if the emitted photons then interact further with other excited molecules they can produce a considerable amplification of that initial incident photon. In order for this to occur and for a laser medium to produce gain there must be a large density of molecules excited in their upper energy levels. In a laser system gain is simply the amount of amplification of light and can be calculated from: $g = \sigma N$, where g is the gain coefficient, σ is the cross section and N is the population inversion density. The cross section σ is an important value, because it is related to the amount of gain within the material and is also related to the important laser parameter $\sigma\tau$, which is a measure of how hard the system needs to be pumped to produce a given gain. So maximising this product is helpful in identifying the best gain materials.

To understand the requirements for a population inversion we need to look at the occupancy of the energy levels. For a two energy level system we are able to describe the population of the different energy levels using Boltzmann statistics:

$$\frac{N_2}{N_1} = e^{-h\nu/K_B T} \qquad (2.9)$$

where N_1 is the density of molecules in the ground energy state E_1 and N_2 is the density of molecules in energy level E_2, K_B is Boltzmann's constant and T is the temperature of the system with an energy gap $h\nu$. For a system under normal conditions N_1 will be greater than N_2. However, to produce amplification N_2 needs to be greater than N_1; this makes for a so called population inversion, which allows for the net optical gain.[49]

A population inversion cannot exist in the simple two level system. This is because as the number of molecules in the excited state approaches that of the ground state, then the probability of the energy being absorbed is equal to the probability of it causing stimulating emission, because both transitions are linked by the Einstein B coefficient. This means that at least one other energy level is required to produce a population inversion, because this insures that the energy gap between absorption and emission is different. There are 2 main arrangements of energy levels used for lasers; these are 3 and 4 energy level systems. In a three level energy system, like that of the ruby laser,[41] the pump excites the atom into a higher energy level, this then non-radiatively decays into a lower excited energy state, before radiatively decaying back to the ground state. In a four level system a similar process happens, but instead of decaying to the ground level, it decays to a higher lying (unpopulated) level in the ground state before a fast vibronic transition to the ground state minimum. In both these situations a population inversion can be produced, and the system can produce gain.

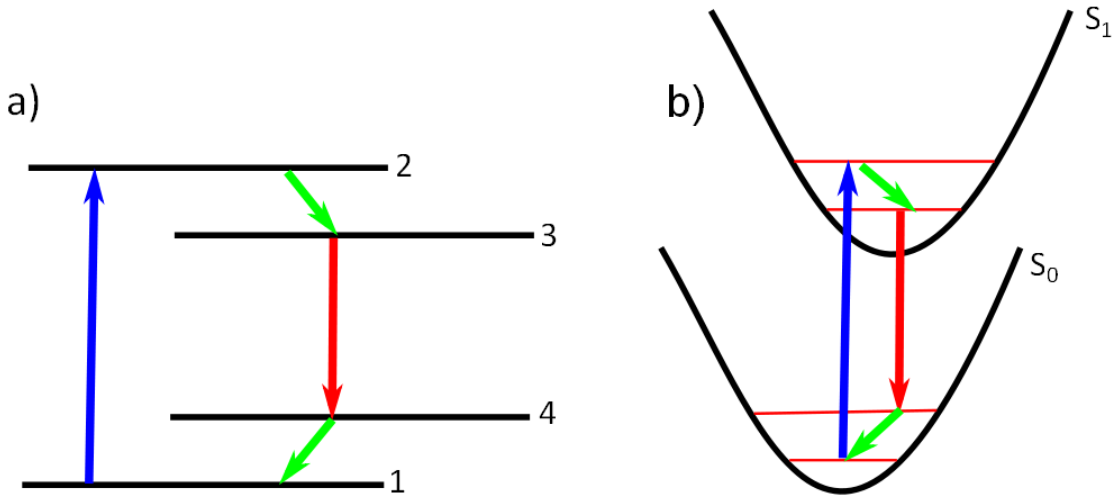

Figure 2.13: a) Simple diagram of a 4 level energy system for a laser, and b) the Franck-Condon diagram for an organic semiconductor laser. Blue arrow is the absorption, the red is the lasing emission and the two green arrows are the fast radiative transitions.

An organic semiconductor can be classed as a 4 level system, which is outlined in Figure 2.13. In an organic semiconductor, the molecule is excited into a higher S_1 energy level; it then loses some energy via a vibronic relaxation which brings it down

to the lowest S_1 energy level. Once it is in the lowest S_1 state it can then radiatively decay to a high level S_0 state before decaying vibronically to the lowest point of the S_0 ground state. These two vibronic transitions need to happen very quickly, so that a population inversion can exist between states 3 and 4, because the decay between these two states is where the lasing action occurs from.[33]

There are several other processes that can compete with the stimulated emission. One major process is excited state absorption, in which a molecule in the excited state absorbs the extra incoming radiation and causes the exciton to be raised to an even higher S_n energy level. There are also effects at high pumping intensities of exciton-exciton annihilation, which causes a scattering of the two excitons with one going into a higher energy state and one going into a lower energy state. As well as this, there can be problems with self-absorption within the system, this is a problem in which high energy emitted photons are absorbed by low energy absorbing states. Self-absorption is not a great problem in organic semiconductor films, due to their broad gain spectra. Also due to the conformational disorder, there is a red shift in emission; this is because the excitons in a film tend to diffuse along the chain or to a neighbouring molecule to low energy sites, before recombining.

2.4.2 Cavity design

For lasing to occur, the round trip gain must be greater than the round trip losses. If it is greater, then the laser oscillation can build up exponentially during repeated passes of the cavity. The point at which the gain overcomes the losses in the cavity is known as the threshold condition.[50] To fulfil the lasing criteria outlined above one must use a selective cavity, which allows for the feedback of a resonant mode back and forth through the gain media.

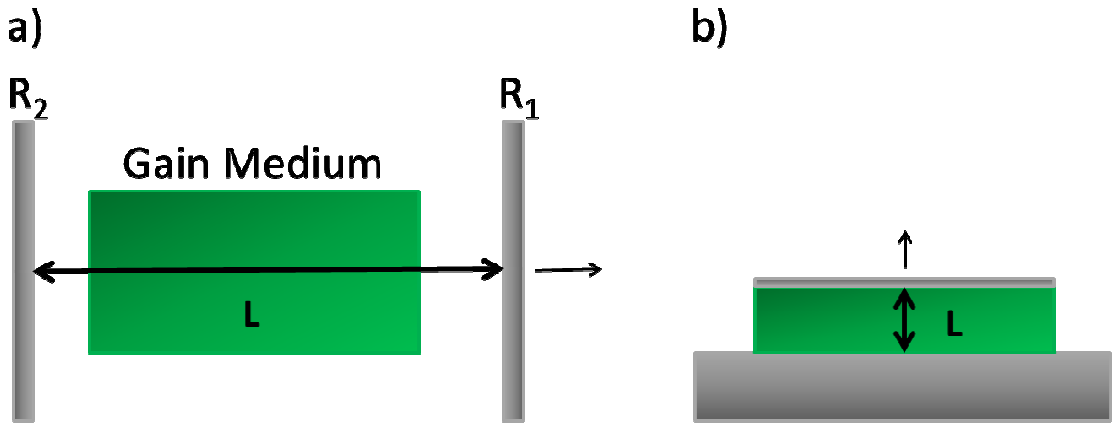

Figure 2.14: a) Fabry-Perot laser cavity with the gain medium sandwiched between a pair of mirrors, b) schematic of a microcavity laser, in this case the mirrors are in contact with the gain medium.

The simplest cavity is the classic Fabry-Perot resonator, where the gain medium is placed between a pair of highly reflective mirrors to provide the feedback. The mirrors in such a cavity, must be exactly positioned to allow the laser to operate at a specific frequency; this is because the laser light must be unchanged in both amplitude and phase after one round trip to keep the coherence. As a result of this, after a number of round trips within the cavity there will be a discrete set of laser modes, which are determined from the following relation:

$$m\frac{\lambda}{2} = nL \qquad (2.10)$$

Where λ is the operating wavelength of the laser, n is the refractive index of the gain medium, L is the cavity length and m is an integer. The reason why the wavelength is divided by 2 is that the round trip needs to be equal to an integer multiple of the wavelength.

This type of cavity is typical for gas and crystal lasers and has also been employed in making organic microcavity lasers; this was the first reported solid state organic semiconductor laser, reported by Tessler et al.[46] Microcavity lasers have been actively pursued, as they have many similarities to the Vertical Cavity Surface Emitting Laser (VCSEL),[51] which have become popular for inorganic semiconductors. A disadvantage of these is that similar to the case of the Fabry-Perot cavity, the mirrors need to be

carefully positioned so that a standing wave is supported in the cavity. The other option for a Fabry-Perot is cleaving the ends of the waveguide to define the cavity. This however has a problem in organic molecules as they do not cleave particularly well, leaving the end facets rough, so that a stable resonant mode cannot be setup. This means that mirrors must be used; these mirrors need to be placed in contact with the gain medium, but due to the nature of organic molecules having low glass transition temperatures, it makes depositing dielectric mirrors difficult. These types of cavities, however, can have exceptionally high Q (quality) factors, and are one of the favoured designs for realising electrically pumped lasing.[52]

A different class of laser resonator which has found a lot of popularity for use with organic semiconductors is the distributed feedback resonator (DFB). These structures do not require mirrors, but rather use the scattered light from periodic wavelength scale structures to reflect the light back and forth. Under certain conditions this light combines coherently to create a counter propagating "Bragg scattered" mode in the waveguide. The feedback conditions for this are given by:

$$m\lambda = 2n_{eff}\Lambda \qquad (2.11)$$

Where λ is the wavelength of the light in nm, m is an integer, Λ is the period of the grating in nm and n_{eff} is the effective refractive index of the waveguide mode. For lasing to be detected from the DFB structure it must occur for the second order m=2, as the first order is the feedback within the plane, and the second order is the outcoupled laser. DFB structures can have one dimensional (1D) and two dimensional (2D) periodic structures. The 1D structure is shown in Figure 2.15, whilst a 2D resonator combines the periodic features of a one dimensional grating in two dimensions. In this case the feedback structures lie perpendicular to one another. These are more like photonic crystals with either square or hexagonal lattices. In such structures the feedback can be supported in several different directions, with it possessing the characteristic symmetry of the resonator; this is the reason for their distinctive cross shaped output beam. Two dimensional resonators have been found to have a very low divergence of only a few mrad and an output beam quality superior to that from a one dimensional DFB laser.[53]

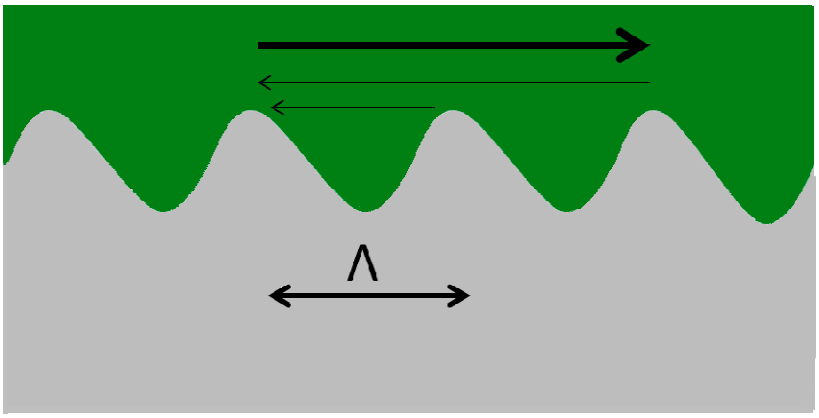

Figure 2.15: A 1-dimensional distributed feedback laser, with an illustration of the feedback shown as the black arrows in the gain medium, also shown is the period Λ.

The advantage of using this type of structure is that it can be made directly into glass or quartz via holography and etching, and then the organic semiconductor film can be spun directly onto the surface. This type of structure can also be patterned onto the surface of the film via nanoimprint lithography[54] or by solvent assisted micromoulding.[55]

There are a number of other cavity designs which can be made using organic semiconductors, due to their advantages of simple processing such as microring[56] and microsphere lasers.[57] Microring lasers have been reported to be produced from dipping an optical fibre in a solution of organic semiconductor and then the laser cavity being formed around the fibre.[56] These lasers operate with the waveguided light propagating in a whispering gallery mode around the laser, and are found to be very multimodal due to this. The performance of lasing structures like these have been well covered in a review by Samuel and Turnbull.[33]

2.4.3 Pump sources

All organic lasers are currently optically pumped. There has been a great deal of research performed to develop an electrically pumped laser; however, these have so far proved fruitless. There are a number of reasons why this has yet to be achieved, the main three are the following: Firstly, when electronically exciting a molecule there is a build-up of molecules in the triplet state which limits the gain available in the cavity, with the triplets accounting for approximately 75% of the charges.[58] Secondly,

the mobility of carriers in organic semiconductors are much lower than in inorganic semiconductors; so the current needs to be much higher than is required from organic light emitting diodes. Thirdly, due to the nature of the contacts between the organic layers and the electrodes there are high losses associated with these. Due to the low mobility of the materials it is difficult to place the contacts far apart to limit these losses.[59] Because of this there has also been a great deal of work on the reduction in size of the pump sources; this has led to a reduction from a large regenerative amplified laser, as was reported by Tessler et al.,[46] to use of diode lasers[60,61] before finally being demonstrated in using an inorganic light emitting diode by Yang et al..[19]

2.5 References

1 Bardeen, J. & Brattain, W. H. The Transistor, A Semi-Conductor Triode. *Physical Review* **74**, 230-231 (1948).

2 Arns, R. G. The other transistor: early history of the metal-oxide semiconductor field-effect transistor. *Engineering Science and Education Journal* **7**, 233-240, doi:10.1049/esej:19980509 (1998).

3 Optics.org. *Cree smashes white LED record – again*, <http://optics.org/news/2/5/8> (2011).

4 Sze, S. M. *Physics of Semiconductor Devices*. second edn, (Wiley Interscience, 1981).

5 Solar & Junction. *Solar Junction Breaks World Record with 43.5% Efficient CPV Production Cell*, <http://sj-solar.com/downloads/Solar_Junction_World_Record_%20Efficiency_14April11.pdf> (2011).

6 Schäffler, F. High-mobility Si and Ge structures. *Semiconductor Science and Technology* **12**, 1515 (1997).

7 Shirakawa, H., Louis, E. J., MacDiarmid, A. G., Chiang, C. K. & Heeger, A. J. Synthesis of electrically conducting organic polymers: halogen derivatives of polyacetylene, (CH). *Journal of the Chemical Society, Chemical Communications*, 578-580 (1977).

8 Nobelprize.org. *The Nobel Prize in Chemistry 2000*, <http://www.nobelprize.org/nobel_prizes/chemistry/laureates/2000>

9 Jones, M. *Organic Chemistry*. Third edn, 8-12 (W. W. Norton & Company).

10 Atkins, P. W. *The Elements of Physical Chemistry*. Second edn, 335-355 (Oxford University Press, 1997).

11 Valeur, B. *Molecular Fluorescence: Principles and Applications*. (Wiley-VCH, 2001).

12 Pope, M. & Swenberg, C. E. *Electronic Processes in Organic Crystals and Polymers*. 2nd edn, (Oxford University Press, 1999).

13 Barrow, G. M. *Introduction to Molecular Spectroscopy*. 231-238 (McGraw-Hill International, 1962).

14 Wilson, J. & Hawkes, J. F. B. *Optoelectronics an Introduction*. 174-176 (Prentice/Hall International, 1983).

15 Gierschner, J., Cornil, J. & Egelhaaf, H.-J. Optical Bandgaps of &pgr;-Conjugated Organic Materials at the Polymer Limit: Experiment and Theory. *Adv. Mater.* **19**, 173-191 (2007).

16 Grimme, J. & Scherf, U. Planar para-phenylene oligomers. *Macromolecular Chemistry and Physics* **197**, 2297-2304, doi:10.1002/macp.1996.021970720 (1996).

17 Izumi, T., Kobashi, S., Takimiya, K., Aso, Y. & Otsubo, T. Synthesis and Spectroscopic Properties of a Series of β-Blocked Long Oligothiophenes up to the 96-mer: Revaluation of Effective Conjugation Length. *Journal of the American Chemical Society* **125**, 5286-5287, doi:10.1021/ja034333i (2003).

18 Morgado, J., Moons, E., Friend, R. H. & Cacialli, F. Optical and morphological investigations of non-homogeneity in polyfluorene blends. *Synth. Met.* **124**, 63-66, doi:10.1016/s0379-6779(01)00423-4 (2001).

19 Yang, Y., Turnbull, G. A. & Samuel, I. D. W. Hybrid optoelectronics: A polymer laser pumped by a nitride light-emitting diode. *Appl. Phys. Lett.* **92**, doi:16330610.1063/1.2912433 (2008).

20 Saragi, T. P. I., Spehr, T., Siebert, A., Fuhrmann-Lieker, T. & Salbeck, J. Spiro Compounds for Organic Optoelectronics. *Chem. Rev.* **107**, 1011-1065, doi:10.1021/cr0501341 (2007).

21 Franco, I. & Tretiak, S. Electron-Vibrational Dynamics of Photoexcited Polyfluorenes. *Journal of the American Chemical Society* **126**, 12130-12140, doi:10.1021/ja0489285 (2004).

22 Ma, W., Kim, J. Y., Lee, K. & Heeger, A. J. Effect of the Molecular Weight of Poly(3-hexylthiophene) on the Morphology and Performance of Polymer Bulk Heterojunction Solar Cells. *Macromolecular Rapid Communications* **28**, 1776-1780, doi:10.1002/marc.200700280 (2007).

23 Hosoi, K., Mori, T., Mizutani, T., Yamamoto, T. & Kitamura, N. Effects of molecular weight on polyfluorene-based polymeric light emitting diodes. *Thin Solid Films* **438–439**, 201-205, doi:10.1016/s0040-6090(03)00749-1 (2003).

24 Ma, W., Yang, C., Gong, X., Lee, K. & Heeger, A. J. Thermally Stable, Efficient Polymer Solar Cells with Nanoscale Control of the Interpenetrating Network Morphology. *Adv. Funct. Mater.* **15**, 1617-1622, doi:10.1002/adfm.200500211 (2005).

25 Li, G. *et al.* "Solvent Annealing" Effect in Polymer Solar Cells Based on Poly(3-hexylthiophene) and Methanofullerenes. *Adv. Funct. Mater.* **17**, 1636-1644, doi:10.1002/adfm.200600624 (2007).

26 Ryu, G., Stavrinou, P. N. & Bradley, D. D. C. Spatial Patterning of the β-Phase in Poly(9,9-dioctylfluorene): A Metamaterials-Inspired Molecular Conformation Approach to the Fabrication of Polymer Semiconductor Optical Structures. *Adv. Funct. Mater.* **19**, 3237-3242, doi:10.1002/adfm.200900788 (2009).

27 Burn, P., Lo, S. C. & Samuel, I. The Development of Light-Emitting Dendrimers for Displays. *Adv. Mater.* **19**, 1675-1688, doi:10.1002/adma.200601592 (2007).

28 Kanibolotsky, A. L. *et al.* Synthesis and Properties of Monodisperse Oligofluorene-Functionalized Truxenes: Highly Fluorescent Star-Shaped Architectures. *Journal of the American Chemical Society* **126**, 13695-13702, doi:10.1021/ja039228n (2004).

29 Lo, S.-C. & Burn, P. L. Development of Dendrimers: Macromolecules for Use in Organic Light-Emitting Diodes and Solar Cells. *Chem. Rev.* **107**, 1097-1116, doi:10.1021/cr050136l (2007).

30 Chaskar, A., Chen, H.-F. & Wong, K.-T. Bipolar Host Materials: A Chemical Approach for Highly Efficient Electrophosphorescent Devices. *Adv. Mater.* **23**, 3876-3895, doi:10.1002/adma.201101848 (2011).

31 Adachi, C., Baldo, M. A., Forrest, S. R. & Thompson, M. E. High-efficiency organic electrophosphorescent devices with tris(2-phenylpyridine)iridium doped into electron-transporting materials. *Appl. Phys. Lett.* **77**, 904-906 (2000).

32 Adachi, C., Baldo, M. A., Thompson, M. E. & Forrest, S. R. Nearly 100% internal phosphorescence efficiency in an organic light-emitting device. *J. Appl. Phys.* **90**, 5048-5051 (2001).

33 Samuel, I. D. W. & Turnbull, G. A. Organic semiconductor lasers. *Chem. Rev.* **107**, 1272-1295, doi:10.1021/cr050152i (2007).

34 Tsiminis, G. *et al.* Two-photon absorption and lasing in first-generation bisfluorene dendrimers. *Adv. Mater.* **20**, 1940-+, doi:10.1002/adma.200702498 (2008).

35 Li, B., Li, J., Fu, Y. & Bo, Z. Porphyrins with Four Monodisperse Oligofluorene Arms as Efficient Red Light-Emitting Materials. *Journal of the American Chemical Society* **126**, 3430-3431, doi:10.1021/ja039832y (2004).

36 Goodson, T. G. Optical Excitations in Organic Dendrimers Investigated by Time-Resolved and Nonlinear Optical Spectroscopy. *Accounts of Chemical Research* **38**, 99-107, doi:10.1021/ar020247w (2004).

37 Atkins, P. & Friedman, R. *Molecular Quantum mechanics*. 158-159 (Oxford University Press, 2011).

38 Terenziani, F., Sissa, C. & Painelli, A. Symmetry Breaking in Octupolar Chromophores: Solvatochromism and Electroabsorption. *The Journal of Physical Chemistry B* **112**, 5079-5087, doi:10.1021/jp710241g (2008).

39 Jahn, H. A. & Teller, E. Stability of Polyatomic Molecules in Degenerate Electronic States. I. Orbital Degeneracy. *Proceedings of the Royal Society of London. Series A - Mathematical and Physical Sciences* **161**, 220-235, doi:10.1098/rspa.1937.0142 (1937).

40 Haar, D. t. *The Old Quantum Theory*. 1st edn, 167-183 (Pergamon Press, 1967).

41 Maiman, T. H. Stimulated Optical Radiation in Ruby. *Nature* **187**, 493-494 (1960).

42 Svelto, O. *Principles of Lasers*. (Springer, 1998).

43 Siegman, A. E. *Lasers*. (University Science Books, 1986).

44 Hall, R. N., Fenner, G. E., Kingsley, J. D., Soltys, T. J. & Carlson, R. O. Coherent Light Emission From GaAs Junctions. *Physical Review Letters* **9**, 366-368 (1962).

45 Schäfer, F. P. & Drexhage, K. H. (Springer, Berlin, 1990).

46 Tessler, N., Denton, G. J. & Friend, R. H. Lasing from conjugated-polymer microcavities. *Nature* **382**, 695-697 (1996).

47 Grivas, C. & Pollnau, M. Organic solid-state integrated amplifiers and lasers. *Laser & Photonics Reviews*, n/a-n/a, doi:10.1002/lpor.201100034 (2012).

48 Chénais, S. & Forget, S. Recent advances in solid-state organic lasers. *Polymer International* **61**, 390-406, doi:10.1002/pi.3173 (2012).

49 Siegman, A. E. *Lasers*. Pages 26-27 (University Science Books, 1986).

50 Siegman, A. E. *Lasers*. Page 39 (University Science Books, 1986).

51 Jewell, J. L., Harbison, J. P., Scherer, A., Lee, Y. H. & Florez, L. T. Vertical-cavity surface-emitting lasers: Design, growth, fabrication, characterization. *Quantum Electronics, IEEE Journal of* **27**, 1332-1346, doi:10.1109/3.89950 (1991).

52 Koschorreck, M. *et al.* Dynamics of a high-Q vertical-cavity organic laser. *Appl. Phys. Lett.* **87**, 181108 (2005).

53 Heliotis, G. *et al.* Emission Characteristics and Performance Comparison of Polyfluorene Lasers with One- and Two-Dimensional Distributed Feedback. *Adv. Funct. Mater.* **14**, 91-97, doi:10.1002/adfm.200305504 (2004).

54 Mele, E. *et al.* Polymeric distributed feedback lasers by room-temperature nanoimprint lithography. *Appl. Phys. Lett.* **89**, 131109 (2006).

55 Lawrence, J. R., Turnbull, G. A. & Samuel, I. D. W. Polymer laser fabricated by a simple micromolding process. *Appl. Phys. Lett.* **82**, 4023-4025 (2003).

56 Frolov, S. V., Shkunov, M., Vardeny, Z. V. & Yoshino, K. Ring microlasers from conducting polymers. *Phys. Rev. B* **56**, R4363-R4366 (1997).

57 Berggren, M., Dodabalapur, A., Bao, Z. & Slusher, R. E. Solid-state droplet laser made from an organic blend with a conjugated polymer emitter. *Adv. Mater.* **9**, 968-971, doi:10.1002/adma.19970091208 (1997).

58 Segal, M., Baldo, M. A., Holmes, R. J., Forrest, S. R. & Soos, Z. G. Excitonic singlet-triplet ratios in molecular and polymeric organic materials. *Phys. Rev. B* **68**, 075211 (2003).

59 Samuel, I. D. W., Namdas, E. B. & Turnbull, G. A. How to recognize lasing. *Nat. Photonics* **3**, 546-549, doi:10.1038/nphoton.2009.173 (2009).

60 Vasdekis, A. E. *et al.* Diode pumped distributed Bragg reflector lasers based on a dye-to-polymer energy transfer blend. *Opt. Express* **14**, 9211-9216 (2006).

61 Riechel, S. *et al.* Very compact tunable solid-state laser utilizing a thin-film organic semiconductor. *Opt. Lett.* **26**, 593-595 (2001).

3

Experimental methods

3.0 Introduction

This chapter will explore the experimental methods that were employed throughout this work. The aim of this chapter is to highlight the key measurement techniques and the equipment used, so that a full understanding of the results can be gained. The work outlined in the results chapters begins with photophysical characterisation of the molecules, so this chapter will initially focus on absorption and photoluminescence spectroscopy techniques. After this the lifetimes of the molecules were measured using time-resolved photoluminescence techniques, and then ultrafast anisotropy measurements were performed on a family of star-shaped molecules, to study the energy transfer within the molecule. This used fluorescence upconversion spectroscopy which can measure dynamics down to 100 fs. The final part of the work will focus upon lasing performance of a family of star-shaped molecules and the characterisation of these molecules. There will also be a brief review of the chemistry methods and density functional theory calculations performed by our collaborators.

As outlined above, section 3.1 covers sample preparation and the steady state absorption and emission measurements; this also includes the instruments that were employed to perform them. Section 3.2 discusses the techniques used to determine the photoluminescence quantum yield for both solids and solutions. Section 3.3 covers time resolved measurements, first discussing the titanium sapphire laser system used to excite the sample, before moving on to discuss the streak camera for measurements on the picosecond-nanosecond timescale, then upconversion spectroscopy techniques for the femtosecond time regime. This will be concluded with a description of anisotropy measurements and the fitting of their results. Section 3.4 explores the laser

systems used to pump the organic lasers and then the measurement techniques employed for measuring organic semiconductor lasers. This also looks at the characterisation of the films by measuring the gain, loss and ASE of the samples. The final two sections will conclude this chapter on methods, with Section 3.5 discussing the techniques used by other parties involved in this work in the synthesis of the molecules and Section 3.6 covering the theory and methods behind the Density Functional Theory calculations used throughout this work.

3.1 Steady state measurements and sample preparation

3.1.1 Sample Preparation

Most materials were supplied in powder form from the Chemistry department at the University of Strathclyde by the group headed by Professor Peter Skabara, with the majority of synthesis being performed by Dr Alexander Kanibolotsky. The rest of the materials were procured from American Dye Source Inc.. The synthesis and purification techniques employed by the Chemists at Strathclyde University are covered in Section 3.5, and the details of each of the materials used will be provided in the relevant chapters. Once all materials were obtained, they were stored in an oxygen free glove box; this aims to prevent sample degradation due to the effects of oxygen. For sample preparation the materials were removed briefly from the glovebox and out into the cleanroom, in which it is housed. The materials were only exposed to these ambient conditions for brief periods, before being returned to the glovebox for storage.

Samples were then carefully weighed out in sealable glass vials, before the solvent was added. For solution measurements either spectroscopic grade toluene or tetrahydrofuran was used, whilst for films spectroscopic grade toluene was used as the solvent for spin-coating. In measurements where a definite concentration is required for determining the molar extinction coefficient, a known concentration was measured before being carefully diluted to a weaker concentration capable of being measured.

Films were prepared in the same way as the solutions, but at higher concentrations of 20 mg ml^{-1}. Films were then deposited onto the substrates using a spin-coater; this rotates the films at a defined speed for a set period of time in order for the solvent to

evaporate; conditions used were typically spin speeds of 1000 and 2000 rpm for a duration of 1 minute, which results in films between 150 and 100 nm. All sample preparation was carried out in the cleanroom, to protect the samples from any contaminants or particulates of dust which can degrade the performance of the films.

Solutions were then transferred from the vials into either 1 cm path length quartz cuvettes for the steady state measurements or a rotating cuvette for the ultrafast measurements. The rotating cuvette consists of a pair of quartz windows, which are separated by a 0.5 mm Teflon spacer; these are then clamped together by an aluminium housing. Filling the cuvette is then performed by sliding one of the windows slightly back and then pipetting the solution in before closing it and sealing it with the housing. When the measurements are performed the cuvette is rotated at approximately 200 rpm by an electric motor.

3.1.2 Steady state measurements

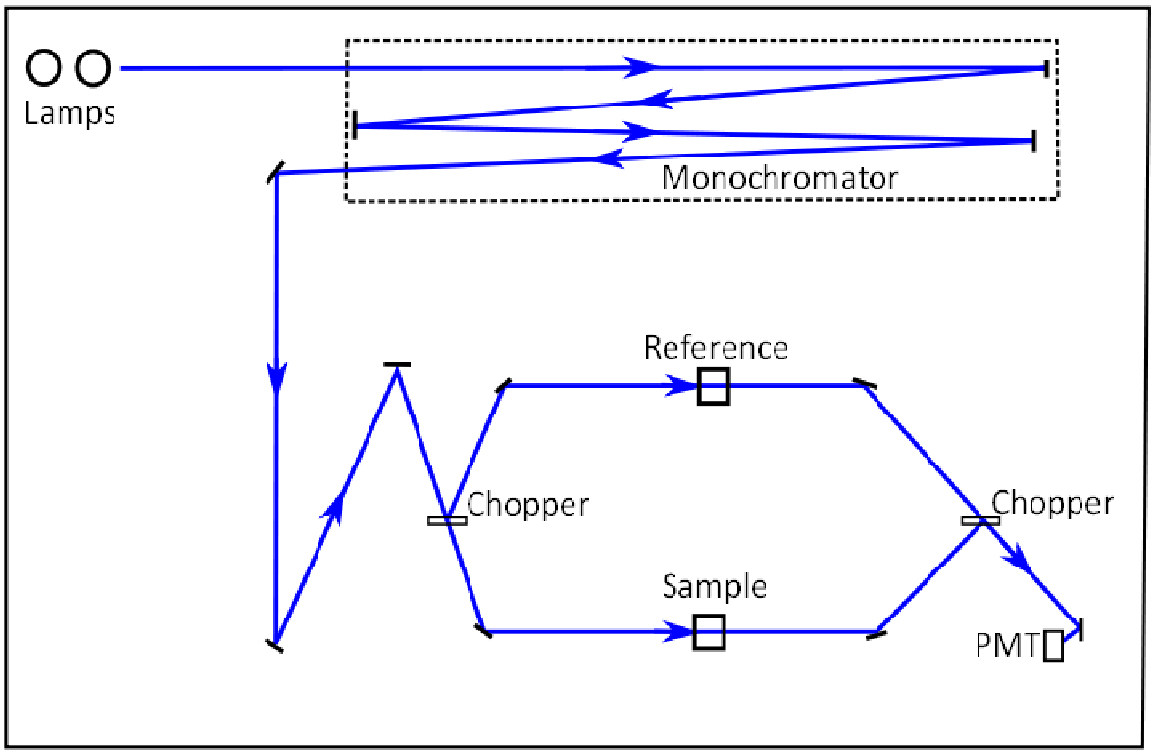

Figure 3.1: Absorption spectrometer, showing the path from the lamps through the monochromator to the sample and reference.

Absorption measurements were carried out using a Varian Cary 300 UV-Vis spectrometer. This uses a halogen lamp for the visible light source and a deuterium lamp for the UV. The output light from these bulbs is passed through a scanning monochromator to allow for the probe wavelength to be changed. Measurements are then performed using a dual beam experiment, with one being passed through the sample and the other being passed through a reference path. The change in intensity is due to absorption and is given by the following formula:

$$A = -log_{10}\left(\frac{I}{I_o}\right) \qquad (3.1)$$

Where A is the absorbance, I is the intensity and I_o is the input intensity. In order to correct for other effects which could affect the absorption, such as reflections and solvent absorption, the measurements were performed against a reference sample. The reference for the films was chosen to be a quartz disc identical to the one which the film was spun onto. For the solution measurement the reference was chosen to be another quartz cuvette containing the same solvent used to dissolve the sample.

As shown in equation 3.1 the absorption is determined by a change in intensity of the beam as it passes through a sample. This change in intensity is found to be proportional to the path length l, concentration c and the molar extinction coefficient ε. This relationship is described by the Beer-Lambert Law:

$$A = \varepsilon c l \qquad (3.2)$$

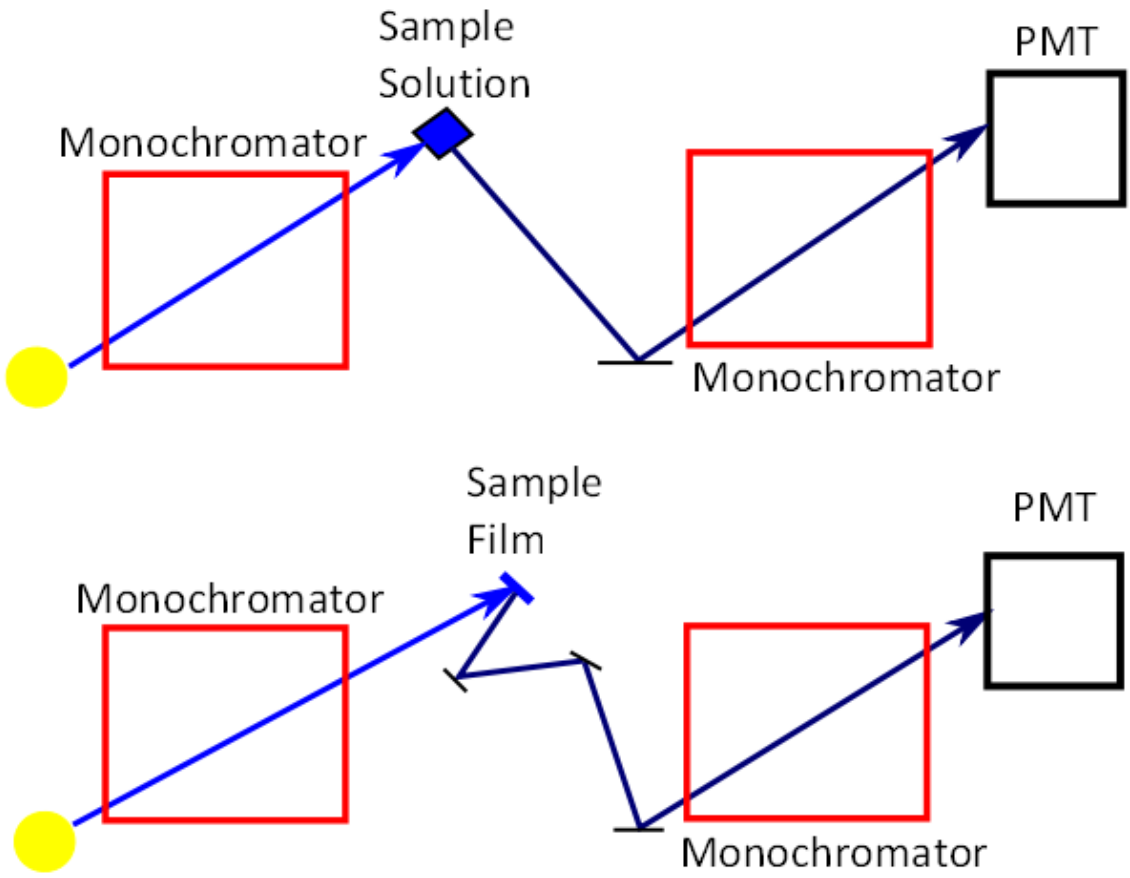

Figure 3.2: Fluorescence spectrometer, showing the path from the lamps through the monochromator to the sample and back through the scanning monochromator to the PMT. The top shows the collection orientation for solution and the bottom for film samples.

Fluorescence measurements were performed using a Jobin-Yvone Fluoromax 2 spectrophotometer. This uses a xenon lamp as the excitation source; this is then passed through a monochromator, which selects a specific excitation wavelength. This is then focussed onto the sample. The excitation is perpendicular to detection for solutions and at a small angle to the collection of emission for films; the front face emission from films is then collected by a pair of mirrors, which change the emission path and focus it onto the collection optics. The emission is then detected using a photomultiplier tube, which detects the light and turns it into an electrical signal. To get spectral information on the sample the emission is first passed through a scanning monochromator, which scans through the entire range of the emission wavelengths. The excitation and emission wavelengths can all be controlled by simple computer

software, which records the emission intensity from the sample against the recording wavelength. All the emission spectra were then corrected for the sensitivity of the photomultiplier tube.

When converting the emission spectra into energy, all spectra were multiplied by a wavelength squared correction; this accounts for the fact that although a translation into energy is simple, the bandpass in energy is not constant.[1] This means that in order to get the corrected spectra, one needs to apply the following correction:

$$I(E) = \lambda^2 I(\lambda) \qquad (3.3)$$

Where $I(E)$ is the intensity at energy E, λ is the wavelength and $I(\lambda)$ is the intensity at wavelength λ.

To cool samples to 77 K an Oxford Instruments Optistat DN liquid nitrogen cryostat was used. It has an inner sample chamber where the liquid samples are carefully positioned in sealed glass cuvettes. Surrounding this is a reservoir for the liquid nitrogen, which is surrounded by a vacuum chamber which isolates the sample chamber from the ambient room conditions. Before performing any measurements the vacuum chamber needs to be pumped out and the sorb activated. The role of the sorb is to capture any of the gas produced by outgassing, as the sample is cooled from room temperature to 77 K. This maintains the vacuum and prevents condensation forming on the optical windows. To isolate the sample in the sample chamber, helium was used as an exchange gas. Helium is used rather than a vacuum because it has better thermal properties.

Part of the work outlined in the following chapters involved using a cryostat to cool the samples to 77 K for absorption and fluorescence measurements. Although the basic concept for the measurements are the same as outlined above, there are a few small subtleties, due to the shape and size of the cryostat; this means that special sample mounts needed to be used in both measurements and that the reference sample in absorption is the empty cryostat itself.

3.2 Photoluminescence quantum yield

As outlined in Chapter 2 the photoluminescence quantum yield (PLQY) is an important quantity to know for a material, because it provides information on the number of photons emitted to the number of photons absorbed. This can then be used to provide information on the lifetimes of the radiative and non-radiative states when one knows the natural lifetime. Also depending on whether the sample is a film or suspended in solution can affect the PLQY, because in a film there are a number of quenching factors caused by intermolecular interactions; this increases the number of non-radiative pathways open to the molecule and can thus decrease the PLQY.

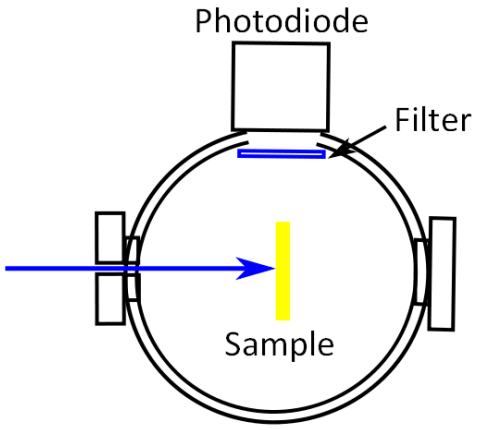

Figure 3.3: Film PLQY measurement, showing the sample inside the integrating sphere, with the filter and photodiode at the top of the sphere.

In this work the film PLQY was determined using the Greenham method.[2] In this, the sample is placed at the centre of an integrating sphere, which is used to collect all the light emitted by the sample. Samples were excited using the 325 nm laser line from a helium cadmium laser, which is shone through a small aperture at the front of the integrating sphere. Emission is then detected using a calibrated photodiode, which is positioned at the top of the integrating sphere. A filter is placed in front of the photodiode to prevent any of the incident excitation light being detected as luminescence. In order to account for the effect of reflectance of the pump light and absorption, reflectance and transmission measurements were taken using a calibrated power meter, and the incident power recorded. With this information one can then calculate the Greenham x factor which is given by:

$$x = \frac{X_{sample} - (R+T)X_{Sphere}}{(1-R-T)X_{laser}} \qquad (3.4)$$

Where R is the reflectance, T is the transmission, X_{sample} is the measurement from the laser onto the sample, X_{Sphere} is the measurements from the sphere and X_{laser} is the signal without the sample or filter in place.

After this the emission spectrum of the sample, the spectral reflectivity and the efficiency of the photodiode needs to be taken into account. The emission spectrum of the sample was measured as above. The other two values come from their calibration specifications. This is the so called y term in the Greenham formulation and is given by:

$$y = \int \frac{S_{sphere}(\lambda)L(\lambda)G(\lambda)F(\lambda)}{S_{lamp}(\lambda)} d\lambda \times \left(\frac{S_{sphere}(\lambda_{ex})G(\lambda_{ex})}{S_{lamp}(\lambda_{ex})} \int L(\lambda) d\lambda \right) \qquad (3.5)$$

Where $L(\lambda)$ is the emission spectrum, $G(\lambda)$ is the quantum efficiency of the photodiode, $F(\lambda)$ is the transmission of the filter, $S_{sphere}(\lambda)$ is the spectral response of the sphere and $S_{lamp}(\lambda)$ is the spectrum of the lamp. The PLQY is then simply x/y.

In comparison, the solution PLQY is a relatively straightforward measurement. This uses the measurement of the solution against a reference solution with a known PLQY.[3] In this case the sample is made into a dilute solution, with an absorption at the excitation wavelength of 0.1. The reference samples chosen were quinine sulphate in 0.1 Mol sulphuric acid, which has a known PLQY of 0.54[4] and 2-aminopyridine diluted into 0.1 Mol of sulphuric acid, which has a known PLQY of 0.6.[5] Quinine sulphate was used for the majority of measurements for the samples which emit at ~ 450 nm.

The PLQYs are then calculated by measuring the absorption at a set wavelength, and the emission spectrum when excited at the absorption wavelength. The PLQY can thus be determined from the following relation:[3]

$$Q_x = Q_r \left(\frac{A_r(\lambda_r)}{A_x(\lambda_x)} \right) \left(\frac{I(\lambda_r)}{I(\lambda_x)} \right) \left(\frac{n_x}{n_r} \right) \left(\frac{D_x}{D_r} \right) \qquad (3.6)$$

Where r and x are the reference and measured samples respectively. Q is the PLQY, $I(\lambda)$ is the intensity of the excitation pulse at wavelength λ, $A(\lambda)$is the absorbance at

wavelength λ, n is the refractive index of the solvent and D is the integrated area under the emission spectrum.

3.3 Time-resolved measurements

In organic semiconductors there are three main timescales depending upon which processes are being recorded. There is phosphorescence which occurs on a microsecond to millisecond timescale and is typically measured by time-gated CCD instruments to measure spectra and time-correlated single photon counting (TCSPC) to measure the dynamics. Then there are fluorescence lifetime measurements, which occur on the picosecond to nanosecond timescale, and can be measured by a streak camera or fast TCSPC methods. Finally there are intermolecular processes, which can occur on a femtosecond to picosecond timescale and require techniques such as sum frequency generation for upconversion spectroscopy or transient absorption to resolve. For the work presented in this document, the focus will be placed upon the latter two timescales with the streak camera and fluorescence upconversion spectroscopy both being employed.

All ultrafast measurements require a laser with an ultrashort pulse length, in order to resolve the transition. Typically this requires a laser with a pulse width shorter than the time period of the transition. Up until the invention of the self-mode locked titanium sapphire laser by Spence, Kean and Sibbet,[6] here at St Andrews in 1991, ultrafast measurements were limited by difficult to maintain equipment. Most of the work was performed using mode locked dye lasers, which were able to produce pulse lengths of under a picosecond. But the invention of the mode locked Ti:Sapphire laser then opened up an easy and commercially realisable way to produce ultrafast light sources, with pulse lengths of ~100 fs or shorter. All ultrafast measurements in this work used a Mai Tai titanium sapphire laser manufactured by Spectra Physics.

As outlined in Chapter 2, all lasers require a gain medium in which light of certain wavelengths can be amplified. In a titanium sapphire laser the titanium atoms are doped into an artificial sapphire (Al_2O_3) crystal. For this to lase it needs a pump source; this is performed using a continuous wave (CW) Neodymium (ND^{3+}) Yttrium Vanadate

laser (YVO^4). Using a CW pump source and without any other form of control, the laser would produce a CW output in the region between 750-1000 nm. However, as we require short pulses, there must be a form of optical control applied to the laser pulse, which reduces its duration down to 100 fs. Pulse reduction in Ti:Sapphire laser is created by passive mode locking using Kerr lenses. Using this the Mai Tai is able to produce pulses with 100 fs FWHM, which are tuneable between 750 and 850 nm via simple computer software. This wavelength range is good for organic semiconductors because it means that the output beam can be frequency doubled, so that the excitation source is 375-425 nm, which is suitable for many organic semiconductors.

3.3.1 Streak Camera

To detect the photoluminescence of a sample and to measure radiative decay processes on a picosecond to nanosecond timescale this work used a Hamamatsu Synchroscan Streak Camera. This measures the intensity of a pulse vs time and position, with a resolution of 2 ps.[7]

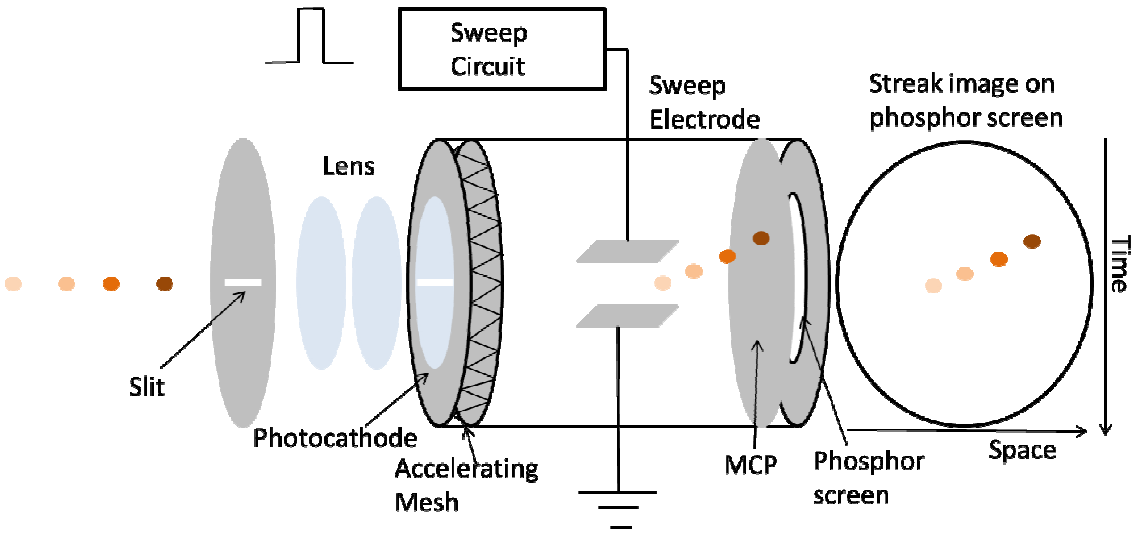

Figure 3.4: Schematic of a streak camera, figure inspired by Hamamatsu Guide to streak cameras. [7]

The emission light from the sample is focussed on the entrance slit to the streak camera. Upon entering, the pulse is then focussed onto a photocathode, where the

incident light is converted into a number of electrons; their number is proportional to the intensity of the incident light. These emitted electrons are then accelerated towards a phosphor screen at the back of the detector. As they are travelling along this path, the electrons pass through an electric field created by a pair of parallel plates. The field is controlled, so that it creates a sweep effect, which deflects the incoming electrons in different paths relative to their arrival time across the plate. The sweep is triggered by the laser pulse, and a measurement delay which can be controlled via the computer software and a delay unit. The deflected electrons then strike a micro-channel plate (MCP), which is an electron multiplier consisting of a number of glass capillaries which are formed into a disk shaped plate. As the electrons enter the capillaries they strike the specially coated walls and produce a number of electrons with each collision. This means that a single electron can be multiplied by as much as a 1000 times by this process, which allows weak signals can be detected. The emission from the MCP is then impacted against a phosphor screen, which converts the electrons back into light, and the temporal profile of the incident pulse can be resolved. The light emission on the phosphor screen is then imaged by a charge coupled device (CCD) camera. The CCD then converts the image on the phosphor screen back to an electrical signal, which can be measured by the computer and a digital readout of the dynamics recorded.

3.3.2 Upconversion spectroscopy

To resolve times faster than a few picoseconds one needs to move away from electronic components, where noise from electronic jitter can affect the results. This means that the system needs to be optically controlled to resolve dynamics on this timescale. These can be performed in two ways, either by transient absorption or upconversion spectroscopy. Transient absorption looks at excited state processes, where a molecule is excited into an upper state and then a second pulse, delayed by a set amount, is directed upon the sample. The change in absorption of the second beam with respect to time and wavelength provides a lot of information on the dynamics of the photoexcitations. The results, however, are often difficult to interpret as there are a number of competing processes occurring; each of these needs to be

understood and accounted for to provide an accurate description of what is occurring within the molecule. Studying the fluorescence on the other hand, is a much more straightforward process, and can be monitored on the femtosecond timescale via upconversion spectroscopy.

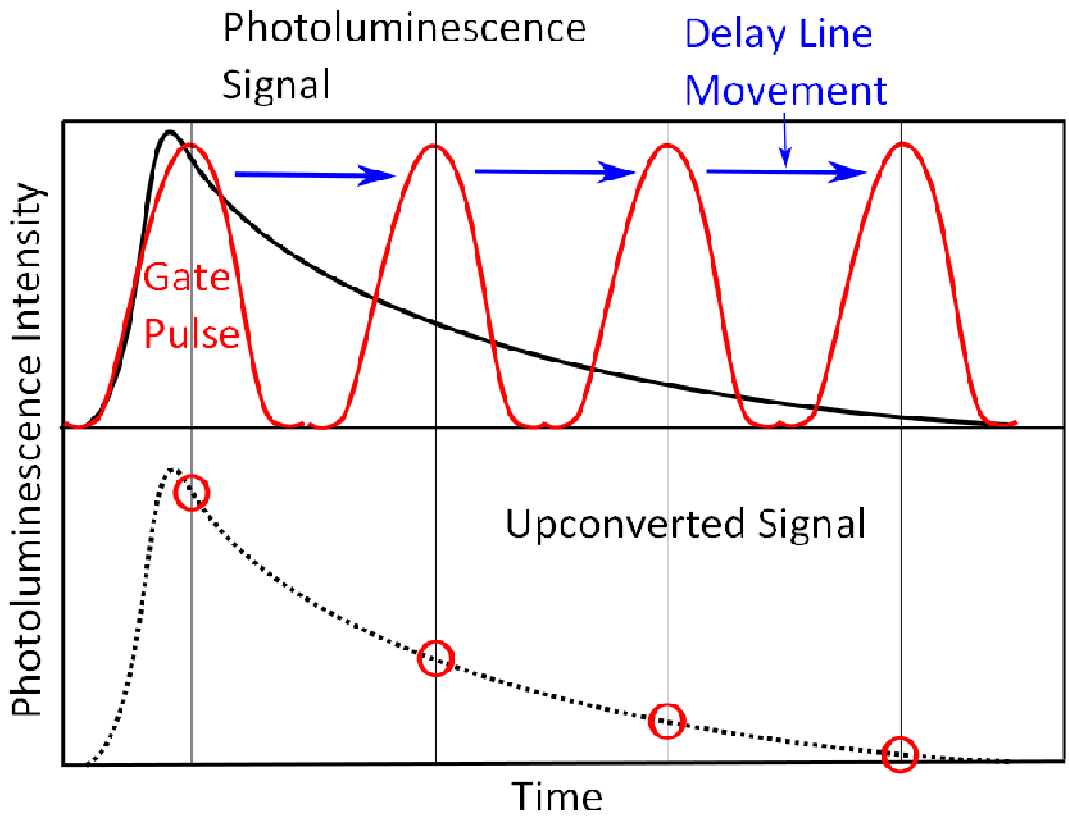

Figure 3.5: Upconversion principle, top shows the decay of a fluorescence trace with the gating pulse overlaid. The lower figure shows the upconverted signal.

Upconversion spectroscopy is an important technique and is well covered by a review by Shah.[8] The basic principles of upconversion are similar to those employed in an optical parametric oscillator, only reversed. In upconversion light of two frequencies are brought together into a non-linear optical crystal, to produce sum frequency generation within the crystal. In this process, when the two pulses mix, they produce a third wavelength of light, which is equal to frequency of the other two wavelengths combined. The frequency of the generated light can be calculated from the following formula:

$$\nu_{up} = \nu_{PL} + \nu_{gate} \qquad (3.7)$$

Where ν_{up} is the frequency of the upconverted light, ν_{PL} is the selected frequency of the photoluminescence and ν_{gate} is the frequency of the gate pulse. This principle is used in spectroscopy to detect time dynamics of fluorescence on a very fast timescale. The equipment for this technique outlined in Figure 3.6, is a CPD systems FOG 100 upconversion spectrometer. The pump and gate pulses are created by frequency doubling a single laser pulse. The pump is the frequency doubled light and the residual light is then the gate. These two pulses can then be combined back together in a non-linear crystal to produce a sum frequency generated signal. The process of sum frequency generation only occurs when the two pulses are incident on the crystal at the same time, so the dynamics of the molecule can be built up by progressively delaying the timing of the gate with respect to the photoluminescence as is shown in Figure 3.5. This sampling of the photoluminescence with time allows for femtosecond resolution of the dynamics to be obtained by accurate control of the delay line. The software then detects the signal produced at a certain timescale for a set time period, before moving to the next time window. An accurate picture of the fast dynamics can be obtained from this method. The time resolution of the sample is then limited by the thickness of the crystal and the pulse width of the laser beam.

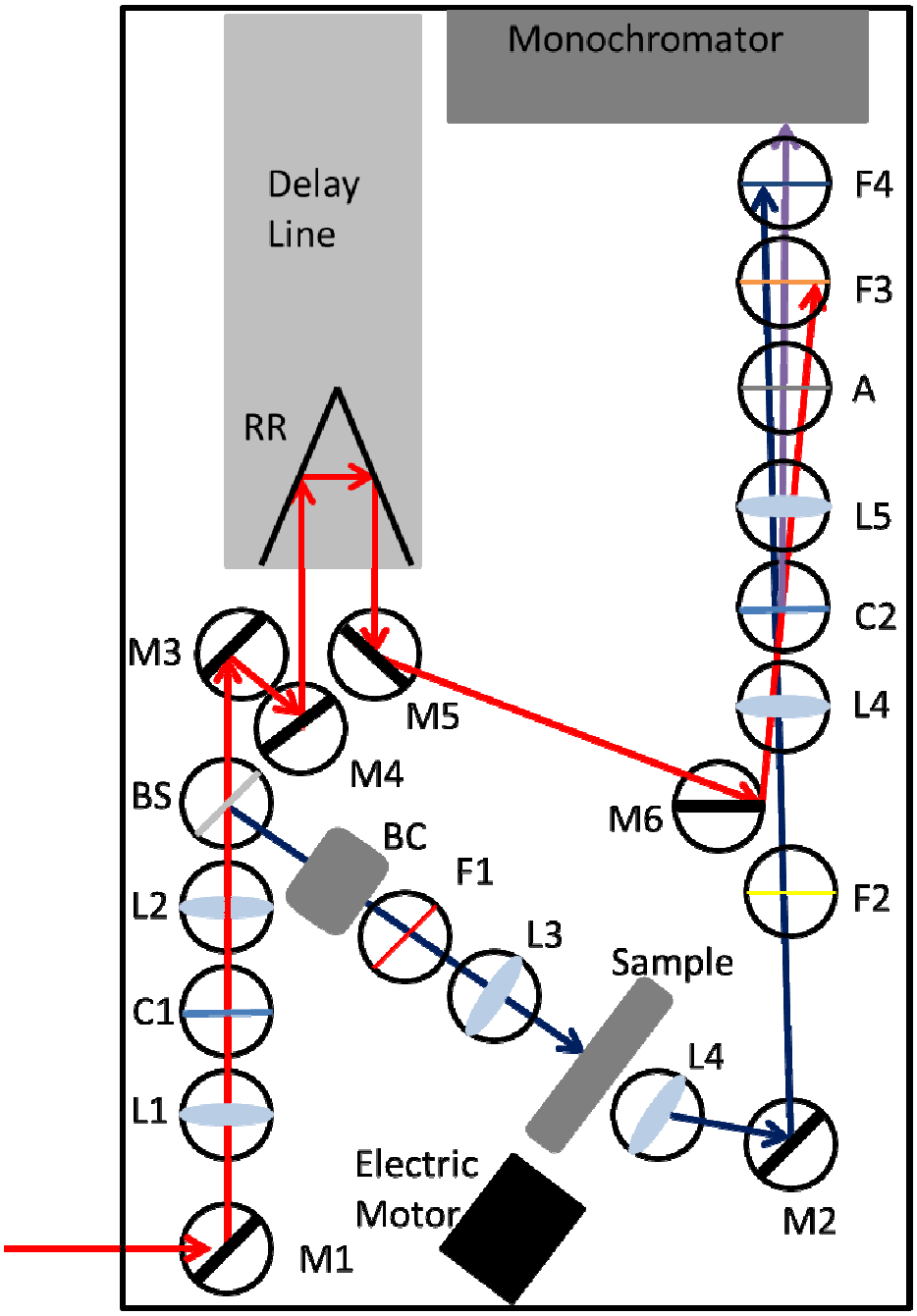

Figure 3.6: Experimental setup of the fluorescence upconversion measurement system.

The laser output from the Mai Tai titanium sapphire laser is directed into to the optical setup. Although this setup is tuneable for a number of wavelengths, for clarity of explanation of the setup we will assume that the initial pump light is 800 nm. The light from the laser enters from an aperture in the box which encloses all the equipment, the light is then directed into the optical path by mirror M1. The light is then focussed by lens L1 onto a type 1 beta barium borate frequency doubling crystal, which is 1 mm thick. This splits the beam into two wavelengths, where there is around 200 mW of the

residual 800 nm light and 100 mW of the frequency doubled 400 nm light. The two wavelengths are then collimated by a 6 cm focal length lens L2, before passing to a dichroic beamsplitter (BS). This beamsplitter reflects the 400 nm light along the excitation path and transmits the 800 nm light along the gate path.

The 400 nm excitation pulse first passes through a Berek compensator (BC): this allows for the polarisation of the excitation light to be controlled, and is very important in the case of the anisotropy measurements discussed later. It then passes through a filter (F1), which is there to remove any residual 800 nm light that was reflected at the beamsplitter. After passing through this, it is then focussed, using lens (L3), onto the rotating sample cell. The focussing is as tight as possible in order to increase the collection of the emitted photoluminescence. High concentrations are used in these measurements to ensure that as much of the 400 nm light is absorbed as possible, so that it does not affect the results when detected. The emitted photoluminescence is then collected and focussed by lens L4 with a focal length of 4 cm to a movable steering mirror (M2). This directs the collected photoluminescence towards the second frequency doubling crystal. Before travelling to this crystal it passes filter (F2), which removes any remaining pump light. Once passed through the filter the light is then focussed onto a type 1 BBO sum frequency generating crystal, where it is overlapped with the gate light.

As this is the point at which the two beams come together, it is appropriate to discuss the second path, that of the residual 800 nm gate pulse. This light has its path adjusted by mirrors M3 and M4, so that the beam is directed onto the gold coated retroreflectors of the delay line. The delay line is used to vary the time of the path between the excitation pulse and the gating pulse so that a sweep of the dynamics can be made. The delay is controlled by simple computer software and is capable of adjusting the time of the pulses in steps by a minimum of 6.5 fs. The light from the optical delay line is then steered towards the sum frequency generating crystal by mirrors (M5 and M6). It is then passed at an angle through lens L5, which is where the paths of the two beams re-join. The slight angle of the two beams with respect to each other allows for the light to be directed away from the detector after the passing through the sum frequency generating crystal, whilst the upconverted light is directed

towards the detector. Before arriving at the detector the UV upconverted light is focussed by lens L6 onto the monochromator. Any residual light from either photoluminescence or gate must be filtered out so that they are not detected with the upconverted light. This filtering is in part done by the spatial separation of the two beams after passing the crystal, and part done by an aperture (A) and then two filters (F3 and F4). The first filter (F3) is a dichroic and reflects any residual pump light; the second (F4) is a Schott glass filter which only allows transmission of the UV upconverted light. The monochromator is then set to detect the desired UV wavelength as indicated by entering the gate wavelength and the chosen emission wavelength into the computer software. The position of the monochromator is controlled by a simple micrometre screw. The monochromator provided with this system is a Solar/TII single monochromator CPD systems model 2022.

3.3.3 Anisotropy measurements

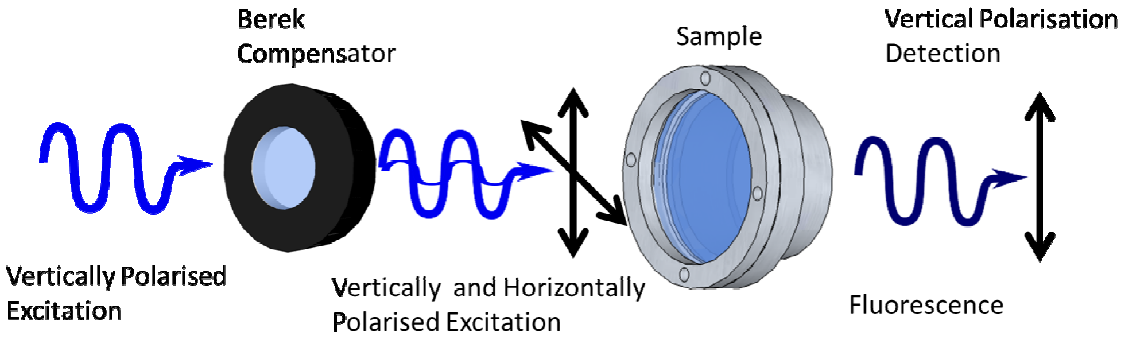

Figure 3.7: Anisotropy measurement: vertically polarised light arrives from the laser and its polarisation relative to the detector is then controlled by a Berek compensator. This is used to excite the sample and fluorescence is then collected by the detector.

In spectroscopy, fluorescence anisotropy is a measure of the change in the intensity of the emission angle relative to that of the excitation. This in turn provides information on energy transfer and the change in the orientation of the emission dipole relative to the absorption one. Because of this, it is a very useful tool for studying intramolecular energy transfer. The anisotropy can be determined by measuring the emission intensity parallel and perpendicular to the pump beam using the following formula:[9]

$$r = \frac{I_{\parallel} - I_{\perp}}{I_{\parallel} + 2I_{\perp}} \qquad (3.8)$$

Where r is the anisotropy, $I_{\parallel}$ is the intensity recorded parallel to the pump and $I_{\perp}$ is the intensity detected perpendicular. In this experiment the excitation light is rotated with respect to the detection using a Berek compensator. The two traces can then be recorded for the two different orientations so that multiple scans of $I_{\parallel}$ and $I_{\perp}$ can be run before averaging them, and then combining them as in equation 3.8. To change the orientation of the polarisation of the pulse involves the rotation of a Berek compensator; this rotation also changes the delay times between the excitation of the $I_{\parallel}$ pulse and the $I_{\perp}$. This means that, if it was unaccounted for it would affect the early time dynamics being monitored within the sample. To get the time difference between differently oriented pulses water Raman measurements were performed. These results were fitted with a Gaussian, and the time difference between the two pulses is then equal to the temporal delay caused by the Berek compensator. This was found to be 39 for 380 nm, 32 fs for 400 nm and 38 fs for 420 nm. This temporal shift was then added to the perpendicular results before fitting.

3.3.4 Fitting anisotropy decay

The first stage with all the scan data is to average them, reducing any noise from the signals. After this, the temporal shifts were added to the perpendicular results, and the anisotropy calculated. The anisotropy fitting was done by a so called sum difference fitting technique, where the sum is the denominator of equation 3.8 and the difference is the numerator to the equation. The fitting was performed using the "Globals WE" software package, developed by the University of Illinois at Urbana-Champagne, by the Laboratory of Fluorescence Dynamics.[10] The fitting of the anisotropy decay follows the method outlined by Souter et al..[11] This fits the sum as a series of exponentials, $S(t)$:

$$S(t) = \sum_n A_n e^{\frac{-t}{\tau_n}} \qquad (3.9)$$

The best fit for the sum equation $S(t)$ was then multiplied by a trial function $A(t)$:

$$A(t) = r_1 e^{\frac{-t}{\tau_1}} + r_2 e^{\frac{-t}{\tau_2}} + r_{inf} \quad (3.10)$$

This was found to work best for a two exponential decay and an offset, as described in equation 3.10.

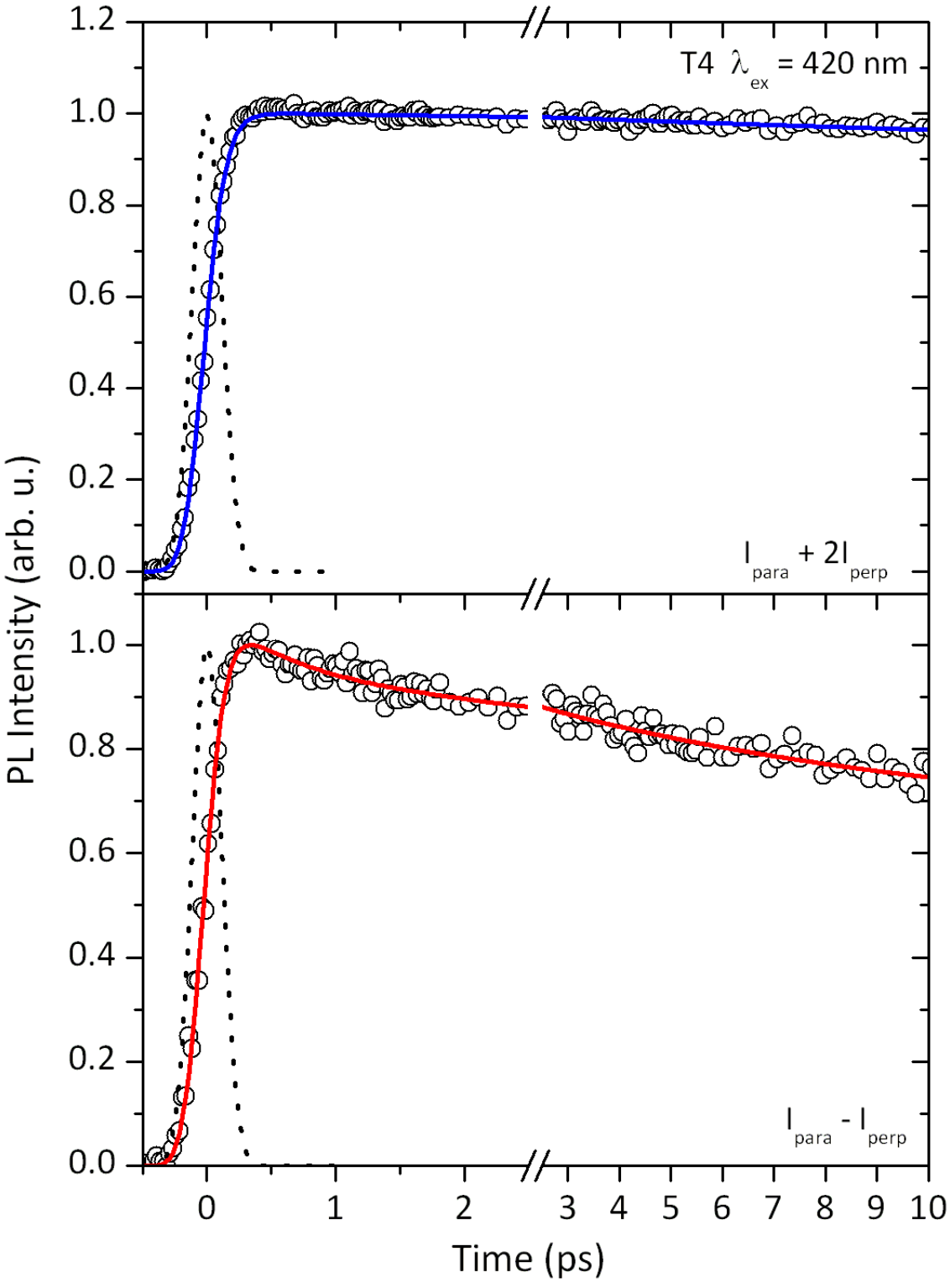

Figure 3.8: Anisotropy fitting: the top figure shows the sum fit from equation 3.8, whilst the bottom shows the fitting for the difference part of the equation 3.8.

The resultant fit is then compared against the sum fit and the instrument response function, to provide the difference fit for the data, such that:

$$D(t) = [S(t) \times A(t)] \otimes IRF \qquad (3.11)$$

From this it is shown that the trial $A(t)$, is equal to the anisotropy. Therefore the terms in the A(t) best fit are equal to the terms governing the anisotropy, so that r_1 and r_2 are the amplitudes of time decays τ_1 and τ_2, and r_{inf} is the anisotropy at the end of the data scan.

3.4 Organic semiconductor lasers

3.4.1 Experimental setup

As mentioned in section 2.3 all organic semiconductor lasers require an external optical pump source to excite them. Measurements of lasers and amplified spontaneous emission (ASE) were performed using a Q-switched Nd:YAG pump laser, with a 4 ns pulse length. A Nd:YAG laser uses a Yttrium aluminium garnet (YAG) crystal doped with a small amount of neodymium (Nd^{3+}) as the gain medium. The laser then produces emission at 1064 nm from the neodymium emission; this can then be frequency doubled to produce green 532 nm, or tripled to produce 355 nm. The use of Q-switching allows the laser to produce its 4 ns pulses. All the materials presented in this study absorb in the UV region of the spectrum, so the third harmonic of this laser is an ideal pump source. This laser source is usually used for pumping of an OPO cavity, but in the case of 355 nm the emission light is able to bypass the cavity and be directed out of the housing. The optical set up to the sample is shown in Figure 3.9.

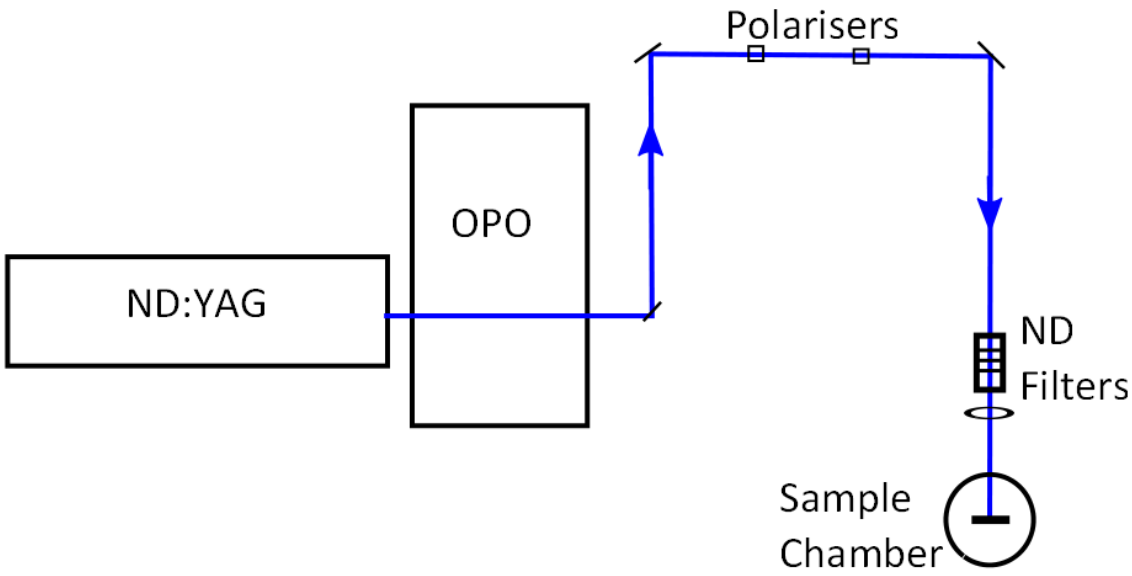

Figure 3.9: Experimental setup for Laser and ASE measurements.

In order to carry out the characterisation of any laser material, it is important to have an understanding of how the molecule behaves at high pump intensities, without the presence of a cavity. This can be done by measuring the ASE of the sample, because this is a very similar process to lasing, but without the resonant wavelength being selected by the cavity. ASE measurements can provide information on losses and gain within the films, as well as the threshold for the onset of ASE.

For all laser and ASE measurements the samples were placed inside a vacuum chamber, which helps to prevent photo-degradation of the samples at high pump energy intensities. The vacuum chamber consists of a cylindrical glass chamber, with a fixed bottom plate. The mount for the sample then projects from the base plate. The mount holds the sample in the middle of the chamber, with the sample being fastened in position by a small screw. The top plate is removable to allow insertion of the sample and connects the chamber to the vacuum pump via a tube. It also connects to a three dimensional adjustable stage, which allows the sample position to be controlled with respect to the pump beam. The vacuum chamber is then sealed by compressing an ‘o’ ring between the top plate and a metal ring. Initial pumping is carried out by a BOC Edwards rotary pump before a turbo molecular pump is used to reduce the pressure further. Under this pumping the vacuum chamber is at 10^{-3} to 10^{-4} mbar of pressure.

The optical setup for the ASE and lasing measurements is shown in Figure 3.9. The same setup is used for both experiments, but there are differences on all the individual measurements. Initially this part will concentrate on the main path and then the nuances of each of the experiments will be explained in detail in the sections on the individual measurements. The 355 nm pump light is passed out of the OPO box and then is directed using mirror M1. The light is then redirected using mirror M2 and passes through a pair of polarisers P1 and P2, which are used to attenuate the beam. The beam then travels onto the adjustable mirror M3 which steers the beam towards the sample; an aperture is used to remove any stray reflections from the beam. The beam then passes through a series of neutral density (ND) filters, which are suitable for the UV light and are used attenuate the beam further; changing these allows for the excitation energy to be varied. There is then a focussing lens which focuses the pump onto the sample. The focal length of this lens is ~10 cm and a circular one is used for the lasing measurements and a cylindrical one for the ASE measurements. The choice of a cylindrical lens is made for the ASE measurements, because when ASE is confined to a long narrow stripe most of the output is emitted out of the end of the stripe, so this increases collection.

3.4.2 Gain, loss and ASE measurements

The ASE threshold measurements are performed by focussing the light from the pump source into a stripe of ~0.3 x 3 mm. The pump energy is measured using a calibrated Newport photodiode pulse energy meter and the pump energy is adjusted by changing the number of neutral density filters before the sample. The ASE is measured perpendicular to the pump and in the plane of the film with a Jobin Yvone Triax 180 spectrometer connected to a CCD detector. Light is coupled into the spectrograph via a fibre, and to increase the capture angle, a lens coupling system is used; this is placed against the wall of the chamber, so as to collect as much light as possible.

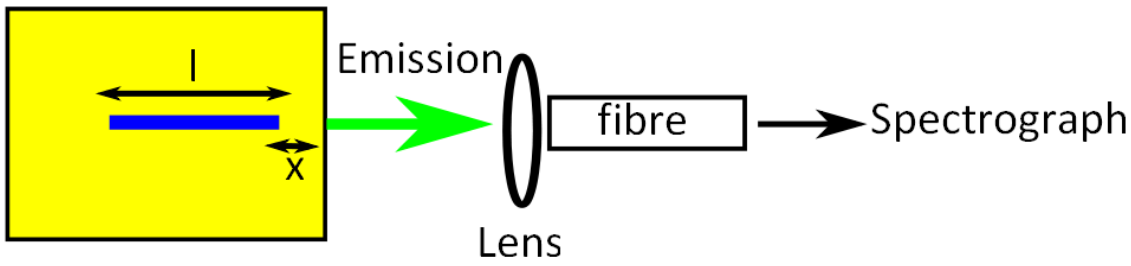

Figure 3.10: Amplified Spontaneous Emission measurement setup: the beam has a length l and is at a distance x from the edge of the film. The emission is emitted perpendicular to the film, where it is collected by a fibre coupled to a spectrograph.

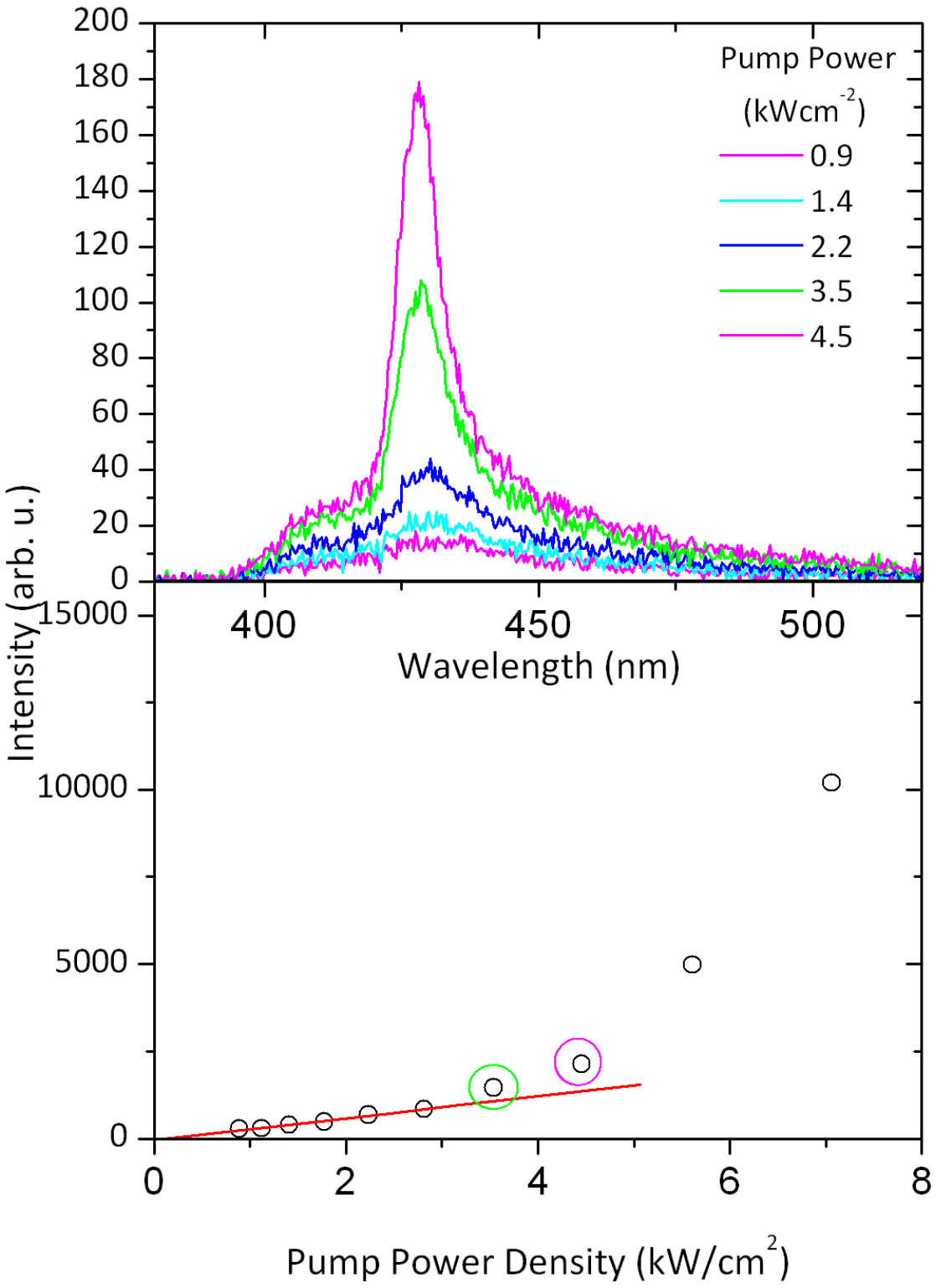

Figure 3.11: Results from an ASE measurement. Top shows the change in spectra with increasing pump intensity; bottom shows the corresponding increase in the intensity of the emission with increasing pump intensity. The threshold has been highlighted by the (green circle), and the (pink circle) is the point above threshold corresponding to the same colours in the spectra above.

The ASE threshold measurement identifies the point at which amplified spontaneous emission is produced from the material; this is done by measuring the ASE output from the film and plotting it against the input power. This input energy is varied by changing the number of ND filters in front of the sample. The threshold is then determined as the point at which the spectra shows a distinctive line narrowing caused by ASE. This point is also typically shown as the point at which output starts to follow a nonlinear dependence to the pump power density.

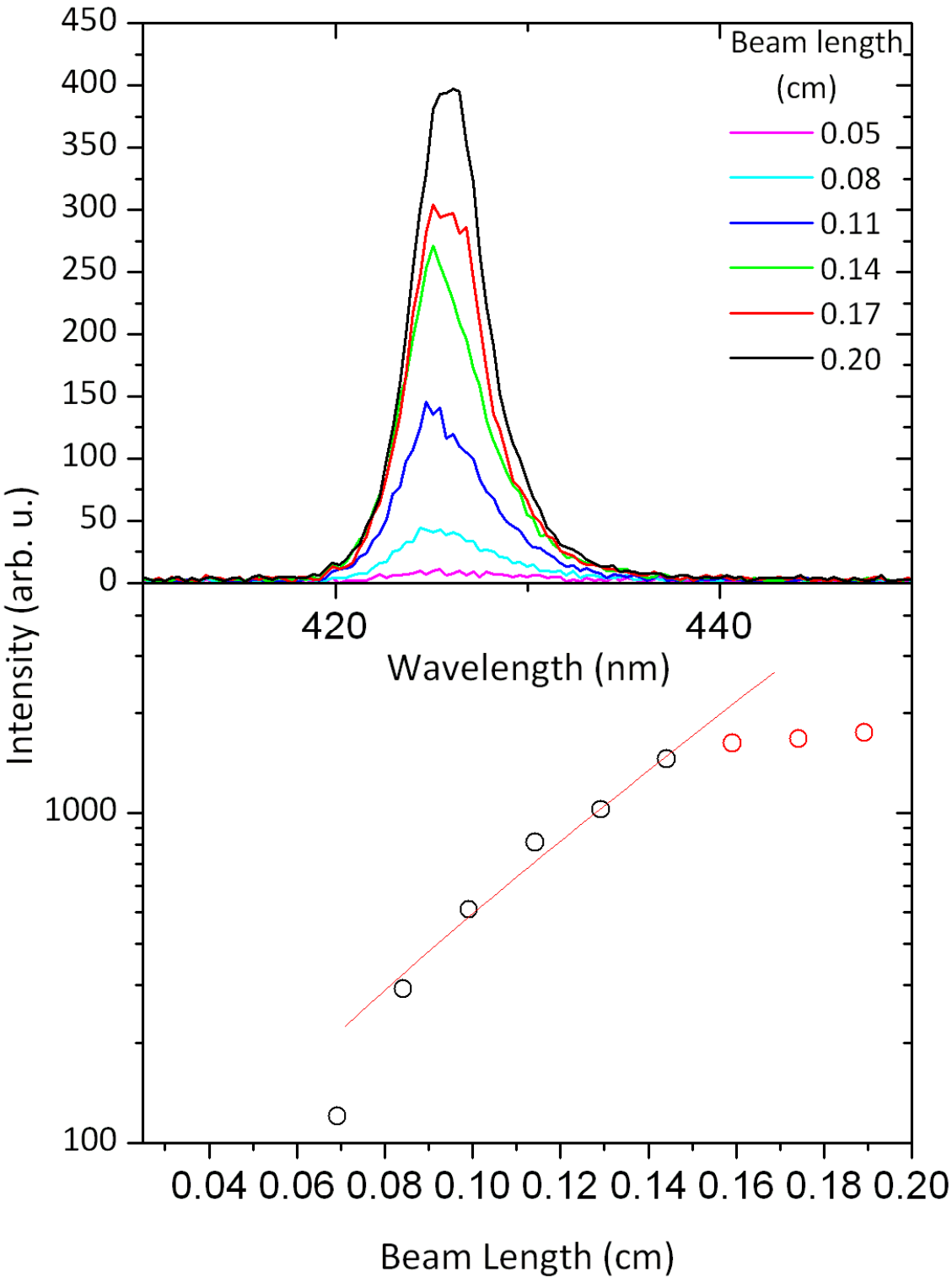

Figure 3.12: Results for a typical gain measurement. Top shows the increase in intensity in the spectra with increasing beam length, whilst the bottom shows the fit to the data from equation 3.12.

Gain measurements are performed by changing the length of the stripe at a fixed excitation energy. The growth of the output intensity should grow with the following relation:[12]

$$I(\lambda, l) = \frac{AI_{exc}}{g(\lambda)}(e^{g(\lambda)l} - 1) \qquad (3.12)$$

Where I_{exc} is the excitation intensity, λ is the wavelength and $g(\lambda)$ is the gain per unit length at the wavelength.

The change in stripe length is achieved by using a variable rectangular aperture, which is controlled by a micrometre screw. This allows for accurate control of the aperture, so that an accurate length of the stripe can be determined. In the measurements the initial output is seen to follow equation 3.12, but at a certain point there is a levelling off of the intensity relative to the length of the increasing pump stripe. This is due to gain saturation in the system, where at high intensities the light becomes so intense that it reduces the available gain.[13] As a result of this, it is the rising data that is fitted by equation 3.12 to calculate the gain coefficient.

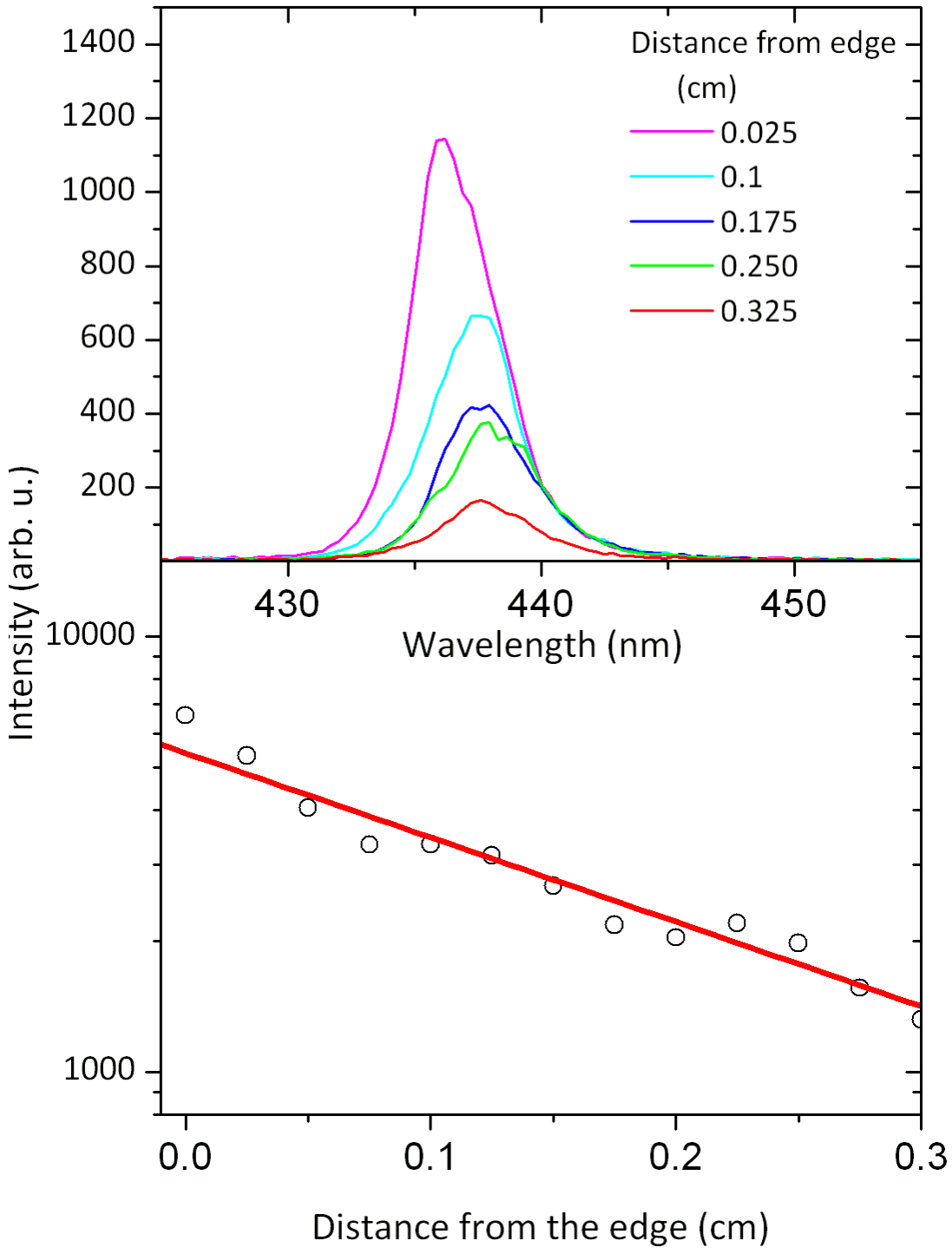

Figure 3.13: Results for a typical loss measurement. Top shows the spectra decreasing in intensity with increasing distance from the edge, whilst the bottom shows the fit to the data from equation 3.13.

Loss measurements are performed at the same time as the ASE and gain measurements on the same film. Loss measurements are performed by moving the stripe away from the edge of the film and thus monitor the reduction in the ASE intensity due to the losses in the film. The film losses can then be determined by:[12]

$$I_{out} = I_0 e^{-\alpha x} \qquad (3.13)$$

Where I_0 is the initial input intensity with the beam at the edge, I_{out} is the output intensity at distance x and α is the loss. Despite the fact that the stripe is being moved away from the edge of the film, the detector is much bigger than the solid angle of emission at that distance and so does not need to be taken into account when considering this experiment.

For all these experiments the intensity is taken as the integrated area under the ASE peak. The beam size is measured using a Coherent LaserCamIIID CCD beam profiler. This is then combined with the pump energy and duration of the pulse, which in this case is 4 ns, to calculate the power density of the beam.

3.4.3 Laser measurements

As outlined above, laser measurements use almost the same setup as the ASE measurements, apart from the fact that the film is spun onto a DFB grating and the lens that focuses the beam is a circular rather than cylindrical lens. Again the input power is controlled by changing the number of ND filters used before the sample. In this case the sample is placed at a very small angle to the pump beam so that the laser emission can be detected from the surface.

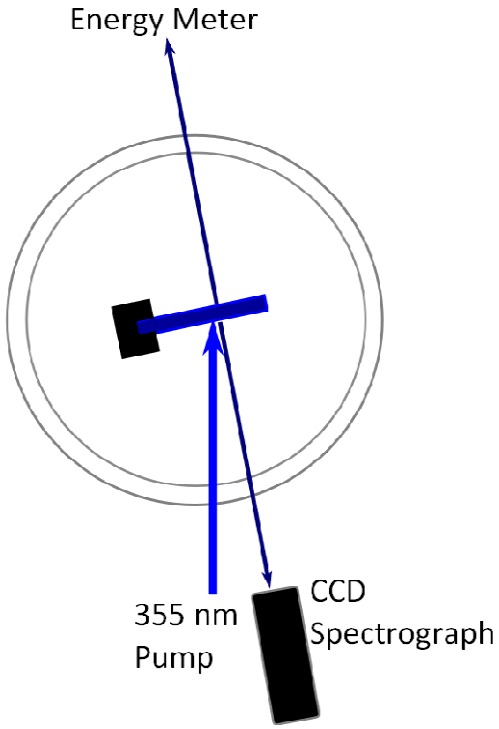

Figure 3.14: Laser measurement setup, the emission is collected from the front using a lens setup for an optical fibre coupled to the CCD spectrograph, and at the back by a calibrated pulse energy meter.

The laser threshold measurements were done in the same way as the ASE measurements, with the power being varied by changing the number of ND filters. The threshold was determined from integrating the area under the full width of the laser peak, which is typically less than a nanometre wide. This was then plotted against the input intensity and the change in slope of the output intensity was determined as the lasing threshold. This point corresponds with the line narrowing observed in the spectrum corresponding to the onset of lasing. There is also an increase in the background photoluminescence resulting from the higher pump powers.

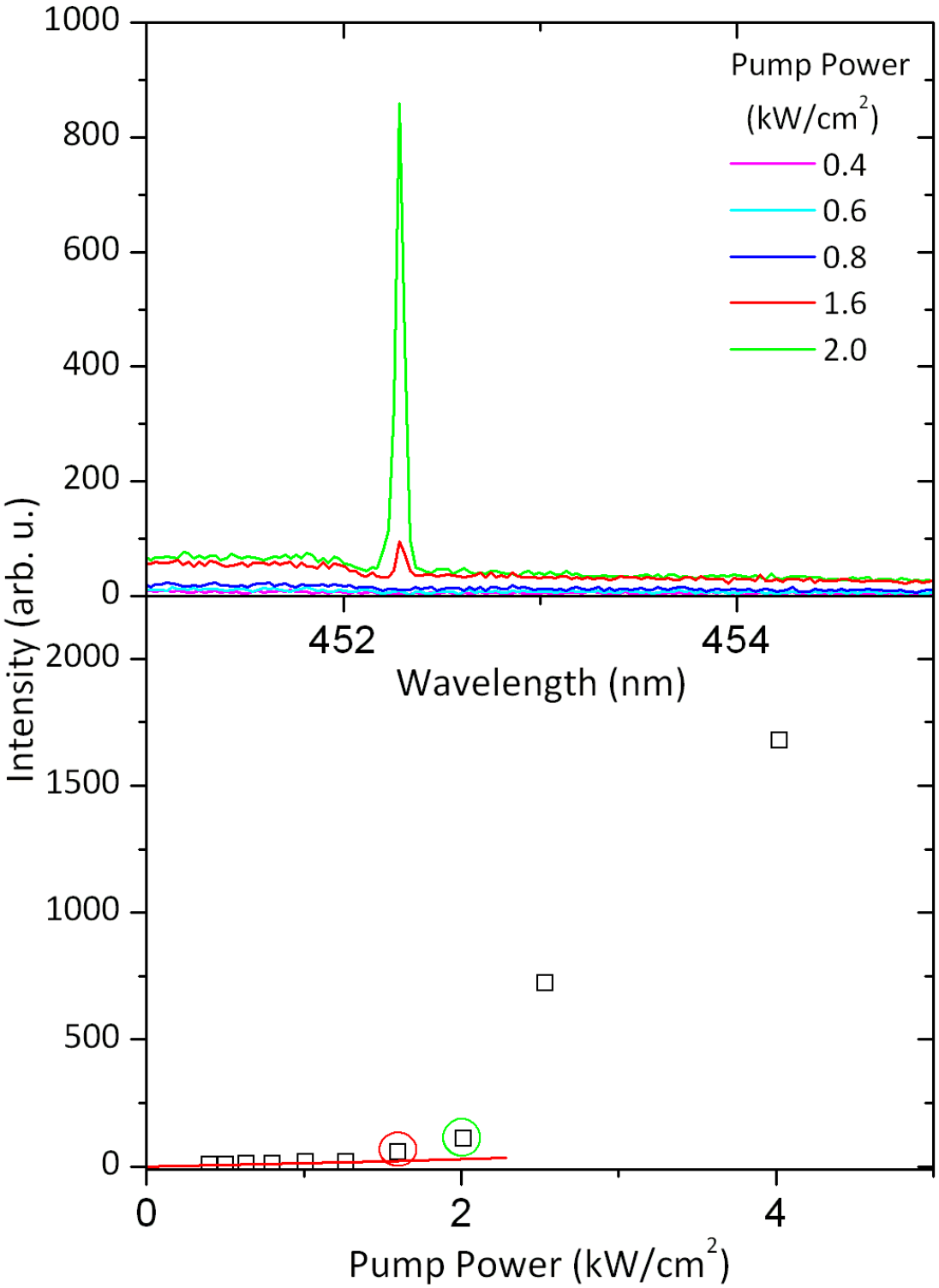

Figure 3.15: Results from a laser measurement. Top shows the change in spectra with increasing pump intensity; bottom shows the corresponding increase in the intensity of the emission with increasing pump intensity. The threshold has been highlighted by the (red circle), whilst the (green circle) corresponds to the point above the threshold, as shown in the spectra above.

Efficiency measurements were performed by replacing the CCD spectrograph with a calibrated Molectron energy meter and recording the input intensity using an oscilloscope. This is then compared against the measured input power and the slope of the line of the two plotted against one another corresponds with the efficiency of the device.

3.5 Material synthesis

One of the key components of this research is the ability to test and analyse new materials; these materials were either procured from American dye sources inc. or synthesised by the Organic Chemistry group at Strathclyde University. In order to get high quality materials with high levels of purity for this study the synthesis of the molecules was of great importance. This is because the better the quality of the materials the greater the trust that can be placed on the physical findings.

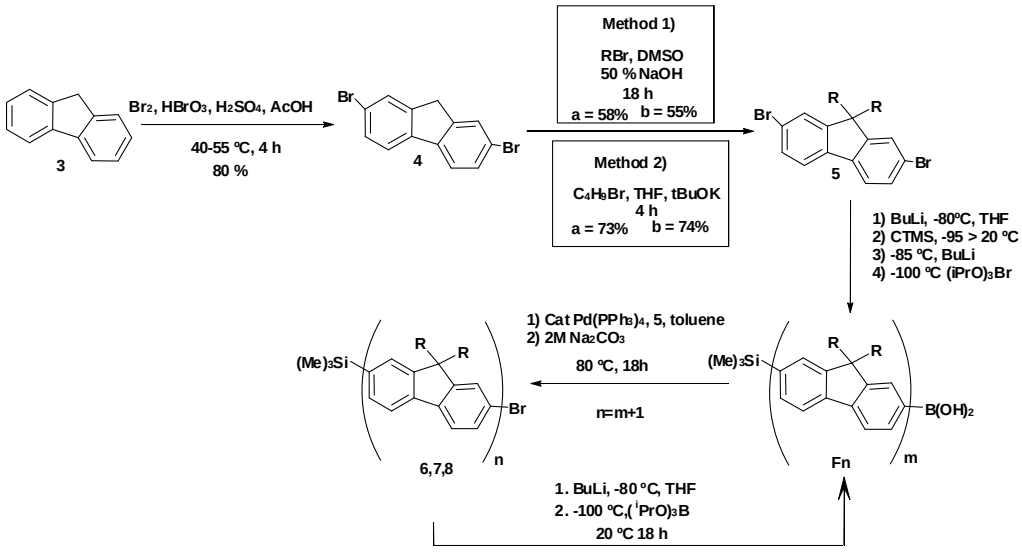

Scheme 3.1- Synthesis of oligofluorenes TMS protected (Scheme by Clara Orofino)

The synthesis of the monodisperse oligofluorene is shown in Scheme 3.1. The base flourene unit is initially brominated and is then lithiated at the 9,9-position using butyl lithium, this is then followed by the addition of the bromo-alkyl chain of choice to alkylate the fluorene unit. 2,7-dibromo-9,9-dialkylfluorene is the building block employed throughout the iterative synthesis of the oligofluorenes. Butyl lithium is then

added to deprotonate one of the bromine atoms, followed by the addition of triisopropylborate to add the $B(OH)_2$ functionality. Butyl lithium is added again followed by the addition of chloro-trimethylsilane (TMS) which yields monofluorene boronic acid. The use of a TMS (trimethylsilane group) allows the chemists to protect that position and as a scaffold to be able to functionalise the molecule further. Once this building block has been created, iterative synthesis using Suzuki coupling of the compound with the fluorene boronic acid is used to increase the length of the oligoluorene chain. This is followed by functionalising the 2- position of the Fn molecules with $B(OH)_2$ by the addition of butyl lithium. These last two steps are repeated until oligofluorenes of the required length are produced. If the molecules are intended to be stand alone oligofluorne molecules, then a final step of deprotecting the molecules from the TMS functionality is performed using a simple treatment of trifluoroacetic acid.

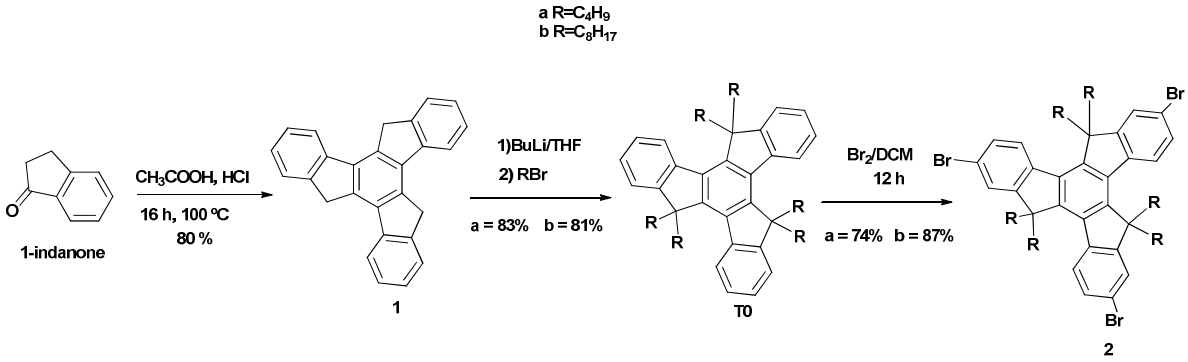

Scheme 3.2- Synthesis of the truxene core (Scheme by Clara Orofino)

In order to synthesise the truxene-cored molecules, the tribromohexaalkyltruxene core is synthesised following the procedure depicted in Scheme 3.2. The truxene compound is generated by cyclisation of commercially available 1-indanone under acidic conditions, followed by alkylation of the methylenic positions by lithiation with butyllithium and addition of the bromoalkyl chain to produce T0. Final bromination of the C2, C7 and C12 positions with bromine yields the truxene core.

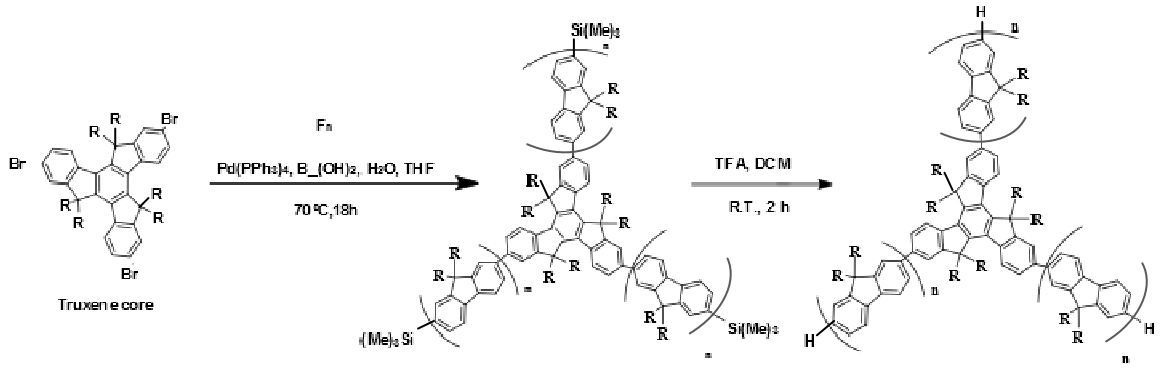

Scheme 3.3- Synthesis of the oligofluorenyltruxenes Tn (Scheme by Clara Orofino)

Once the fluorene arms of the desired length are synthesised, they are then coupled to the required core. The truxene (T1-T4) are synthesised by coupling the tribromohexaalkyltruxene (truxene core) with the TMS protected oligofluorenes of the desired length via Suzuki coupling. The final step consists of deprotecting the molecules from the TMS functionality by simple treatment with a trifluoroacetic acid.

After each step the molecules are purified by column chromatography on silica gel. In this purification technique, the components of a mixture are forced to equilibrate between an immobile stationary phase (silica gel, in our case) and a moving phase by the addition of an eluent (a solvent or mixture of solvents). The components of the mixture have different affinities for the stationary phase and the eluent. The compounds with a greater affinity for the moving phase travel faster along the column than those with greater affinity for the stationary phase. This principle combined with the vertical diffusion of a material along a long column allows for the separation of the mixture into different fractions.[14] This method works well for purification, because it is able to handle large quantities of the mixture. The collected desired fraction then undergoes a crystallisation or reprecipitation phase. By using pure compounds at each stage increases the yield and purity of the final compound, which is key in its final performance in the device.

As a final check of the purity ^{1}HNMR and thin layer chromatography are used. Using NMR provides information on the protons within the molecule, and can provide information about their relative positions. Nuclear magnetic resonance (NMR) spectroscopy only works for spin 1/2 atoms such as ^{1}H or ^{13}C, this is because they

generate their own magnetic field, without the presence of an external magnetic field, which is randomly oriented. However, if an external magnetic field is applied, the atom can align either with or against the external magnetic field. Once this has been applied, the sample is scanned by radio waves 1-100 m in wavelength, the purpose of this is to apply enough energy to change the alignment orientation of the atom by it absorbing the incident energy. Using this the absorbance over a particular energy range, the number and type of protons can be recorded[15] (eg. aromatic protons, aliphatic protons, aldehydes, etc). It works because the absorption frequency of the different protons within system is different, resulting from their interaction with the surrounding electrons, so the absorption peaks appear at different points along the spectrum. The values for the different absorption conditions are known so that the structure of a molecule can be determined by comparing the peaks in the experimental NMR absorption spectra against known positions for each distinct nucleus. By integrating under the peak it is possible to determine the number of protons which occupy that specific absorption point. As such NMR provides most of the information on the purity of a molecule because the characteristic peaks in the spectrum and can often be traced back to the initial products. The results for this can compared against the known spectrum for a pure molecule to compare the traces to see if there are any impurities within the system.

Thin layer chromatography (TLC) works on the same principle as the column chromatography outlined above, but this technique is qualitative to assess the purity of the material and is also used in combination with column chromatography to assess the progress of the purification. In this technique a small quantity of material is placed on a glass or aluminium plate coated in an adsorbent material (silica in this case). The plate is then inserted in a container with a small amount of the eluent. Capillary action forces the eluent to move upwards along the plate and the compounds present in the adsorbed mixture move along and separate, showing any impurities as a difference from the position of the bulk of the material.

3.5 Density Functional Theory

Quantum chemistry is a growing field of research, with improved computers and computer programmes, the size of molecules which can be studied by quantum chemistry is increasing. With the improved programmes and techniques there is also an increase in the accuracy of the results from these calculations. One of the reasons why there is growing interest is that the use of quantum chemistry allows for the calculation of properties of new molecular designs without them having to go through long and costly synthesis processes to see if a material will have for example a desired transition energy.

In the work covered in this thesis the quantum chemistry calculations were performed by Prof. Ian Galbraith, Dr Stefan Schumacher and Jean-Christophe Denis at Heriot Watt University. The calculations were used to provide greater physical information of the properties of the molecules and as a comparison for the experimentally determined results. The use of these techniques allowed for a greater understanding of the self trapping process in oligofluorenes and the energy transfer properties of the star-shaped molecules.

Theoretical quantum chemistry is the calculation of properties of molecules through use of calculations and computational means. There are several different ways of calculating the properties, these can either use ab-initio or empirical methods. The typical aim of both of these methods is to use the theories of quantum mechanics to determine physical properties of an atom or a molecule. However, to do this for a large molecule leaves the problem that there are N number of particles within the molecule with each having 3 degrees of freedom, so the calculations can soon become enormous. The solution to this problem is to introduce a number of simplifications into the system to reduce the number of variables, with the aim of making the calculation much simpler.

The main approximation used in theoretical calculations is the Born-Oppenheimer approximation, which states that because nuclei are much heavier than electrons they move much more slowly in comparison with the electrons, so the motion of the nuclei

can be neglected.[16,17] This greatly reduces the number of variables that need to be calculated, so that only the movement of the electrons needs to be considered.

Density functional theory or DFT is a method used to perform quantum chemistry calculations. In this it uses a functional, which is a function of a function, to describe the electron density. This allows for a simplified calculation in which the electron density can be represented as a single body and so can only move within the three space dimensions. This assumption is possible due to the Hohenberg-Kohn theorem,[18] which asserts that the ground state properties of a many body electron system can be uniquely determined by the ground state electron density. This allows for accurate calculations of the ground state of a molecule using DFT. If one wants to study the excited states of molecules then it necessitates a move away from DFT to Time Dependent Density Functional Theory TD-DFT. This is similar to DFT but has a time dependent external potential which acts upon the molecule to describe the excited state. This works because of the Runge-Gross theorem,[19]which states that there is a correlation between the time dependent external potential and the time dependent electron density. TD-DFT can therefore be used to calculate the transition energies and the transition dipole moments of the molecules.

As stated above a in order to perform calculations with DFT and TD-DFT a functional must be used. The functional provides a description of the ground state energy which is dependent on the number of electrons N and the nuclear potential of the molecule.[20] For the work outlined in this thesis the B3LYP functional was used, because this has been found to provide accurate calculations for systems like the ones studied in this thesis.[21,22] The results from the calculations using B3LYP were found to provide a very good agreement with the experimental results obtained in this body of work.

Density functional theory as well as requiring a functional to describe the electron density, also requires a basis set which is used to provide a description of the molecular orbital's of the molecules. In the case of the theoretical work in this thesis, the 6-31G basis set was used, because when used in combination with the B3LYP functional has been found to provide very good results for fluorene based molecules.[21,22]

All the calculations were performed using the Gaussian 09 computer programme. In order to perform the calculations for our molecules, DFT was used to optimize the ground-state energy, whilst the excited state was optimized using TD-DFT. When calculating the transition energies and transition dipole moments TD-DFT was used. In the case of the C_3 symmetric molecules a small symmetry breaking must be introduced in order for the lowest energy excited state to be seeded.

3.7 References

1 Lakowicz, J. R. *Principles of Fluorescence Spectroscopy*. 2 edn, 52 (Kluwer Academic/Plenum Publishers, 1999).

2 Greenham, N. C. *et al.* Measurement of Absolute Photoluminescence Quantum Efficiencies in Conjugated Polymers. *Chem. Phys. Lett.* **241**, 89-96 (1995).

3 Crosby, G. A. & Demas, J. N. Measurement of photoluminescence quantum yields. Review. *The Journal of Physical Chemistry* **75**, 991-1024, doi:10.1021/j100678a001 (1971).

4 Melhuish, W. H. Quantum Efficiencies of Fluorescence of Organic Substances: Effect of Solvent and Concentration of the Fluorescenct Solute. *The Journal of Physical Chemistry* **65**, 229-235, doi:10.1021/j100820a009 (1961).

5 Rusakowicz, R. & Testa, A. C. 2-Aminopyridine as a standard for low-wavelength spectrofluorimetry. *The Journal of Physical Chemistry* **72**, 2680-2681, doi:10.1021/j100853a084 (1968).

6 Spence, D. E., Kean, P. N. & Sibbett, W. 60-fsec pulse generation from a self-mode-locked Ti:sapphire laser. *Opt. Lett.* **16**, 42-44 (1991).

7 Hamamatsu. Guide to Streak Cameras. (2008).

8 Shah, J. Ultrafast luminescence spectroscopy using sum frequency generation. *Quantum Electronics, IEEE Journal of* **24**, 276-288, doi:10.1109/3.124 (1988).

9 Lackowicz, J. *Principles of Fluorescence Spectroscopy*. 2 edn, 291-321 (Kluwer Academic/Plenum Publishers, 1999).

10 Beechem, J. M. & Gratton, E. Fluorescence Spectroscopy Data Analysis Environment: A Second Generation Global Analysis Program. 70-81, doi:10.1117/12.945370 (1988).

11 Soutar, I., Swanson, L., Imhof, R. E. & Rumbles, G. Synchrotron-generated time-resolved fluorescence anisotropy studies of the segmental relaxation of

poly(acrylic acid) and poly(methacrylic acid) in dilute methanolic solutions. *Macromolecules* **25**, 4399-4405, doi:10.1021/ma00043a024 (1992).

12 McGehee, M. D. *et al.* Amplified spontaneous emission from photopumped films of a conjugated polymer. *Phys. Rev. B* **58**, 7035-7039 (1998).

13 McGehee, M. D. & Heeger, A. J. Semiconducting (Conjugated) Polymers as Materials for Solid-State Lasers. *Adv. Mater.* **12**, 1655-1668, doi:10.1002/1521-4095(200011)12:22<1655::aid-adma1655>3.0.co;2-2 (2000).

14 Jones M. Organic Chemistry, Third edition, 749-752 (W.W. Norton & Company) 2005.

15 Jones M. Organic Chemistry, Third edition, 768-770 (W.W. Norton & Company) 2005.

16 Szabo A. & Ostlund N., Modern Quantum Chemistry, 43, (Dover Publications inc.) 1996.

17 Born M. and Oppenheimer R. Zur Quantentheorie der Molekeln. Annalen der Physik. **389**, 457-484,doi: 10.1002/andp.19273892002 1927.

18 Hohenberg P. and Kohn W. Inhomogeneous Electron Gas. Phys. Rev. **136**, B864-B871 doi: 10.1103/PhysRev.136.B864 (1964).

19 Runge E. and Gross E. K. U. Density-Functional Theory for Time-Dependent Systems. Phys. Rev. Lett. **52**, 997–1000 doi: 10.1103/PhysRevLett.52.997 (1984)

20 Koch W. and Holthausen M.C. A chemists guide to density functional theory. Second edition. 34 Wiley-VCH Weinheim (2001)

21 Jansson, E., Jha, P. C. & Agren, H. Chain length dependence of singlet and triplet excited states of oligofluorenes: A density functional study. *Chem. Phys.* **336**, 91-98 (2007).

22 Igumenshchev K.I., Tretiak S., & Chernyak V.Y. Excitonic effects in a time-dependent density functional theory J. Chem. Phys. **127**, 114902, DOI:10.1063/1.2773727 (2007)

4

Optical transitions in oligofluorene molecules

4.0 Introduction

This chapter presents a study of the optical transitions in oligofluorene molecules of differing lengths. This study focuses in particular on the transition energies and dipole moments of these molecules with respect to their arm length. To study these transitions, the molar absorption coefficient, photoluminescence quantum yield (PLQY) and fluorescence lifetimes of the molecules were measured. The results show that, as the number of oligofluorene units increases, there is a general redshift in the absorption and emission spectra of the molecules, an increase in PLQY and a reduction in the fluorescence lifetimes. These results are then compared with Density Functional Theory (DFT) and Time Dependent Density Functional Theory (TD-DFT) calculations of transition energies and transition dipole moments. The comparison shows that there is also an increase in the transition dipole moments, which follows an $\sim n^{0.5}$ trend in absorption, with increasing number of fluorene units from $2 \leq n \leq 12$, whereas a clear saturation is observed in fluorescence. This behaviour is attributed to structural relaxation in the longer molecules and subsequent exciton localisation (self-trapping) in the centre of the molecules for both the alpha and beta phase conformations.

Section 4.1 provides an introduction to fluorene molecules and their importance as a material for a number of different devices. Section 4.2 outlines the theory behind the calculation of transition dipole moments in organic semiconductor molecules and their importance for studying molecular behaviour. Section 4.3 covers the absorption and emission spectra of the molecules and their molar extinction coefficients; this will also

introduce vertical transition energies and a comparison with the theoretical calculations. Section 4.4 describes the transition dipole moments and discusses their relationship with the number of fluorene units in the chain. The theoretical work was performed using density functional theory (DFT) and time dependent density functional theory (TD-DFT) by Dr Stefan Schumacher and Prof Ian Galbraith at Heriot Watt University using the Gaussian03 programme. Section 4.5 presents a discussion about the results and what they imply about the photophysical properties of the molecules, focussing in particular on self-trapping. Finally, section 4.6 presents a conclusion on the findings from the research presented in this chapter and its applications.

4.1 Fluorene polymers and oligomers

Polyfluorene has been one of the cornerstone materials of organic semiconductor research since the 1970s when it was favoured as an organic material due to its high molecular rigidity.[1] Since then it has been used in a number of devices because of its versatility, and as such it has found popularity in use in organic Light Emitting Diodes (OLEDs),[2-5] lasers[6-8] and optical amplifiers[9]. Two of the reasons why it is so popular are that it is a highly efficient emitter[3-5] and that it has a high charge carrier mobility.[10] Being a stable emitter in the blue region of the spectrum, it also covers an important wavelength range and by the addition of different functional groups can be tuned to emit across the entire visible spectrum.[2]

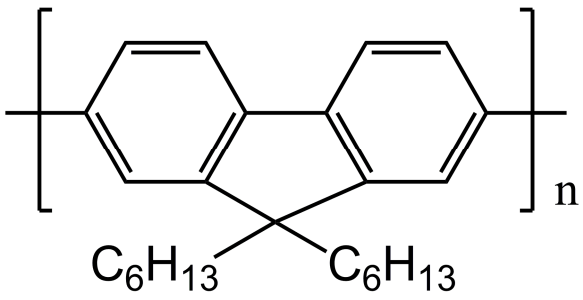

Figure 4.1: Molecular diagram of a fluorene unit with hexyl side chains coming from the central C_9 carbon bridge to increase solubility.

The structure of a single fluorene unit is shown in Figure 4.1. A fluorene unit consists of two phenyl rings connected via a single central bond binding them into a rigid biphenyl

unit. These are then further connected via a bridging non conjugated (sp^3) carbon atom. This bridging unit is very useful to the fluorene unit as not only does it lock the two phenyl rings into position, so that they cannot be twisted, it also provides a great option for functionalising the fluorene units. This allows for the properties to be adjusted in the molecule without altering the main conjugated backbone.[11] This can be done by making a spirofluorene unit, or using alkyl side chains to increase the solubility of the molecule. A spirofluorene unit is created by bonding two fluorene units to each other via a shared C_9 carbon bridge. This is done to prevent the molecule from π stacking - because the fluorene units sit at 90° to each other - and thus increases the stability of the molecule.[11] This study however, concentrates on molecules which have hexyl and octyl alkyl side chains to increase solubility.

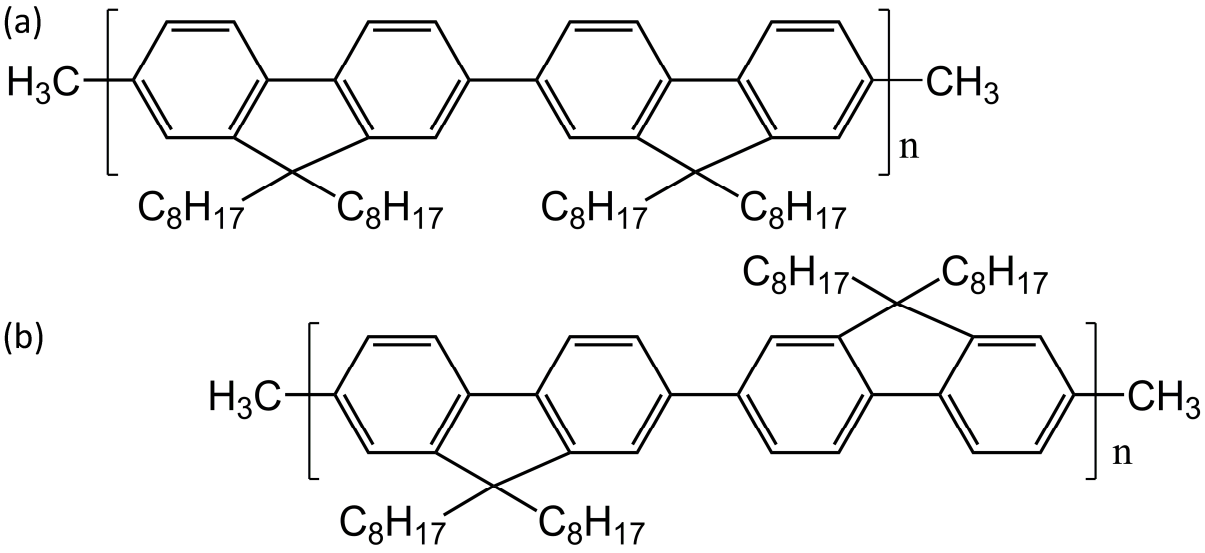

Figure 4.2:(a) Shows the molecular structure of alpha phase PFO, (b) beta phase PFO; note the planarisation of the chain in beta phase caused by the 180° angle between the fluorene units.

Fluorene molecules also possess another distinct characteristic which is not seen in most other molecules: they have a glassy phase and a crystalline beta (β) phase. In the glassy phase the orientation of the fluorene molecules is thought to be random. Whilst in the beta phase (β) of polyfluorene, it is believed that the fluorene molecules alternate by 180° within the films,[12] thus making them more planar and giving them improved charge transfer characteristics along the chain, as shown in Figure 4.2(b). Only small amounts of β phase PFO occur naturally in a good quality sample using high

quality solvents. It has been found that by using poor quality solvents, such as o-xylene, the proportion of beta phase produced can be as high as 30%, and values as high as 42% can be achieved using 1,8 diiodooctane as an additive to the solution.[13-15] The beta phase is not just confined to the polymer; reports have observed it in oligofluorene molecules of only 5 repeat units, when inserted into a poly(methyl methacrylate) PMMA matrix.[16] Studies on β phase have shown two interesting features relating to it. Firstly, it only appears in fluorene units functionalised with octyl alkyl chains at the C_9 bridging point. Secondly, the conjugation length in the beta phase is longer than that of the alpha phase consisting of 30±12 repeat fluorene units.[16] This increase in the conjugation length and the more planar nature of the beta phase, in comparison with the alpha phase, explain why it has lower energy transitions. These important features of fluorene make it a very desirable material to study, as it has a number of unique characteristics which gives it many advantageous properties.

Despite the vast amount of research that has been carried out on fluorene molecules for technological applications, there has been very few studies carried out to understand the microscopic nature of the excitons. A promising method of studying the photophysical properties of a polymer is to use the oligomer approach. This studies the effect of increasing the number of repeat units within a well-defined chain, in order to understand how the properties scale with increasing chain length.[17] This type of approach has worked well on studies of poly(p-phenylene viylene) (PPV)[18] and polythiophene (PT).[19] However, it has only been applied to oligofluorene in limited studies. By studying the photophysical properties of absorption it was possible to determine the effective conjugation of α phase polyfluorene, which was found to be 12 repeat units.[20] This was done by plotting the peak absorption against 1/n repeat units and extrapolating to the x-axis intercept. However, theoretical studies have been carried out and have shown that the extent of the delocalised exciton is only around 3 repeat fluorene units within the chain.[21] This type of approach has been used to look at the optical transitions, but this was only extended to oligofluorenes with up to 7 repeat units.[22] These studies found that the transition energies decrease with increasing conjugation length and that there is a relative saturation in the transition energies for $n \geq 4$.[22,23] It has also been shown that the oscillator strength and the

transition dipole moments scale linearly.[23-25] The previous work on determining the transition dipole moments in fluorescence were all limited, by assuming a PLQY of 1.[23-25] These calculations therefore are only able to provide a guide to the true nature of the fluorescence transition dipole moment. In this work experimental and theoretical methods have been used jointly to study the excited singlet state and the transition dipole moments within the molecules.

This chapter will investigate the effects of increasing the number of fluorene units on the optical transitions in a family of oligofluorene molecules; this aims to cover the effects of increasing the number of fluorene units on the transition energies and transition dipole moments. Transition dipoles in absorption are determined from the molar absorption coefficient, and in fluorescence using the PLQY and the fluorescence lifetime. Experimental transition energies and dipole moments are in good agreement with values obtained from TD-DFT. The results show that the fluorescence transition dipole saturates at shorter oligomer lengths than in absorption. This effect can be explained by self-trapping.

4.2 Transition dipole moments

The transition dipole moment is an important quantity to know for light emitting materials as it provides information on the strength of interaction between the molecule and the incident radiation. For this reason it is able to provide information on the strength of the absorption and emission from the molecule, and as such it would be desirable if an accurate theoretical calculation could be made for the molecule. This chapter and the following one will compare the experimental results obtained in absorption from the molar extinction coefficient and in fluorescence, from the emission spectrum and the radiative lifetime of the molecule, with values determined from TD-DFT calculations.

The importance of studying the interaction of light with an absorbing medium was first set out by Albert Einstein in 1916.[26] Einstein argued, from the thermodynamics of black body radiation, that for a two level energy system, there are three possible mechanisms which can occur. Firstly, if the molecule is in the lowest energy ground

state it can absorb energy (light) and be promoted to the upper energy level. Once it is in the upper energy level it then has two ways of decaying from the upper energy level back to the ground state level. The first mechanism for this decay to occur is spontaneous emission, and the second method is stimulated emission; in which the excited molecule interacts with incident radiation, causing the emission of an identical photon. There is more on these processes in Chapter 2. From this Einstein related the three processes with two coefficients; he labelled spontaneous emission the A coefficient, and absorption and stimulated emission the B coefficient.

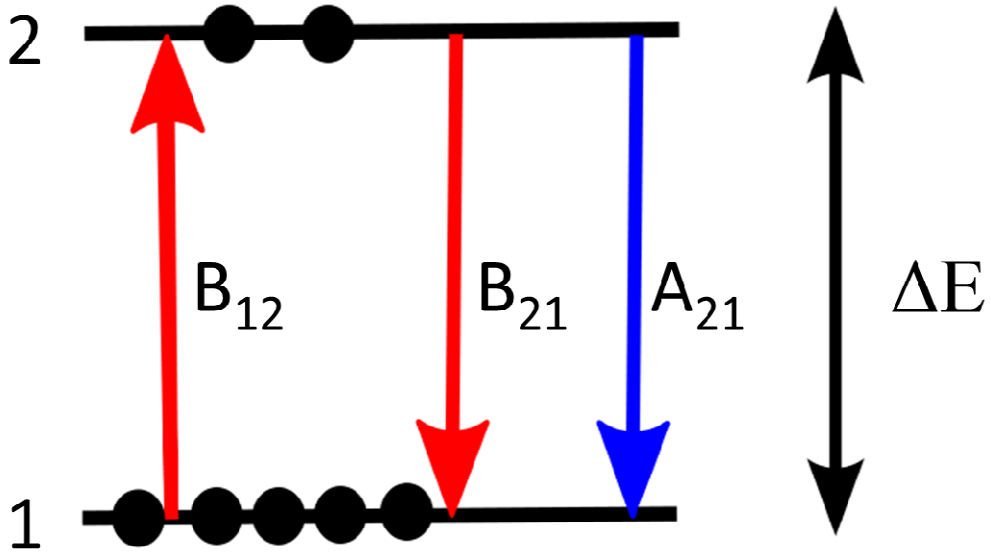

Figure 4.3: Energy level diagram for a two level system 1 and 2 with an energy separation ΔE, and showing the three possible transitions and their Einstein coefficients.

By using the model shown in Figure 4.3 for the possible transitions Einstein came up with a series of equations to calculate the transition rates for these three processes.

$$\Gamma_{absorption} = n_1 B_{12} \rho \qquad (4.1)$$

$$\Gamma_{stimulated} = n_2 B_{21} \rho \qquad (4.2)$$

$$\Gamma_{spontaneous} = n_2 A_{21} \qquad (4.3)$$

Where $\Gamma_{absorption}$ is the rate of absorption, $\Gamma_{stimulated}$is the rate of stimulated emission and the rate of spontaneous emission is given by $\Gamma_{spontaneuos}$, A and B are the Einstein coefficients relating to the transition and ρ is the photon density.

The ideas that were first proposed by Einstein were further developed for molecular systems firstly in 1948 by Förster,[27] who studied the rate of energy transfer between molecules and secondly by Strickler and Berg[28] in 1962. The work by Strickler and Berg focussed on determining the relationship between absorption and emission to calculate the fluorescence lifetime of the molecule. Förster's work focussed upon the absorption and emission dipole strengths of the molecules to build a formula for energy transfer via dipole-dipole coupling. His model provides an accurate description of many energy transfer processes from a donor molecule to an acceptor molecule.

If we consider the absorption transition B_{12}, then the Einstein coefficient for this transfer can be calculated by considering the rate of change in the system as a result of the absorption of radiation. This can be written as:

$$B_{12} = \frac{8\pi^3}{3h^2}|d_{ab}|^2 \qquad (4.4)$$

where d_{ab} is the transition dipole moment and h is Planck's constant. So in order to calculate the absorption transition dipole moment, we need to be able to relate the probability of absorption from the ground state (1) to an excited state (2) to measurable quantities. The probability of the absorption transition is given by the Einstein coefficient of induced absorption and as can be seen from equation 4.4, is proportional to the square of the transition dipole moment. To relate this quantity to the experimental absorption, we need to relate this to measureable quantities using the Beer-Lambert law, explained in more detail in Chapter 3. The Beer-Lambert law relates the change in intensity of a beam of intensity I, as it passes through a distance dl, which is proportional to the path length dl the concentration C and molar extinction coefficient ε.[29]

$$dI = -\ln(10)\varepsilon CIdl \quad (4.5)$$

If we consider a 1 M solution, then the rate of energy absorption per cm^3 of solution is:

$$\frac{-\mathrm{dI}(\nu)}{dt} = \frac{h\nu N B_{12}}{1000} I(\nu) \quad (4.6)$$

Where N is Avogadro's constant, and ν is the wavenumber. As I is the amount of energy flowing through a cross sectional area of 1 cm^2 in 1 s, we need to relate the change in intensity with time.

As $dI(\nu)/dt = [dI(\nu)/dl] \times dl/dt = (c/n)\, dI(\nu)/dl$, so:

$$B_{12} = \frac{\mathrm{cln}(10)}{nN'h\nu} \varepsilon_A(\nu) \quad (4.7)$$

Where N' is Avogadro's number divided by 1000, and n is the refractive index.

By combining these two equations for B_{12} we can then relate the Einstein coefficient with the measurable rate of absorption for the molecules to calculate the transition dipole moment.

As the absorption band for a single transition, extends over a number of frequencies, we get this relation for the extinction coefficient:[27,30]

$$\varepsilon_A(\tilde{\nu}) = \frac{8\pi^3}{3} \frac{N'\tilde{\nu}}{hcnln(10)} \sum_{i=1}^{m} |d_{ab}\,(\tilde{\nu})|^2 \quad (4.8)$$

By rearranging and integrating over the absorption band we can calculate the transition dipole moment:

$$|d_{ab}|^2 = \frac{3}{8\pi^2} \frac{hcnln(10)}{N'} \int [\varepsilon\,(\tilde{\nu})/\tilde{\nu}]\, d\tilde{\nu} \quad (4.9)$$

And so on working through all the constants, one obtains the equation for the absorption transition dipole moment, for a single transition:

$$|d_{ab}|^2 = 9.186 \times 10^{-3} n \int [\varepsilon\,(\tilde{\nu})/\tilde{\nu}]\, d\tilde{\nu} \quad (4.10)$$

where $\int [\varepsilon(\tilde{\nu}/\tilde{\nu})]\, d\tilde{\nu}$ is the integration over the absorption band for the transition. The formula provides values in Debyes (D) which are equal to 3.336x10^{-30} Cm.

Once the light has been absorbed and the electron has been promoted to a higher energy level, it will not remain there forever and will decay back to the ground energy

level. So if we consider a number of molecules in energy levels 1 and 2 in a black-body system then the radiation density can be given by Planck's radiation law:

$$\rho(\nu) = \frac{8\pi h\nu^3}{c^3}\frac{1}{e^{h\nu/K_BT}} \qquad (4.11)$$

Where c is the vacuum speed of light, K_B is Boltzmann's constant, T is temperature of the system, h is Planck's constant and ν is the wavenumber.

At equilibrium the ratio of the number of molecules in the higher energy state (2) N_2 and in the ground state (1) N_1 will be given by Boltzmann's distribution:

$$\frac{N_1}{N_2} = e^{-\Delta E/K_BT} \qquad (4.12)$$

Where ΔE is the energy difference between states 1 and 2 and is equal to $h\nu$. In this system electrons can be excited into a higher energy state by induced absorption, which is given by the Einstein B coefficient in equation 4.4. Now if we use equations 4.1 and 4.3, which describe the rate of up and down transitions for absorption and spontaneous emission, and the fact that in a balanced system the two rates must be equal, then we can determine the relevant Einstein A_{21} coefficient:

$$A_{21} = \frac{8\pi h\nu^3}{c^3}B_{12} \qquad (4.13)$$

From this we then need to obtain the probability of emission, which has to take into account all emission modes and polarisations. This also needs to account for the spread of transition energies, and can be done by relating equation 4.12 to the Fermi golden rule to calculate the probability of a transition and we obtain:[31]

$$\Gamma = \frac{n\langle E^3\rangle}{3\varepsilon_0\pi\hbar c^3}|d_f|^2 \qquad (4.14)$$

Where d_f is the fluorescence transition dipole moment, $\langle E^3\rangle = \int E^3\, I(E)dE / \int I(E)dE$ is averaged over the spectrum and obtained from the fluorescence intensity $I(E)$ in units of relative intensity at the photon energy E, n is the refractive index of the solvent, $\hbar = h/2\pi$ is Planck's constant and ε_0 is the permittivity of free space.

As $\Gamma = 1/\tau_{rad}$, which is equivalent to the Einstein A_{21} coefficient, we can rearrange this to give us the transition dipole moment:

$$\left|d_f\right|^2 = \frac{3\pi\hbar^4\varepsilon_0 c^3}{n\tau_{rad}}\langle E^{-3}\rangle \qquad (4.15)$$

Where $\langle E^{-3}\rangle = \int E^{-3}\, I(E)dE / \int I(E)dE$ and τ_{rad} is the radiative lifetime which is obtained from the fluorescence lifetime τ_f and the quantum yield QY using:

$$\tau_{rad} = \tau_f / QY \qquad (4.16)$$

The classical unit for the transition dipole moment is the Debye because this provides the numbers in a convenient size, 1D = 3.336x10^{-30} Cm, however in this study the results are presented as a multiple of elementary charge and a distance in angstrom (eÅ), 1 eÅ= 0.208 D. These units were chosen because they are more illustrative of how much electrons are displaced during an optical transition.

As can be seen the transition dipoles are an important quantity to know accurately and can be measured via spectroscopic techniques. The measurements for these quantities also provide a lot of information on the absorption and emission of the molecule making them an ideal study. The measured values of these can then be directly compared with values obtained via TD-DFT calculations in order to provide both an accurate description of the molecules interaction with light and as an accuracy check for the calculations.

4.3 Absorption and emission in oligofluorene

In this study all the nomenclature refers to the number of fluorene units within a chain; so for example O3 corresponds to an oligofluorene unit with 3 repeat fluorene units, only polyfluorene (PFO) is named differently. The different molecules come from two separate sources; samples of O3 and O5 as well as our PFO were procured from American Dye Source Inc. (ADS036FO, ADS056FO and ADS129BE respectively). O1-O4 was obtained from our collaborators at the Organic Chemistry Group at the University of Strathclyde headed by Professor Peter Skabara with the synthesis being performed by Dr Alexander Kanibolotsky. All the fluorene oligomers studied were functionalised

with two hexyl side groups per repeat unit to improve solubility. The PFO studied is poly(9,9-dioctylfluorene-2,7-diyl), which was functionalised with two octyl side groups per fluorene unit and is end capped with dimethylphenyl units. Solutions were made in spectroscopic grade tetrahydrofuran (THF) and 2-methyltetrahydrofuran, obtained from Sigma Aldrich.

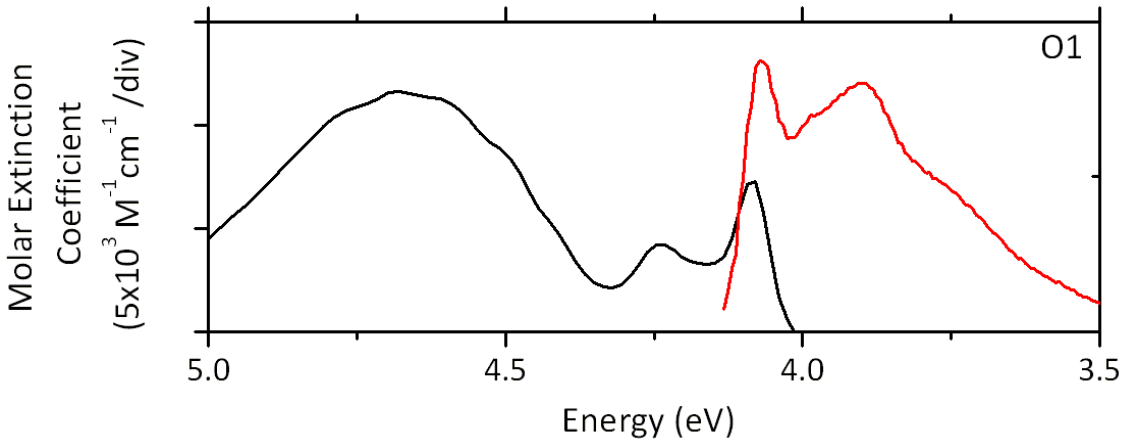

Figure 4.4: Absorption (molar extinction coefficient) and emission spectra of the O1 oligofluorene molecule.

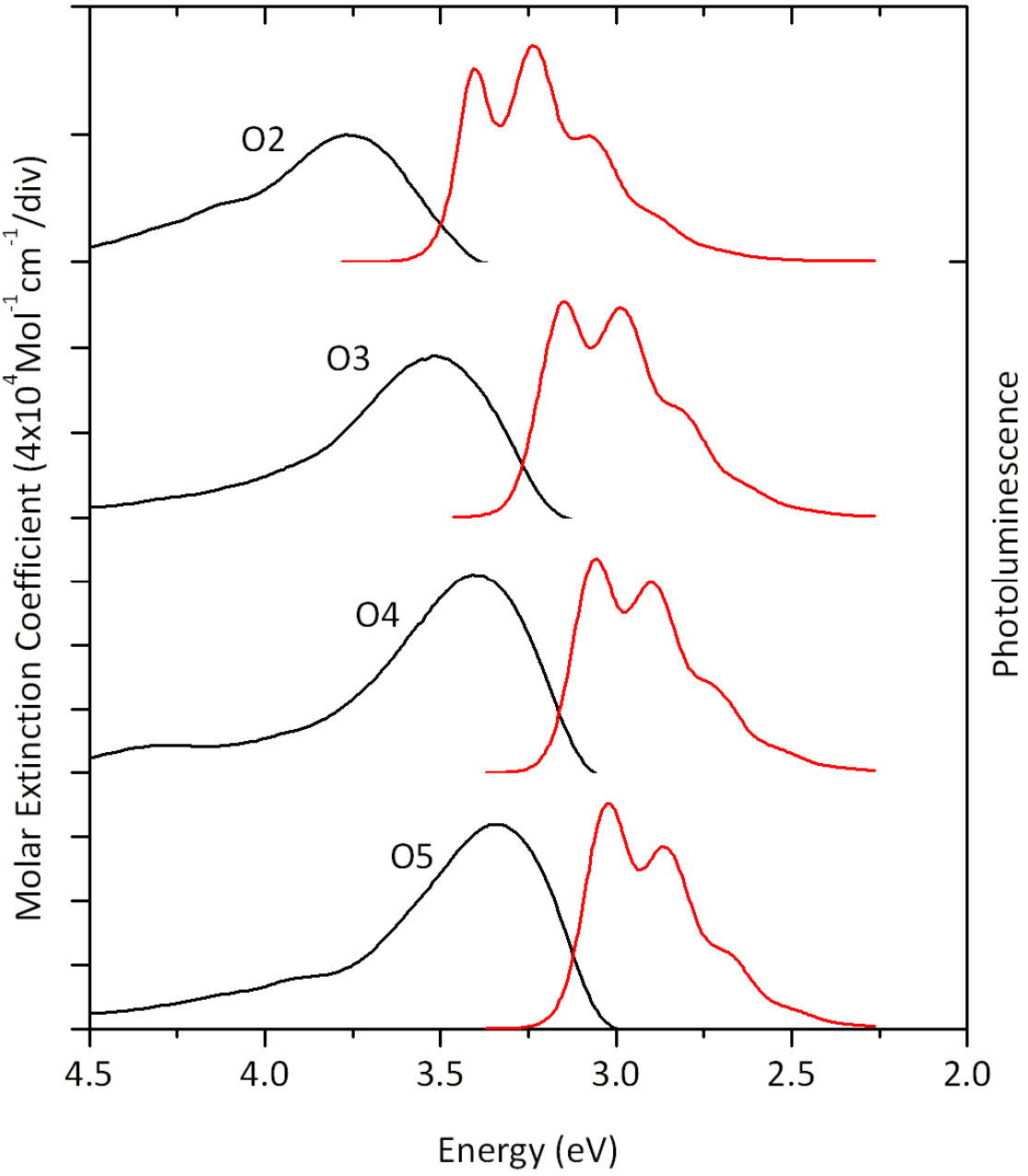

Figure 4.5: Room temperature absorption (molar extinction coefficient) and photoluminescence spectra for O2-O5 oligofluorene molecules.

Room temperature solution absorption and emission spectra for all the oligofluorenes studied is presented in Figures 4.4 and 4.5. The O1 results show that the absorption energy for this molecule is much lower than the others and that there is not a lot of broadening of the S1 absorption transition as is seen in the other molecules. The results for O2-O5 clearly show that as you increase the number of fluorene units, you get a redshift in absorption and emission. All emission spectra show two vibronic peaks

separated by ~0.16 eV, which is characteristic of the bond stretch between carbon-carbon bonds, and is a typical emission feature in conjugated polymers. There is also an increase in the molar extinction coefficient, as the number of oligofluorene units increases.

In order to compare the values for the transition dipole moments and transition energies with those calculated via TD-DFT in isolated molecules at 0 K, measurements were also performed at 77 K to freeze the solutions, using an Oxford Instrument Optistat DN liquid nitrogen bath cryostat, with helium as the exchange gas.

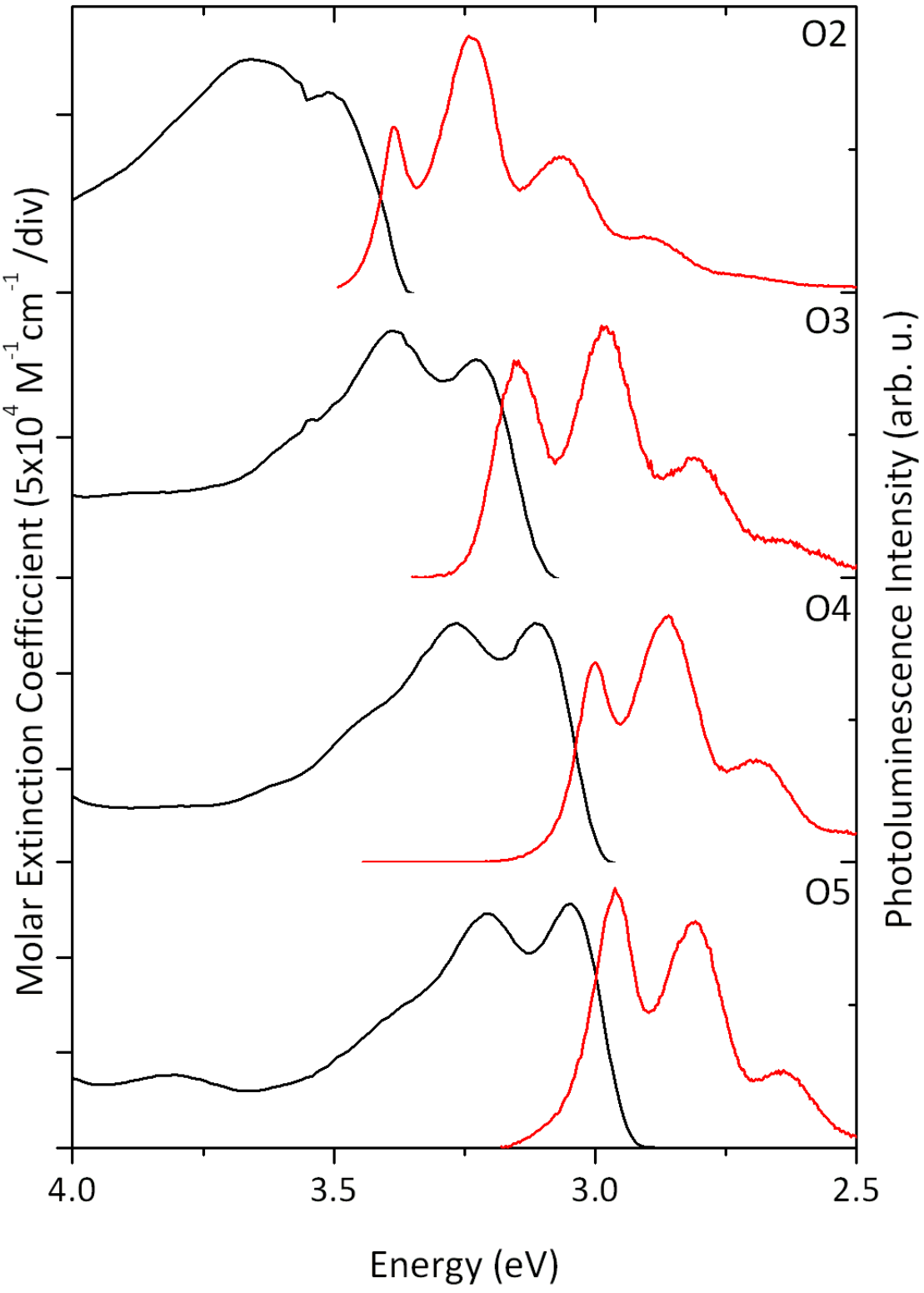

Figure 4.6: 77 K absorption (molar extinction coefficient) and photoluminescence spectra for O2-O5 oligofluorene molecules.

Figure 4.6 presents the absorption and emission spectra of the O2-O5 oligofluorene molecules at 77 K. The molecules show the same redshift trend, with increasing number of fluorene units. There is also a slight narrowing of the 0-0 peak due to self absorption resulting from the higher concentrations used. Results show a clear vibronic structure in absorption which is not present in the room temperature absorption. The 77 K results also present an increase in the molar extinction coefficient of approximately 10% over the room temperature results. These results can be explained by a reduction in the conformational disorder of the molecules, because they are frozen into the solvent matrix. This also results in a small redshift of the absorption and emission spectra, relative to the room temperature measurements.

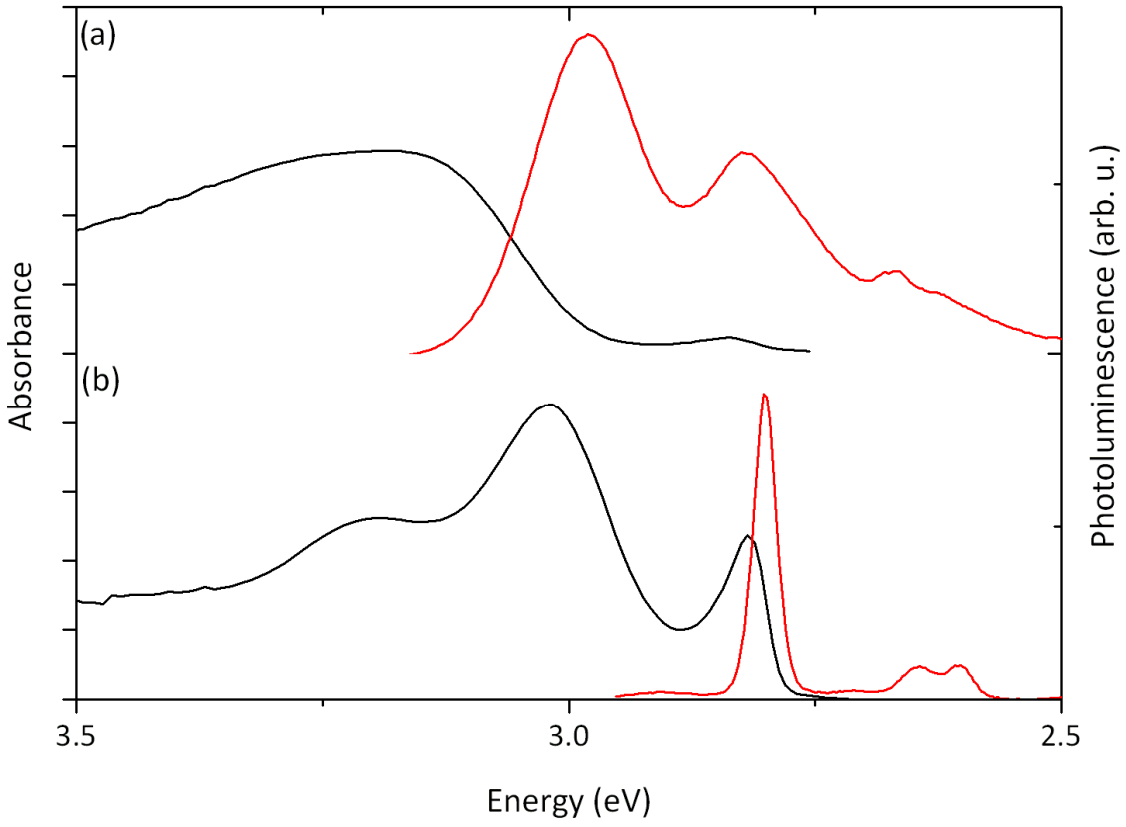

Figure 4.7: Absorption and photoluminescence spectra of PFO at room temperature (a) and at 77 K (b). Note that in the room temperature measurement the spectra are dominated by the alpha phase absorption and emission, whilst at 77 K the beta phase is dominant.

Figure 4.7 presents the data for the emission and absorption of PFO at room temperature (a) and at 77 K (b). As can be clearly seen there is a large difference

caused by the formation of beta phase at 77 K. At room temperature the absorption peak is at 3.15 eV, whereas at 77 K the vibronic peaks of the absorption separate with the 0-0 peak at 2.82 eV and the 0-1 peak at 3.0 eV. The main difference between the two absorption results is the narrower 0-0 absorption peak at 2.82 eV, which is only present in the low temperature spectrum. The position of this peak agrees well with the reports for beta phases in both films and in matrices reported in previous studies.[12,15,32] This lower energy peak is the result of the planar nature and the longer conjugation length of the beta phase. There is also a large difference in the emission spectra. The room temperature spectra show similar features to the other oligofluorenes measured, with a dominant 0-0 peak, and a separation between 0-0 and 0-1 peaks of ~0.16 eV. The 77 K emission spectrum is very different: it has a very small Stokes shift of only 3 nm and the 0-0 peak at 2.8 eV is very narrow with a full width half maximum of 5 nm. This is then considerably separated from the two further vibronic peaks, which are red shifted by 0.15 and 0.19 eV, relative to the 0-0 peak; these peaks are attributed to the stretching modes of the double and single carbon bonds respectively. This indicates that emission is entirely from the beta phase, which is the lower energy state of the PFO molecule. Due to the emission all coming from the β phase there must be efficient energy transfer from the glassy phase into the β phase. The beta phase must also be very uniform, because there is not a lot of broadening of the spectra caused by differing structural conformations. The observations of the lower energy emission peaks and red shifted absorption are characteristic of the beta phase conformation of PFO, and suggest that it is possible to transform isolated chains into the planar beta phase. This agrees with reports of beta phase being observed in short oligofluorenes in PMMA matrices[16] and in the single molecule level in a Zeonex matrix.[33,34]

In order to be able to compare our values with those of the theoretical models, the vertical transition energies in absorption and emission were calculated from the spectra. The experimental vertical transition energies E_{vert} are calculated for absorption (abs) and emission (em) using:[17]

$$E_{Vert}(abs) = \int EA(E)dE / \int A(E)dE \qquad (4.17)$$

and

$$E_{vert}(em) = \int EI(E)dE / \int I(E)dE \qquad (4.18)$$

where $A(E)$ is the absorbance and $I(E)$ is the fluorescence intensity at energy E. The vertical transition energy is the energy directly up (absorption) or down (fluorescence) from the minima of the potential energy surface of the absorbing or emitting state, as shown in Figure 2.6. The 0-0 energies can provide a simple measure of the energy; however, they are not the same results as the values from the DFT calculations which directly calculate the vertical transition energy. The differences between these different measures are shown in Table 4.1, alongside their theoretical comparison.

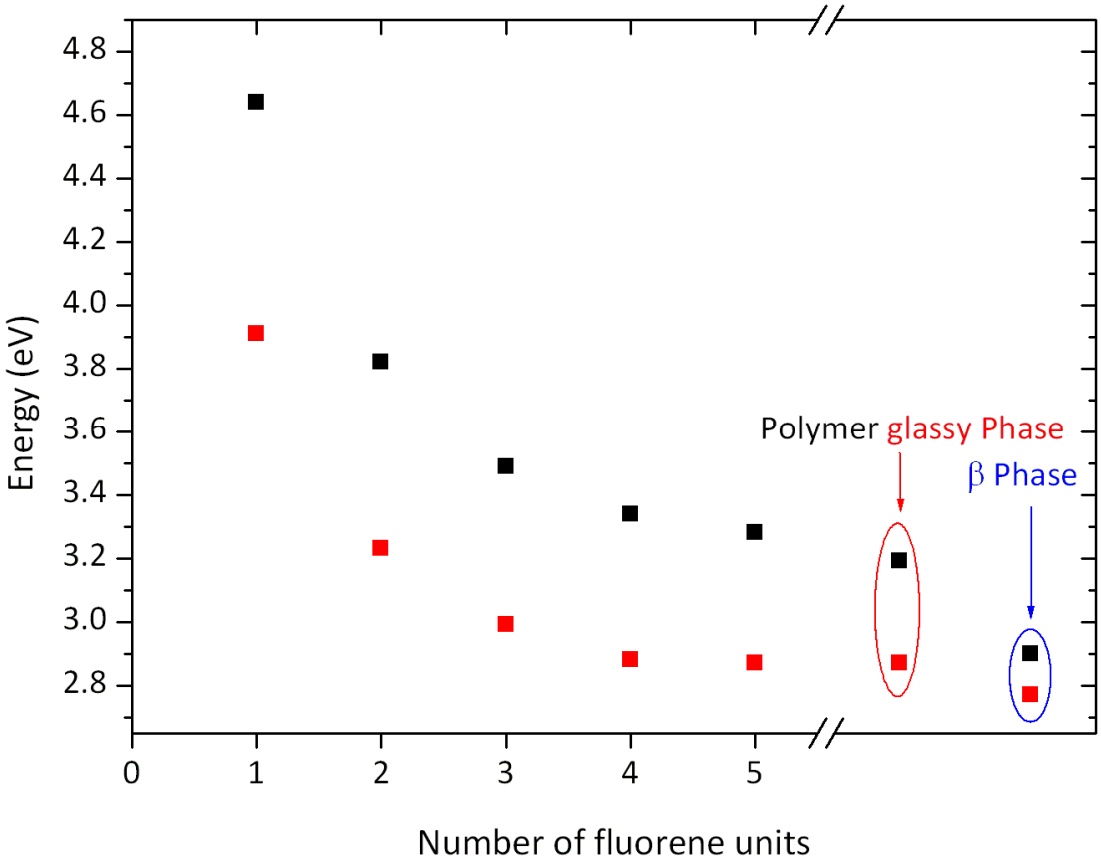

Figure 4.8: Experimental vertical transition energies of the studied fluorene molecules. The polymer values are circled on the right side in both alpha and beta phase: absorption (black squares) and photoluminescence (red squares).

The results in Figure 4.8 show that there is a decrease in the vertical transition energy with increasing number of fluorene units. The energy difference shows a convergence as the molecular length increases. This is due to the fact that adding another fluorene

unit has a smaller proportional effect on the overall length of the molecule, so there is a smaller percentage change in conjugation length, and thus transition energy.

Table 4.1: Experimental 0-0 energy and the vertical transition energies (in eV) measured in absorption (Abs) and emission (PL).

Material	Experimental 0-0 energy (eV)		Experimental vertical transition energies (eV)		Theoretical vertical transition energies (eV)	
	Abs	PL	Abs	PL	Abs	PL
O1	4.08	4.07	4.64	3.91	4.70	4.24
O2	3.78	3.41	3.82	3.23	3.86	3.31
O3	3.51	3.15	3.49	2.99	3.51	2.98
O4	3.41	3.06	3.34	2.88	3.35	2.88
O5	3.34	3.02	3.28	2.87	3.27	2.85
$O8_{alpha}$	…	…	…	…	3.17	2.82
$O8_{beta}$	…	…	…	…	2.86	2.69
$O12_{alpha}$	…	…	…	…	3.13	2.82
$O12_{beta}$	…	…	…	…	2.79	2.69
α phase PFO	3.20	2.98	3.19	2.87	…	…
β phase PFO	2.86	2.80	~2.9	2.77	…	…

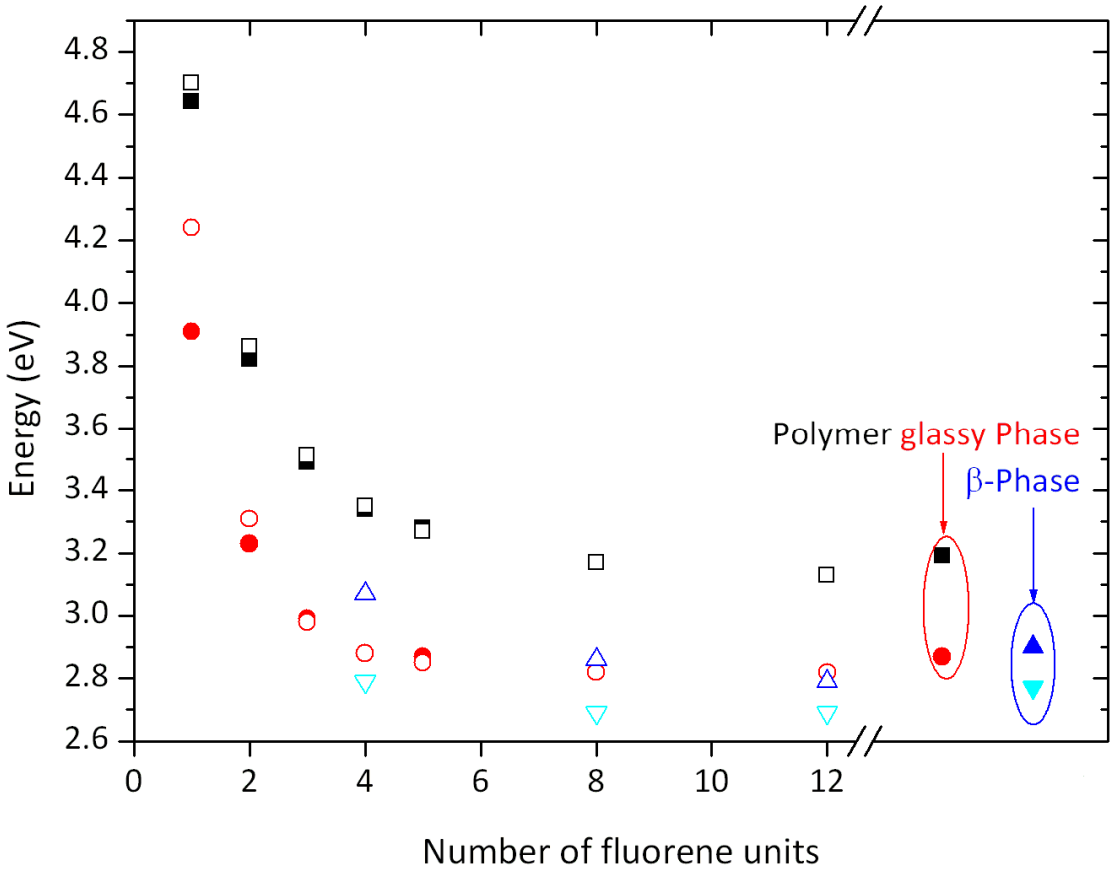

Figure 4.9: Comparison of the transition energies between the experimental (solid shapes) and theoretical values (hollow shapes). Absorption (black squares), emission (red circles), and beta phase (blue triangles: up absorption (blue) down emission (cyan)).

When the experimental results are compared to the theoretically calculated vertical transition energies in Figure 4.9, a very good agreement is observed. The difference between the two values is typically less than 0.05 eV for all, apart from the monomer and dimer. This shows that using DFT and TD-DFT is an accurate way of calculating the transition energies of the molecules. For the monomer and the dimer however, the agreement is not so good, with the difference being 0.08 eV for the dimer, and 0.3 eV for the monomer. The reason for such a large discrepancy in the monomer values is not known, but agrees with other experimental and theoretical work.[23] The theoretical work also shows that, at shorter chain lengths, the beta phase should have lower transition energies than the alpha phase molecule. This agrees with the absorption and emission spectra recorded for the different phases in the PFO molecules. As we approach the pentamer (n=5), and longer length oligofluorene

molecules, signs of convergence appear because there is only a small decrease in the transition energy beyond this. For the TD-DFT values the difference between the transition energies is less than 0.05 eV between the O5 and O12 molecule, whilst the total spread is ~1.5 eV for the family. If this is compared against the results for the oligo-para-phenylenes, oligophenylenevinylenes and oligothiophenes, this convergence is usually seen at 18-22 double bonds, along the shortest path of the conjugated backbone. These results are covered in a review article by Gierschner et al.,[17] looking at comparing experimental and theoretical results in oligomers. This value of 18-22 double bonds agrees well with the observation from the pentamer, which has 20 double bonds along the conjugated backbone.

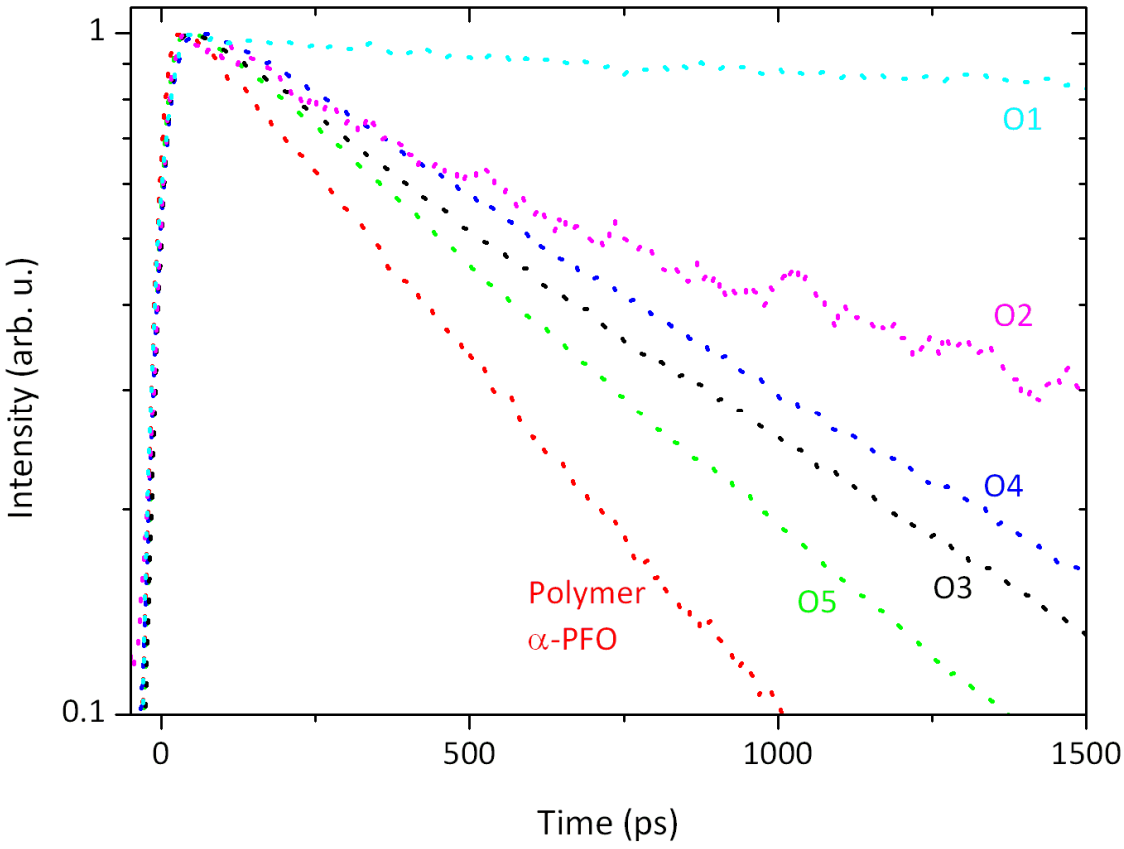

Figure 4.10: Fluorescence lifetimes of all the fluorene molecules measured at room temperature.

Figure 4.10 shows the time resolved fluorescence measurements of all the fluorene molecules. The experiments were performed using a Streak camera, as described in Chapter 3. All the molecules show a mono-exponential decay, which is detection

wavelength independent, with a decrease in the lifetime of the molecules with increasing chain length. The fluorescence lifetimes decrease from 6.5 ns for the O1 molecule to 0.58 ps for the O5 molecule and then to 0.42 ns for the PFO molecule.

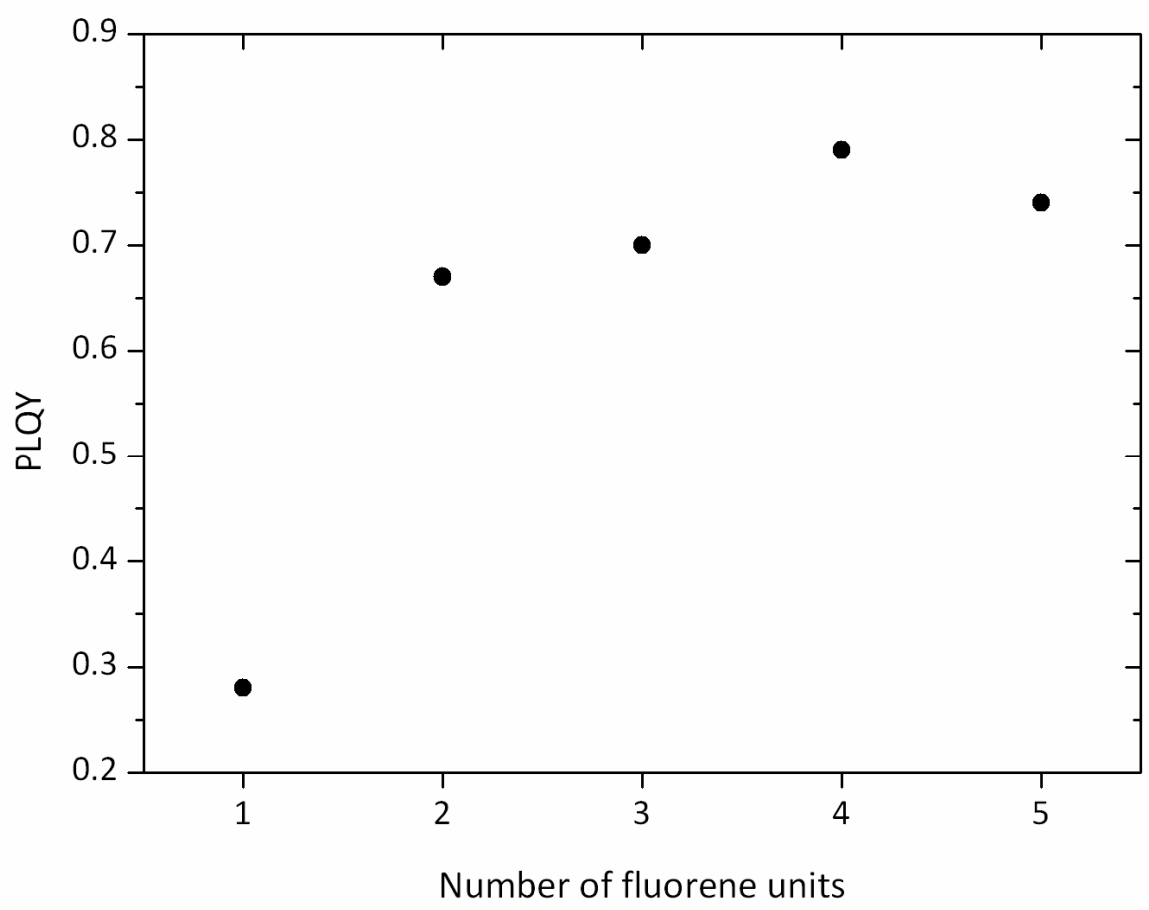

Figure 4.11: Photoluminescence quantum yields (PLQY) of the fluorene oligomers.

Figure 4.11 shows the change in PLQY with chain length of the oligofluorenes measured. The techniques for measuring the solution PLQY are described in Chapter 3 and use a reference of quinine sulphate for O2 to PFO molecules and 2-aminopyridine for the O1 molecule. The different reference standards are used because the absorption and emission spectra are more closely matched, with the spectra of the molecules to which it is being compared to. The materials show an increase in PLQY with increasing number of repeat fluorene units. The largest change is between O1 (28%) and O2 (67%), whereas from the O2 to the O5 there is only a change of 12%, to 79% for the O4 molecule. Polyfluorene has a similar PLQY of 78%. Results for the lifetime and PLQY can be combined to provide the radiative rate of the molecule using

Formula 4.15. The radiative lifetime is an important property of the molecule as it provides information on how fast the photon emission is from the excited state. It is also an important quantity in determining the transition dipole moment using equation 4.15. Results for this are shown in Table 4.2.

Table 4.2. PLQY, fluorescence and radiative lifetimes of the oligofluorene molecules

Material	PLQY	Fluorescence lifetime (ns)	Radiative lifetime (ns)
O1	0.28 ± 0.02	6.5 ± 0.2	23 ± 1.8
O2	0.67 ± 0.07	0.97 ± 0.06	1.4 ± 0.16
O3	0.70 ± 0.06	0.70 ± 0.01	1.1 ± 0.09
O4	0.79 ± 0.07	0.74 ± 0.02	1.0 ± 0.09
O5	0.74 ± 0.06	0.58 ± 0.01	0.75 ± 0.05
PFO	0.78 ± 0.08	0.42 ± 0.01	0.54 ± 0.05

4.4 Transition dipole moment

The next important photophysical property to study for the molecule is the transition dipole moment, because this provides information on the interaction of the molecule with light. The calculations were carried out using equations 4.10 for absorption and 4.15 for fluorescence as outlined in Section 4.2. By performing these calculations a directly comparable value for the TD-DFT results was obtained.

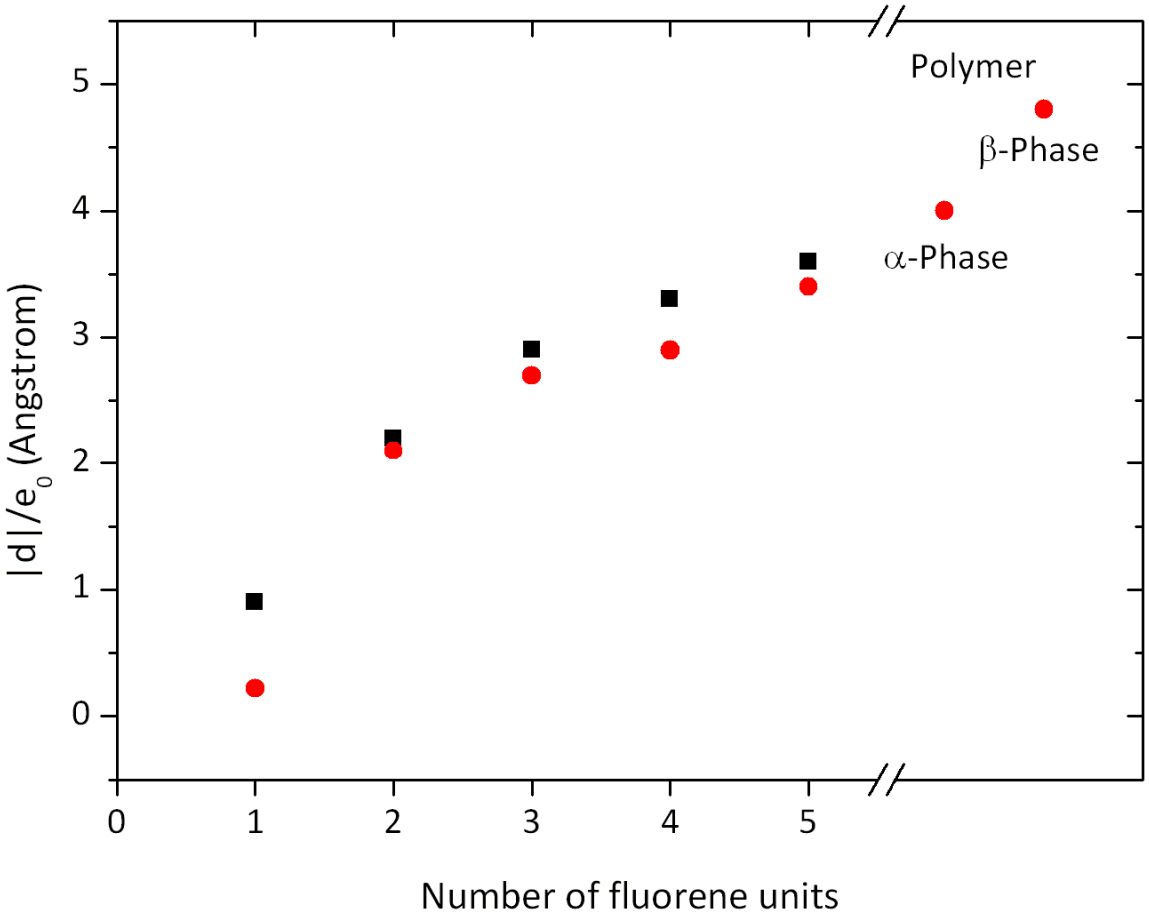

Figure 4.12: Experimentally determined transition dipole moments; absorption dipoles (black squares), fluorescence dipoles (red circles).

In figure 4.12 we show the experimentally determined absorption and emission transition dipole moments. The graph shows a clear trend of increasing transition dipole moment with increasing number of fluorene units. Apart from the O1 molecule there is very little difference between the absorption and photoluminescence transition dipole moments. The absorption transition dipole moments are slightly greater than the fluorescence transition dipole moments.

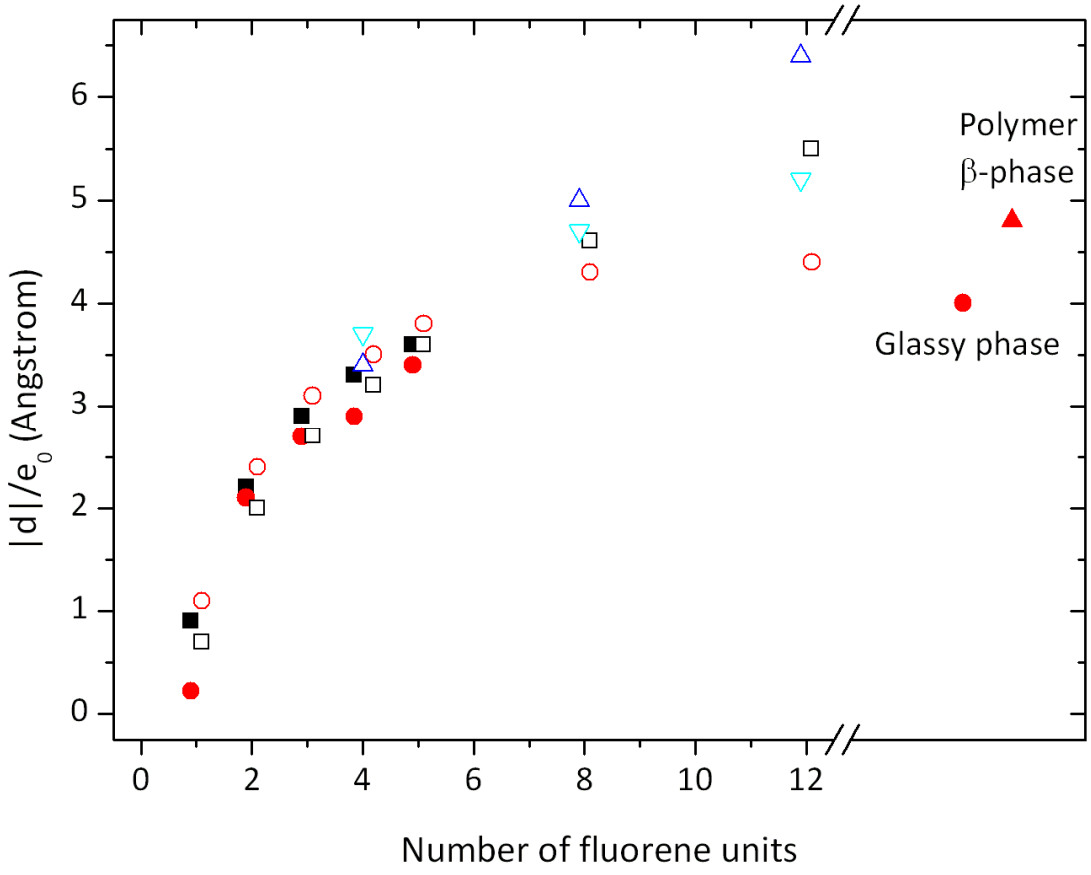

Figure 4.13: Comparison of the experimental and theoretical TD-DFT transition dipole moments. Experimental dipoles solid shapes and theoretical results open symbols, absorption (squares) and emission (circles), Beta phase triangles; fluorescence (down) and absorption (up).

Figure 4.13 shows the comparison between the experimental and theoretical transition dipole moments. A good agreement between the experimental and theoretical values is observed, with both showing an increase in the transition dipole moment with increasing molecular length. The beta phase transition dipole moments are found to be greater than their alpha phase equivalents; this agrees with reports of increased conjugation length in beta phase fluorene molecules.[16] The results also show an increase in the difference between the absorption and fluorescence transition dipole moments; with the fluorescence being much smaller than the absorption. This saturation after ~5 repeat units is mainly seen in the theoretical results due to the longer chain lengths studied. Transition dipole moments for the beta phase conformations are ~20% larger than for the alpha phase, in both theory and

experiment. Experimental values for the fluorescence dipole in PFO are found to agree with the calculated TD-DFT values for oligomers with 8-12 repeat units, which indicates that the effective conjugation length is between 8 and 12 repeat units. This agrees with the report for the effective conjugation length being 12 repeat units.[20] The fluorescence dipoles are within 10% of the reported values for the ladder type oligo-para-phenylenes for the same number of benzene rings, 2 per repeat unit.[35] This indicates that the photophysical properties of the 2 molecules are similar.

The agreement between experimental and theoretical values is better than previously reported.[23] When compared to some other measurements on oligofluorene molecules, these results show the importance of including the radiative lifetime, and not just the natural lifetime, in the fluorescence transition dipole moment calculations. As can be seen from Table 4.2, there is quite a large difference in the PLQYs of the molecules, and this produces a significant difference between the fluorescence lifetime and the radiative lifetime. If we used this simplification, we would therefore, be overestimating the size of the fluorescence transition dipole moments. The previous studies did not measure PLQY values, and this simplification led to overestimations of the transition dipole moments.[23-25]

With the theoretical calculations extending to 12 repeat units, it was possible to model the behaviour of the alpha and beta phase molecules at chains approaching the expected conjugation length of the alpha phase polymer. These results show that the beta phase has higher transition dipole moments than the alpha phase in both absorption and fluorescence. Also, that both phases show the same saturation in fluorescence with increasing chain length.

Table 4.3: Experimental and theoretical transition dipole moments in absorption and emission.

	Experimental Transition Dipole moments $\|d\|/e_0$ (Å)		Theoretical Transition Dipole moments $\|d\|/e_0$ (Å)	
Material	Abs	PL	Abs	PL
O1	0.9 ± 0.2	0.22 ± 0.04	0.7	1.1
O2	2.2 ± 0.2	2.1 ± 0.2	2.0	2.4
O3	2.9 ± 0.2	2.7 ± 0.2	2.7	3.1
O4	3.3 ± 0.3	2.9 ± 0.2	3.2	3.5
O5	3.6 ± 0.3	3.4 ± 0.3	3.6	3.8
$O8_{alpha}$	…	…	4.6	4.3
$O8_{beta}$	…	…	5.0	4.7
$O12_{alpha}$	…	…	5.5	4.4
$O12_{beta}$	…	…	6.4	5.2
α phase PFO	…	4.0 ± 0.3	…	…
β Phase PFO	…	4.8 ± 0.3	…	…

4.5 Self-trapping

As outlined above, by moving to longer length oligofluorene molecules we can address some of the important issues in the polymers, such as exciton behaviour in absorption and emission, which other studies have been unable to access.

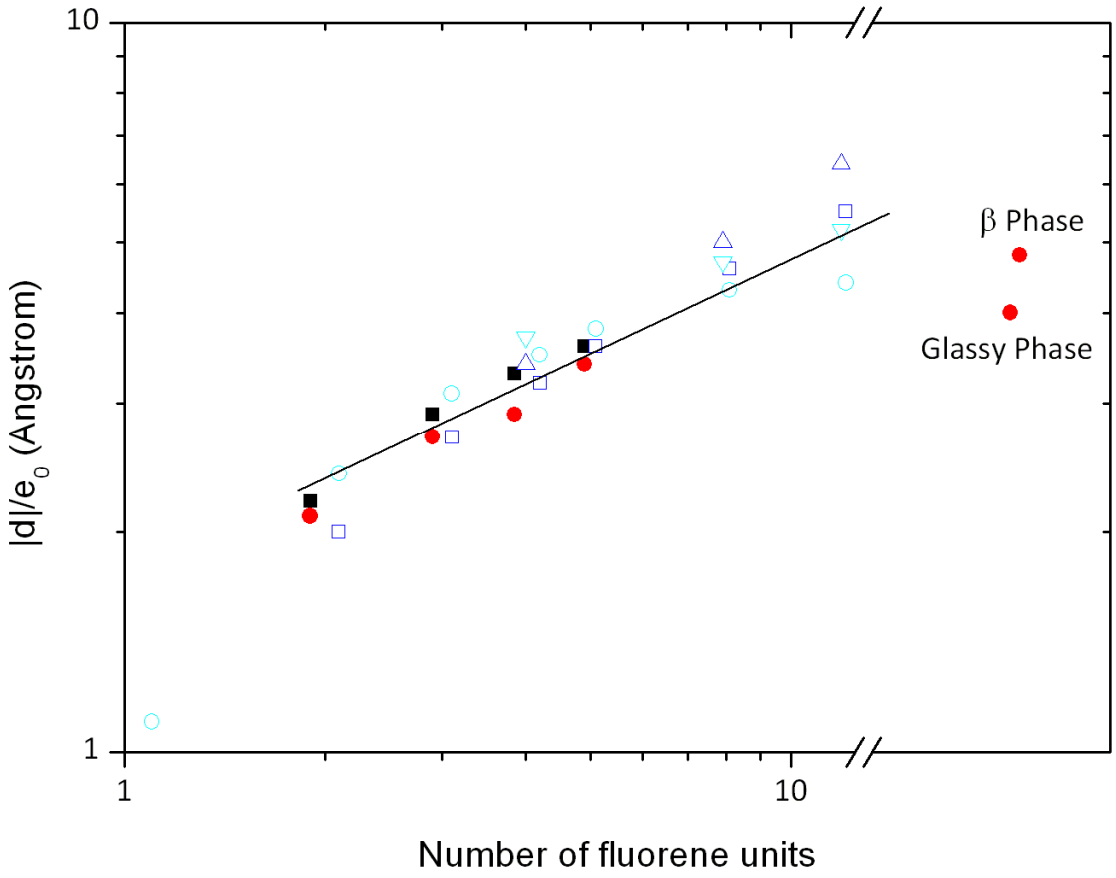

Figure 4.14: Transition dipole moment vs. oligomer length on a double logarithmic plot. Experimental dipoles (solid) shapes and theoretical results (hollow) symbols, absorption (squares) and emission (circles). Beta phase triangles, fluorescence (down) and absorption (up). The solid line shows a fit to the approximate $n^{0.5}$ for the absorption dipole for oligomers n≥2.

Figure 4.14 shows the transition dipole moments as a function of oligomer length on a double logarithmic plot. The absorption transition dipoles on this scale can be fitted by a straight line dependence for 2≤n≤12 with a slope of 0.5, which implies an $n^{0.5}$ dependence upon the number of repeat fluorene units n. Slightly higher values of the exponent have previously been reported for shorter molecules, extending to only 7 repeat units.[24,25] However, for the fluorescence transition dipole moments this trend is only followed between 2≤n≤5 repeat units; above this a deviation from the line is observed, in both the experimental values and theoretical calculations. The results show that a saturation of the fluorescence transition dipole moment occurs with increasing chain length in fluorescence, with the calculated values showing that there is little change in the transition dipole moments from 8 to 12 repeat units.

From the results of both the experimental and theoretical work, a clear trend appears; as the chain length increases there is less of an effect on the photophysical properties of adding another fluorene unit. When the number of fluorene units approaches 5, the behaviour in terms of PLQY, absorption and emission transition energies and dipole moments tends to be very close to that of the polymer in the alpha phase.

The fact that there is a saturation of the emission transition dipole moments, when compared against the absorption values, suggests that an effect is occurring, which is reducing the effective conjugation length of this transition. The results in absorption show that the transition occurs across the entire molecule because the transition dipole moments continue to scale linearly on the plot, whilst in fluorescence there is a clear deviation from this line. This suggests that a self-trapping effect is occurring, which can be understood as: in fluorescence the exciton is localised or “trapped” on a smaller part of the molecule for oligomers longer than 5 repeat fluorene units. Self-trapping is an effect which occurs when the local conditions of the molecule such as the dihedral angles or bond lengths change, causing the exciton to localise on a particular point on the chain.

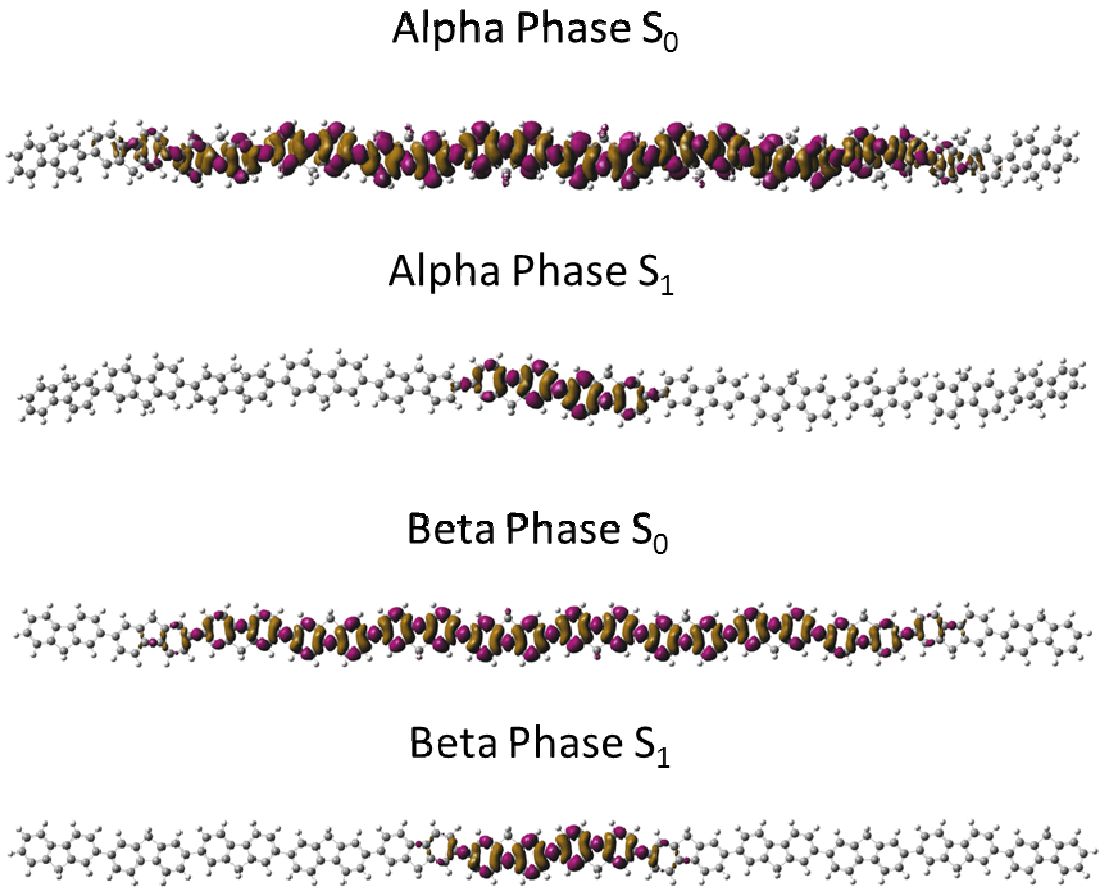

Figure 4.15: Visualisation of the change in the single particle electron density upon photo excitation for an alpha and beta phase oligofluorene molecule. It shows the extent of the exciton localisation between absorption and fluorescence. Images by Dr Stefan Schumacher.

Figure 4.15 shows the calculated electron density of a 12 unit oligofluorene molecule in both absorption and emission. The results clearly show that the absorption transition is delocalised across the entire molecule, in contrast to the emission, which is localised over 2-3 fluorene units. These plots agree well with the trend seen in the dipole data, suggesting that this is the same process which is being observed. The results also show that the excited state S_1 geometry is similar in both the alpha and beta phase conformations. The results suggest that the self-trapping occurs due to a decrease in the bond length alternation in the excited state. The change in the bond length was found to be similar in both conformations, from the TD-DFT calculations,

and the small differences explain the slower saturation in the beta phase conformation.

If we combine both the results a clearer picture of the mechanisms comes into place. As the molecular length increases there is an increase in the transition dipole moments in both absorption and emission. When approaching 5 repeat fluorene units the trend for the emission deviates from that of the absorption; at this point increasing the number of fluorene units has a smaller effect. This is because emission is localised to ~3 repeat units, so adding more fluorene units has little effect on the emission transition dipole moment. The calculations on absorption show that, even at 12 repeat units, the absorption occurs across the entire molecule. Even at such lengths the absorption transitions are still dependent upon the boundary conditions of the calculations, implying that there is still no saturation. This means that the absorption for the polymer would be similar to that of the long oligofluorene calculations, because the average conjugation length for the polyfluorene has been found to be 12 repeat units.[20]

Our results for the photophysical properties of the molecule do highlight a key point that has not been addressed in the other studies of oligofluorene molecules: that is the importance of taking into account the radiative lifetime of the molecule. This is important, because the results for the PLQYs show that the values decrease rapidly with shortening molecular length, meaning that the fluorescence lifetime is not equal to the radiative lifetime as it has been argued.[23-25] This has produced a better agreement between the theoretical and experimental results. By accounting for this fact it has been possible to build a more accurate picture of the experimental fluorescence transition dipole moments than those presented in other photophysical studies.

4.6 Conclusion

This work has investigated the optical transition energies and dipole moments between the ground and first excited singlet state for a family of oligofluorene molecules. The results of this study provide an insight into the behaviour of oligofluorene and polyfluorene through a detailed study of their photophysical properties. The study looked at the difference in behaviour with increasing number of repeat fluorene units from 1-5 to the polymer. These results were then compared with values calculated from DFT and TD-DFT to provide an accurate picture of the photophysical properties. The results show that increasing the number of fluorene units within the chain increases the PLQY and transition dipole moments, whilst decreasing the transition energies and fluorescence lifetimes. In PLQY there is a greater increase between 1 and 2 repeat units and after that there is only a small increase in the PLQY from 2 to 5 repeat units.

The results also show that the transition dipole moments increase with increasing number of fluorene units, with the absorption dipoles scaling with an $n^{0.5}$ trend for $2 \leq n \leq 12$. Fluorescence results, on the other hand, only follow this trend between $2 \leq n \leq 5$ repeat units. This shows that in fluorescence a self-trapping process is occurring, which was confirmed by the theoretical calculations showing changes in both dihedral angle and primarily bond length, causing the excited state wavefunction to shrink. Results for the absorption showed that the absorption transition, even at 12 repeat units, takes place across the entire molecule. The very good agreement between the experimental and theoretical results for the transition dipole moments shows the importance of using the PLQY to calculate the radiative lifetime and not just using the fluorescence lifetime. The fact that the theoretical calculations are able to predict the properties of oligofluorene molecules accurately is a big advantage for designing and understanding the important characteristics of different molecules.

4.7 References

1 Bell, V. L. Polyimide structure–property relationships. I. Polymers from fluorene-derived diamines. *Journal of Polymer Science: Polymer Chemistry Edition* **14**, 225-235, doi:10.1002/pol.1976.170140119 (1976).

2 Neher D. Scherf U. Polyfluorenes (Springer, Berlin, 2008).

3 Pei, Q. & Yang. Efficient Photoluminescence and Electroluminescence from a Soluble Polyfluorene. *Journal of the American Chemical Society* **118**, 7416-7417, doi:10.1021/ja9615233 (1996).

4 Grell, M., Bradley, D. D. C., Inbasekaran, M. & Woo, E. P. A glass-forming conjugated main-chain liquid crystal polymer for polarized electroluminescence applications. *Adv. Mater.* **9**, 798-802, doi:10.1002/adma.19970091006 (1997).

5 Grice, A. W. *et al.* High brightness and efficiency blue light-emitting polymer diodes. *Appl. Phys. Lett.* **73**, 629-631 (1998).

6 Theander, M. *et al.* Lasing in a Microcavity with an Oriented Liquid-Crystalline Polyfluorene Copolymer as Active Layer. *Adv. Mater.* **13**, 323-327 (2001).

7 Heliotis, G. *et al.* Blue, surface-emitting, distributed feedback polyfluorene lasers. *Appl. Phys. Lett.* **83**, 2118-2120 (2003).

8 Yang, Y., Turnbull, G. A. & Samuel, I. D. W. Hybrid optoelectronics: A polymer laser pumped by a nitride light-emitting diode. *Appl. Phys. Lett.* **92**, doi:16330610.1063/1.2912433 (2008).

9 Amarasinghe, D., Ruseckas, A., Vasdekis, A. E., Turnbull, G. A. & Samuel, I. D. W. High-Gain Broadband Solid-State Optical Amplifier using a Semiconducting Copolymer. *Adv. Mater.* **21**, 107-110, doi:10.1002/adma.200801930 (2009).

10 Kreouzis, T. *et al.* Temperature and field dependence of hole mobility in poly(9,9-dioctylfluorene). *Phys. Rev. B* **73**, 235201 (2006).

11 Franco, I. & Tretiak, S. Electron-Vibrational Dynamics of Photoexcited Polyfluorenes. *Journal of the American Chemical Society* **126**, 12130-12140, doi:10.1021/ja0489285 (2004).

12 Grell, M., Bradley, D. D. C., Ungar, G., Hill, J. & Whitehead, K. S. Interplay of Physical Structure and Photophysics for a Liquid Crystalline Polyfluorene. *Macromolecules* **32**, 5810-5817, doi:10.1021/ma990741o (1999).

13 Bansal, A. K., Ruseckas, A., Shaw, P. E. & Samuel, I. D. W. Fluorescence Quenchers in Mixed Phase Polyfluorene Films. *The Journal of Physical Chemistry C* **114**, 17864-17867, doi:10.1021/jp105545r (2010).

14 Shaw, P. E., Ruseckas, A., Peet, J., Bazan, G. C. & Samuel, I. D. W. Exciton–Exciton Annihilation in Mixed-Phase Polyfluorene Films. *Adv. Funct. Mater.* **20**, 155-161, doi:10.1002/adfm.200900879 (2010).

15 Peet, J., Brocker, E., Xu, Y. & Bazan, G. C. Controlled β-Phase Formation in Poly(9,9-di-n-octylfluorene) by Processing with Alkyl Additives. *Adv. Mater.* **20**, 1882-1885, doi:10.1002/adma.200702515 (2008).

16 Tsoi, W. C. *et al.* Observation of the β-Phase in Two Short-Chain Oligofluorenes. *Adv. Funct. Mater.* **18**, 600-606, doi:10.1002/adfm.200700530 (2008).

17 Gierschner, J., Cornil, J. & Egelhaaf, H.-J. Optical Bandgaps of &pgr;-Conjugated Organic Materials at the Polymer Limit: Experiment and Theory. *Adv. Mater.* **19**, 173-191 (2007).

18 Grimme, J. & Scherf, U. Planar para-phenylene oligomers. *Macromolecular Chemistry and Physics* **197**, 2297-2304, doi:10.1002/macp.1996.021970720 (1996).

19 Izumi, T., Kobashi, S., Takimiya, K., Aso, Y. & Otsubo, T. Synthesis and Spectroscopic Properties of a Series of β-Blocked Long Oligothiophenes up to the 96-mer: Revaluation of Effective Conjugation Length. *Journal of the American Chemical Society* **125**, 5286-5287, doi:10.1021/ja034333i (2003).

20 Klaerner, G. & Miller, R. D. Polyfluorene Derivatives: Effective Conjugation Lengths from Well-Defined Oligomers. *Macromolecules* **31**, 2007-2009, doi:10.1021/ma971073e (1998).

21 Franco, I. & Tretiak, S. Electron-Vibrational Dynamics of Photoexcited Polyfluorenes. *Journal of the American Chemical Society* **126**, 12130-12140, doi:10.1021/ja0489285 (2004).

22 Wasserberg, D., Dudek, S. P., Meskers, S. C. J. & Janssen, R. A. J. Comparison of the chain length dependence of the singlet- and triplet-excited states of oligofluorenes. *Chem. Phys. Lett.* **411**, 273-277, doi:10.1016/j.cplett.2005.06.039 (2005).

23 Jansson, E., Jha, P. C. & Agren, H. Chain length dependence of singlet and triplet excited states of oligofluorenes: A density functional study. *Chem. Phys.* **336**, 91-98 (2007).

24 Anemian, R., Mulatier, J. C., Andraud, C., Stephan, O. & Vial, J. C. Monodisperse fluorene oligomers exhibiting strong dipolar coupling interactions. *Chem. Commun.*, 1608-1609, doi:10.1039/b201414a (2002).

25 Chi, C., Im, C. & Wegner, G. Lifetime determination of fluorescence and phosphorescence of a series of oligofluorenes. *The Journal of Chemical Physics* **124**, 024907 (2006).

26 Haar, D. T. *The Old Quantum Theory*. 1st edn, 167-183 (Pergamon Press, 1967).

27 Förster, T. Zwischenmolekulare Energiewanderung und Fluoreszenz. *Annalen der Physik* **437**, 55-75, doi:10.1002/andp.19484370105 (1948).

28 Strickler, S. J. & Berg, R. A. Relationship between Absorption Intensity and Fluorescence Lifetime of Molecules. *The Journal of Chemical Physics* **37**, 814-822 (1962).

29 Barrow, G. M. *Introduction to Molecular Spectroscopy*. 66-72 (McGraw-Hill, 1962).

30 Knox, R. S. & van Amerongen, H. Refractive index dependence of the Forster resonance excitation transfer rate. *J. Phys. Chem. B* **106**, 5289-5293, doi:10.1021/jp013927+ (2002).

31 Craig, D. P. & Thirunacchandran, T. *Molecular Quantum Electrodynamics*. 89-97 (Academic Press, 1984).

32 Ariu, M. *et al.* Exciton migration in β-phase poly(9,9-dioctylfluorene). *Phys. Rev. B* **67**, 195333 (2003).

33 Becker, K. & Lupton, J. M. Dual Species Emission from Single Polyfluorene Molecules: Signatures of Stress-Induced Planarization of Single Polymer Chains. *Journal of the American Chemical Society* **127**, 7306-7307, doi:10.1021/ja051583l (2005).

34 Da Como, E., Becker, K., Feldmann, J. & Lupton, J. M. How Strain Controls Electronic Linewidth in Single β-Phase Polyfluorene Nanowires. *Nano Letters* **7**, 2993-2998, doi:10.1021/nl071207u (2007).

35 Rant, U. *et al.* Influence of the degree of conjugation on excited state lifetimes in phenylene-based materials. *Synth. Met.* **127**, 241-245, doi:10.1016/s0379-6779(01)00630-0 (2002).

5

Optical excitations in star-shaped oligofluorene molecules

5.0 Introduction

This chapter will present a detailed study of the optical transitions of star-shaped oligofluorene molecules. The molecules studied here have oligofluorene arms attached to a central core and possess 3 fold rotational symmetry. One family have a large rigid meta-linked central truxene core, and the other one is a meta linked benzene-cored moiety. This chapter will present a detailed study of the low energy transitions of these molecules. The results for the optical transitions of these new star-shaped molecules are compared with those from the oligofluorenes, studied in chapter 4. It will then compare these experimental results with results obtained from Time Dependent Density Functional Theory (TD-DFT) calculations. Both sets of results show that the star-shaped molecules present many advantages over linear oligofluorenes including higher photoluminescence quantum yields, greater transition dipole moments and molar extinction coefficients.

Section 5.1 will examine why C_3 symmetric star-shaped molecules are of growing importance and interest; concluding this section will be an outline of the importance of the truxene and benzene-cored molecules. Section 5.2 presents the basic photophysical measurements outlining the absorption coefficients, photoluminescence spectra and the lifetime data of the molecules. Section 5.3 will look at the nature of the transitions within

these molecules analysed from TD-DFT results. Section 5.4 will compare the experimentally determined transition energies with those calculated from DFT and TD-DFT. Section 5.5 will cover the transition dipole moments in all the molecules and the considerations that need to be employed when calculating them. These results will then be compared with the results obtained from the TD-DFT calculations and the values will be discussed and compared. Section 5.6 presents a discussion of the results, which will cover what information the results provide regarding the symmetry of the molecule and the degeneracy that these symmetry considerations impose. Section 5.7 will discuss the conclusions of this chapter. In this chapter all the theoretical work was performed by Jean-Christophe Denis, Dr Stefan Schumacher and Prof Ian Galbraith at Heriot Watt University.

5.1 Star-shaped molecules

As outlined in the theory section of this document, chapter 2, there is a growing demand to move away from polymers and into dendrimers[1,2] and star-shaped molecular systems.[3] In comparison with polymers, small molecular systems present many interesting advantages: such as no polydispersity, well defined conjugation lengths and synthetic reproducibility.[4,5] As well as these benefits, they also offer the opportunity to move away from 1 dimensional polymer systems into 2 and 3 dimensional systems.

In a star-shaped molecule there are two defining parameters. One is the length and composition of arms, which typically determines the absorption and emission characteristics. The other is the core, which determines the symmetry and the conjugation between arms; if there is conjugation then this also determines the nature of the optical transitions. The other constraint imposed by the core is the symmetry; star shaped molecules have been found to have dihedral $D_{2,3,6}$ and cyclic $C_{2,3}$ symmetry depending upon the core and the bonding positions to the core. Knowing the degrees of symmetry within a molecule is important for constructing the molecular orbitals and analysing spectroscopic properties. This particular study focuses on 2 molecules which have C_3 symmetry; this means that it has 3 identical orientations separated by 120^o. For this symmetry the molecules must have 2 degenerate transitions.[6] This means that in the system the two lowest energy levels within the molecule have the same energy levels, and that the two states have an equal probability of being excited. If the molecule is perfectly symmetrical,

then the whole molecule can be excited during absorption. A symmetry breaking process then occurs, which is similar to the well-known Jahn-Teller effect[7] for a symmetric system. The Jahn-Teller effect describes a situation in which two degenerate states cannot be stable, so that the molecule must undergo a fast distortion to lift the degeneracy between the two levels, to lower the system's energy.

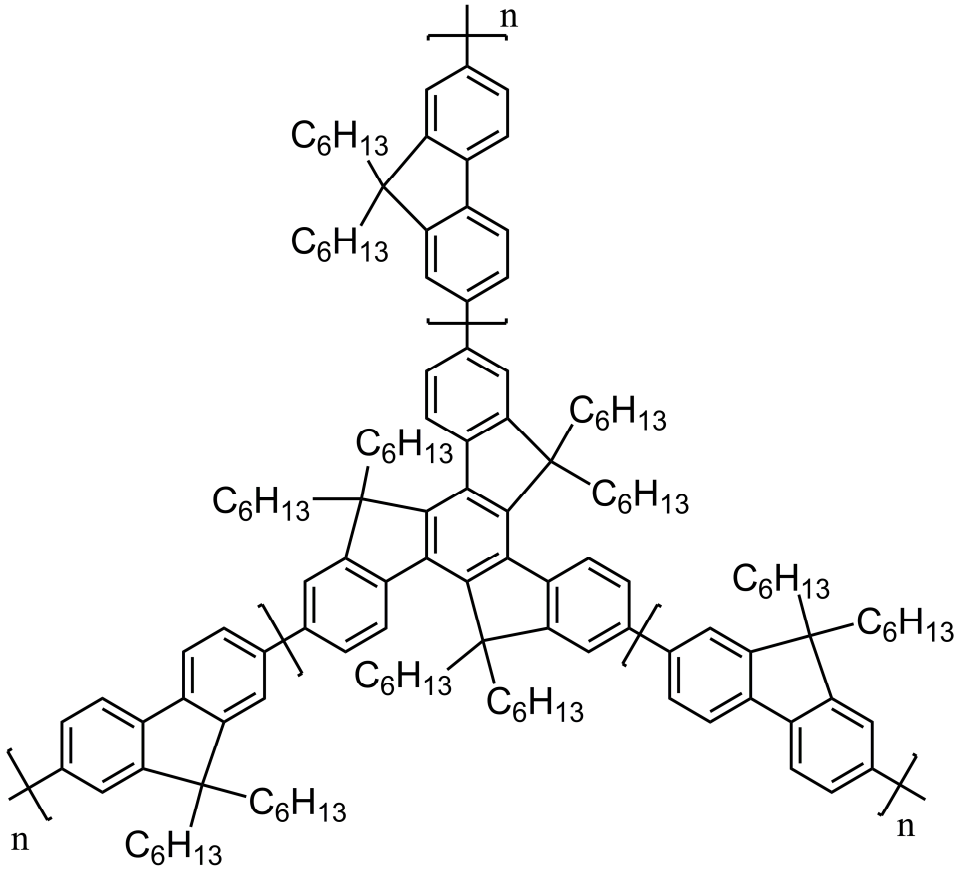

Figure 5.1: Truxene-cored molecular structure, for the work in this chapter n=1-4.

As with all organic materials, choosing the right building blocks is important in order to get the desired photophysical properties. Truxene is a core material that has shown a great deal of promise in a number of different devices. It is formed from three overlapping fluorene units sharing a central benzene ring; attached to this are three equal length fluorene arms with repeat units (n) 1-4, as shown in figure 5.1. As was shown in the previous chapter, fluorene is a very good material for organic lasers and OLEDs, as it has a number of very desirable photophysical properties. With the advantage of these desirable properties truxene-cored materials have been used in lasers and have been found to have low losses and to be very broadly tunable throughout the blue part of the spectrum.[8-11] Truxene has

also been shown to be a material which is versatile and has been used in organic field effect transistors,[12] and as fluorescence probes.[13] To look at the properties of star-shaped molecules without symmetry constraints, iso-systems have been developed in which the core has been fused to break the symmetry of the molecule. By doing this it was found that there is increased coupling between the arms.[14,15]

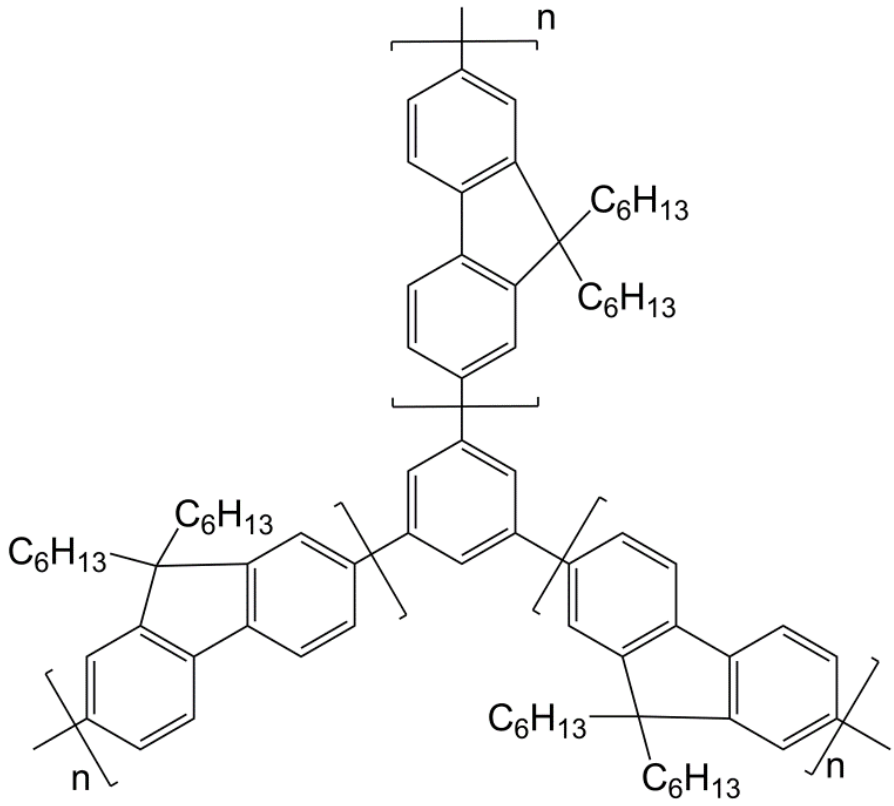

Figure 5.2: Benzene-cored molecular structure, for the work in this chapter n=1-4.

The other family of materials studied are a benzene-cored moiety with 3 fluorene arms connected to the meta positions of a central benzene core, as is shown in figure 5.2. The use of benzene-cored molecules in star-shaped molecules is much more prevalent.[3] This is because it offers a number of options for the attachment of arms. Benzene-cored molecules have been synthesised with 6, 4 and 3 arms attached to the core. The 6 arm molecules had phenylenevinylenes for arms and were found to self-assemble.[16] Cruciform's have been made with 4 arms, connected to a central benzene core. This was found to enhance the morphological and thermal stabilities of the material, and also to increase the solubility and ease of processability.[17] The use of three arm molecules is even more widespread and these molecules have been used in OFETs[18] and OLEDs.[19]

The fact truxene-cored molecules present so many desirable properties makes a study of their photophysical properties and of the effect of conjugation length very timely, because little has been done to study this molecular family. There have been some basic studies of benzene and truxene-cored molecules, but these only focussed on the basic spectral properties.[4,5] The one theoretical study carried out on truxene investigated molecules with 0-2 repeat fluorene units on each arm and focussed on Raman spectroscopy and the ground energy state geometry.[20] This found that there is not a lot of inter arm connection due to the meta linkages in the core, and that interactions between the arms and the core happen at the periphery of the core. It also found that as the arm length is increased, they play a more dominant part in the photophysical properties.

This chapter will study the effects on the optical transitions of changing the core and increasing the number of fluorene units in the arms of two families of star-shaped molecules. This will aim to understand these effects and relate them to the molecular structure by studying the optical spectra, PLQY and transition dipole moments of the molecules. Transition dipoles in absorption are determined from the molar absorption coefficient, and in fluorescence using the PLQY and the fluorescence lifetime. Experimental transition energies and dipole moments are in good agreement with values obtained from TD-DFT. The results show that the fluorescence transition dipole saturates at shorter oligomer lengths than in absorption. This effect can be explained by self-trapping.

5.2 Optical spectra, photoluminescence quantum yields and lifetimes

This work compares the photophysical properties of two families of star-shaped molecules. The molecules are named in relation to the core structure and to the number of fluorene units on the arms, so that a truxene-cored molecule with two fluorene units on the arms would be T2, and B2 would be a similar benzene-cored molecule. These molecules are then compared with the oligofluorene molecules which are named in the same way as in chapter 4, with O for oligofluorene and then the number of repeat fluorene units. The materials studied, except the O3 and O5 oligofluorene, were synthesised at the University of Strathclyde by Prof Peter Skabara and Dr Alexander Kanibolotsky.[4] The O3 and O5 molecules

were procured from American dye source Inc. All solutions were made with HPLC grade toluene or tetrahydrofuran (THF) sourced from Sigma Aldrich.

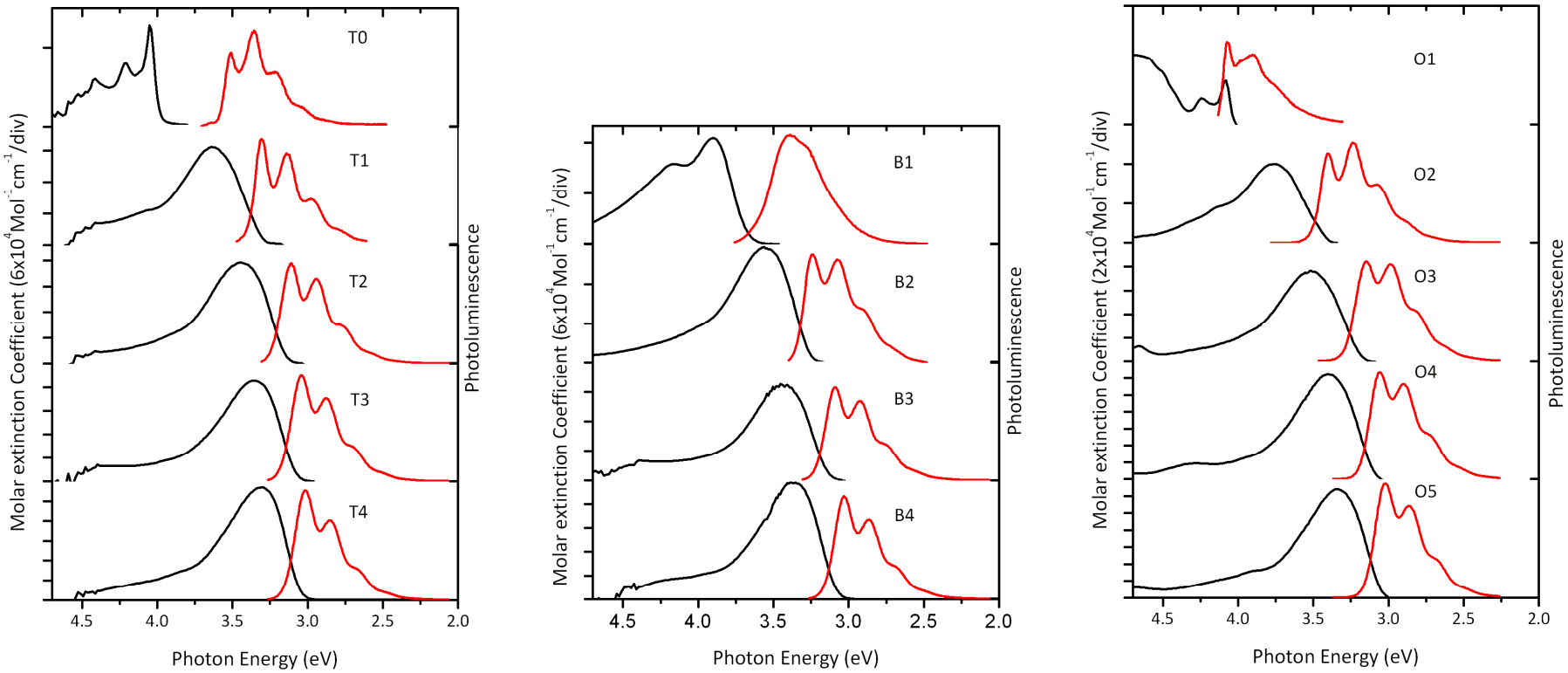

Figure 5.3: Absorption (molar extinction coefficient and photoluminescence spectra of the truxene-cored (left), benzene-cored (centre) and oligofluorene (right) molecules. Molar extinction is marked in terms of divisions on the y-axis. Note the change in the scale of the y-axis for the oligofluorene molecules.

Figure 5.3 shows the molar extinction coefficient and the photoluminescence spectra for all the molecules. All molecules show a slight red-shift in both absorption and emission with increasing number of fluorene units. All the molecules show an increase in molar extinction coefficient with increasing oligofluorene unit length. For a given length of star-shaped molecule the value of the peak molar extinction coefficients are equivalent. In the star-shaped molecules the molar absorption coefficients are around three times greater for the 2-4 repeat units than that of the equivalent oligofluorene molecules. This difference can be explained by the absorption taking place across all three arms in the star-shaped molecules. The extra conjugation of the core and the arms also redshifts the absorption and emission spectrum with respect to their equivalent oligofluorenes. The extra conjugation however does not extend between the arms, because they are connected to the meta positions of the central benzene ring. This is more prominent in the truxene molecules where there is an equivalent extra fluorene unit added to each arm, whilst the benzene core has a smaller effect on the photophysical properties. The molecules also show a structured photoluminescence spectrum with vibronic peaks separated by ~0.16 eV, which is characteristic of the bond stretch between carbon atoms, and is frequently seen in conjugated polymers.

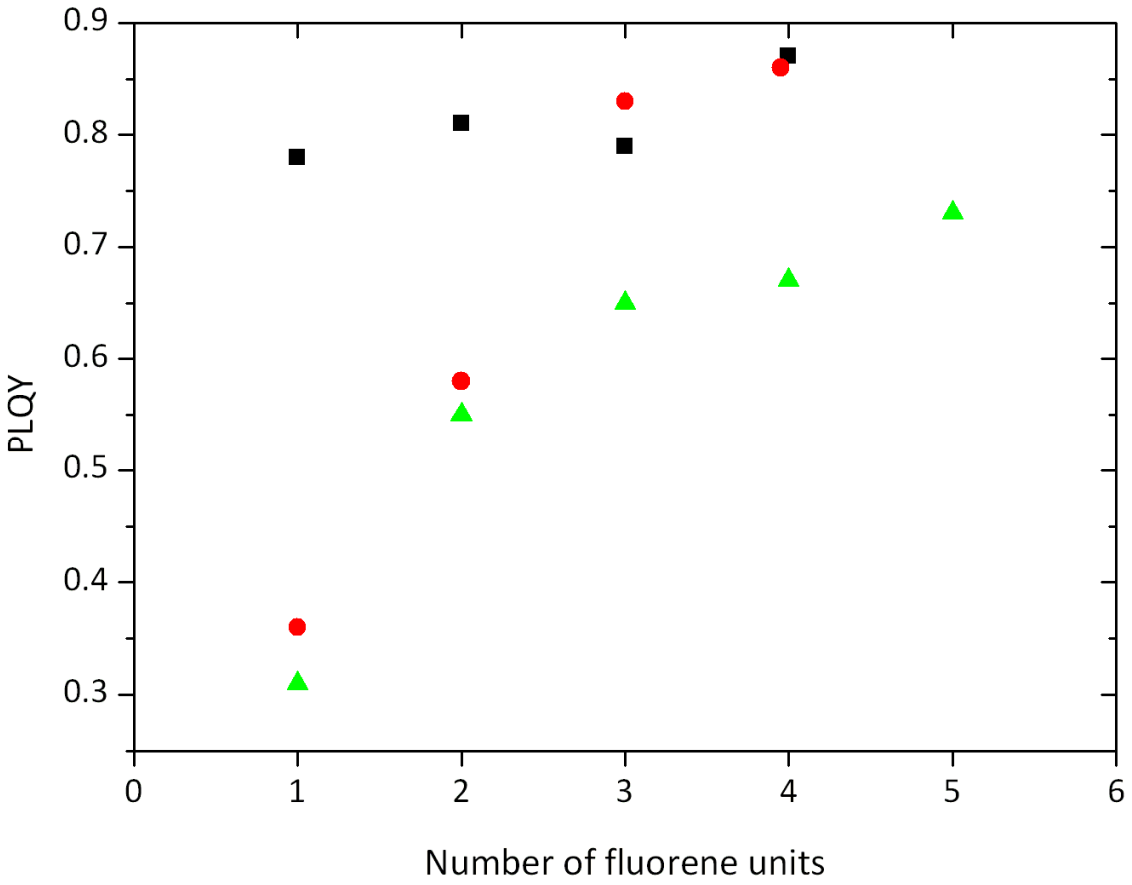

Figure 5.4: Photoluminescence quantum yield for all the molecules: truxene-cored (black squares), benzene-cored (red circles) and oligofluorenes (green triangles).

Figure 5.4 shows the solution photoluminescence quantum yields (PLQY) for all fluorene based molecules studied. All the molecules show the same trend of an increasing PLQY with increasing number of fluorene units. The PLQY for the star shaped molecules is greater than that of the oligofluorene molecules for the same length. Throughout the family the truxene-cored molecules, with arms, have high values for the PLQY, with all being greater than 75%. Only the T0 molecule, the truxene core itself, has a low PLQY of 7% (not shown); this suggests that the arms are critical for the performance. Over the range of truxene molecules there is only a small increase from 78% for T1 to 87% for T4. The benzene-cored molecules show a much greater increase in PLQY, and follow a similar trend to the oligofluorene molecules. The PLQY of the benzene cored molecules increases from 36% for B1 to 84% for B4. These values agree well with the values reported by Zhou et al.[5] for the benzene-cored and Kanibolotsky et al.[4] for the truxene-cored molecules. The PLQY for the star-shaped

molecules with 3 and 4 repeat unit arms are similar, suggesting that after 3 units the photophysics becomes dominated by the arms. This agrees with reports from Raman and DFT studies on the truxene molecules which observed a similar trend.[20]

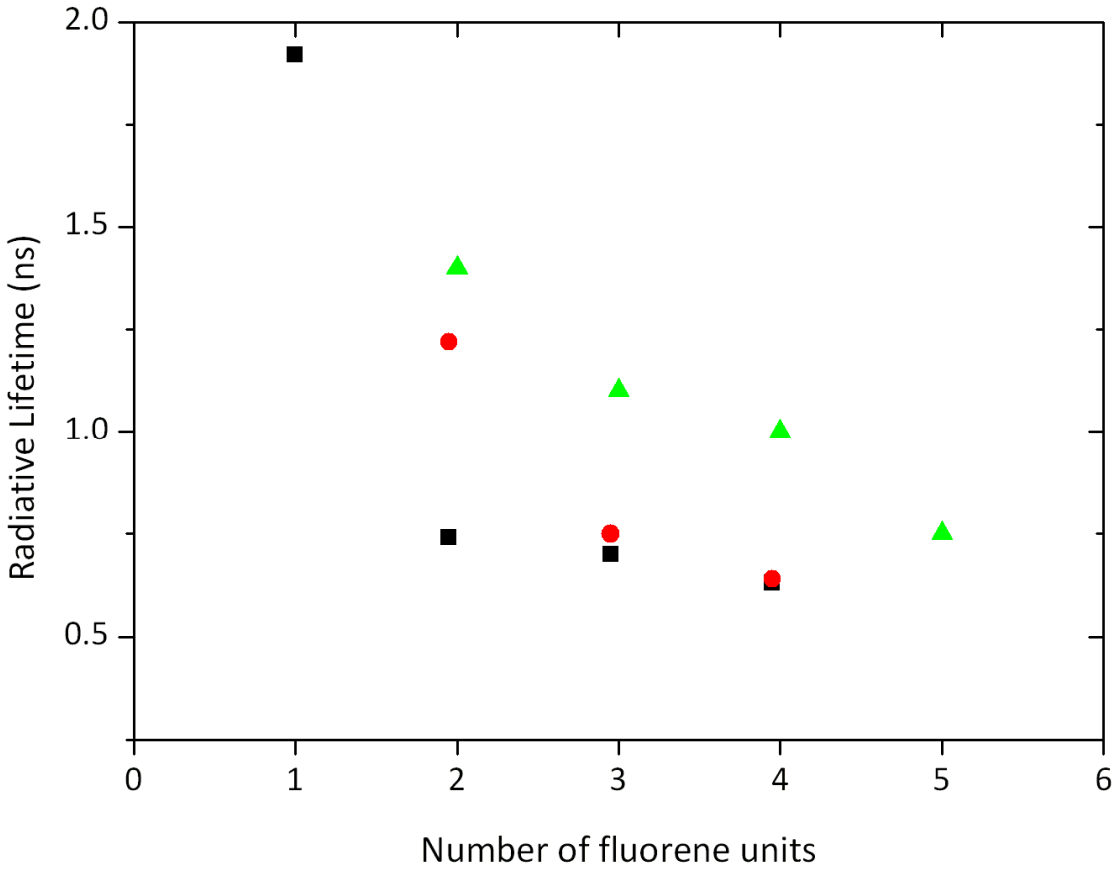

Figure 5.5: Radiative lifetime data for all the molecules: truxene-cored (black squares), benzene-cored (red circles) and oligofluorenes (green triangles).

Figure 5.5 shows the radiative lifetime data for the benzene and truxene cored molecules, where the natural radiative lifetime is determined from the photoluminescence quantum yield and time resolved luminescence measurements. This can then be calculated using $\tau_R = \tau/PLQY$. Throughout, there is a trend that increasing the length of the arms reduces the lifetimes of the molecules. All molecules show a mono-exponential decay, which is detection wavelength independent, similar to the oligofluorene molecules. Both families of star-shaped molecules have shorter radiative lifetimes than their equivalent oligofluorenes. The lifetimes of the truxene molecules with arms are always lower than their equivalent benzene-cored material counterparts. The lifetime of the truxene molecules decrease from 1.9 ns for the T1

molecule to 0.63 ns for the T4 molecule, whilst the benzene-cored molecule's lifetime decreases from 42 ns to 0.64 ns for the B1 to B4 respectively. The radiative lifetimes for the star-shaped molecules with 3-4 repeat units lie between 600 and 750 ps. The radiative lifetimes of the one arm unit molecules are substantially greater than for longer arm molecules, especially in the case of the B1 molecule. The radiative lifetime of the T0 molecule of 400 ns is very large in comparison with the other molecules studied; the reason for the long lifetime is due to the molecules symmetry. The radiative lifetimes of the star-shaped molecules are still lower than the radiative lifetime measured for polyfluorene, reported in chapter 4, which was calculated as 0.54 ps. However, the PLQY of the truxene T1-T4 and B3 and B4 are higher than the PLQY for polyfluorene.

Table 5.1: Photoluminescence, lifetime and radiative lifetime of the truxene-cored, benzene cored oligofluorenes.

Material	PLQY	Lifetime (ns)	Radiative Lifetime (ns)
T0	0.07 ± 0.01	6.5 ± 1.0	400 ± 80
T1	0.78 ± 0.08	1.48 ± 0.04	1.9 ± 0.2
T2	0.81 ± 0.07	0.60 ± 0.01	0.74 ± 0.06
T3	0.79 ± 0.06	0.56 ± 0.01	0.7± 0.05
T4	0.87 ± 0.07	0.54 ± 0.01	0.63 ± 0.05
B1	0.36 ± 0.02	15 ± 1.0	42 ± 3
B2	0.58 ± 0.05	0.70 ± 0.01	1.2 ± 0.1
B3	0.83 ± 0.06	0.62 ± 0.01	0.75 ± 0.06
B4	0.86 ± 0.07	0.55 ± 0.01	0.64 ± 0.05
O1	0.31 ± 0.03	6.5 ± 0.2	23 ± 2
O2	0.55 ± 0.05	0.97 ± 0.06	1.4 ± 0.2
O3	0.65 ± 0.05	0.70 ± 0.01	1.1 ± 0.1
O4	0.67 ± 0.06	0.74 ± 0.02	1.0 ± 0.09
O5	0.73 ± 0.06	0.58 ± 0.01	0.75 ± 0.06

5.3 Transition densities

Quantum chemistry calculations were used to probe the nature of the absorption and emission transitions. As outlined in the introduction, these showed that for these C_3 symmetric molecules there are two degenerate transitions which have orthogonal transition dipole moments. The absorption is found to be delocalised across the entire molecule and that after a symmetry breaking process, there are three stable minima in the potential energy surface which correspond to the three arms of the molecules.

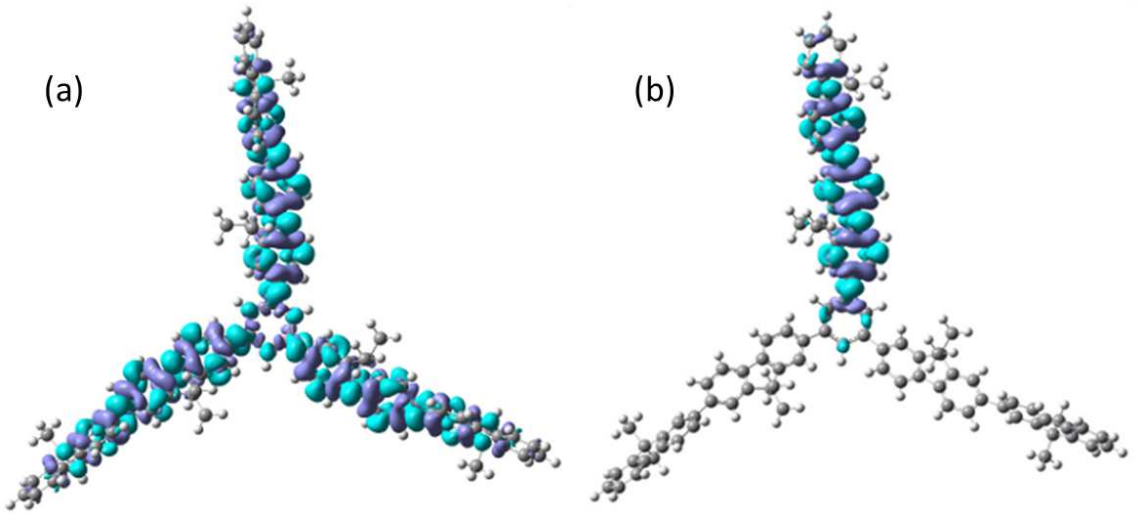

Figure 5.6: Visualisation of the change in electron density, for the B2 molecules in absorption (a) and in one of the three emission states (b). For the absorption transition the incident excitation is circularly polarised.

More detailed quantum chemistry calculations were performed to look in detail at both the absorption and emission transitions in B1 and B2. The calculations of the change in the electron density in a symmetric B2 molecule show that after absorption the exciton is delocalised across the entire molecule, whilst just prior to fluorescence it is localised on a single arm. This is shown in figure 5.6. The absorption transition shows that most of the electron density is localised at the centres of the arms, similar to the oligofluorenes, however a small amount is delocalised across the meta-linked benzene core. After absorption, a small symmetry breaking is enforced to mirror the Jahn-Teller effect.[7] After this symmetry breaking, it is found that the exciton always localises on one of the arms, as shown in Figure 5.6(b). Which arm it localises on depends upon the conditions of the symmetry breaking, as it always goes to the lowest energy arm.

The symmetry breaking is usually caused by a change in the geometry of the system, which affects the potential energy surface. Once the exciton localises, the arm is then planarised by the exciton similar to what was observed in the oligofluorenes[21] in Chapter 4. However, as these measurements occur at room temperature, there is a greater chance that the molecule will not possess perfect symmetry, and thus the excitation will only excite a single mode on an arm. In steady state measurements, it is possible to excite both modes even with the spectrally narrow beam. This then creates a similar situation where the exciton is still delocalised across the entire molecule and then localises on a single arm with the lowest energy.

5.4 Transition energies

To compare the theoretical results with the experimental values for the transition energies, a quantity needs to be chosen, which allows this to be done easily. As with the oligofluorenes in Chapter 4, the emission spectra can be calculated, but at an even higher computational cost due to their size. As such a more useful measure and direct comparison is the vertical transition energy, which corresponds to the direct vertical transition from the centre of the potential energy well in the Franck Condon principle as outlined in Chapter 2 Figure 2.6(a). This can be directly calculated using DFT and the experimental absorption and emission vertical transition energies can be determined from the recorded absorption and emission spectrum, for $E_{vert}(abs)$ and (em) for absorption and emission respectively using:[22]

$$E_{vert}(abs) = \frac{\int EA(E)dE}{\int A(E)dE} \qquad (5.1)$$

and

$$E_{vert}(em) = \frac{\int EI(E)dE}{\int I(E)dE} \qquad (5.2)$$

where $A(E)$ is the absorbance and $I(E)$ is the fluorescence intensity (in photons) at the energy E and the integration is over the absorbance and emission bands.

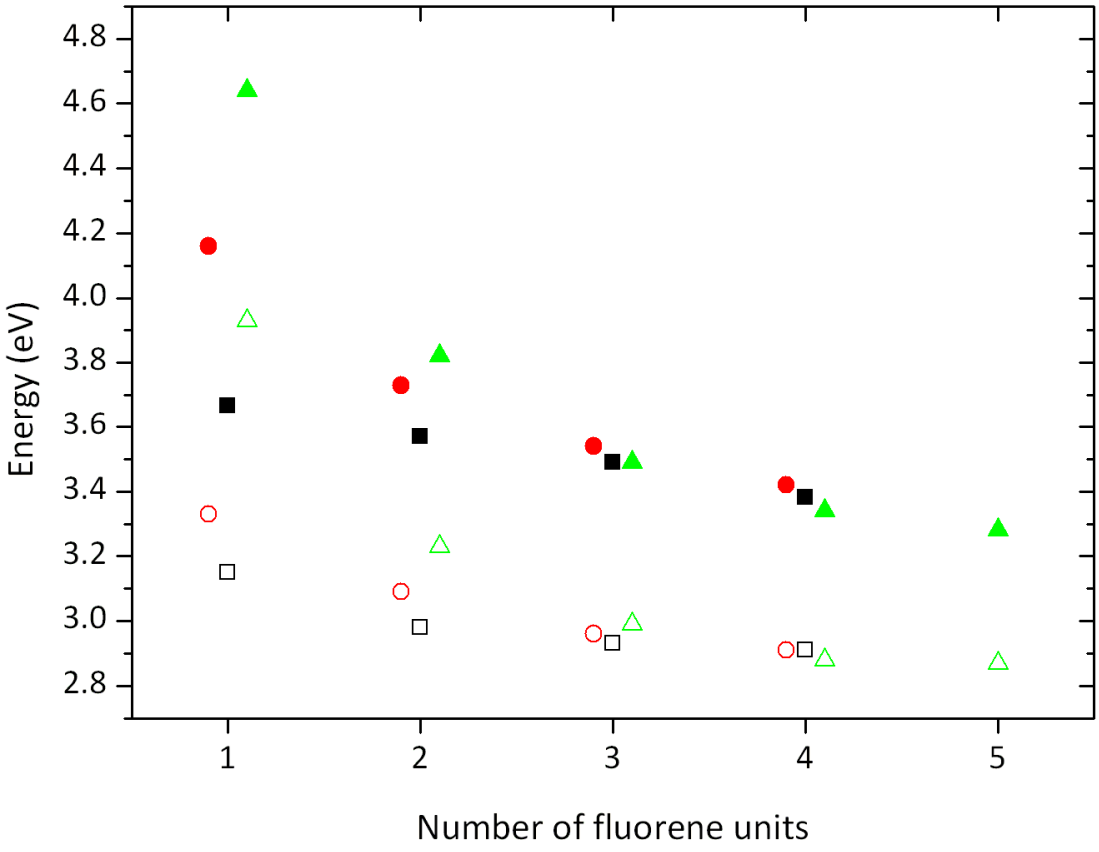

Figure 5.7: Experimental vertical transition energies: truxene-cored (black squares), benzene-cored (red circles), and oligofluorenes (green triangles), absorption (solid shapes) and fluorescence (hollow symbols).

The values were measured and calculated for all three families, and the measured values are shown in Figure 5.7. As can be seen there is a clear trend of decreasing transition energy with increasing arm length, in both absorption and fluorescence. For the 3-4 repeat fluorene unit arm lengths the transition energies are closer together with increasing arm length. For the B1, O1 and T1 there is a substantial spread in the transition energies: this is due to the core which, where present, constitutes an increasingly large part of the molecule. For example, in T1 the effective size of the core along the line of the arm makes it a bifluorene unit, rather than a single fluorene unit. As a result of this the transition energies in both star-shaped molecules are red-shifted when compared against the oligofluorenes; with the truxene-cored molecules having absorption and emission characteristics similar to n+1 number of oligofluorene units. There is a smaller effect caused by the shared single benzene ring in the benzene-cored molecule.

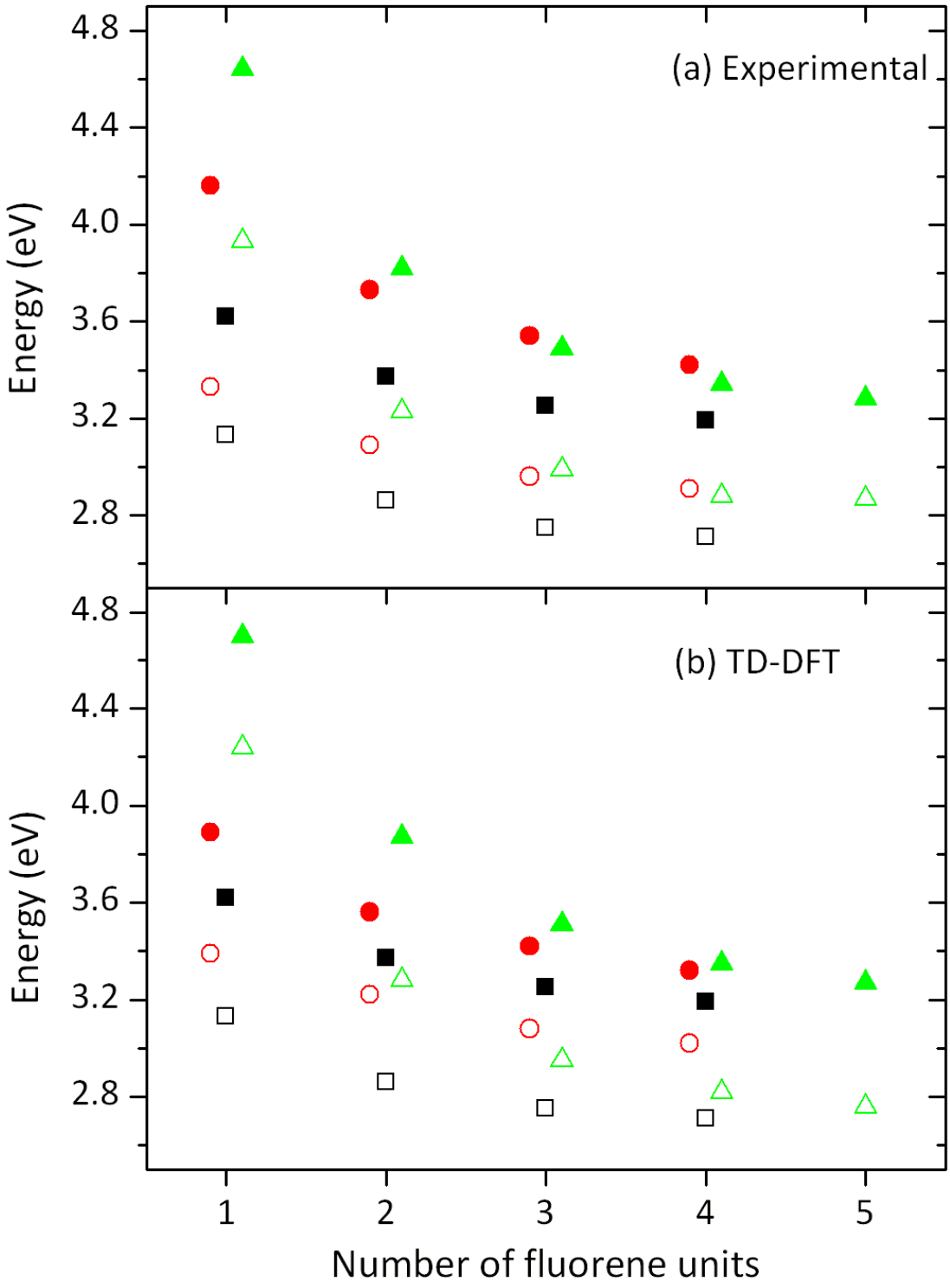

Figure 5.8: Experimental vertical transition energies (a) and TD-DFT values (b): truxene-cored (black squares), benzene-cored (red circles), and oligofluorenes (green triangles), absorption (solid shapes) and fluorescence (hollow symbols).

Figure 5.8 shows the comparison between the experimental (a) and the TD-DFT calculations (b). As can be seen there is a very good agreement between the experimental and theoretical values, with the redshifts in absorption and emission clearly shown in the figure. As with the previous chapter, the difference between the experimental and theoretical values in the short T0, O1 and B1 molecules is larger than in the other molecules; this was also seen in short chain linear oligofluorenes by Jansson et al..[23] This does however agree with other theoretical studies of short chain length molecules. The agreement between the experimental and theoretical values is not quite as good as in the previous chapter; this can be explained because the results for the oligofluorenes were measured at 77 K. It was decided not to measure all the molecules at low temperature for this study as it would provide results more applicable to devices operating at room temperature. The values for these are shown in Table 5.2 for a clearer comparison

Table 5.2: Experimental and TD-DFT vertical transition energies E_{vert} in eV.

Material	Absorption Vertical Transition Energy E_{vert} (eV)		Fluorescence Vertical Transition Energy E_{vert} (eV)	
	Experimental	Theory	Experimental	Theory
T0	4.25	4.34	3.31	4.16
T1	3.66	3.62	3.14	3.13
T2	3.57	3.37	2.97	2.86
T3	3.49	3.25	2.91	2.75
T4	3.38	3.19	2.89	2.71
B1	4.16	4.03	3.31	3.51
B2	3.73	3.53	3.07	3.01
B3	3.54	3.33	2.95	2.82
B4	3.42	3.24	2.90	2.74
O1	4.64	4.7	3.91	4.18
O2	3.9	3.81	3.25	3.23
O3	3.65	3.47	3.00	2.91
O4	3.52	3.31	2.95	2.78
O5	3.41	3.24	2.93	2.72

5.5 Transition dipole moment

When a molecule absorbs or emits light it must undergo a transition from one state into another; the strength of this transition is given as the transition dipole moment for the molecule. This is an important parameter to know, because it provides information on how the molecule interacts with radiation during absorption and how it emits light during fluorescence. Calculations and measurements were performed on these fluorene molecules to determine this value for each member of the family. The theory behind the experimental determination is presented in Chapter 4. As outlined, when calculating the absorption transition it is important to consider the number of

transitions within the absorption band; due to the symmetry of the star-shaped molecules, the molecules have two degenerate transitions, whose dipoles are orthogonal to each other.[24] As these transitions lie within the same absorption band, the calculation for the absorption transition dipoles needs to be summed over during the calculation. So from chapter 4.2, we have:[25,26]

$$\varepsilon_A(\tilde{\nu}) = \frac{8\pi^3}{3}\frac{N\prime\tilde{\nu}}{hcn_0 \ln(10)}\sum_{i=1}^{m}|d_a(\tilde{\nu})|^2 \quad (5.3)$$

Where N' is Avogadro's number divided by 1000, m is the number of dipole allowed transitions, $d_a(\tilde{\nu})$ is the transition dipole moment strength density, c is the speed of light in a vacuum, $\tilde{\nu}$ is the wavenumber in units of cm^{-1} and h is Planck's constant. In the case of this experiment, m=2 for the star shaped molecules and 1 for the oligomers. In the case of m=2 the two transitions d_1 and d_2 are equal so d_1=d_2. This has been shown for other star shaped molecules with C_3 symmetry[24] and was also shown in the quantum chemistry calculations performed on the molecule. So, by rearranging equation 5.3 for the star-shaped molecules and integrating over the absorption band we obtain:

$$|d_a|^2 = 4.593 \times 10^{-3} n_0 \int[\varepsilon(\tilde{\nu})/\tilde{\nu}]d\tilde{\nu} \qquad (5.4)$$

Where d_a is the frequency integrated transition dipole moment measured in Debyes, for one of the degenerate transitions.

There is only a single transition in fluorescence, because the exciton localises on to a single arm. As such the formula for calculating the transition dipole moment in fluorescence is the same as that outlined in chapter 4, using:[27]

$$|d_f|^2 = \frac{3\pi\varepsilon_0\hbar^4c^3\langle E^{-3}\rangle}{n_0\tau_{rad}} \quad (5.5)$$

Where $|d_f|$ is the fluorescence transition dipole moment, $\langle E^{-3}\rangle = [\int E^{-3}I(E)dE]/\int I(E)dE$ and $I(E)$ is the fluorescence intensity expressed in number of quanta, ε_0 is the vacuum dielectric constant, $\hbar = h/2\pi$ is Planck's constant, c is the speed of light in a vacuum and τ_{rad} is the natural radiative lifetime.

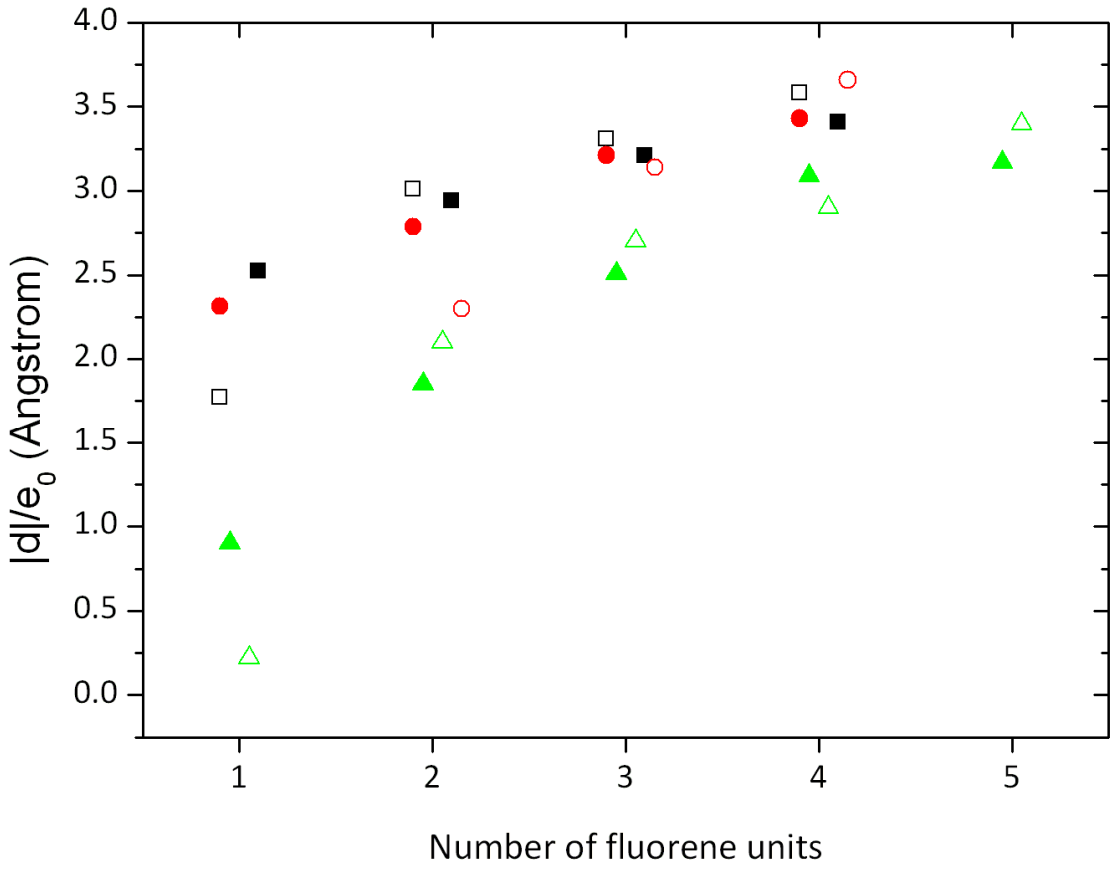

Figure 5.9: Experimentally determined transition dipole moments: truxene-cored (black squares), benzene-cored (red circles), and oligofluorenes (green triangles), absorption (solid shapes) and fluorescence (hollow symbols).

Figure 5.9 shows the transition dipole moments for all the experimental results on the fluorene molecules studied. The figure shows an increase in the transition dipole moments with increasing number of fluorene units. The star-shaped molecules always present larger transition dipole moments than their oligofluorene equivalents. The oligofluorenes show the same trend as was presented in Chapter 4, with an increasing transition dipole moment which starts to saturate as we increase the number of the fluorene units. The star-shaped molecules follow a similar trend, but as we approach longer arm lengths the transition dipole moments in both absorption and emission saturate more.

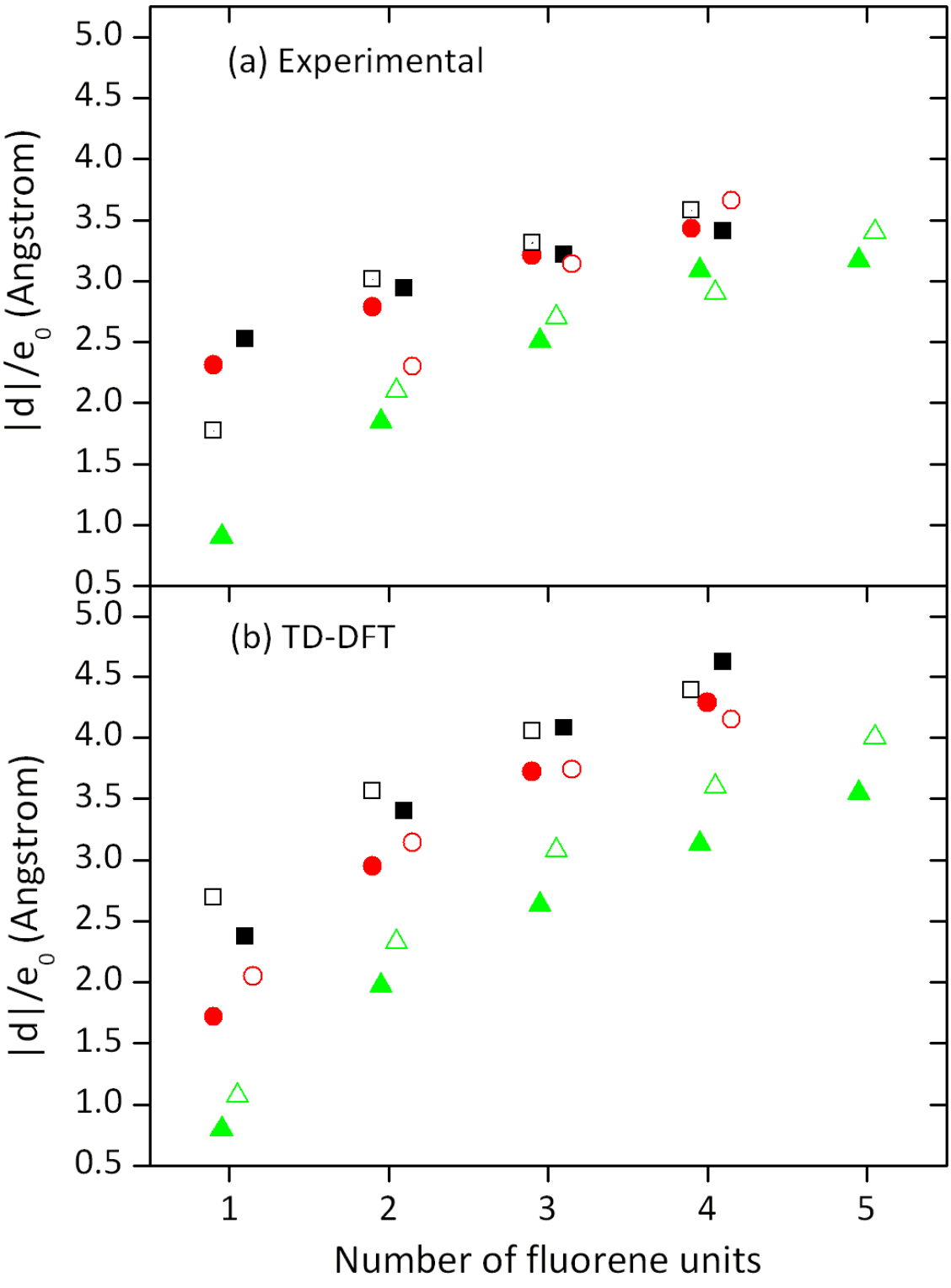

Figure 5.10: Experimentally determined transition dipole moments (a) and TD-DFT values (b): truxene-cored (black squares), benzene cored (red circles), and oligofluorenes (green triangles), absorption (solid shapes) and fluorescence (hollow symbols).

Figure 5.10 compares the experimentally determined values with the theoretical TD-DFT calculated values. The TD-DFT results presented correspond to the lowest optically active transitions. For all but the T0, T1 and B1, this is the transition from the ground state into one of the two lowest excited singlet states. In the other three molecules, this lowest energy state was found to be dark, in agreement with Oliva et al..[20] So the lowest bright singlet transition is into the degenerate second and third excited singlet state. For the T0, this is from the ground state into the third excited state. The results show a very good agreement, with all the values showing an increase in transition dipole moment with increasing number of fluorene units. Theoretical results follow the same trend as the experimental results, with the truxene-cored dipoles always being larger than the benzene-cored dipoles. The results for the TD-DFT transition dipole moments in the star-shaped molecules do not show the same saturation for 3 and 4 unit arm lengths. The reason that these can be seen in the experimental results, but not in the theoretical values, is due to conformational issues at room temperature. The good agreement between the experimental and theoretical transition dipole moments in both absorption and emission shows the importance of incorporating the number of transitions into calculations for the transition dipole moments in these C_3 symmetric molecules. The results for the dipoles are presented in Table 5.3.

Table 5.3: Experimental and TD-DFT transition dipole moments in absorption and fluorescence.

Material	Absorption		Fluorescence	
	Transition dipole moment $\|d\|/e_0$ (Å)		Transition dipole moment $\|d\|/e_0$ (Å)	
	Experimental	Theory	Experimental	Theory
T0	1.2 ± 0.2	1.03	...	1.07
T1	2.5 ± 0.3	2.37	2.0 ± 0.2	2.69
T2	2.9 ± 0.3	3.4	3.0 ± 0.2	3.56
T3	3.2 ± 0.3	4.08	3.3 ± 0.3	4.05
T4	3.4 ± 0.3	4.62	3.6 ± 0.3	4.39
B1	2.3 ± 0.2	1.72	0.3 ± 0.02	2.05
B2	2.7 ± 0.3	2.95	2.3 ± 0.2	3.14
B3	3.2 ± 0.3	3.72	3.3 ± 0.3	3.74
B4	3.4 ± 0.3	4.29	3.7 ± 0.3	4.15
O1	0.9 ± 0.2	0.8	0.2 ± 0.04	1.07
O2	1.9 ± 0.2	1.97	2.1 ± 0.2	2.33
O3	2.5 ± 0.2	2.63	2.7 ± 0.2	3.08
O4	3.1 ± 0.3	3.13	2.9 ± 0.2	3.60
O5	3.2 ± 0.3	3.55	3.4 ± 0.3	4.00

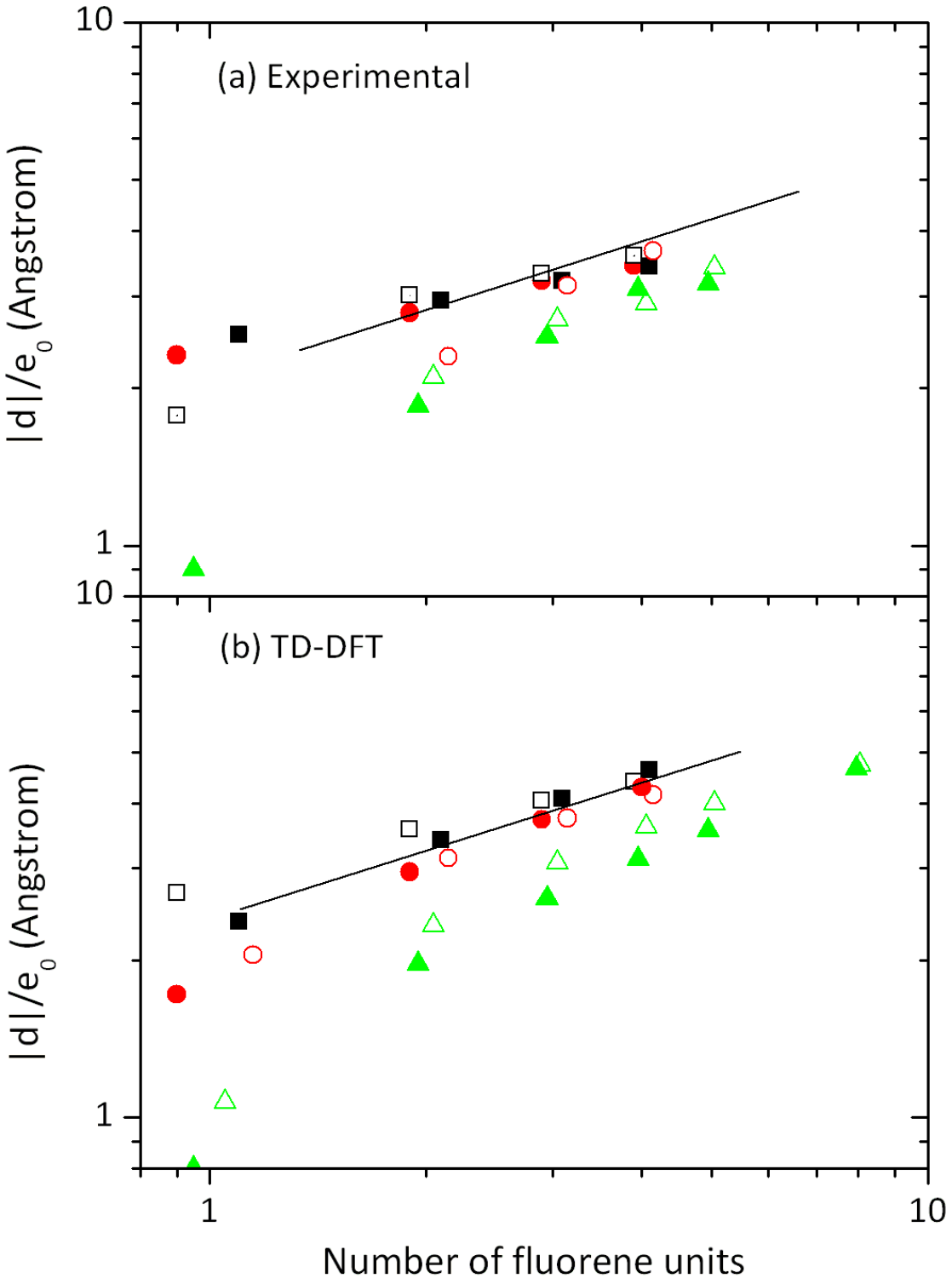

Figure 5.11: Experimentally determined transition dipole moments (a) and TD-DFT values (b) plotted on a log-log plot with a line fit of $n^{0.5}$: truxene-cored (black squares), benzene-cored (red circles), and oligofluorenes (green triangles), absorption (solid shapes) and fluorescence (hollow symbols).

As shown in Chapter 4, the transition dipole moments for oligofluorene molecules followed a ~$n^{0.5}$ trend for the absorption for 2≥n≥12. Figure 5.11 plots the same trend for comparison on double logarithmic plot for both the experimental and theoretical values for the star-shaped molecules. The theoretical results show that this trend roughly holds for the star-shaped molecules as well as for the oligofluorene molecules. The experimental results show a weaker trend than the theoretical calculations, in both absorption and fluorescence. This could be due to the conformational disorder that is outlined above, which will be particularly relevant in room temperature solutions.

5.6 Discussion

As can be seen from the comparison with the oligofluorene molecules, by changing the geometry from a simple linear molecule to a branched star-shaped one offers many advantages. These are the increase in PLQY, especially in the case of the truxene, the increase in the molar extinction coefficient and transition dipole moments. The reason why the molecules provide these improvements is that, due to their cores, the arms are held in a well linked system. For the star-shaped molecules this allows the transition to occur over the entire molecule. This makes them ideal candidates for devices that require optical pumping.

One of the considerations that need to be made, when making these comparisons, is what is the effect of the core? As the results show, the core causes an increase in the conjugation length. So it is not always a fair comparison to compare the results for a certain length oligofluorene, with that of the same number of repeat units, on the arm of a truxene molecule for example. This extra conjugation is definitely the reason for the redshift in absorption and emission when compared to the oligofluorene molecules. But on the other hand, the PLQY values for the truxene-cored and benzene cored molecules are greater than those of the oligofluorenes, even if a n+1 comparison is applied to account for the extra conjugation length. The difference between the values is about 10% for the T4, T3, B4 and B3 over the 3-5 length oligofluorenes. For the truxene cored molecules the entire family has higher PLQYs than for any of the oligofluorene molecules. This is again shown in the longer length star-shaped

molecules, when comparing the radiative lifetimes; the truxene-cored and benzene-cored molecules have shorter radiative lifetimes than the oligofluorenes of similar lengths. The truxene-cored molecules have lower values than the benzene-cored molecules and lower values than the extra fluorene unit in the core should account for, when compared against the oligofluorenes. With the smaller increase in the transition dipole moments in the longer length star shaped molecules, in experiment the comparison is not as clear. But the theoretical results show much higher transition dipole moments observed for the star-shaped molecules than the oligofluorenes.

These results show that, by having linked chromophores, well separated at well-defined angles, there are many photophysical improvements to the molecule. If we break this down to look at which core structure is better, then there is a clear case that the truxene core provides the best photophysical improvements. Both cores have a central benzene unit, with the arms linked at the meta positions so only a small amount of delocalisation exists across the core. The increase in the photophysical properties must then be a result of the highly rigid and planar nature of the truxene core. The use of the three fused fluorene units must greatly increase the rigidity allowing it to support the arms of the molecule better than just a simple benzene-cored molecule. The results of this study show that a lot of improvements to the photophysical performance of a molecule can be made by changing its geometry. The results also show that by careful consideration one can produce improved performance by selecting a suitable core for the application.

5.7 Conclusion

As the number of applications for star-shaped molecules increases as well as the number of star-shaped molecules, it is important to build up an understanding of the effects of changing the core and molecular size. In this work the optical properties of two families of star-shaped molecules have been studied. These molecules have two different cores with differing levels of conjugation and are studied to identify the effect of increasing the arm lengths of the molecules. The use of fluorene as the arm material allows the results to be compared against the results for linear oligofluorene molecules from Chapter 4. This also allows for deductions to be made as to the

advantages presented by the core. The results show that there is an increase in the PLQYs for the star-shaped molecules and a redshift in both absorption and emission resulting from the increase in the conjugation of the core. Experimental results show a slight increase in the transition dipole moments in both absorption and emission for the star-shaped molecules when compared with the oligofluorenes.

The experimental results have been compared against the results for calculations of the molecular behaviour from TD-DFT calculations, and are found to provide a good quantative agreement. The results highlight the importance of taking into account the number of transitions present within a molecule when calculating the transition dipole moments in absorption, which for the star-shaped molecules studied is 2. The results from the TD-DFT calculations show that under perfect symmetry considerations, the molecule absorbs over the entire molecule. After absorption across the entire molecule there is then a small symmetry breaking change in the molecular conditions, which causes the exciton to localise at the minimum on the potential energy surface. This corresponds to the exciton being localised on a single arm. The transition dipole moments are shown to present a similar trend to that of the oligofluorenes with the transition dipole moments in the theoretical calculations scaling with a rough $n^{0.5}$ trend. In experiment, however the results show that this increase is slightly weaker as there is the presence of conformational disorder in the larger molecules resulting in a saturation being observed.

It has also been argued that the increase in the photophysical properties of the molecule is not just due to the extra conjugation of the molecules from the cores. The cores also appear to separate the chromophores, allowing for efficient absorption across the entire molecule and transfer to a single arm for emission. From the discussion the best option for the material system is the highly conjugated truxene-core, which is a very rigid central core as it is based on three linked fluorene units. Many of the properties highlighted in this study, such as the high PLQY and high molar extinction coefficients make these materials perfect for light emitting devices, especially those that require optical pumping, such as organic lasers, which will be discussed in Chapter 7.

5.8 References

1 Burn, P. L., Lo, S. C. & Samuel, I. D. W. The development of light-emitting dendrimers for displays. *Adv. Mater.* **19**, 1675-1688, doi:10.1002/adma.200601592 (2007).

2 Lo, S.-C. & Burn, P. L. Development of Dendrimers: Macromolecules for Use in Organic Light-Emitting Diodes and Solar Cells. *Chem. Rev.* **107**, 1097-1116, doi:10.1021/cr050136l (2007).

3 Kanibolotsky, A. L., Perepichka, I. F. & Skabara, P. J. Star-shaped pi-conjugated oligomers and their applications in organic electronics and photonics. *Chem. Soc. Rev.* **39**, 2695-2728, doi:10.1039/b918154g (2010).

4 Kanibolotsky, A. L. *et al.* Synthesis and Properties of Monodisperse Oligofluorene-Functionalized Truxenes: Highly Fluorescent Star-Shaped Architectures. *Journal of the American Chemical Society* **126**, 13695-13702, doi:10.1021/ja039228n (2004).

5 Zhou, X. H., Yan, J. C. & Pei, J. Synthesis and relationships between the structures and properties of monodisperse star-shaped oligofluorenes. *Organic Letters* **5**, 3543-3546, doi:10.1021/ol035461e (2003).

6 Jacobs, P. W. M. *Group theory with applications in chemical physics*. 81 (Cambridge University Press, 2005., 2005).

7 Jahn, H. A. & Teller, E. Stability of Polyatomic Molecules in Degenerate Electronic States. I. Orbital Degeneracy. *Proceedings of the Royal Society of London. Series A - Mathematical and Physical Sciences* **161**, 220-235, doi:10.1098/rspa.1937.0142 (1937).

8 Tsiminis, G. *et al.* Low-threshold organic laser based on an oligofluorene truxene with low optical losses. *Appl. Phys. Lett.* **94**, doi:24330410.1063/1.3152782 (2009).

9 Wang, Y. *et al.* Broadly tunable deep blue laser based on a star-shaped oligofluorene truxene. *Synth. Met.* **160**, 1397-1400, doi:10.1016/j.synthmet.2010.04.016 (2010).

10 Lai, W.-Y. *et al.* Enhanced Solid-State Luminescence and Low-Threshold Lasing from Starburst Macromolecular Materials. *Adv. Mater.* **21**, 355-360 (2009).

11 Xia, R. D., Lai, W. Y., Levermore, P. A., Huang, W. & Bradley, D. D. C. Low-Threshold Distributed-Feedback Lasers Based on Pyrene-Cored Starburst Molecules with 1,3,6,8-Attached Oligo(9,9-Dialkylfluorene) Arms. *Adv. Funct. Mater.* **19**, 2844-2850, doi:10.1002/adfm.200900503 (2009).

12 Sun, Y. M. *et al.* Oligothiophene-Functionalized Truxene: Star-Shaped Compounds for Organic Field-Effect Transistors. *Adv. Funct. Mater.* **15**, 818-822 (2005).

13 Yuan, M. S., Liu, Z. Q. & Fang, Q. Donor-and-acceptor substituted truxenes as multifunctional fluorescent probes. *J. Org. Chem.* **72**, 7915-7922, doi:10.1021/jo071064w (2007).

14 Yang, J.-S., Huang, H.-H. & Ho, J.-H. Electronic Properties of Star-Shaped Oligofluorenes Containing an Isotruxene Core: Interplay of Para and Ortho Conjugation Effects in Phenylene-Based π Systems. *The Journal of Physical Chemistry B* **112**, 8871-8878, doi:10.1021/jp800448p (2008).

15 Yang, J.-S., Lee, Y.-R., Yan, J.-L. & Lu, M.-C. Synthesis and Properties of a Fluorene-Capped Isotruxene: A New Unsymmetrical Star-Shaped π-System. *Organic Letters* **8**, 5813-5816, doi:10.1021/ol062408s (2006).

16 Tomović, Ž. *et al.* Star-Shaped Oligo(p-phenylenevinylene) Substituted Hexaarylbenzene: Purity, Stability, and Chiral Self-assembly†. *Journal of the American Chemical Society* **129**, 16190-16196, doi:10.1021/ja0765417 (2007).

17 Li, Z. H., Wong, M. S. & Tao, Y. Two-dimensional oligoarylenes: synthesis and structure–properties relationships. *Tetrahedron* **61**, 5277-5285, doi:10.1016/j.tet.2005.03.077 (2005).

18 Ponomarenko, S. A. *et al.* Star-Shaped Oligothiophenes for Solution-Processible Organic Field-Effect Transistors. *Adv. Funct. Mater.* **13**, 591-596, doi:10.1002/adfm.200304363 (2003).

19 Huang, J. *et al.* Benzene-cored fluorophors with TPE peripheries: facile synthesis, crystallization-induced blue-shifted emission, and efficient blue luminogens for non-doped OLEDs. *J. Mater. Chem.* **22**, 12001-12007 (2012).

20 Moreno Oliva, M. *et al.* Electronic and Molecular Structures of Trigonal Truxene-Core Systems Conjugated to Peripheral Fluorene Branches. Spectroscopic and Theoretical Study. *The Journal of Physical Chemistry B* **111**, 4026-4035, doi:10.1021/jp065271w (2007).

21 Schumacher, S. *et al.* Effect of exciton self-trapping and molecular conformation on photophysical properties of oligofluorenes. *J. Chem. Phys.* **131**, doi:15490610.1063/1.3244984 (2009).

22 Gierschner, J., Cornil, J. & Egelhaaf, H.-J. Optical Bandgaps of &pgr;-Conjugated Organic Materials at the Polymer Limit: Experiment and Theory. *Adv. Mater.* **19**, 173-191 (2007).

23 Jansson, E., Jha, P. C. & Agren, H. Chain length dependence of singlet and triplet excited states of oligofluorenes: A density functional study. *Chem. Phys.* **336**, 91-98 (2007).

24 Terenziani, F., Sissa, C. & Painelli, A. Symmetry Breaking in Octupolar Chromophores: Solvatochromism and Electroabsorption. *The Journal of Physical Chemistry B* **112**, 5079-5087, doi:10.1021/jp710241g (2008).

25 Förster, T. Zwischenmolekulare Energiewanderung und Fluoreszenz. *Annalen der Physik* **437**, 55-75, doi:10.1002/andp.19484370105 (1948).

26 Knox, R. S. & van Amerongen, H. Refractive index dependence of the Forster resonance excitation transfer rate. *J. Phys. Chem. B* **106**, 5289-5293, doi:10.1021/jp013927+ (2002).

27 Craig, D. P. & Thirunacchandran, T. *Molecular Quantum Electrodynamics*. 89-97 (Academic Press, 1984).

6

Anisotropy decay in truxene-cored molecules

6.0 Introduction

This chapter presents a study of the ultrafast energy transfer in star-shaped truxene-cored oligofluorene molecules. This study focuses on the photoluminescence anisotropy decay of two members of the family, measured using upconversion fluorescence spectroscopy. The results for these molecules are then compared against the dynamics of linear oligofluorene molecules with equivalent conjugation lengths, to identify the effect of the fixed geometry in the star-shaped systems. The results show that there is a fast ~ 500 fs initial decay, followed by a slower 3-10 ps second decay component. The amount of anisotropy decay and thus the energy transfer was found to be dependent on the pump wavelength. This happens because, as one tunes the pump to the lower energy side of the absorption spectrum, one is only able to access lower energy states.

Section 6.1 provides an overview of anisotropy measurements and energy transfer within branched molecules. Section 6.2 presents and discuss the absorption and emission characteristics of the truxene-cored molecules and their linear oligofluorene counterparts. Section 6.3 presents the results for the photoluminescence anisotropy, showing a comparison with the linear oligofluorenes. This is then followed by the results for the anisotropy at different pump wavelengths. Section 6.4 discusses the results and provides an explanation of the relaxation processes within the molecule. Also presented are some time dependent density functional theory TD-DFT

calculations, performed by Jean-Christophe Denis and Prof. Ian Galbraith at Heriot Watt University. These calculations show the energy requirements for a series of different conformational changes, which break the symmetry and cause a significant splitting between the two absorption transitions of the molecule. Section 6.5 concludes the chapter and highlights the key findings from the study.

6.1 Anisotropy and energy transfer

6.1.1 Anisotropy measurements

Anisotropy is a measure of how a measured quantity changes with respect to the orientation of observation. In photophysical measurements this is done by exciting a sample with a polarised light source, and detecting the resulting emission using a polarised detector; in this case either the excitation light can have its polarisation changed or a polariser can be used in the detection, so that only light emitted parallel or perpendicular to the excitation is detected. In the case of the experiments presented in this chapter, it is the orientation of the excitation light that is varied with respect to the detection polarisation. In both experimental cases the anisotropy is measured using:

$$r = \frac{I_{\parallel} - gI_{\perp}}{I_{\parallel} + 2gI_{\perp}} \qquad (6.1)$$

Where r is the anisotropy, $I_{\parallel}$ is the intensity recorded parallel to the excitation source and $I_{\perp}$is the intensity recorded perpendicular to the excitation source. Anisotropy is therefore a measure of the difference between the detected intensity parallel and perpendicular to the excitation light divided by the total detectable emitted intensity. The g factor in this equation is a measure of the sensitivity of the detection of the parallel and perpendicular emission; it can be calculated from: $g = S_{\parallel}/S_{\perp}$, where S is the sensitivity. In the case of our experiment the g factor was found to be 1. This was also shown from the anisotropy results for the short straight 3 unit oligofluorene molecule which was found to have an initial anisotropy of 0.4 consistent with the theoretical value for a rod like molecule. The initial expected anisotropy of a rod like molecule can be calculated by firstly considering the molecule to have parallel

absorption and emission dipoles. A representation of a rod like molecule in an anisotropy measurement is shown in figure 6.1.

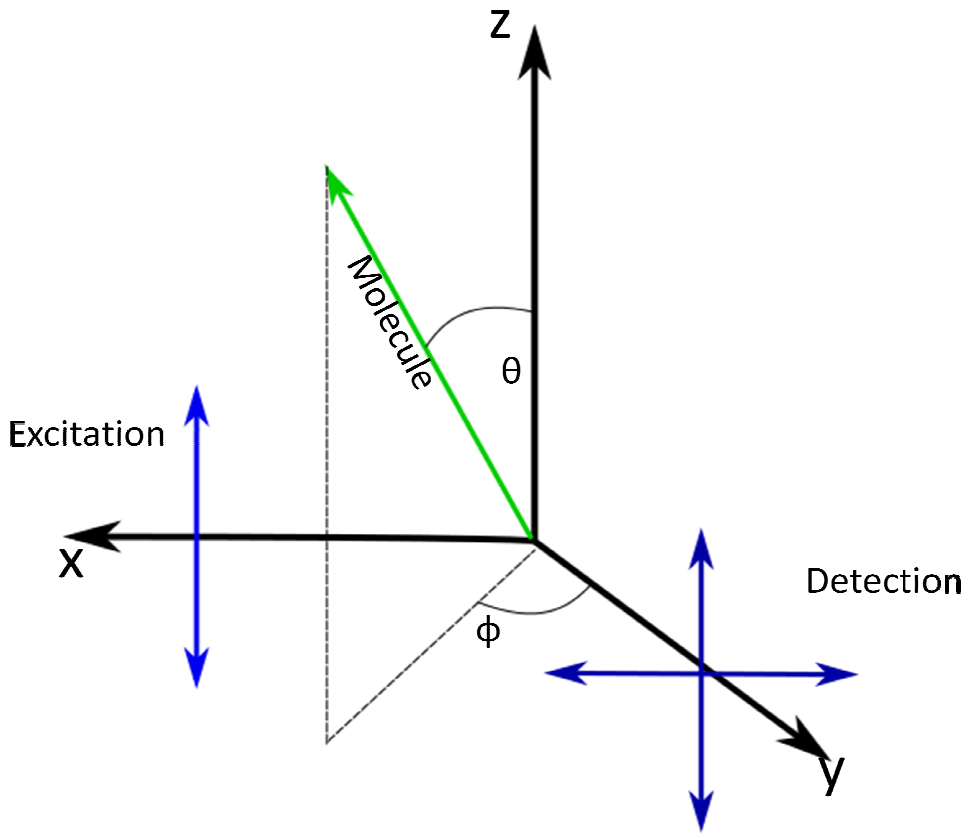

Figure 6.1: schematic of an anisotropy measurement showing the excitation and detection relative to a molecule. Figure inspired by Principles of fluorescence spectroscopy (Figure based on figure 10.4 Principles of fluorescence spectroscopy Lakowicz.)[1]

The molecule is positioned at an angle θ from the z axis and at an angle ϕ relative to the x and y axes. The excitation is shown as coming in along polarised relative to the z axis, whilst the detection is performed relative to the x and z axis. From angular considerations the intensity parallel to the excitation beam is $I_{\parallel} = cos^2\theta$, whilst the perpendicular intensity is given by $I_{\perp} = sin^2\theta sin^2\phi$. By initially applying an angular averaging over ϕ and then over θ and substituting the results back into equation 6.1 it can be calculated that for a rod like molecule the expected initial anisotropy is 0.4.

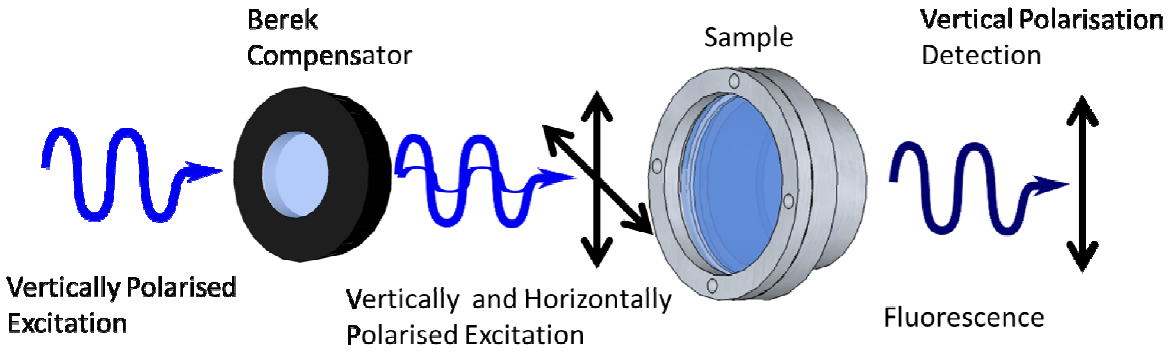

Figure 6.2: Anisotropy measurement setup. Polarised excitation light is incident on the sample either parallel or perpendicular to the orientation of the detection polarisation.

It is also possible to monitor the dynamics of the molecule, such as spectral diffusion, whilst obtaining the anisotropy data. This is done by measuring the total intensity which is equal to $I_{total} = I_{\parallel} + 2I_{\perp,}$the reason for this can be seen in figure 6.1, due to the orientation of the detector only the perpendicular emission propagating in x direction can be detected, but due to the symmetry of emission there is an equal amount of emitted perpendicular emission in the y that cannot; hence the need for the $2I_{\perp,}$ term. The total intensity can also be approximated with the polarisation set at the so called "magic angle". The "magic angle" is measured at 57.4°, and when considering the intensity at the magic angle $\cos^2$=0.333 and $\sin^2$=0.666, so the detected intensity is equal to $I_{\parallel} + 2I_{\perp}$.[1] In this experiment the parallel and perpendicular intensities were measured and the total intensity or magic angle data reconstructed from:

$$I_{magic} = (I_{\parallel} + 2I_{\perp})/3 \qquad (6.2)$$

6.1.2 Energy Transfer

There has been increasing interest in branched[2] and dendrimer like molecules,[3,4] in which different functional groups can be included in the arms, making them suitable for a range of applications.[5,6] Energy transfer within these branched molecules[7] has been studied with an aim of developing improved molecules for applications such as light harvesting systems[6,8,9], OLEDs[3,4] and lasers.[10-12] Anisotropy measurements have often been used to measure energy transfer within polymer chains.[13-15] This technique has now been employed to study the energy transfer processes in branched molecules.

To address this issue of energy transfer within branched molecules there have been a number of theoretical and experimental studies performed on different types of molecules. Experimental measurements have been performed using fluorescence[16-18] or transient absorption spectroscopy.[19,20] Both these methods are suitable for studying the depolarisation in the molecule. Fluorescence anisotropy is the easier of the two to interpret, as one only needs to consider the S_1-S_0 transition. Transient absorption on the other hand pumps the molecule into a higher unknown S_n energy state and then sends a second pulse to probe this. As the higher lying energy states are unknown, there could be other processes involved, which could affect the anisotropy results.[17]

Fluorescence anisotropy measurements have been employed to study the energy transfer dynamics in a particular class of small molecules which possess C_3 symmetry. These molecules can be branched from a number of different cores with benzene[21-23] and nitrogen being used.[7,16,19,24] Triphenylbenzene derivatives have been studied and it was concluded that when the symmetry is broken the exciton localises on one of the arms.[22] After this initial localisation the excitons were then able to move from arm to arm via a hopping mechanism.[25] Studies on nitrogen-cored styrylbenzene dendrimers also show a rapid depolarisation as the energy transfers to the core.[24] Theoretical studies were performed on phenylacetylene dendrimers and it was found that the exciton localises on the branching point.[23]

The majority of these experimental results suggest that the energy transfer occurs to a single arm.[19] Rates for the depolarisation to an arm are found to be different for different cores, but most molecules show a fast depolarisation on a sub picosecond time scale. In the nitrogen-cored three branch molecules, this very fast depolarisation is attributed to coherent energy transfer.[19] This dephasing process takes place from an absorption state across the entire molecule to a localisation on a single arm.

If the exciton localises on an arm, rather than the core, then there is evidence that in many systems further energy transfer can occur within the molecule. This has been proposed to be a hopping process between the arms of the molecules, with the exciton transferring via a Förster type mechanism.[25] Because of the Förster type nature of this energy transfer process, the timescale for this localisation is an order of

magnitude slower than the initial depolarisation, and typically occurs on a picosecond timescale. The localisation process is claimed to be dependent upon the chromophore's relaxation time and the angle between chromophores.[7,25] These results show that depending upon a number of considerations there are a lot of different molecular processes which can occur, all of which affect the amount and rate of depolarisation.

As this review has shown, there is a lot of understanding to be gained about these large branched symmetric molecules. The nature of the energy transfer appears to be dependent on both the size of the molecule and its core structure. By using ultrafast fluorescence anisotropy measurements, it is hoped that a better understanding of this process can be achieved for truxene-cored oligofluorene molecules.

6.2 Absorption and emission characteristics of the molecules

In this study the anisotropy of two truxene-cored oligofluorene molecules is compared with that of their linear oligofluorene counterparts. The study was performed on the T2 and T4 truxene-cored molecules which have chains of 2 and 4 fluorene units in each arm respectively. These are compared with O3 and O5 oligofluorene molecules, which are chains of 3 and 5 fluorenes respectively. The structures of the molecules are shown in the inset to Figure 6.3. Initial studies on the photophysical properties of the molecules have been presented in Chapters 4 and 5. The particular choice of oligofluorene molecules for this comparison was made because the truxene-core consists of three fluorene units fused through the meta-positions of a shared central benzene ring, making the truxene-core equivalent to an extra fluorene unit added to each arm.[26] The truxene cored molecules were synthesised by Dr Alexander Kanibolotsky and Prof Peter Skabara at Strathclyde University.[27] The O5 and O3 were procured from American Dye Source Inc., ADS056FO and ADS036FO respectively. Unless stated all measurements were performed in spectroscopic grade toluene procured from Sigma Aldrich.

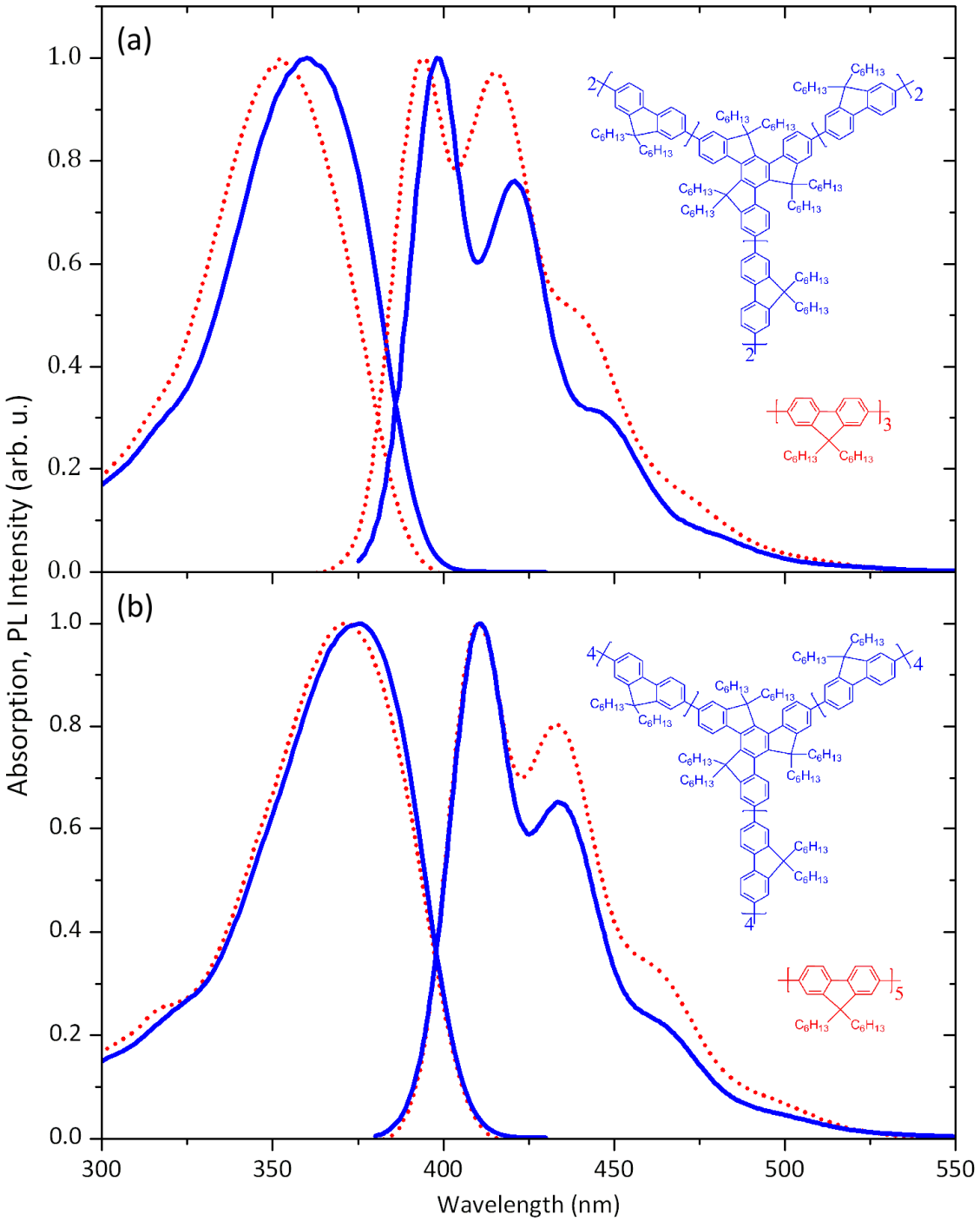

Figure 6.3:(a) Absorption and emission spectra of T2 (blue) and O2 (red dashed) lines, (b) absorption and emission spectra of the T4 and O5 molecules (same colours). The molecular structures are inset in the figure.

The similarity in the absorption and emission of the truxene-cored and oligofluorene molecules is presented in Figure 6.3. As can be seen from the data shown in figure 6.3(a) there is a small 6 nm blue shift for the absorption and emission of the O3 with respect to the T2 molecules, whilst there is a very good agreement between the

spectra of O5 and T4 molecules, shown in Figure 6.3(b). The spectra presented in Figure 6.3 were measured at low concentrations with a peak absorption of 0.1, and as such do not present any effects of self-absorbance.

6.3 Anisotropy

The anisotropy measurements were carried out at a higher concentration of 6 mg ml^{-1}. This was done to ensure that in these measurements absorbance was greater than 1 at the pump wavelength, and that as little of the pump pulse was transmitted through the sample as possible. If pump light passes through the sample it can interfere with the data at times when the pulse is still incident, and because the pump light is orientated “parallel”, it will detrimentally affect the results of the anisotropy measurements. The downside of using higher concentrations is the increase in self-absorption, meaning that it is difficult to detect photoluminescence on the 0-0 peak. The experimental setup used a frequency doubled Ti:Sapphire laser, which is tuneable from 375-425 nm; this meant that the experiment could only probe the absorption from the peak to the red-edge tail. For further information on the experimental setup see Chapter 3.

Anisotropy measurements were performed by varying the polarisation of the excitation parallel and perpendicular to the detection. These two signals were then combined to calculate the anisotropy or to reconstruct the magic angle data using formulae 6.1 and 6.2 respectively.

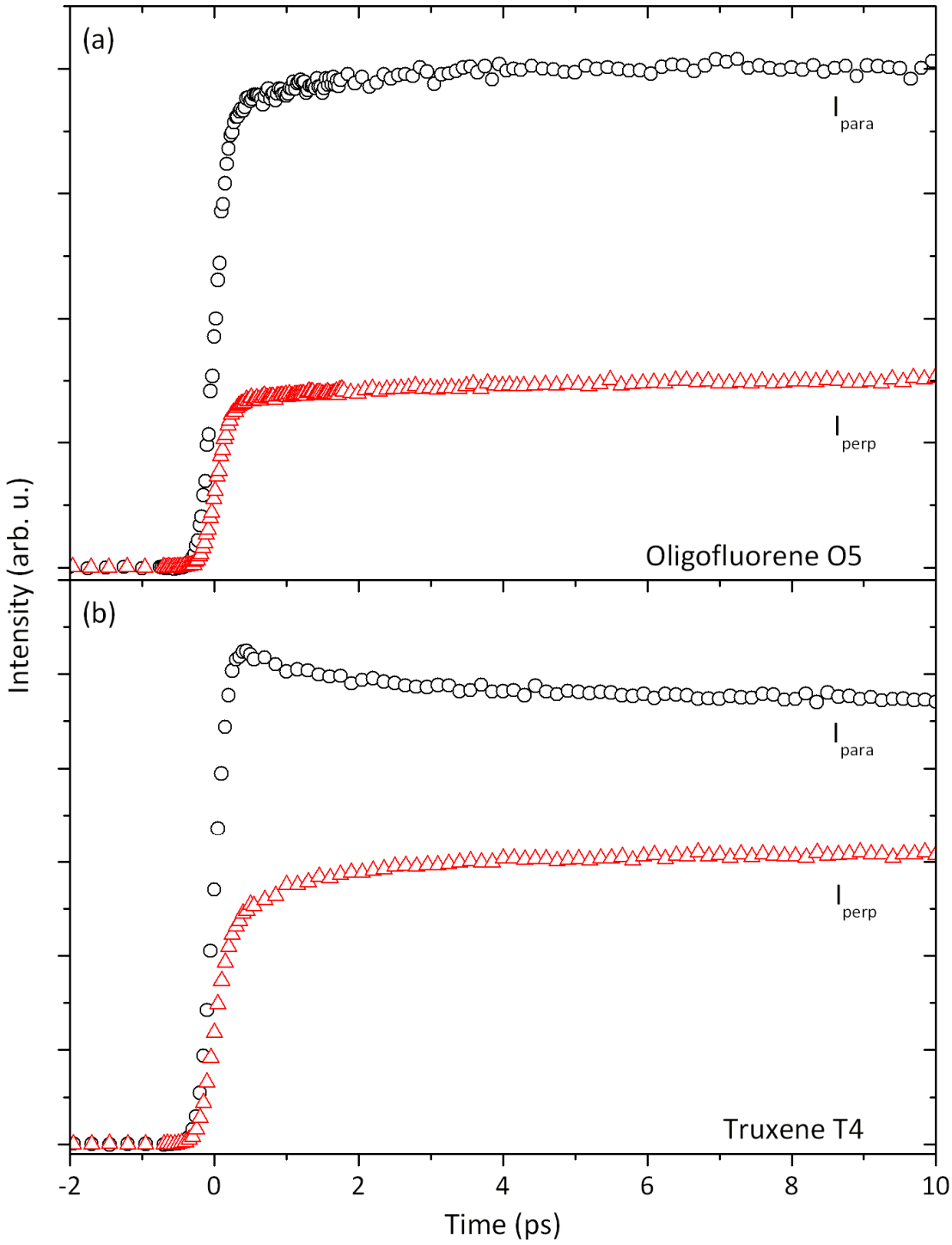

Figure 6.4: Measured fluorescence intensity: parallel (black open circles) and perpendicular (open red triangles) of O5 (a), and truxene T4 (b). Excitation wavelength used was 380 nm, whilst the detection was 440 nm.

Figure 6.4(a) presents the time-resolved parallel and perpendicular intensities from the O5 linear oligofluorene molecule when excited at 380 nm and detected at 440 nm. The

data shows that the intensity recorded for the parallel excitation $I_{\parallel}$ is about twice as great as that of the perpendicular $I_{\perp}$. The difference in the intensities of these two signals does not change greatly with time. Figure 6.4(b) presents the parallel and perpendicular signals for T4, at the same excitation and detection wavelengths. As can be seen in the data, there is a large difference in the initial intensity between the parallel and perpendicular traces. At early times during the formation of the states, there is a fast decrease in the parallel trace and a corresponding increase in the perpendicular trace, as energy is transferred away from the parallel direction. There is also a slow decay present in the parallel signal, which corresponds to a similar increase in the perpendicular trace. This hints at a larger level of fast dipole reorientation within the star-shaped molecules when compared with the linear equivalent.

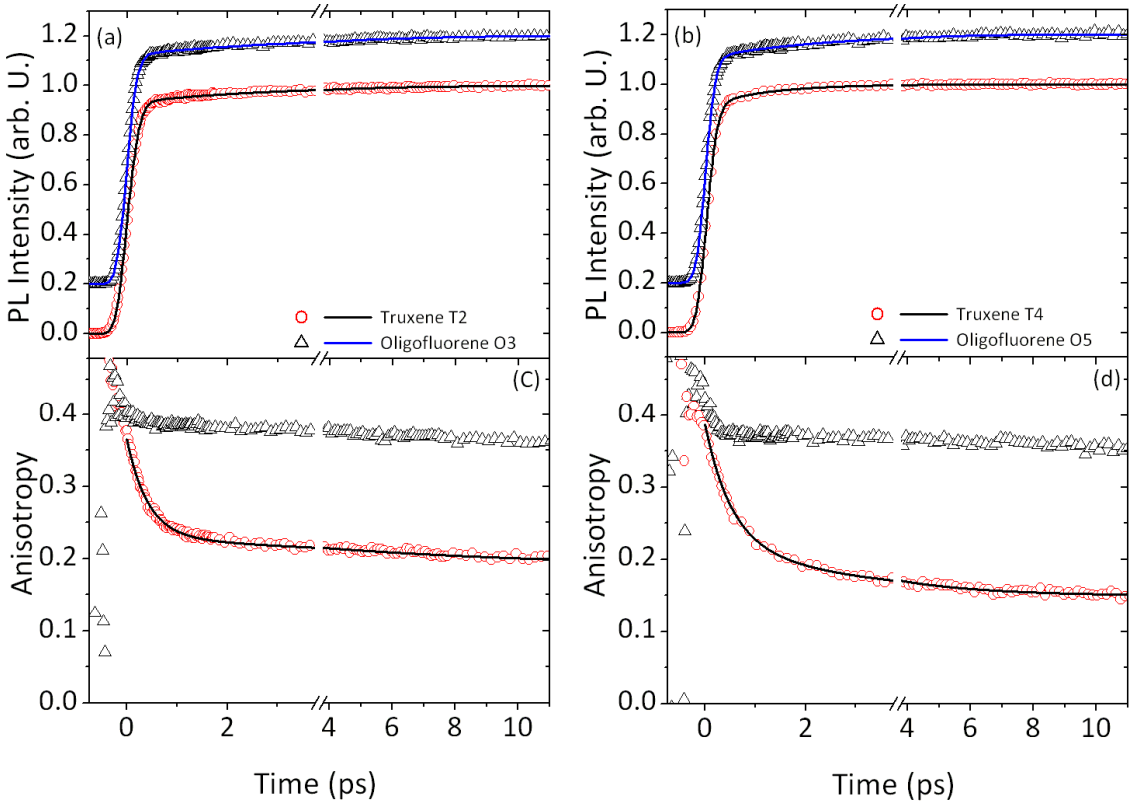

Figure 6.5 (a): Fluorescence magic angle (top panels) and anisotropy (bottom panels) data and fits for the four molecules studied. The data on the left panels (a and c) contain comparisons between O3 and T2, while those on the right (b and d) contain comparisons between O5 and T4. The magic angle data are offset vertically for clarity

Figure 6.5 presents a comparison of the anisotropy and the magic angle data for the truxene and oligofluorene molecules. An excitation of 380 nm was used, whilst a detection wavelength of 420 nm was used for T2 and O3 molecules and 440 nm was

used for T4 and O5. The detection wavelengths were chosen to measure a similar emission point in the photoluminescence spectra; this is close to the 0-1 peak to avoid the effects of self-absorption. Figure 6.5 (a) shows a comparison of the reconstructed magic angle data from T2 and O3 using formula 6.2, and panel (b) in Figure 6.5 shows the same reconstructed magic angle data for the T4 and O5 molecules. All the molecules show an initial rise of ~90 fs and a slower rise over the period of 10 ps. The slow rise in the magic angle data can be attributed to spectral relaxation, because we are detecting on the red side of the 0-1 emission peak for all of the molecules.

Figure 6.5 (c) presents the anisotropy results for the O3 and T2 molecules. Both molecules show an initial anisotropy of ~0.4 at t=0. O3 then undergoes a very slow mono-exponential decay which reduces the anisotropy to 0.35 after 10 ps and is attributed to rotational diffusion in this small molecule. T2, on the other hand, shows a bi-exponential decay with an initial fast component, which reduces the anisotropy from 0.37 to 0.25, and a slower second decay which reduces the anisotropy further to 0.19. Both of these decays are too fast for rotational diffusion in a molecule this large. Figure 6.4 (d) presents the data for the anisotropy decay of T4 and O5 molecules. The O5 anisotropy data is very similar to that of the O3, showing an initial anisotropy value of 0.38 with a slow mono-exponential decay to 0.35 after 10 ps. T4, like T2, shows a fast initial decay from 0.39 to 0.23 and then a slower second decay component, which reduces the anisotropy further to 0.15. Dynamics were fitted using the sum difference fitting technique[28] outlined in Chapter 3. The fitting values of the decays are shown as the solid black line on the traces in figure 6.5 and are summarised in Table 6.1. The results show the decays of the star-shaped truxene-cored molecules differ greatly from those of the constituent oligofluorenes. This suggests that there is a large amount of anisotropy decay caused by the shape of the molecule.

These results specifically highlight two interesting issues regarding the anisotropy decay of the star-shaped molecules. Firstly, there is a difference in the final anisotropy values for the two truxene-cored molecules, with the T4 having a lower final anisotropy of 0.15, whilst the T2 has a final anisotropy value of 0.19. Secondly, the initial anisotropy of the truxene-cored molecules, being approximately 0.4, is the same as the oligofluorenes. This is interesting because for a C_3 symmetric molecule, the

predicted initial anisotropy is 0.7, whilst the final anisotropy for a fully depolarised C_3 symmetric molecule to a random arm is predicted to be 0.1.[29] An initial anisotropy value of 0.4 is more readily associated with the anisotropy of a rod like molecule, whose absorption and emission dipoles are parallel.

The difference observed in the final anisotropy values between the two truxene-cored molecules is considered first. The main difference between the two molecules is that there are 2 extra fluorene units on each arm of T4, which causes a red-shift in the absorption. This means that, when exciting the T2 molecule at 380 nm, we are exciting into a lower energy state relative to that in T4. To investigate if this might be the cause of the effect, the excitation wavelength dependence of the T4 anisotropy was measured. T4 was chosen, rather than T2, due to constraints of the laser system being used, which had a range of 375-425 nm, allowing for access to the higher energy absorption states of T4. To investigate this effect, T4 was excited at 380, 400 and 420 nm with detection wavelengths of 440 nm used for 380 nm excitation, and 500 nm for the 400 nm and 420 nm excitation. A detection wavelength of 500 nm was chosen for the 400 and 420 nm excitation wavelengths, to remove any effects from solvent Raman signals, which can detrimentally affect the early time dynamics of the anisotropy. Raman signals are a problem as they preferentially align with the parallel signal, and become a greater problem when exciting the red edge of the absorption. This is because there is less absorption, and hence less emission in this region, so Raman makes up a greater percentage of the total signal. The choice of 500 nm for the detection wavelength does not affect the results, as our experiments showed that the final anisotropy values are detection wavelength independent. This was also shown in the study by Sissa et al.,[30] for a similar system.

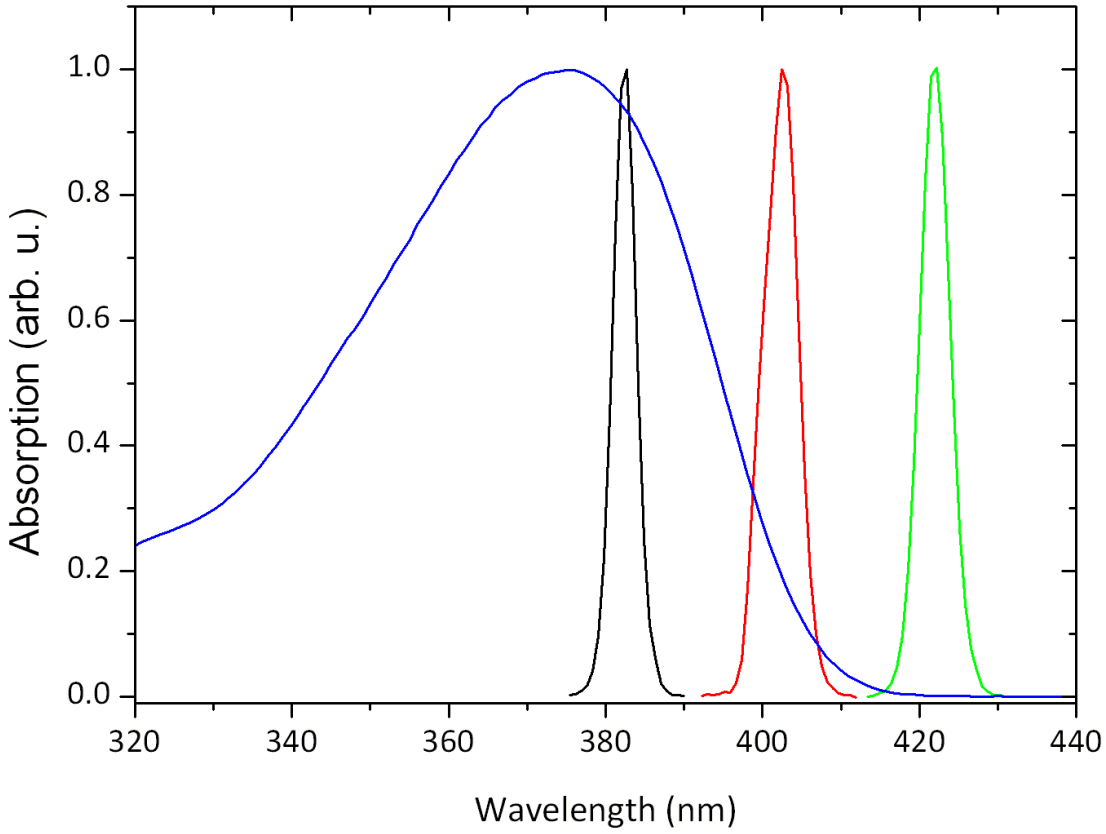

Figure 6.6: Absorption of the Truxene T4 (blue line) and the laser spectra at the 380 nm (black), 400 nm (red) and 420 nm (green) pump wavelengths.

Figure 6.6 shows the absorption of the T4 molecule. Overlaid onto this is the laser spectrum of the pump at the three different excitation wavelengths. The data shows how the absorption decreases towards 420 nm, meaning that measuring fluorescence when pumping at 420 nm is much more difficult than when pumping at 380 nm, as there is a considerable reduction in absorption.

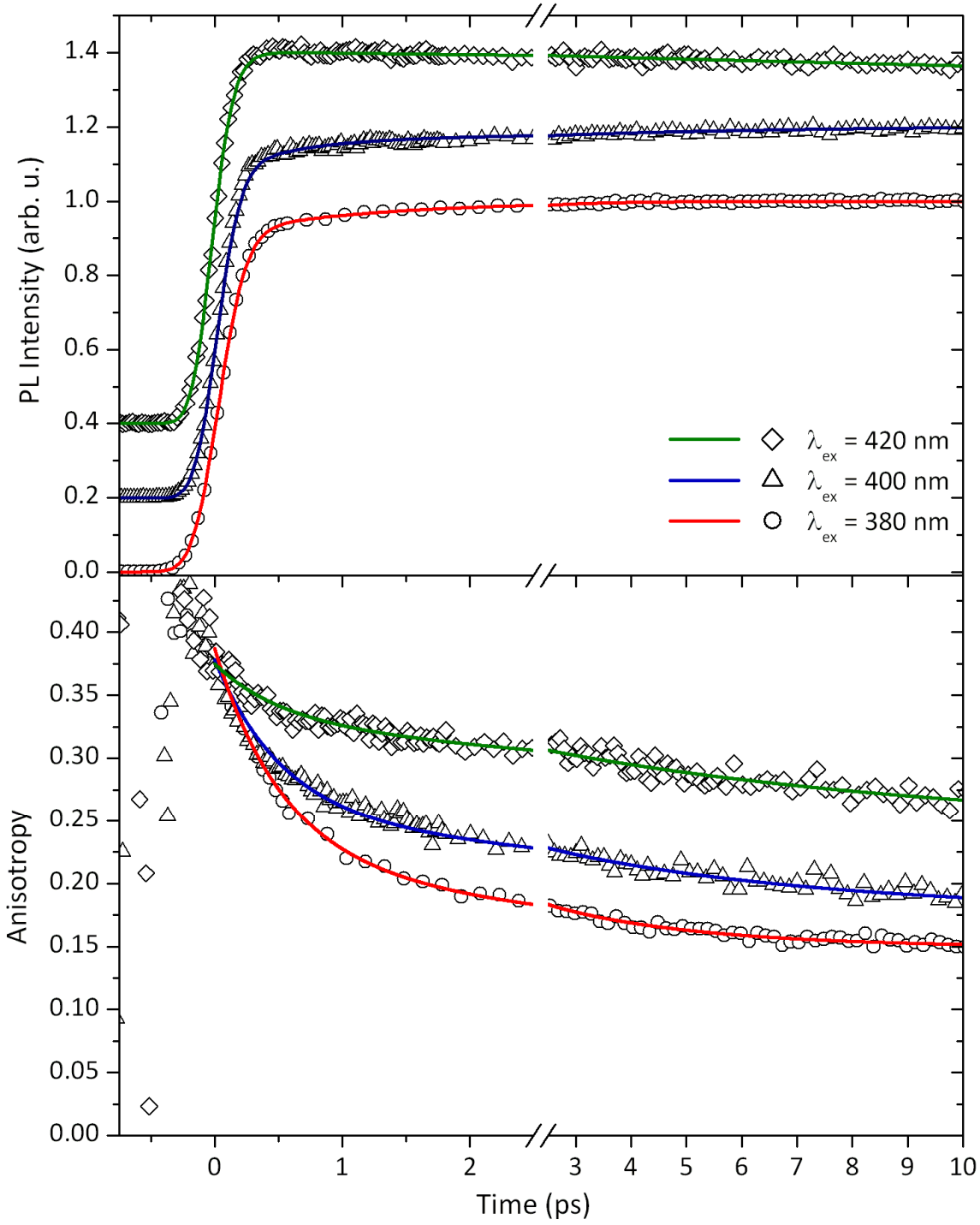

Figure 6.7 (a): The reconstructed magic angle data for T4 at the different pump wavelengths, offset for clarity, (b) the corresponding anisotropy plots at the different pump wavelengths and their fits. Open diamonds and green solid line correspond to 420 nm, open triangles and solid blue line 400 nm, and open circles and red solid line 380 nm.

Figure 6.7(a) shows the reconstructed magic angle data for the T4 molecule. All these are fitted using the sum fit procedure and all the fast rises show an ~90 fs rise time.

The results again show a sharp rise coinciding with the absorption of the molecules. After this there is a slow rise on the 380 and 400 nm excitation wavelengths and a slow decrease at 420 nm. These slow dynamics are due to spectral shift with the higher energy excitations decreasing to lower energy emission states due to spectral diffusion.

Figure 6.7(b) presents the anisotropy results for the T4 molecule when excited at 380, 400 and 420 nm. The results show that at all excitation wavelengths the anisotropies exhibit a bi-exponential decay. The magnitude of the fast initial decay is dependent upon the excitation wavelength; longer excitation wavelengths lead to a smaller amount of the fast anisotropy decay than for shorter wavelengths. For 380 nm excitation there is a fast initial anisotropy decay from 0.4 to 0.225 and then a slower anisotropy decay which further reduces the anisotropy to 0.15. For the 400 nm excitation there is a fast initial anisotropy decay from 0.4 to 0.27 and then a slower second decay to 0.18. For the 420 nm excitation there is a fast initial anisotropy decay from 0.38 to 0.34 and then a slower final anisotropy decay to 0.26 after 10 ps.

Table 6.1: Fitting times for the anisotropy decays. R_0 is the anisotropy at time zero, τ_1 is the first fitting time constant whilst A_1 is the pre-exponential decay factor. τ_2 is the second decay time component with A_2 being the pre-exponential decay factor, and R_{inf} is the anisotropy at 20 ps. The fitting formula is in Chapter 3 as formula 3.10.

	λ_{ex} (nm)	λ_{det} (nm)	R_o	τ_1 (fs)	A_1	τ_2 (ps)	A_2	R_{inf}
T2	380	420	0.37 (± 0.01)	415 (±27)	0.76 (± 0.04)	8.4 (± 0.33)	0.24 (± 0.01)	0.19 (± 0.001)
T4	380	440	0.39 (± 0.01)	513 (± 22)	0.67 (± 0.02)	2.9 (± 0.09)	0.33 (± 0.01)	0.15 (± 0.001)
T4	400	500	0.38 (± 0.01)	520 (± 50)	0.6 (± 0.05)	5.2 (± 0.2)	0.4 (± 0.01)	0.18 (± 0.001)
T4	420	500	0.38 (± 0.01)	520 (± 75)	0.34 (± 0.1)	7.9 (± 0.5)	0.66 (± 0.01)	0.24 (± 0.002)

From the fittings, whose values are shown in Table 6.1, one can see that the initial anisotropy for all conditions is very close to 0.4, and the initial anisotropy decay rate is similar at 415 fs for T2 and 520 fs for T4. The amplitude of this fast decay shows a

strong dependence on excitation wavelength in the T4 molecule. By changing the pump wavelength from 380 nm to 420 nm the magnitude of this decay reduces from 0.67 to 0.34. The second decay time constant also shows an excitation wavelength dependence, with higher excitation energies having a faster decay time than lower energy ones.

One possible reason for the lower than expected initial anisotropy for a C_3 symmetric molecule, is that the molecule is distorted by the polarity of the solvent, as has been suggested by Sissa et al..[30] Experiments were carried out to investigate this using cyclohexane as a comparison against the toluene results. While toluene is not a very polar solvent, only having a polarity of 2.4, it was still important to rule out solvent polarity as the cause of the symmetry breaking; cyclohexane was chosen as it has a lower polarity, of only 0.2, so is almost non polar.

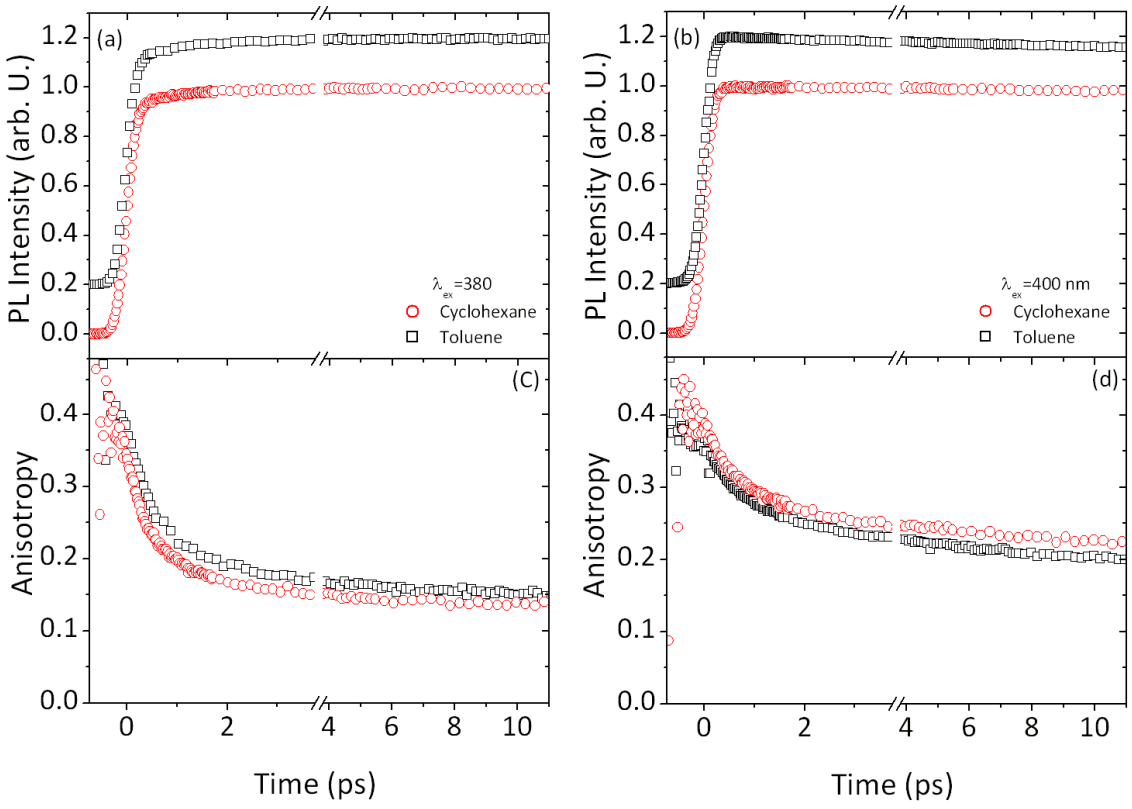

Figure 6.8: (a) shows the results for the reconstructed magic angle data for T4 pumped at 380 nm and 440 nm detection in toluene (black open squares) and cyclohexane (red open circles); (b) shows the magic angle results for 400 nm excitation and 440 detection. (c) shows the anisotropy at 380 nm excitation, whilst (d) shows anisotropy at 400 nm excitation.

The data presented in Figure 6.8 compares the anisotropy decay of T4 molecules in toluene and cyclohexane. The magic angle data for excitation at 380 nm and detection at 440 nm is shown in figure 6.8(a), whilst (b) shows it for 400 nm excitation and 440 nm detection. The anisotropy results for the 380 nm excitation are presented in (c) and those for the 400 nm excitation in (d). As can be seen from the anisotropy results, both solvents show the same characteristic of having an initial anisotropy of 0.4. The anisotropy after 10 ps is lower for cyclohexane than for toluene when excited at 400 nm, but higher when excited at 380 nm. The final anisotropy values are 0.15 at λ_{ex}=380 nm and 0.20 for λ_{ex}=400 nm in toluene and 0.14 at λ_{ex}=380 and 0.22 at λ_{ex}=400 nm in cyclohexane, showing that there is a small solvent effect. However, this effect is small and, because the molecules show similar behaviour, the initial anisotropy value cannot be explained as a result of the polarity of the solvent. This means that there must be another cause for the initial anisotropy of 0.4. The same experiments were performed on the oligofluorene as a reference, but no change in the anisotropy dynamics was observed for the oligofluorene molecules.

6.4 Discussion of results

6.4.1 Initial 0.4 anisotropy value

The fact that the anisotropy values after 10 ps are excitation wavelength dependent shows that red-edge effects are being observed. Moreover, the results show a different initial anisotropy result from the predicted value for a C_3 symmetric molecule with two degenerate energy states. The expected value for the anisotropy of a rod like molecule is 0.4, which is due to the fact that the absorption and emission dipoles are parallel.[1] Whilst for a C_3 Symmetric molecule with two degenerate states the expected initial anisotropy is 0.7,[29,31] this is due to the shape of the molecule, presenting an increased probability of the light being absorbed by the molecule. However, there have been very few experiments which observe an initial anisotropy value of 0.7, with a number of differing reasons as to why this value is not observed. One reason is that when observing the fluorescence anisotropy the degeneracy between the two levels has been broken via a Jahn-Teller type effect,[32] causing the exciton to localise onto an

arm.[33] For a C_3 symmetric molecule the final anisotropy value is predicted to be 0.1, because the exciton should have lost its coherence and moved to a random arm.[29] However, there is a problem to consider with this argument: where does the exciton need to localise for it to get this anisotropy value? If it localises on the arm closest to the direction of polarization of the excitation, then one would expect a high anisotropy value. This is because a lot of the large initial anisotropy is retained, as the change in the angle of the dipole moment would be quite small, therefore showing little depolarisation from 0.7. On the other hand if it localises on a random arm the only value that would be observed is 0.1[29,31] and one should not see the anisotropy decay in fluorescence, as it needs to be localised on an arm in order to emit. Others have claimed, along similar lines, that the 0.7 is not seen because the dephasing between the two states[33] leads to emission from a single arm;[34] this is claimed to happen so quickly that the 0.7 value is not observed as it lies beyond the time resolution of most techniques.[19]

Both these arguments are valid for some of the results, however they do not fit well with the results observed for the truxene-cored molecules. At all excitation wavelengths we observe an initial anisotropy of ~0.4, which is closer to the expected value for a rod like molecule, than the results for a localisation to the nearest or random arm would allow. Also with the relatively long ~500 fs anisotropy decay times for the truxene-cored molecules, it should be possible to observe the decay from a value greater than 0.4, as we can resolve anisotropy dynamics down to ~100 fs. One proposal for this result is that it is caused by the symmetry being already broken by interactions with polar solvents at room temperature.[30] The experimental results in this chapter show that anisotropy decays are independent of the solvent, and that there must be a means for a non-polar solvent like cyclohexane to break the symmetry. The problem with this, however, is that it is not just a simple case of breaking the symmetry; the symmetry must be broken in a way that causes a splitting between the two states to be greater than the bandwidth of the laser. If this were not fulfilled, then both modes of the molecule would be excited and it would result in a higher initial anisotropy than the 0.4 observed.

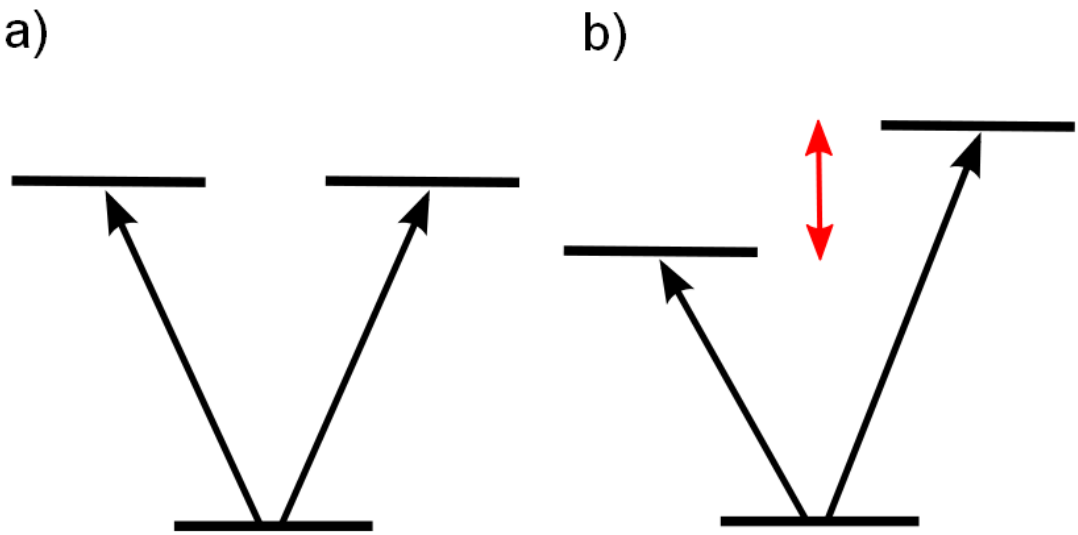

Figure 6.9 a): Schematic of the key energy levels in a degenerate system, b) shows a distorted system with different energy levels, the red arrow corresponds to the energy splitting of the two states.

Figure 6.9 shows a schematic of the relevant two lowest absorption states in a degenerate (a) and non-degenerate system (b). For the degenerate case the energy levels are identical, but for the non-degenerate system a change has been applied to the molecule to either raise or lower one or both of the energy levels. In our experiment the energy difference is represented by the red arrow, and must be considerable so that the energy level splitting is greater than the bandwidth of the laser, which has a full width half maximum of ~3 nm (~3 meV). A possible source of this energy level splitting could be conformational disorder in the molecules.

In order to test this hypothesis of conformational disorder induced splitting, a series of TD-DFT calculations were carried out using the Gaussian09 programme by our collaborators Prof Ian Galbraith and Jean-Christophe Denis at Heriot Watt University. These calculated the energy difference between the two transitions in a molecule with a specific deformation applied, as well as the energy cost of this transformation compared with the minimum energy conformation. These transformations can only be small changes to the molecular geometry, because when working at room temperature the only energy available is of the order of K_BT (26 meV).

Table 6.2: Results for the quantum chemistry calculations for conformational changes to the T2 molecule: performed by Jean-Christophe Denis and Prof. Ian Galbraith at Heriot Watt University. The formation cost is the difference between the symmetric ground state and the energy of the broken symmetry configuration. The degeneracy splitting is the difference in the two electronic energy levels and the 1st absorption state is the lowest energy transition. Cases 1-4 represent a twisting of a fluorene unit by -5°, -10°, +5° and +10° at the end of an arm. Case 5 is a twist of -10° at the beginning of an arm. Case 6 is a rotation of the fluorene unit at the end of the fluorene unit by 5° in the plane of the molecule and case 7 is a rotation of -5° out of the plane of the molecule. Case 8 corresponds to a twist of the final fluorene unit by -10° and a rotation to the same arm by -10° out of the molecular plane. Case 9 corresponds to a twist of a fluorene unit at the end of one arm by -10° and a twist to the final fluorene unit in another arm by +10°.

Case	Formation Cost (meV)	Degeneracy Splitting (nm)	1st Absorption (nm)
1	7	1.96	369.95
2	15	3.98	372.01
3	18	3.24	367.88
4	29	4.41	367.85
5	16	4.87	373.21
6	50	0.19	367.95
7	16	1.19	369.16
8	62	7.11	375.39
9	30	6.2	371.66

Table 6.2 presents the energy cost and the relative splittings for a number of different conformational changes applied to a T2 molecule. The types of molecular deformations were chosen to represent real world possibilities that could occur within

a molecule at room temperature, under normal conditions. For example, it would be possible to completely rotate an arm; however the energy cost for this would be very high, but would only present a small change in the electronic energy levels between the two states. For the calculations the two situations considered are a twist to a fluorene unit within the chain and a movement of a fluorene unit out of the plane by a set angle. This is represented in cases 6 and 7. Thus for the truxene-cored molecules any distortion to the molecule that causes a sufficient energy splitting between the two energy levels to break the symmetry must be a small conformational change rather than a large distortion. From the results, the cases that fit the description of providing a splitting of more than 5 nm with only a small energy cost are those which twist one of the fluorene molecules within the arm as shown in cases 1-5. If this is applied to 2 of the arms, as is shown in case 9, then it is easily possible to produce the required splitting of 6.2 nm, at energy of 30 meV.

Table 6.2 shows that for certain cases there is enough thermal energy at room temperature to get the required energy splittings between the two energy levels, so that a spectrally narrow laser beam on a short time scale would only excite a single mode within the molecule rather than a mixture of both modes. Due to these small conformational changes, the molecule starts to behave more rod like, as only one rather than both of the transition dipoles is excited. As there is only a single dipole being excited the photophysical properties are dominated by the orientation of the excited chromophore rather than that of the entire molecule, which would be the case for a completely C_3 symmetric system.

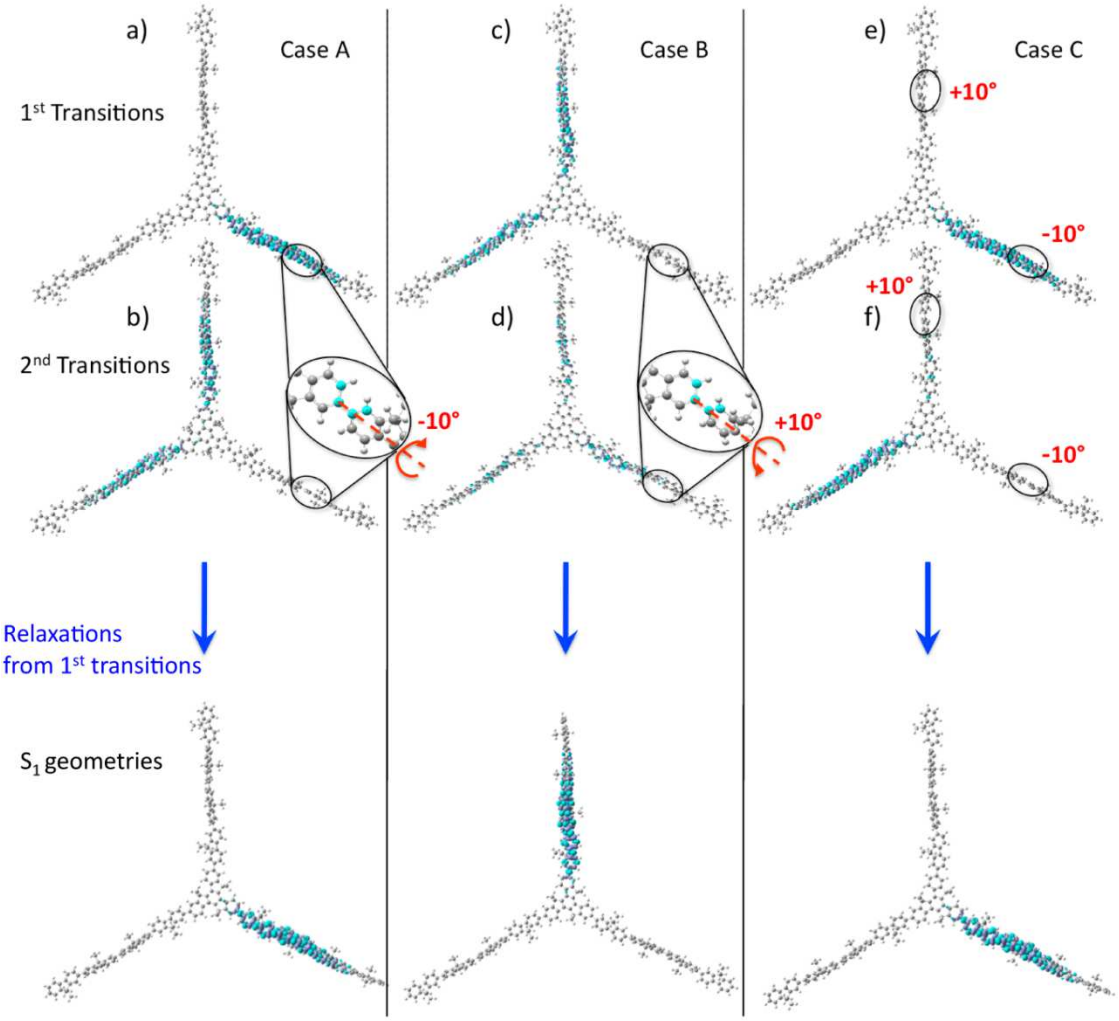

Figure 6.10: Change of the electron density upon photoexcitation of T4, with rotational twists slightly breaking their symmetry. Case A corresponds to a rotational twist clockwise of 10° of the 3rd fluorene unit. Case B represents an anti-clockwise twist of 10° of the third fluorene unit and Case C combines cases A and B. Below the absorption transitions are the S_1 emission geometries for the lowest energy transitions. Reproduced from Ref. 35 with permission from the PCCP owner society. [35]

Calculations were performed for three separate cases of applied twists to the T4 molecules and the electron densities plotted, as shown in Figure 6.10. In Case A the dihedral angle between the second and third fluorene units in one arm was increased, and reduced in Case B by 10^{o}. Case C shows the effect of having the two twists applied to two arms of the molecule. In Case A the energy cost of this transformation to the molecule is 20 meV and leads to a splitting of 4.2 nm of the two optically bright lowest energy transitions. As a result of this twist the first absorption state is at 3.157 eV,

which is lower than in the fully symmetric state and leads to emission being localised on this distorted arm. The reason why the energy of the arm is lower for this type of distortion is that, by increasing the angle of one of the fluorene units, the arm becomes more planar and the π-conjugation is increased. The second transition on this molecule is at 3.191 eV and leads to localisation on the two non-distorted arms. This transition closely resembles one of the two transitions observed in a fully symmetric molecule. In Case B, where the angle of the third fluorene unit within an arm has been increased by $+10^{o}$, such that the dihedral angle increases, and the π-conjugation between the two fluorene units get reduced. The first transition shown in Figure 6.10(c) is at 3.191 eV, and excites the two undistorted arms. The second transition, Figure 6.10(d), which is mainly localised on the distorted arm, has an even higher energy of 3.214 eV. The cost of this symmetry breaking is 18 meV and leads to a splitting of 2.7 nm. If we combine these two distortions on two separate arms of the same molecule, as is shown in Case C, then the first absorption state has an energy of 3.159 eV, and the exciton is localised on the more planar arm, Figure 6.10(e). In the second absorption transition, the exciton is mainly localised on the undistorted arm with a small contribution on the distorted arm, Figure 6.10(f). The energy of this transition is 3.207 eV, the total cost of these two distortions is 30 meV and the resulting splitting is 5.9 nm. Below each of the two absorption transitions the emission geometries are shown, and as can be seen, for all the different distortions the exciton in emission is localised on a single arm.

6.42Anisotropy decay

All the truxene-cored molecules show a bi-exponential decay of the anisotropy with a fast first decay and a slower second. As outlined in the introduction a picosecond anisotropy decay has been attributed to a Förster energy transfer mechanism. To investigate this, calculations of the energy transfer were performed using two different models. Firstly we approached it from a classical Förster point dipole-dipole coupling calculation using:[36,37]

$$k^{Förster} = \frac{1}{\tau_D}\frac{9000(ln10)\kappa^2\phi_D I}{128\pi^5 N_A n^4}\frac{1}{R^6} \qquad (6.3)$$

Where τ_D is the donor lifetime, ϕ_D is the donor fluorescence quantum yield, N_A is Avogadro's number, n is the refractive index of the solvent, which for this experiment was toluene giving $n = 1.50$, I is a spectral overlap between the homogeneous spectral profiles of donor fluorescence $f^{hom}(E)$ and acceptor absorption $a^{hom}(E)$, which have each been normalised to unit area on an energy scale, $I = \int_0^{E_{max}} f^{hom}(E) a^{hom}(E)\, dE$ and E_{max} is the upper energy of the vibronic progression in $S_1 \leftarrow S_0$ absorption, calculated from the steady state absorption and emission spectra, and R is the centre-to-centre separation. The calculation of the separation R between the two arms was chosen to be from a point at the centre of one arm to a point at the centre of another arm. This separation was calculated geometrically from the bond lengths of the molecule. For the two materials this produced an expected energy transfer decay time of 13 ps and 54 ps for T2 and T4 respectively. The calculated decay time for T4 is much larger than that of T2 and too large for T4; experimental results are shown in Table 6.1. This is because this formula underestimates the coupling strength between the arms in the molecule, because of the R^6 dependence. This shows that as these coupled molecules get larger arms one has to move beyond a point dipole coupling approximation.

Thus a second approach was employed using a weak coupling calculation, because this has been found to provide a better description of complex donor acceptor systems; where the interaction between the excited state donor and ground state acceptor are purely due to electronic coupling.[38,39] Calculations of the rate of energy transfer in a weak coupling system can be made by:[36]

$$\frac{1}{\tau_{RET}} = \frac{2\pi}{\hbar} |s \cdot V|^2 J \qquad (6.4)$$

where V is the electronic coupling energy between donor and acceptor chromophores and s is the dielectric screening of the interaction by the surrounding medium. We use $s = 1/n^2$, where $n=1.5$ is the refractive index of the solvent, which follows from the dipole approximation, J is the spectral overlap and is calculated in the same way as for the Förster point dipole calculation. The electronic coupling V between the arms of molecules was determined as $V=(E_3-E_1)/3$, where E_1 and E_3 are the transition energies

from ground state to the lowest energy excited state S_1 and to the dark state S_3 respectively calculated using DFT in the ground state geometry. This approach resulted in a similar value for the decay time for the T2 of 15 ps, however a much shorter decay time was obtained for the T4 molecule of 8 ps.

Table 6.3: Parameters used in the calculation of the energy transfer rate using equation 6.4. V is the electronic coupling calculated from the excited state splitting potential from the DFT calculations performed. J is the spectral overlap, τ_{RET} is the calculated resonant energy transfer values, with the values for the Förster calculations in parenthesis. τ_1 and τ_2 are the fitted times for the first and second exponentials for the anisotropy decays.

Molecule	V (meV)	J (meV^{-1})	τ_{RET} (ps)	τ_1 (ps)	τ_2 (ps)
T2	23 (25)	0.063	15 (13)	0.4	8.3
T4	25 (10)	0.10	8 (54)	0.5	5

The results in Table 6.3 show that using the weak coupling formula produces a better description of the observed energy transfer rate rather than using a point dipole Förster equation. As can be seen, the time for the resonant energy transfer in the Förster equation is far too long; this is because of the R^6 dependence in the point dipole calculation. As a result of this term this method underestimates the coupling strength between the arms and produces a much longer transfer time for T4 than that measured. For T2 however where the separation between the point dipoles is much smaller than for T4, the point dipole approach provides a similar result to the calculated weak coupling time; although both results underestimate the coupling strength between the arms in the T2 molecule. Using the weak coupling approach also predicts T4 to have a shorter decay time than T2, which agrees with the experimental results. These calculations show that the second decay component can be explained as being the result of a weakly coupled resonant energy transfer process between two of the molecules arms.

Using these calculations, assignments can be made as to the nature of the decay processes. Presented above is an outlined description of what is occurring to the molecule in terms of symmetry breaking and parts of the energy transfer. Before excitation, the symmetry is already broken, giving a rod like initial anisotropy. The 500

fs decay is caused by a fast reorientation of the emission dipole moment from the absorption one, resulting from adiabatic geometry changes within the molecule, as the exciton localises on a single arm. The second decay is a weakly coupled energy transfer process between the arms.

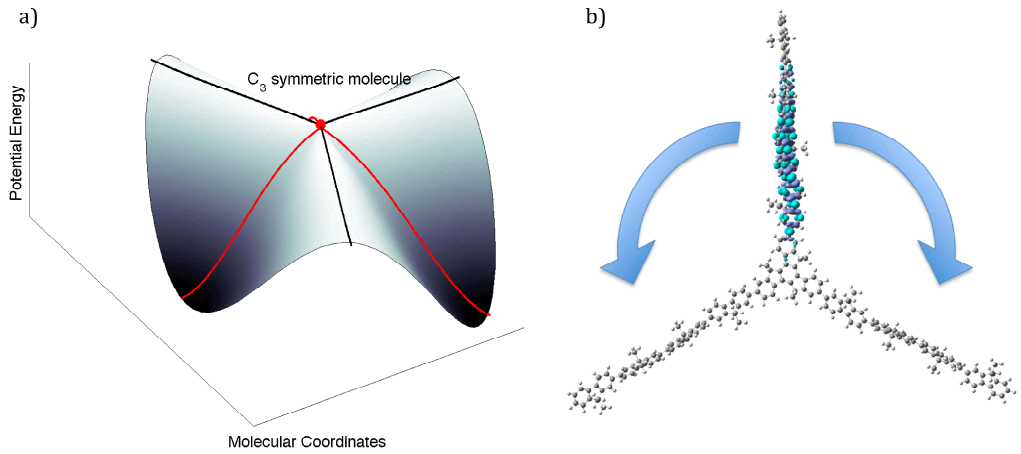

Figure 6.11: Illustrates the two decay mechanisms present within a truxene molecule, on two different timescales. (a) Shows the excited state potential energy surface of a symmetric three armed molecule, movement down this after absorption corresponds to the 500 fs decay. (b) is an illustration of the Förster-type resonant energy transfer hoping, from arm to arm, which occurs on a 3-10 ps timescale. Reproduced from Ref. 35 with permission from the PCCP owner society. [35]

In a perfectly symmetric molecule the potential energy surface (PES) of the molecule resembles a so called “Mexican hat”. This is shown in Figure 6.11. When excited with a high energy photon, the molecule resides close to the top of the potential energy surface, marked by the red dot, from here it then has to find a path to a local minima. This proposal of a Mexican hat type PES for C_3 symmetric molecule was made by Terenziani et al.[40] whose study describes the symmetry breaking effects caused by polar solvents on C_3 symmetric octupolar molecules. In non-polar solvents the lowest excited state was found to have a PES with three equal minima corresponding to the arms of the molecule. When interacting with a polar solvent a symmetry breaking defect occurs to change the energy of one of the three arms and thus raises or lowers one of the minima on the PES so that it is no longer symmetric. Our system is

qualitatively similar with the potential energy surface having three potential minima corresponding to the arms. The image provided in Figure 6.11(a) is only an illustrative sketch of the surface for a symmetric molecule as any distortion to the molecule, like those calculated above, would distort this surface and cause a change to one of the local energy minima, which will affect the final state of the molecule. From the point at which a photon is absorbed by the molecule, it will begin travelling down its potential energy surface to the emitting point localised on one of the arms.

This description fits well with the experimental results, because when we use a high energy excitation (380 nm for T4) there is a large amount of depolarisation, as the photon excites the molecule near the top of the potential energy surface. This results in many potential downhill pathways, which the molecule can travel down to the localised emitting state. The TD-DFT results show that the higher energy absorption states are often spread over a greater proportion of the molecule, covering more than a single arm of the molecule, as shown in Figure 6.10. This state then quickly localises to an emission state on a single arm, which corresponds to the fast ~500 fs decay. On the other hand, when exciting into the very tail of the T4 low energy absorption at 420 nm, we are already exciting close to the lowest energy state. The TD-DFT calculations show that these lower energy absorption transitions are typically localised on a single arm, which means that there is less chance of the localisation moving quickly to another arm. It is also less likely for the molecule to have a lower energy arm available, to which the exciton can resonantly energy transfer to. As a result of this it is more difficult for the exciton to transfer from that arm to a lower energy one, so less depolarisation is observed. This is reflected in the anisotropy decay values in Table 6.1, where the higher the excitation energy, the greater the amount of initial fast decay and also the faster the second energy transfer process.

The depolarisation mechanisms obviously come in two forms: there is the initial 500 fs localisation, which probably is a localisation transition onto a single arm, and then there is the 3-10 ps transition, caused by resonant energy transfer from one arm to another. This first energy transfer process is far slower than that reported for complexes with nitrogen cores, where the fast energy transfer happens over a period of ~50 fs.

6.5 Conclusion

This work has provided important information about the energy transfer process within an important family of materials. The study used upconversion photoluminescence anisotropy measurements to observe the inter arm energy transfer within star-shaped truxene-cored oligofluorene molecules. The results show an initial anisotropy of 0.4, which is expected for a rod like molecule, but not for a C_3 molecule with two degenerate energy states. This symmetry breaking and the resultant energy level splitting has been shown to be independent of solvent polarity. To provide further information on the experimental results a series of TD-DFT calculations were performed to investigate molecular deformations and the resultant splitting of the energy levels. These indicate that small thermal deformations can break the symmetry within the molecule, and cause a splitting between the two absorption transitions, greater than the bandwidth of the laser pulse. The calculations show that a combination of small twists to the fluorene units on the arms of the molecule would be the most probable deformation capable of producing the required splitting. The fact that these deformations require energies less than k_BT at room temperature shows that these could happen due to interactions with the solvent molecules.

Unlike the oligofluorene molecules, both truxene-cored molecules show a fast bi-exponential anisotropy decay, indicating energy transfer within the molecule. This energy transfer process has two different mechanisms which have two separate timescales. The majority of the anisotropy decay happens during the first decay which happens on ~500 fs timescale. This is argued to be a fast localisation onto a low energy single arm from a higher energy absorbing state. The second decay mechanism occurs on a 3-10 ps timescale, and is consistent with a weakly coupled resonant energy transfer between arms. The amount of anisotropy decay has been found to be highly dependent upon the excitation wavelength.

The results present a strong red-edge effect, with less decay observed when exciting at 420 nm than 380 or 400 nm. This can be explained by the nature of the decay: when exciting near the absorption maxima one excites the molecule to near the peak of its potential energy surface, allowing for a greater number of relaxation pathways.

However, if one excites in the tail of the absorption, which is near a local minimum, there are fewer relaxation pathways available for the molecule, resulting in the exciton staying on the absorbing arm.

6.6 References

1 Lackowicz, J. *Principles of Fluorescence Spectroscopy* third edition, Chapter 10 353 - 364 (Springer).

2 Kanibolotsky, A. L., Perepichka, I. F. & Skabara, P. J. Star-shaped pi-conjugated oligomers and their applications in organic electronics and photonics. *Chem. Soc. Rev.* **39**, 2695-2728, doi:10.1039/b918154g (2010).

3 Burn, P. L., Lo, S. C. & Samuel, I. D. W. The development of light-emitting dendrimers for displays. *Adv. Mater.* **19**, 1675-1688, doi:10.1002/adma.200601592 (2007).

4 Lo, S.-C. & Burn, P. L. Development of Dendrimers: Macromolecules for Use in Organic Light-Emitting Diodes and Solar Cells. *Chem. Rev.* **107**, 1097-1116, doi:10.1021/cr050136l (2007).

5 Drobizhev, M., Karotki, A., Rebane, A. & Spangler, C. W. Dendrimer molecules with record large two-photon absorption cross section. *Opt. Lett.* **26**, 1081-1083 (2001).

6 Bar-Haim, A., Klafter, J. & Kopelman, R. Dendrimers as Controlled Artificial Energy Antennae. *Journal of the American Chemical Society* **119**, 6197-6198, doi:10.1021/ja970972f (1997).

7 Goodson, T. G. Optical Excitations in Organic Dendrimers Investigated by Time-Resolved and Nonlinear Optical Spectroscopy. *Accounts of Chemical Research* **38**, 99-107, doi:10.1021/ar020247w (2004).

8 Wasielewski, M. R. Self-Assembly Strategies for Integrating Light Harvesting and Charge Separation in Artificial Photosynthetic Systems. *Accounts of Chemical Research* **42**, 1910-1921, doi:10.1021/ar9001735 (2009).

9 Kopelman, R. *et al.* Spectroscopic Evidence for Excitonic Localization in Fractal Antenna Supermolecules. *Physical Review Letters* **78**, 1239-1242 (1997).

10 Tsiminis, G. *et al.* Low-threshold organic laser based on an oligofluorene truxene with low optical losses. *Appl. Phys. Lett.* **94**, doi:24330410.1063/1.3152782 (2009).

11 Tsiminis, G. *et al.* Two-photon absorption and lasing in first-generation bisfluorene dendrimers. *Adv. Mater.* **20**, 1940-+, doi:10.1002/adma.200702498 (2008).

12 Wang, Y. *et al.* Broadly tunable deep blue laser based on a star-shaped oligofluorene truxene. *Synth. Met.* **160**, 1397-1400, doi:10.1016/j.synthmet.2010.04.016 (2010).

13 Ruseckas, A. & Samuel, I. D. W. Exciton self-trapping in MEH-PPV films studied by ultrafast emission depolarization. *physica status solidi (c)* **3**, 263-266 (2006).

14 Ruseckas, A. *et al.* Ultrafast depolarization of the fluorescence in a conjugated polymer. *Phys. Rev. B* **72**, 115214 (2005).

15 Grage, M. M. L. *et al.* Conformational disorder and energy migration in MEH-PPV with partially broken conjugation. *J. Chem. Phys.* **118**, 7644-7650, doi:10.1063/1.1562190 (2003).

16 Varnavski, O. *et al.* Ultrafast polarized fluorescence dynamics in an organic dendrimer (vol 77, pg 1120, 2000). *Appl. Phys. Lett.* **78**, 3749-3749 (2001).

17 Varnavski, O. P. *et al.* Coherent Effects in Energy Transport in Model Dendritic Structures Investigated by Ultrafast Fluorescence Anisotropy Spectroscopy. *Journal of the American Chemical Society* **124**, 1736-1743, doi:10.1021/ja011038u (2002).

18 Varnavski, O., Leanov, A., Liu, L., Takacs, J. & Goodson, T., III. Femtosecond luminescence dynamics in a nonlinear optical organic dendrimer. *Phys. Rev. B* **61**, 12732-12738 (2000).

19 Varnavski, O., Goodson, T., Sukhomlinova, L. & Twieg, R. Ultrafast Exciton Dynamics in a Branched Molecule Investigated by Time-Resolved Fluorescence,

Transient Absorption, and Three-Pulse Photon Echo Peak Shift Measurements†. *The Journal of Physical Chemistry B* **108**, 10484-10492, doi:10.1021/jp0495996 (2004).

20 Lahankar, S. A. *et al.* Electronic interactions in a branched chromophore investigated by nonlinear optical and time-resolved spectroscopy. *The Journal of Chemical Physics* **120**, 337-344 (2004).

21 Latterini, L., De Belder, G., Schweitzer, G., Van der Auweraer, M. & De Schryver, F. C. Femtosecond polarized transient absorption spectroscopy of a C3-symmetric amino-substituted phenylbenzene derivative. *Chem. Phys. Lett.* **295**, 11-16, doi:10.1016/s0009-2614(98)00930-0 (1998).

22 Verbouwe, W., Van der Auweraer, M., De Schryver, F. C., Piet, J. J. & Warman, J. M. Excited State Localization or Delocalization in C3-symmetric Amino-substituted Triphenylbenzene Derivatives. *Journal of the American Chemical Society* **120**, 1319-1324, doi:10.1021/ja9725615 (1998).

23 Poliakov, E. Y., Chernyak, V., Tretiak, S. & Mukamel, S. Exciton-scaling and optical excitations of self-similar phenylacetylene dendrimers. *The Journal of Chemical Physics* **110**, 8161-8175 (1999).

24 Varnavski, O. *et al.* Investigations of excitation energy transfer and intramolecular interactions in a nitrogen corded distrylbenzene dendrimer system. *The Journal of Chemical Physics* **116**, 8893-8903 (2002).

25 Jimenez, R., Dikshit, S. N., Bradforth, S. E. & Fleming, G. R. Electronic Excitation Transfer in the LH2 Complex of Rhodobacter sphaeroides. *The Journal of Physical Chemistry* **100**, 6825-6834, doi:10.1021/jp953074j (1996).

26 Montgomery, N. A. *et al.* Optical Excitations in Star-Shaped Fluorene Molecules. *The Journal of Physical Chemistry A* **115**, 2913-2919, doi:10.1021/jp1109042 (2011).

27 Kanibolotsky, A. L. *et al.* Synthesis and Properties of Monodisperse Oligofluorene-Functionalized Truxenes: Highly Fluorescent Star-Shaped Architectures. *Journal of the American Chemical Society* **126**, 13695-13702, doi:10.1021/ja039228n (2004).

28 Soutar, I., Swanson, L., Imhof, R. E. & Rumbles, G. Synchrotron-generated time-resolved fluorescence anisotropy studies of the segmental relaxation of poly(acrylic acid) and poly(methacrylic acid) in dilute methanolic solutions. *Macromolecules* **25**, 4399-4405, doi:10.1021/ma00043a024 (1992).

29 Wynne, K. & Hochstrasser, R. M. Coherence effects in the anisotropy of optical experiments. *Chem. Phys.* **171**, 179-188, doi:10.1016/0301-0104(93)85142-u (1993).

30 Sissa, C., Painelli, A., Blanchard-Desce, M. & Terenziani, F. Fluorescence Anisotropy Spectra Disclose the Role of Disorder in Optical Spectra of Branched Intramolecular-Charge-Transfer Molecules. *The Journal of Physical Chemistry B* **115**, 7009-7020, doi:10.1021/jp2027274 (2011).

31 Gurzadyan, G. G., Tran-Thi, T.-H. & Gustavsson, T. Time-resolved fluorescence spectroscopy of high-lying electronic states of Zn-tetraphenylporphyrin. *The Journal of Chemical Physics* **108**, 385-388 (1998).

32 Jahn, H. A. & Teller, E. Stability of Polyatomic Molecules in Degenerate Electronic States. I. Orbital Degeneracy. *Proceedings of the Royal Society of London. Series A - Mathematical and Physical Sciences* **161**, 220-235, doi:10.1098/rspa.1937.0142 (1937).

33 Galli, C., Wynne, K., LeCours, S. M., Therien, M. J. & Hochstrasser, R. M. Direct measurement of electronic dephasing using anisotropy. *Chem. Phys. Lett.* **206**, 493-499, doi:10.1016/0009-2614(93)80174-n (1993).

34 Cho, H. S. *et al.* Excitation Energy Transport Processes of Porphyrin Monomer, Dimer, Cyclic Trimer, and Hexamer Probed by Ultrafast Fluorescence

Anisotropy Decay. *Journal of the American Chemical Society* **125**, 5849-5860, doi:10.1021/ja021476g (2003).

35 Montgomery, N. A. *et al.* Dynamics of fluorescence depolarisation in star-shaped oligofluorene-truxene molecules. *Phys. Chem. Chem. Phys.* **14**, 9176-9184 (2012).

36 Scholes, G. D. LONG-RANGE RESONANCE ENERGY TRANSFER IN MOLECULAR SYSTEMS. *Annual Review of Physical Chemistry* **54**, 57-87, doi:doi:10.1146/annurev.physchem.54.011002.103746 (2003).

37 Förster, T. Zwischenmolekulare Energiewanderung und Fluoreszenz. *Annalen der Physik* **437**, 55-75, doi:10.1002/andp.19484370105 (1948).

38 Hennebicq, E. *et al.* Exciton Migration in Rigid-Rod Conjugated Polymers: An Improved Förster Model. *Journal of the American Chemical Society* **127**, 4744-4762, doi:10.1021/ja0488784 (2005).

39 Hukka, T. I. *et al.* Pathways for Resonant Energy Transfer in Oligo(phenylenevinylene)–Fullerene Dyads: An Atomistic Model. *Adv. Mater.* **18**, 1301-1306, doi:10.1002/adma.200600155 (2006).

40 Terenziani, F., Sissa, C. & Painelli, A. Symmetry Breaking in Octupolar Chromophores: Solvatochromism and Electroabsorption. *The Journal of Physical Chemistry B* **112**, 5079-5087, doi:10.1021/jp710241g (2008).

7

Lasing characteristics of benzene-cored star-shaped oligofluorenes

7.0 Introduction

This chapter will present the lasing results from a family of benzene-cored star-shaped oligofluorene molecules. This work studies the relationship between changing the molecular size and the lasing performance. The work finds that increasing the arm length of the molecules causes a redshift of the absorption and emission spectra and also increases the solid state photoluminescence quantum yield (PLQY). This corresponds to a reduction in the threshold for the onset of amplified spontaneous emission (ASE). The materials were then spun onto distributed feedback gratings to assess their laser performance; it was found that as the arm length increases there is a reduction in the power density required for lasing and that the family are broadly tunable from 402-462 nm. The lasers were also found to have a small divergence, low lasing thresholds of 1.1 kW/cm^2 and efficiencies as high as 6.6%. The lasing performance of these molecules will be compared against the published lasing values and photophysical results for a similar family of oligofluorene molecules with truxene cores. This comparison investigates which criteria are important for low threshold organic lasers, and finds that high PLQY and a reduction in intermolecular interactions are both important features.

Section 7.1 introduces the materials used in organic lasers as well as their results and performance. Section 7.2 presents the solid state photophysical properties of the molecules, by looking at absorption, emission and PLQY of the molecules. Section 7.3 analyses the results of the ASE experiments, which provide a good indication of laser performance and looks at ASE thresholds, and at the material's gain and loss. Section 7.4 presents the lasing

results for the molecules looking at lasing thresholds, tunability and efficiencies. Section 7.5 discusses the results and compares these to the lasing and photophysical results for the truxene-cored molecules, in order to identify what characteristics are required for a low threshold organic laser. Finally section 7.6 concludes the study. The work in this study was performed with the assistance of Dr Georgios Tsiminis.

7.1 Organic semiconductor lasers

The field of organic semiconductor lasers has grown massively over the last two decades, since the first solid state organic semiconductor laser was produced by Tessler et al..[1] The mechanisms and resonator design of organic semiconductor lasers was included in Chapter 2, whilst this section presents the important attributes of the gain media. A more detailed account of organic lasers can be found in several review papers.[2-4] At present all organic semiconductor lasers are optically pumped, but the size of required pump sources has decreased from large regenerative amplifiers to small inorganic Gallium Nitride LEDs.[5-7] Due to this reduction in size, organic semiconductor lasers are seen as an important technology[3] for lab on chip type devices,[8] especially in spectroscopy and sensing.[9] A particularly promising application of organic laser sensors is in explosive sensing, where sensitivities to TNT derivatives has found to be as high as 5 ppb.[10]

Since just after the invention of the laser, organic materials have been used as laser gain materials, with dye lasers becoming a well-established technology.[11] These had the advantage of broad tunability and very short pulse lengths, but because they had to be used in dilute solution meant that relatively compact lasers could not be produced. The problem with using organic dyes as a laser gain material in the solid state is that they have low PLQYs, and as such have to be doped into a host matrix.[12] The reason why dyes have low solid state PLQYs is that there are large intermolecular interactions, and they also have a tendency to form dimers. This poor performance of dyes led to the development of a number of different classes of organic materials for lasers, such as polymers, small molecules and dendrimers. Each of these materials have their own different set of characteristics which will be further explored, but they all present one advantage over traditional organic dyes, in that they have high PLQYs in the neat film.[2] This is a huge advantage for organic materials used in lasers, because it means that they can be processed as neat films. Also due to their

high absorption cross sections, solid state organic lasers can display high gains in a very short path length.

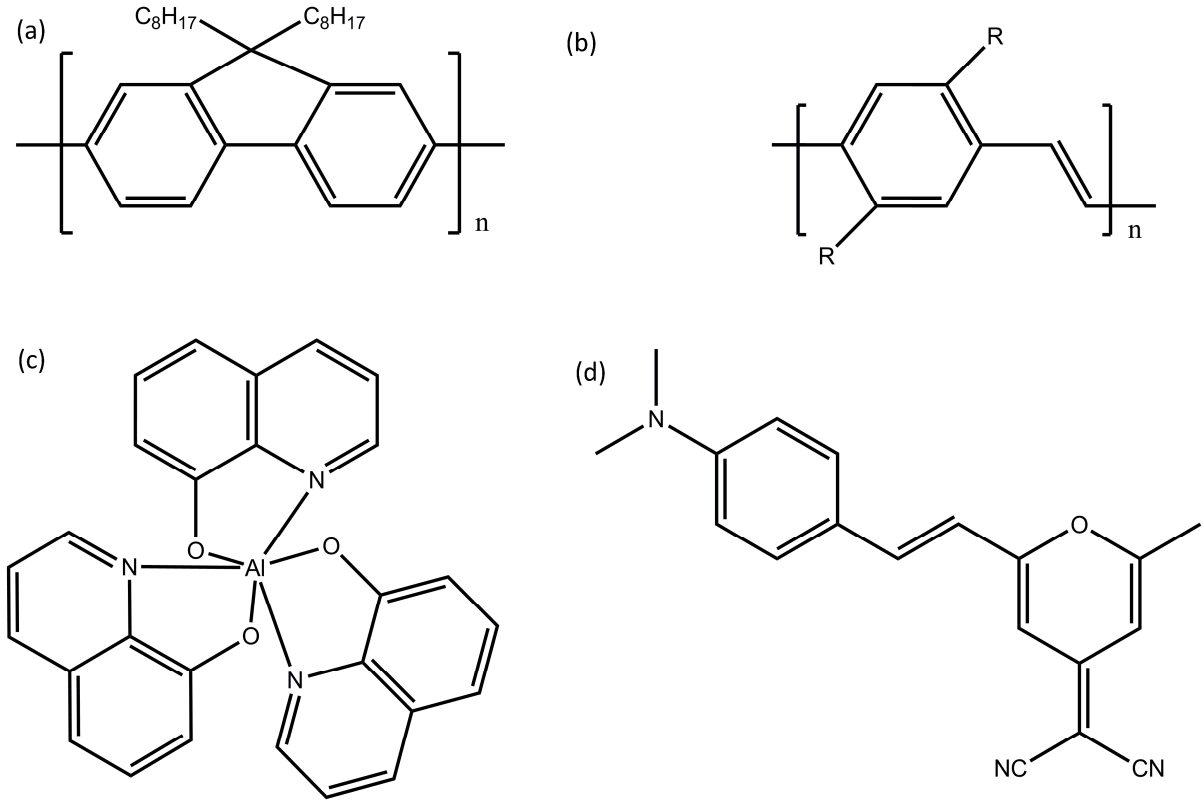

Figure 7.1: (a) Structure of polyfluorene (PFO), (b) poly(para-phenylene vinylene) (PPV) derivative, (c) aluminium tris(quinolate) (Alq_3) and (d) 4(dicyanomethylene)-2-methyl-6p-(dimethylaminostyryl)-4H-pyran (DCM)

Conjugated polymers were used in the first solid state organic semiconductor laser.[1] Since then the two main polymer families which have been studied are polyfluorenes[13,14] and poly(phenylene vinylyene)s.[1,15,16] This is because they both possess high solid state PLQYs and have been reported to have high gains and low lasing thresholds. Other advantages of using these materials are that they are commercially available and can be fabricated via simple solution processing techniques, allowing for low cost fabrication. With the use of two dimensional distributed feedback (DFB) structures, MEH-PPV[17] and polyfluorene[18] lasers have reported slope efficiencies of ~7 and ~10% respectively. These results imply that relatively efficient lasers can be made using organic materials as the gain medium.

As well as conjugated polymers, small molecules have also been used. Aluminium tris(quinolate) (Alq_3) doped with lower energy laser dyes such as DCM and DCM2 are popular material systems. In these systems the absorption occurs in the Alq_3 and then there

is a Förster resonant energy transfer to the acceptor material.[19] Lasers using these materials have been found to have relatively low thresholds of 15 kW/cm^2 and a tunability from 597.8 nm to 713.1 nm.[20] The downside of using these materials is that they have to be thermally evaporated, which makes the laser fabrication more intensive than their solution processable counterparts.

Other small molecules which can be solution processable have also been studied in the form of dendrimers.[21-23] These molecules have a modular design where different parts can be incorporated for different processes, such as adjusting the level of interaction between the dendrons and the core. Typically in a dendrimer the arms can be used for absorption, after which there is a subsequent energy transfer to the core for emission. These types of materials have also been found to be able to lase via a two photon absorption process.[21]

Another category of small molecules is the star-shaped molecules,[24] whose photophysical advantages were highlighted in chapters 2 and 5 of this document. A three armed truxene-cored oligofluorene molecule was found to be a very good lasing material possessing low thresholds and losses.[25-27] The T3 molecule with 3 fluorene unit arms was also found to be broadly tunable over a range of 25 nm from 428-453 nm.[25]

As can be seen from this brief overview there is considerable interest in organic semiconductor lasers with a large variety of suitable materials. Star-shaped molecules are ideal to study the lasing properties and performance in relation to the molecular structure, because they have a well-defined structure whose size can be increased in a controlled way. This means that a study can be performed on a family of molecules and the difference analysed.

This chapter will investigate another family of star-shaped molecules. These have a central benzene-core, with three oligofluorenes arms attached to the meta positions of the central benzene ring. This study investigates the photophysical properties of this family by measuring their absorption, emission and PLQY. It will then cover the ASE results which are used to study the gain and loss of the material without the presence of a laser cavity. The lasing properties will then be measured, when spun onto 1 and 2D DFB gratings. These results will then be compared with those of truxene-cored molecules to provide an insight into what are desirable characteristics in organic semiconductor lasers.

7.2 Solid state photophysics

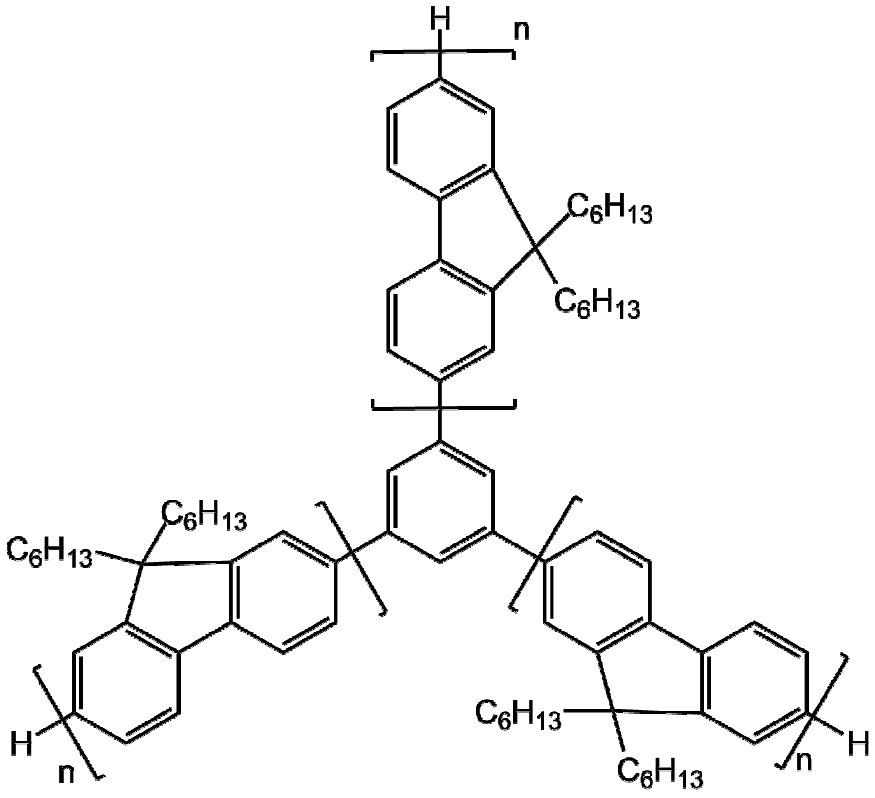

Figure 7.2: Structure of the benzene cored molecule, n=1-4 for this study.

The materials in this study are the same ones which were studied in Chapter 5. They have a central benzene core with three fluorene arms connected via the meta positions, as shown in Figure 7.2. The materials were synthesised at Strathclyde University by Prof Peter Skabara and Dr Alexander Kanibolotsky, and by Prof Igor Perepichka at Bangor University. The films were prepared in toluene obtained from Sigma Aldrich, at concentrations of 20 $mgml^{-1}$. These solutions were then spun onto glass or quartz slides for the photophysical and ASE measurements and onto distributed feedback gratings for the lasing measurements. The films were spun at between 1000 and 2000 rpm, to produce films between 100 and 150 nm thick.

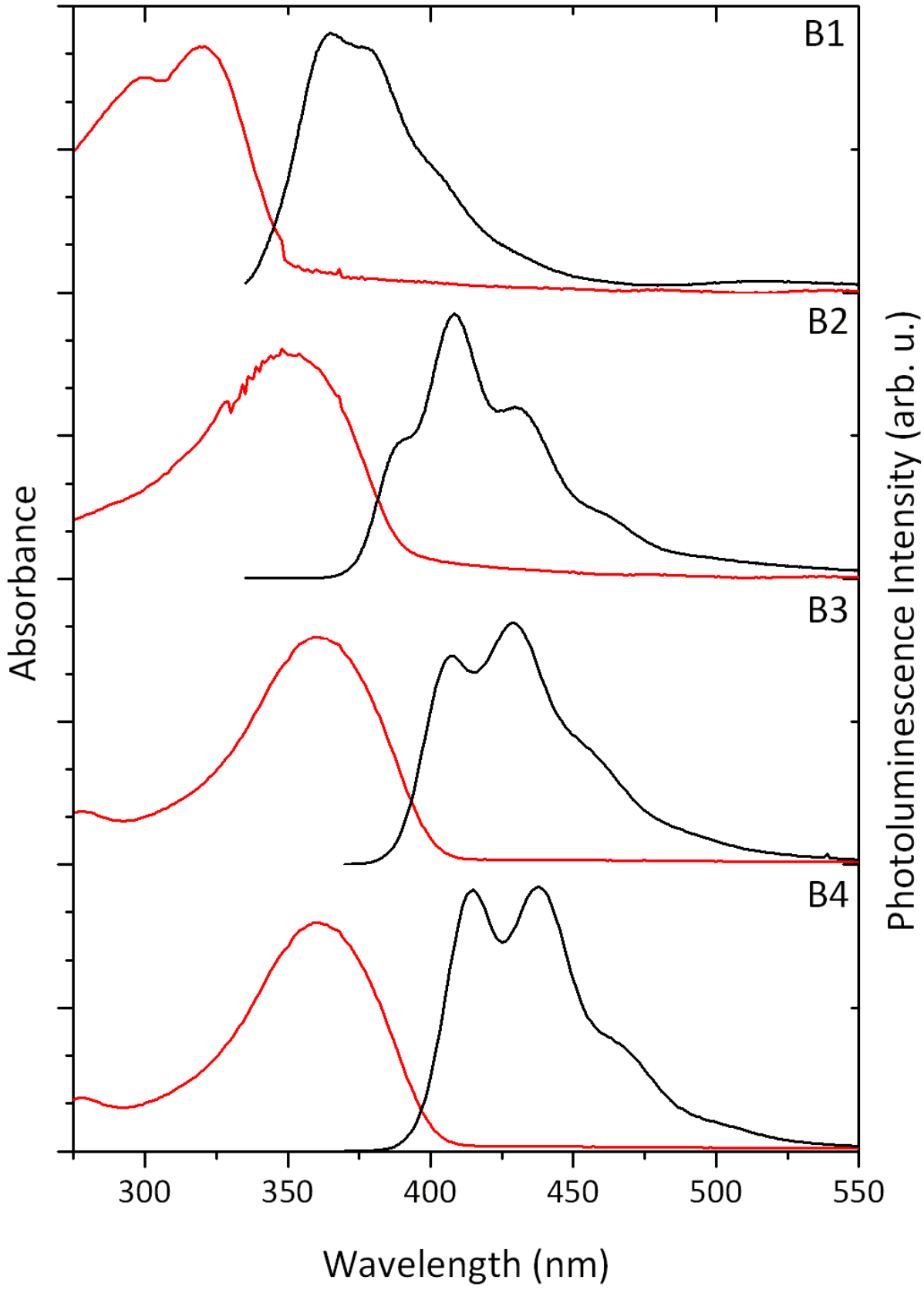

Figure 7.3: Solid state absorption (red line) and emission spectrum (black line) of all the benzene cored molecules in this study.

Figure 7.3 shows the solid-state absorption and emission spectra of the benzene-cored molecules with 1-4 repeat fluorene unit arm lengths. The results show that as the arm length increases the absorption and emission spectra are redshifted and the 0-0 peak become more dominant in photoluminescence. This mirrors the same observed features in solution, as seen in Figure 5.3. All molecules apart from B1 show an absorption peak close to 355 nm, which makes them ideal materials to be pumped using the 3rd harmonic from an neodymium yttrium aluminium garnet (ND:YAG) laser.

The film PLQY data for all the molecules are presented in table 7.1. The PLQY was measured using the Greenham method[28] outlined in Chapter 3. The value of 55% for the B4 molecule is similar to the reported values of 50% for polyfluorene,[29] and only slightly larger than the 47% of B3. These PLQY values agree well with those reported by Zhou et al..[30] There is a clear trend of increasing PLQY with increasing arm length. This is similar to what was observed in the solution measurements from Chapter 5, but with lower absolute values of PLQY in particular for B3 and B4. The PLQY increases from 40-55% between two to four repeat fluorene units.

Table 7.1: Photophysical and lasing result for the benzene-cored molecules

	Solution PLQY (%)	Film PLQY	Emission Dipole (eÅ)	Optical gain (cm^{-1})	Waveguide losses (cm^{-1})	Lasing threshold (kW/cm^2)	Slope efficiency (%)
B1	36	…	0.3	…	…	…	…
B2	58	40	2.3	18.2 ± 1.2	5.0 ± 0.6	2.9 ± 0.6	3.0 ± 0.5
B3	83	47	3.3	21.6 ± 2.1	4.4 ± 0.2	1.1 ± 0.2	5.0 ± 0.4
B4	86	55	3.7	19.6 ± 0.7	3.9 ± 0.3	1.2 ± 0.3	6.6 ± 0.6

7.3 Amplified spontaneous emission, gain and loss

Prior to measuring the laser performance of a material it is helpful to measure the properties of its ASE. Three key parameters can be obtained from this: the ASE threshold, the power density above which ASE is present in a thin film; the gain at a given pump density; and the loss within the films, in the absence of a cavity. To investigate the ASE

properties, films of the materials were optically pumped using the measurement techniques highlighted in chapter 3. No ASE was observed for the B1 molecule and so only results for B2-B4 are presented here.

7.3.1 Measurement techniques

ASE measurements are performed by measuring the output intensity from the film, parallel to the surface and varying the intensity of the stripe input pulse. Gain measurements are performed using the variable slit technique outlined in Chapter 3. In this experiment a laser stripe is focussed through a variable aperture onto the edge of the film and the aperture is opened to increase the length of the pump stripe on the film. As the size of the beam l is increased, the output intensity is expected to change according to the following equation:[31]

$$I(\lambda, l) = \frac{AI_{exc}}{g(\lambda)}(e^{g(\lambda)l} - 1) \quad (7.1)$$

Where I_{exc} is the excitation intensity, λ is the wavelength and $g(\lambda)$ is the gain per unit length at the wavelength.

The loss measurements are performed by moving a stripe of constant intensity away from the edge of the sample and recording the output intensity from this, as it travels through the waveguide. The loss can then be calculated by the following:

$$I_{out} = I_0 e^{-\alpha x} \quad (7.2)$$

Where I_0 is the output intensity when the stripe is at the end of the film and α is the waveguide loss coefficient. Due to the use of a collecting lens on the end of the fibre, the change in the emission solid angle is not an issue in this measurement. This is because the size of the output ASE is much smaller than the diameter of the collecting lens.

7.3.2 ASE results

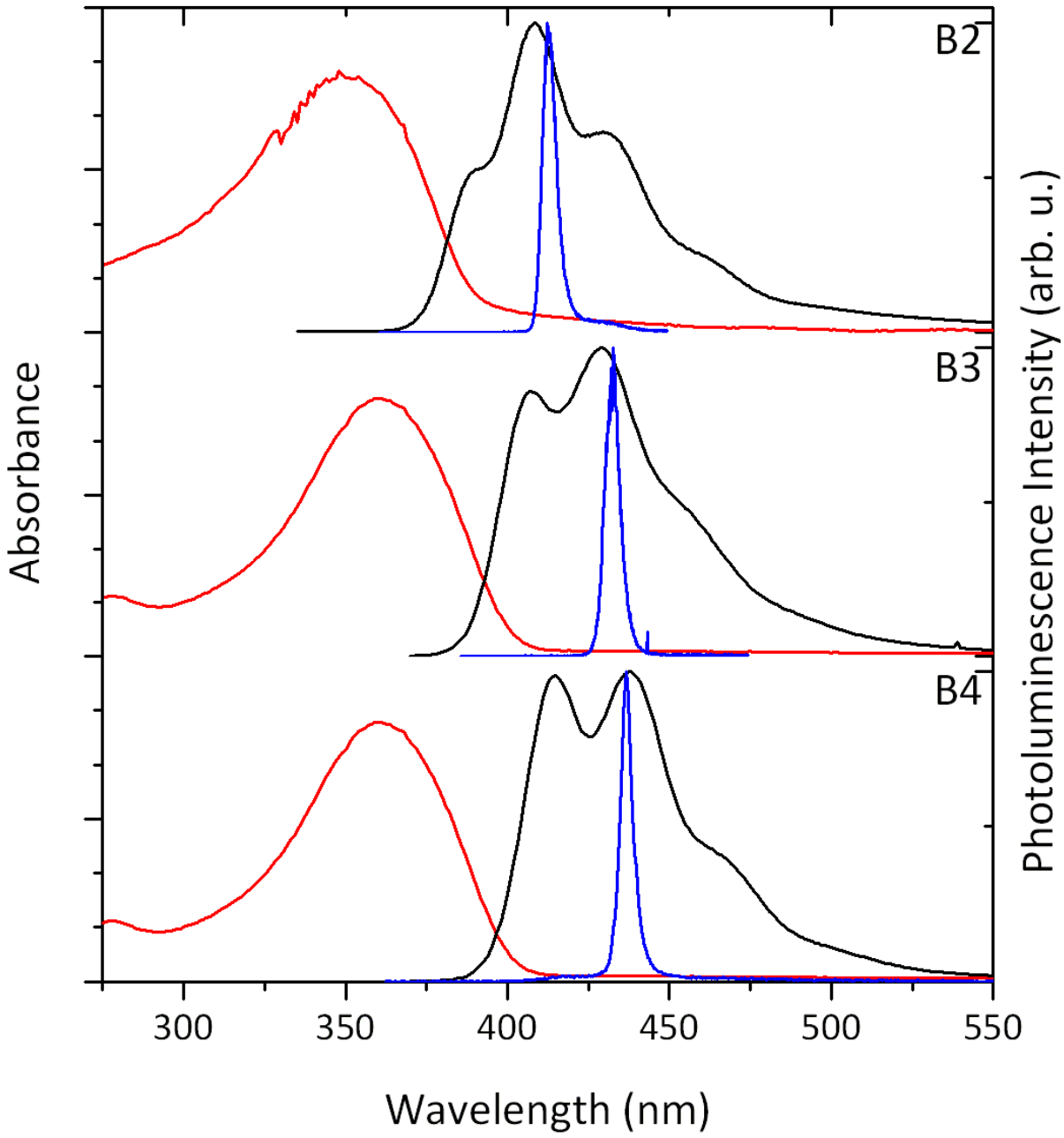

Figure 7.4: ASE spectra (blue line) of the benzene-cored molecules overlaid onto the solid state absorption (red line) and emission spectrum (black line).

In Figure 7.4 the ASE spectra are overlaid onto the emission spectra. The results show that the ASE spectra are considerably narrower, with full width half maxima of less than 7 nm. As can be seen, the ASE peak wavelength redshifts with increasing arm length, and is always located close to the 0-1 peak of the photoluminescence spectra. The narrow emission is

because the net gain in different parts of the spectrum varies, so some wavelengths will exhibit more gain than others, which leads to a spectrally line narrowed ASE peak at the gain maximum.[2] ASE is mostly reported to occur at the 0-0 or 0-1 emission peaks. This is because at these points the gain is at its highest, with the 0-1 peak being more common for ASE, because it is further away from the absorption edge and so is not as significantly affected by self-absorption, which can be an issue at the 0-0 peak.[32]

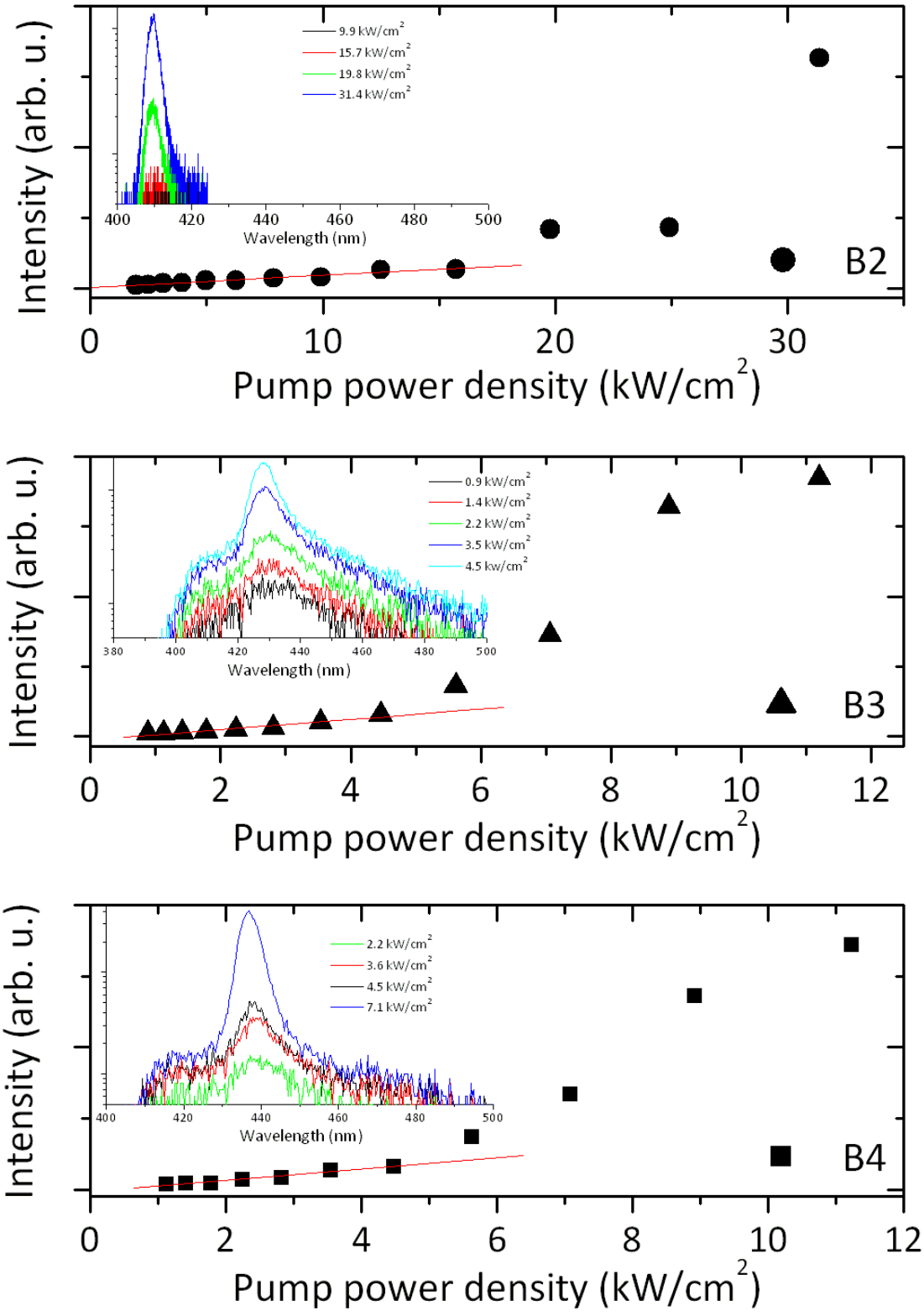

Figure 7.5: ASE thresholds for the B2-B4 molecules. Note the change in scale of the x axis for the B2 molecule. The insets show the spectral narrowing with increasing power.

The ASE threshold results are shown in Figure 7.5. The results show that there is a nonlinear change in the output power dependence of the materials. The point at which the slope changes typically corresponds with the spectral line narrowing of the emission, as shown in the inset to the figures. There is a large difference in the ASE threshold between B2 at 25 ± 5 kW/cm^2 and the 4.5 ± 0.8 kw/cm^2 for both the B3 and B4 molecules. The results show that the ASE threshold reduces with increasing arm length, and that there is a similar performance for both the B3 and B4 molecules.

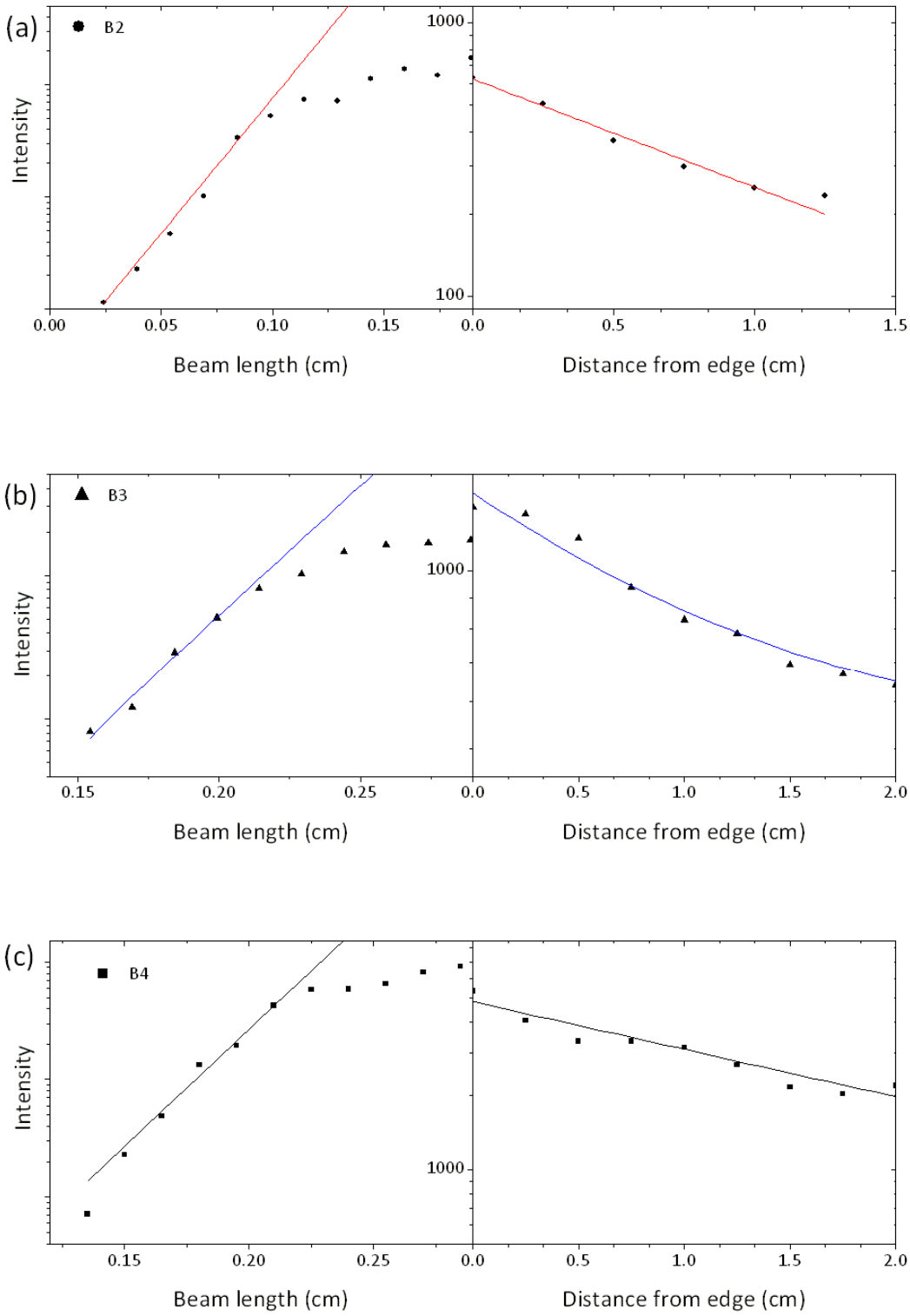

Figure 7.6: Gain and loss of the B2-B4 molecule, with their fits shown as the solid lines. (a) B4 (Black squares and black line fit), (b) B3 (black triangles and blue line fit) and(c) B2 (black circles and red line fit).

Figure 7.6 shows the results for the gain and loss measurements for B2 (a), B3 (b) and B4 (c). As can be seen in all the gain measurement results, as the stripe length is increased the output intensity increases exponentially. The output intensity is seen to increase rapidly at first with increasing pump length, but at longer lengths this increase levels off due to gain saturation. The fit from equation 7.2 is shown as the solid lines on the plot and fits with a gain of 18.2 ± 1.2 cm^{-1} at an excitation density of 49.6 kW/cm^2 for B2, 21.6 ± 2.1 cm^{-1} at 16.5 kW/cm^2 for B3 and 19.6 ±0.7 cm-1 at 20.8 kW/cm^2. The loss results show that as the excitation is moved further from the edge of the film there is a decrease in the output intensity. This decrease in intensity with increasing distance from the edge is expected due to the waveguide losses. The solid lines show the fit to equation 7.2. The loss values are 5.0 ±0.6 cm^{-1} for B2, 4.4 ± 0.2 cm^{-1} for B3 and 3.9 ± 0.3 cm^{-1} for B4. The gain and loss values for all the materials are presented in Table 7.1.

7.4 Laser Results

To assess the laser performance, films were spun on 1 and 2D DFB gratings, fabricated via holography and reactive ion etching into silica substrates. The 1D grating had a period of 270 nm and the 2D a period of 310 nm. The two different gratings were used for the family in order to provide feedback for wavelengths near the ASE peaks as determined by the equation:

$$m\lambda = 2n_{eff}\Lambda \qquad (7.3)$$

where m is the diffraction order, λ is the emission wavelength, n_{eff} is the effective refractive index of the waveguide and Λ is the period of the grating. The films were then excited and the laser emission detected as described in Chapter 3.

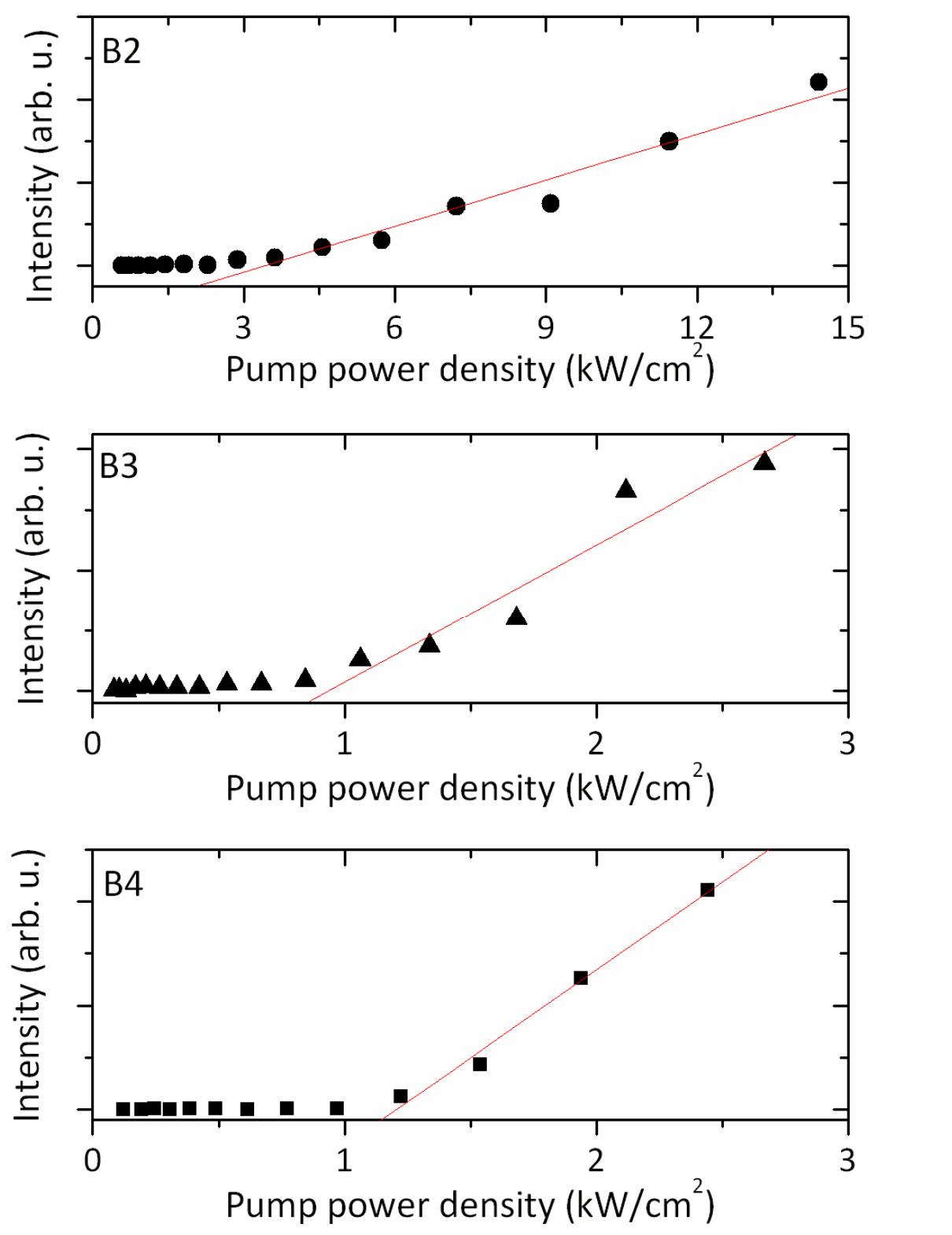

Figure 7.7: Laser threshold results for the B2-B4 molecules.

Figure 7.7 presents the results from the laser threshold measurements for B2-B4. For all the molecules the results show that initially, as the power increases, there is only a small increase in the output intensity, up until a point where the gradient of the output emission

becomes steeper corresponding with the onset of lasing within the films. The lasing thresholds were found to be 2.9 ± 0.6 kW/cm^2 for B2 (1D grating, Λ=270 nm), 1.1 ± 0.2 kW/cm^2 for B3 (2D grating, Λ= 310 nm) and 1.2 ± 0.3 kW/cm^2 for B4 lasers (2D grating, Λ=310 nm).

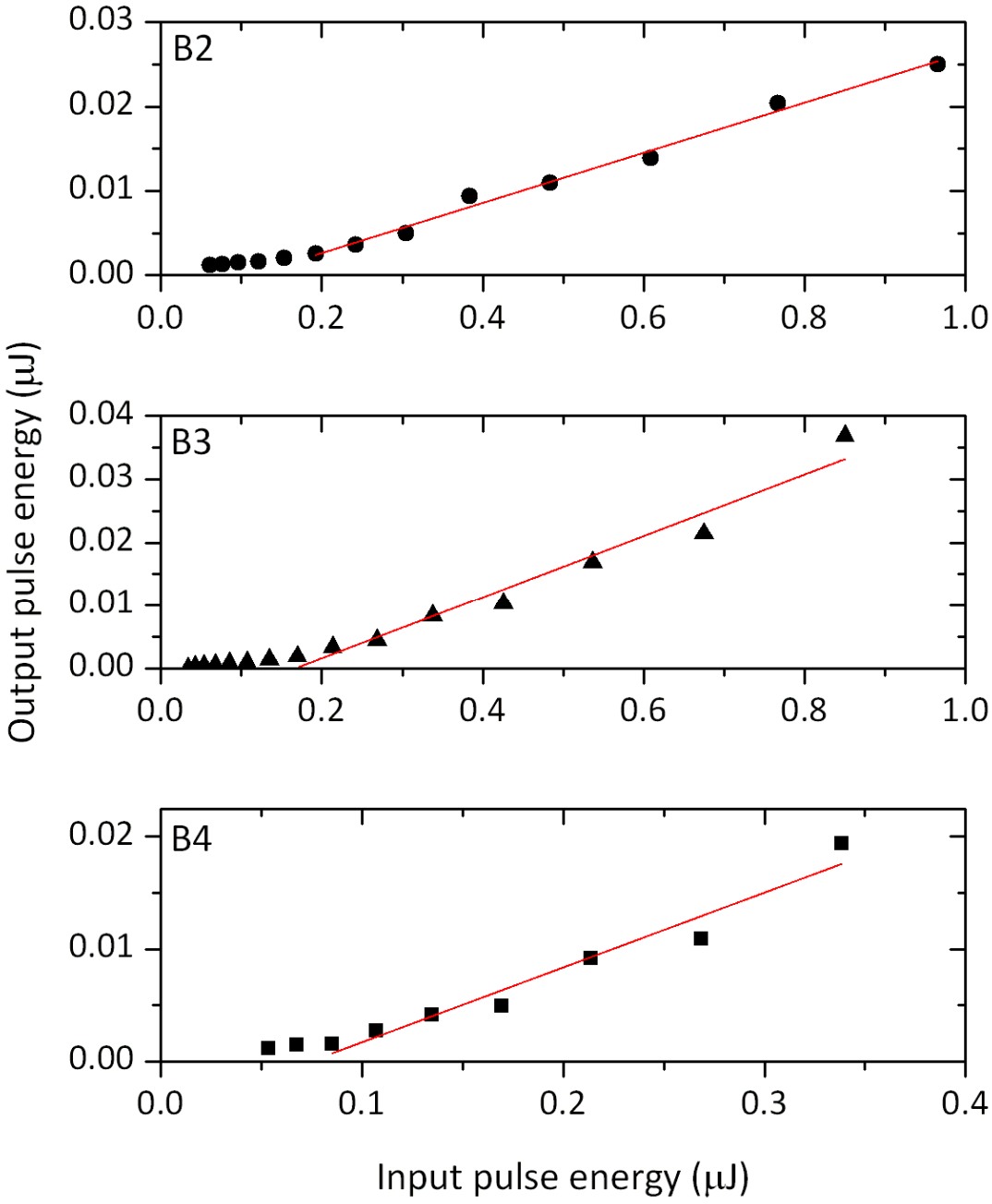

Figure 7.8: Laser efficiency results for the B2-B4 molecules.

For the molecules the output efficiency was also measured by recording the laser output energy against the input energy - for different lasers to the threshold measurements - this is

shown in Figure 7.8. It was found that the output efficiency for the materials was 3.0% ± 0.5% for B2, 5% ± 0.4% for B3 and 6.6% ± 0.6% for B4 .

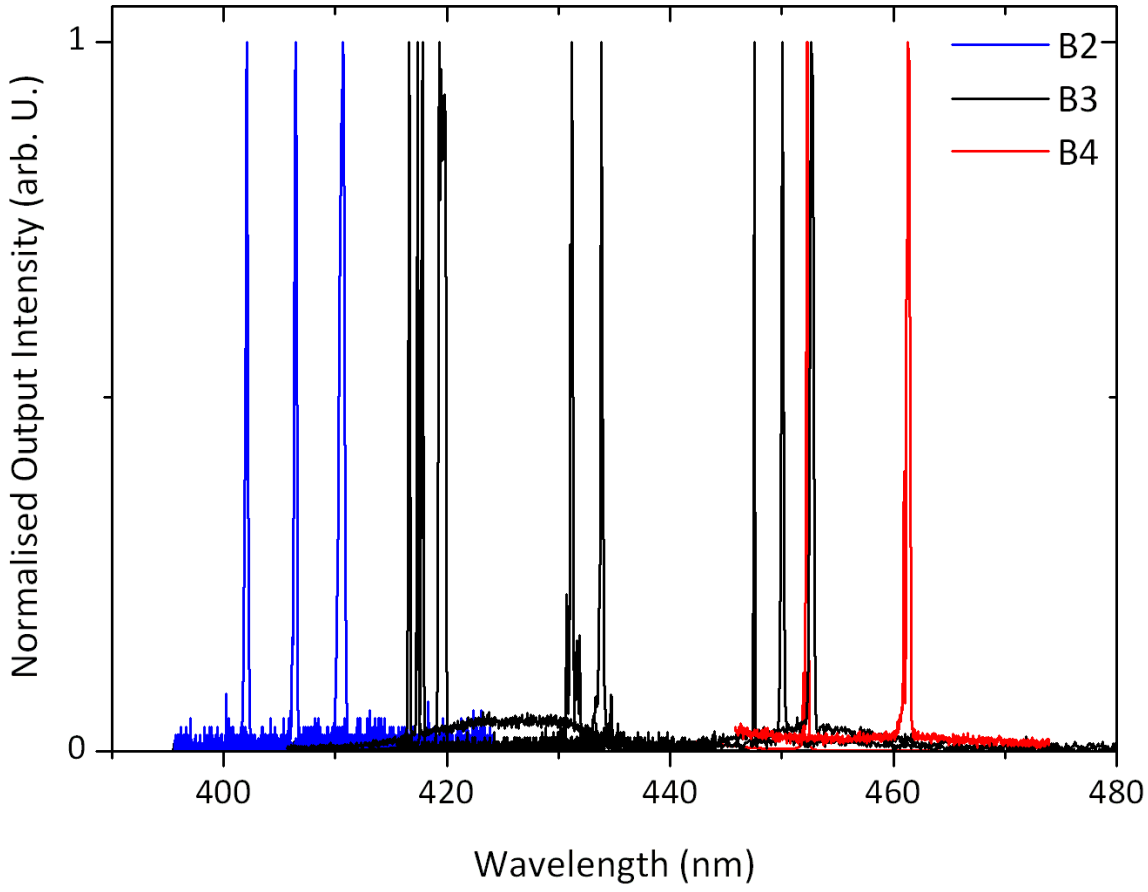

Figure 7.9: Tunability of the benzene-cored lasers, B2 (blue), B3 (black) and B4 (red).

For all molecules, above threshold the lasing line becomes very narrow with a FWHM of less than 0.5 nm, with the peak being located close to the Bragg wavelength for the grating. It is possible to tune the laser emission wavelength by varying a combination of the film thickness and the grating period to produce a change in the Bragg condition from equation 7.3. The results for these tuning experiments are shown in Figure 7.9. The results show that for the benzene-cored materials the lasing wavelength is tunable over 60 nm from 402-462 nm; with B2 being tunable from 402 nm to 410 nm, B3 from 416 nm to 453 nm and B4 from 452 nm to 462 nm.

7.5 Discussion

From the experimental results a clear trend appears: with increasing arm length, there is an improvement in both the lasing and ASE characteristics of the material. It is important to note that, unlike the other studies presented in other chapters this study deals with films, and as such there are a number of factors which can affect the photophysical properties of the film and consequently the laser performance. Two of the key factors are intermolecular interactions and the morphology of the film, each of which can have a detrimental effect on the quality of the gain medium. In order to understand them a comparison can be made with the solution photophysical properties,[33] which were presented in Chapter 5. The results of these are presented in Table 7.1.

In the solution PLQY values there is an increase from 36% for B1 to 86% for B4; there is also an increase in the emission transition dipole moments over this range from 0.3 eÅ to 3.7 eÅ. The results show a clear trend that as the arm length increases the photophysical properties become dominated by the arms, which agrees with the reports for the truxene molecules given by Oliva et al..[34] These results show that the transitions in the longer armed molecules are stronger and more efficient. The results, however, do show that there is a reduction in the PLQY across the family when compared to the solution results. This decrease by a third presents a considerable reduction. It can be explained in terms of an increase in the intermolecular interactions increasing the number of non radiative decay pathways. It is also noticeable that there is a modest decrease in the waveguide losses when going to longer length arms. In this system, increasing the arm length of the molecules leads to a better film morphology and a reduction of the intermolecular interactions. This shows a clear improvement in the laser performance of the molecules with 3 and 4 repeat arm units compared with B2.

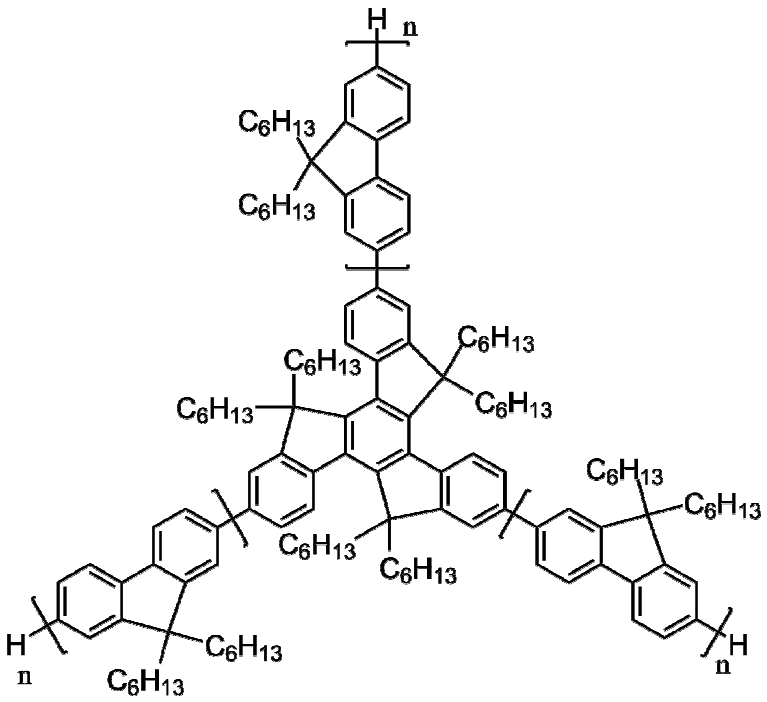

Figure 7.10: Structure of truxene-cored molecules, n=1-4 in this study.

Chapter 5 presented a comparison between the benzene-cored materials and the truxene-cored materials[35] in terms of their solution photophysical properties. This study showed that, by increasing the arm length, there was an increase in the photophysical performance for both families of molecules. The study also showed that the truxene-cored molecules exhibited better photophysical performance throughout the family, which was attributed to the more rigid core. By comparing the lasing and the photophysical results of the benzene and truxene-cored oligofluorene families, an understanding of the important factors for lasing can be determined. This comparison of the results should also provide an insight into what effect the core has on these molecules, and their film photophysics and morphology. The molecules are labelled in the same convention as the benzene-cored molecule in this study, with T designating the truxene core. Lasing studies on T3 were carried out by Tsiminis et al.[25] and on T4 by Wang et al..[26] The results from these studies show that the DFB lasers made from these materials exhibit a much lower lasing thresholds of 515 W/cm^2 and 270 W/cm^2, for the T3 and T4 respectively. The photophysical properties and the lasing performance of the truxene cored molecules is shown in Table 7.2.

Table 7.2: Photophysical and lasing result for the truxene-cored molecules

Material	Solution PLQY (%)	Film PLQY	Emission Dipole (eÅ)	ASE Threshold (kW/cm^2)	Waveguide losses (cm^{-1})	Lasing threshold (kW/cm^2)	Slope efficiency (%)
T1	78	…	2.0	…	…	…	…
T2	81	66	3.0	…	…	…	…
T3	79	73	3.3	2.1	3.5	0.52	…
T4	87	86	3.6	4	2.3	0.27	…

When comparing the solution photophysical properties the largest molecules are equivalent, with the T3, T4, B3 and B4 all having solution PLQYs greater than 80%. However, with the shorter arm lengths there is a larger discrepancy between the PLQYs of the corresponding members of the family. The entire family of truxene-cored molecules have PLQYs greater than 80%, whereas a significant drop off is seen in B1 and B2. Combining the results for the PLQY with the measured lifetimes implies that the truxene-cored materials have an intrinsically lower radiative rate. The similarities in solution are also shown in the emission dipoles, where the 3 and 4 unit arm length molecules have similar values, however the 1 and 2 unit benzene-cored molecules are much lower than their truxene equivalents.

In films, however, there is a much greater difference between the PLQY values for the two families; in the truxene-cored molecules the PLQY remains similar to that observed in solution, with only T2 dropping below 70%. This is in great contrast to data observed for the benzene-cored molecules, where B4 for example has a low film PLQY of only 55%.

By combining all these results, conclusions can be made as to why there is a reduction in the lasing threshold in the truxene-cored molecules. The only photophysical parameter that separates them in terms of performance is the film PLQY, which is 30% lower for the B4 than the T4 molecules. This implies that the level of intermolecular interaction in films of the truxene-cored molecules is lower than in the equivalent benzene-cored molecule. Due to these interactions and the consequent reduction in the PLQY, the benzene-cored molecules must be pumped harder in order to overcome these extra losses to produce gain. The film PLQY is strongly related to the important laser parameter $\sigma\tau$, which due to its influence on

the radiative lifetime, the higher PLQY of the longer armed molecules makes them better lasing molecules. This suggests that the larger and more rigid core with hexyl side chains attached may help to isolate the molecule more and to prevent the molecules from π stacking.

The other aspect that this study highlights is the favourable performance of star-shaped 2D molecules compared with linear 1D molecules.[24] The star shaped molecules discussed in this report show a reduction in the ASE and lasing threshold, when compared with polyfluorene.[29,36] This shows that, by connecting arms of good lasing materials, such as oligofluorenes, to a rigid core at well-defined positions, one can significantly improve the photophysical properties of the material. Moreover, that by further protecting the core by adding side groups as spacers one can achieve solid state efficiency to be close to that of the molecules isolated in solution.

7.6 Conclusion

This study has investigated the performance of a family of star-shaped fluorene oligomers connected to the meta positions of a central benzene-core. The study found that on increasing the arm length there is an improvement of the photophysical properties, with the photophysics of the arms becoming dominant over that of the core. The benzene-cored molecules exhibit good film PLQYs with the longer arm length molecules similar to the PLQY of polyfluorene. They also demonstrate a low lasing threshold of 1.1 kW/cm^2, for the 3 and 4 unit arm length molecules, relatively low optical losses of only 4 cm^{-1}, and slope efficiencies of up to 6.6%. The entire family is found to be broadly tunable over 60 nm in the blue region of the spectrum, from 402 nm to 462 nm.

By combining the results presented in this chapter with the solution photophysical properties of B1-B4 and the same reported for T1-T4 it was possible to understand some of the key features required for a good lasing material. It is found that the truxene-cored molecules have superior lasing properties, due to their much higher PLQYs. This improvement in the film PLQY is argued to be a result of reduced intermolecular interactions. In part this is a result of the core, which separates the molecules more and

prevents π-stacking. The results for both systems highlight the advantages of using organic molecules with 2D star-shaped architecture rather than a linear chain.

7.7 References

1 Tessler, N., Denton, G. J. & Friend, R. H. Lasing from conjugated-polymer microcavities. *Nature* **382**, 695-697 (1996).

2 Samuel, I. D. W. & Turnbull, G. A. Organic semiconductor lasers. *Chem. Rev.* **107**, 1272-1295, doi:10.1021/cr050152i (2007).

3 Grivas, C. & Pollnau, M. Organic solid-state integrated amplifiers and lasers. *Laser & Photonics Reviews*, doi:10.1002/lpor.201100034 (2012).

4 Chénais, S. & Forget, S. Recent advances in solid-state organic lasers. *Polymer International* **61**, 390-406, doi:10.1002/pi.3173 (2012).

5 Vasdekis, A. E. *et al.* Diode pumped distributed Bragg reflector lasers based on a dye-to-polymer energy transfer blend. *Opt. Express* **14**, 9211-9216 (2006).

6 Yang, Y., Turnbull, G. A. & Samuel, I. D. W. Hybrid optoelectronics: A polymer laser pumped by a nitride light-emitting diode. *Appl. Phys. Lett.* **92**, 163306 (2008).

7 Riechel, S. *et al.* Very compact tunable solid-state laser utilizing a thin-film organic semiconductor. *Opt. Lett.* **26**, 593-595 (2001).

8 Vannahme, C. *et al.* Integration of organic semiconductor lasers and single-mode passive waveguides into a PMMA substrate. *Microelectronic Engineering* **87**, 693-695, doi:10.1016/j.mee.2009.12.077 (2010).

9 Woggon, T., Klinkhammer, S. & Lemmer, U. Compact spectroscopy system based on tunable organic semiconductor lasers. *Applied Physics B: Lasers and Optics* **99**, 47-51, doi:10.1007/s00340-010-3953-6 (2010).

10 Rose, A., Zhu, Z., Madigan, C. F., Swager, T. M. & Bulovic, V. Sensitivity gains in chemosensing by lasing action in organic polymers. *Nature* **434**, 876-879, doi:http://www.nature.com/nature/journal/v434/n7035/suppinfo/nature03438_S1.html (2005).

11 Schafer, F. P., Schmidt, W. & Volze, J. Organic Dye Solution laser. *Appl. Phys. Lett.* **9**, 306-309 (1966).

12 Soffer, B. H. & McFarland, B. B. Continuously Tunable, Narrow-Band Organic Dye Lasers. *Appl. Phys. Lett.* **10**, 266-267 (1967).

13 Heliotis, G. *et al.* Blue, surface-emitting, distributed feedback polyfluorene lasers. *Appl. Phys. Lett.* **83**, 2118-2120 (2003).

14 Xia, R., Heliotis, G. & Bradley, D. D. C. Fluorene-based polymer gain media for solid-state laser emission across the full visible spectrum. *Appl. Phys. Lett.* **82**, 3599-3601 (2003).

15 McGehee, M. D. *et al.* Semiconducting polymer distributed feedback lasers. *Appl. Phys. Lett.* **72**, 1536-1538 (1998).

16 Turnbull, G. A., Andrew, P., Barnes, W. L. & Samuel, I. D. W. Photonic mode dispersion of a two-dimensional distributed feedback polymer laser. *Phys. Rev. B* **67**, 165107 (2003).

17 Turnbull, G. A., Andrew, P., Barnes, W. L. & Samuel, I. D. W. Operating characteristics of a semiconducting polymer laser pumped by a microchip laser. *Appl. Phys. Lett.* **82**, 313-315 (2003).

18 Heliotis, G. *et al.* Emission Characteristics and Performance Comparison of Polyfluorene Lasers with One- and Two-Dimensional Distributed Feedback. *Adv. Funct. Mater.* **14**, 91-97, doi:10.1002/adfm.200305504 (2004).

19 Koschorreck, M. *et al.* Dynamics of a high-Q vertical-cavity organic laser. *Appl. Phys. Lett.* **87**, 181108 (2005).

20 Schneider, D. *et al.* Ultrawide tuning range in doped organic solid-state lasers. *Appl. Phys. Lett.* **85**, 1886-1888 (2004).

21 Tsiminis, G. *et al.* Two-photon absorption and lasing in first-generation bisfluorene dendrimers. *Adv. Mater.* **20**, 1940, doi:10.1002/adma.200702498 (2008).

22 Ribierre, J. C., Tsiminis, G., Richardson, S., Turnbull, G. A. & Samuel, I. D. W. Amplified spontaneous emission and lasing properties of bisfluorene-cored dendrimers. *Appl. Phys. Lett.* **91**, doi:08110810.1063/1.2761833 (2007).

23 Lawrence, J. R., Turnbull, G. A., Samuel, I. D. W., Richards, G. J. & Burn, P. L. Optical amplification in a first-generation dendritic organic semiconductor. *Opt. Lett.* **29**, 869-871 (2004).

24 Kanibolotsky, A. L., Perepichka, I. F. & Skabara, P. J. Star-shaped pi-conjugated oligomers and their applications in organic electronics and photonics. *Chem. Soc. Rev.* **39**, 2695-2728, doi:10.1039/b918154g (2010).

25 Tsiminis, G. *et al.* Low-threshold organic laser based on an oligofluorene truxene with low optical losses. *Appl. Phys. Lett.* **94**, doi:24330410.1063/1.3152782 (2009).

26 Wang, Y. *et al.* Broadly tunable deep blue laser based on a star-shaped oligofluorene truxene. *Synth. Met.* **160**, 1397-1400, doi:10.1016/j.synthmet.2010.04.016 (2010).

27 Lai, W.-Y. *et al.* Enhanced Solid-State Luminescence and Low-Threshold Lasing from Starburst Macromolecular Materials. *Adv. Mater.* **21**, 355-360 (2009).

28 Greenham, N. C. *et al.* Measurement of Absolute Photoluminescence Quantum Efficiencies in Conjugated Polymers. *Chem. Phys. Lett.* **241**, 89-96 (1995).

29 Xia, R., Heliotis, G., Hou, Y. & Bradley, D. D. C. Fluorene-based conjugated polymer optical gain media. *Org. Electron.* **4**, 165-177, doi:10.1016/j.orgel.2003.08.009 (2003).

30 Zhou, X.-H., Yan, J.-C. & Pei, J. Synthesis and Relationships between the Structures and Properties of Monodisperse Star-Shaped Oligofluorenes. *Organic Letters* **5**, 3543-3546, doi:10.1021/ol035461e (2003).

31 McGehee, M. D. & Heeger, A. J. Semiconducting (Conjugated) Polymers as Materials for Solid-State Lasers. *Adv. Mater.* **12**, 1655-1668, doi:10.1002/1521-4095(200011)12:22<1655::aid-adma1655>3.0.co;2-2 (2000).

32 McGehee, M. D. *et al.* Amplified spontaneous emission from photopumped films of a conjugated polymer. *Phys. Rev. B* **58**, 7035-7039 (1998).

33 Montgomery, N. A. *et al.* Optical Excitations in Star-Shaped Fluorene Molecules. *The Journal of Physical Chemistry A* **115**, 2913-2919, doi:10.1021/jp1109042 (2011).

34 Moreno Oliva, M. *et al.* Electronic and Molecular Structures of Trigonal Truxene-Core Systems Conjugated to Peripheral Fluorene Branches. Spectroscopic and Theoretical Study. *The Journal of Physical Chemistry B* **111**, 4026-4035, doi:10.1021/jp065271w (2007).

35 Kanibolotsky, A. L. *et al.* Synthesis and Properties of Monodisperse Oligofluorene-Functionalized Truxenes: Highly Fluorescent Star-Shaped Architectures. *Journal of the American Chemical Society* **126**, 13695-13702, doi:10.1021/ja039228n (2004).

36 Heliotis, G., Bradley, D. D. C., Turnbull, G. A. & Samuel, I. D. W. Light amplification and gain in polyfluorene waveguides. *Appl. Phys. Lett.* **81**, 415-417, doi:10.1063/1.1494473 (2002).

8

Conclusion

Since the first demonstration of the solid state organic semiconductor laser, there has been a great deal of work carried out on improving cavity designs and laser performance. However, these improvements have mostly been achieved working with the best available materials; there has been little work on developing dedicated new laser materials. With the development of OLEDs switching to emission via phosphorescence and new solar cell materials, focus has shifted away from new highly efficient fluorescent materials. As a result of this the majority of organic semiconductor lasers still use the same materials that were used from the early examples, such as poly(p-phenylenevinelyne) and polyfluorene.[1-3] Polyfluorene has been shown to be a very good lasing material, however there has been little work done to study and understand why this is the case.

Recently however, some work has been done on developing new laser materials using differing architectures. By moving away from a simple one dimensional structures into two dimensional structures some improvements in the lasing performance have been observed. These include a reduction in lasing thresholds and optical losses.[4,5] These benefits have been observed in other devices too, where an increase in the dimensionality has led to similar improvements in performance.[6-8] One of the best examples of this is shown in OLEDs, where dendrimer materials have been observed to improve the performance of the devices.[6]

The aim of the project was to assess what characteristics are important for good lasing materials. The work began by studying a family of fluorene oligomers, which are known to be a very good lasing material, and have been well studied in other optical devices. The results for the oligofluorene molecules were then fed into a study of a

pair of two-dimensional fluorene derivatives. These molecules have three fixed length oligofluorene arms connected to central cores. One of the cores is a single benzene unit, in which the arms are connected to its meta-positions. The other is a oliofluorene truxene-core in which three fluorene units are fused through a shared central benzene unit.

Investigations were carried out on all these molecules to understand their photophysical properties; this was done by studying their absorption and emission properties through both experiment and theoretical DFT and TD-DFT calculations. The results from this part of the project, then led to a study focusing upon the inter arm energy transfer within the truxene-cored molecules. Once the photophysics of the molecules had been analysed, the final part of the study was then designed to look at the lasing performance of the family of benzene-cored molecules. The results for these were then compared against the photophysical results and the lasing results obtained for the truxene-cored molecules to identify the key characteristics of a good lasing material.

The photophysical results for the oligofluorene and polyfluorene molecules showed that with increasing length there was an increase in the molar extinction coefficient, PLQY and transition dipole moments. A similar trend was also observed for the star-shaped molecules. However, these were found to have three times greater molar extinction coefficients than their linear oligofluorene equivalents. They also possessed higher PLQYs with the truxene-cored molecules all having a PLQY greater than 0.7, whilst the benzene-cored molecules followed a similar increasing trend to that of the oligofluorenes, but with the PLQY being higher throughout the family. It was also observed that both families of star-shaped molecules have higher transition dipole moments than the oligofluorenes.

The experimental results and the results from the theoretical calculations for the oligofluorene molecules showed that at longer chain lengths there was a significant difference between the strengths of the absorption and fluorescence transition dipole moments; this is because the fluorescence transition dipole begins to saturate at chain lengths greater than 5 repeat units. This saturation was probed further by theoretical

DFT and TD-DFT studies, which showed that the saturation was the result of an exciton localisation process occurring in the excited state. The absorption transition on the other hand, was always found to occur across the entire molecule.

The star-shaped molecules were found to present C_3 symmetry in the calculations, with there being two possible absorption transitions that could be excited by a single photon. The TD-DFT calculations showed that whilst it was possible for the absorption transition to occur across the entire molecule the emission transition only ever takes place from a single arm. Due to the symmetry of the molecules it was found that when performing the calculations that a small imposed symmetry breaking was required in order for the molecule to emit light, this symmetry breaking changes the energy levels of the system and forces the exciton to localise onto a single arm for emission. The arm that the exciton transferred to was found to be dependent upon the symmetry breaking conditions imposed and it was always found to go to the arm with the lowest energy.

To study this energy transfer experimentally ultrafast luminescence anisotropy measurements were performed; this was done to provide information on the change in direction of the emission dipole relative to the absorption one. The results show that the symmetry of these large molecules is already broken whilst the molecule is in solution; this meant that only one of the two absorption transitions is excited. The excited transition can either be localised to one arm or spread across two. TD-DFT results were used to probe the nature of the symmetry breaking deformation; this needed to be large enough to cause an energy level splitting between the transitions which is greater than the bandwidth of the laser; otherwise the excitation pulse would excite both transitions and the molecule would behave as though it were symmetric. The most likely cause for the symmetry breaking defect was found to be the twisting of one of the fluorene units within the arm. The results from these calculations typically showed that the transitions which are spread over two arms are the higher energy transitions, whilst the lower energy transitions typically only occur on a single arm. This leads to an excitation energy dependence upon the anisotropy behaviour, in which it was found that there are two decay processes occurring, both of which are faster than rotational diffusion. Initially there is a ~400 fs first decay which is attributed

to a fast localisation process from a transition spread across two arms onto a single arm for emission. There is then a slower excitation energy dependent second decay of 3-8 ps, which is attributed to the exciton hopping between arms.

The lasing performance of the benzene-cored molecules was measured; they were found to be good laser materials, with ASE thresholds as low as 4.5 kW/cm^2 and gains as high as 21.6 cm^{-1}. The lasing emission was found to be tuneable across 60 nm from 402-462 nm throughout the family. As well as this they also presented low lasing thresholds of 1.1 kW/cm^{-2}, and lasing efficiencies as high as 6.6%.

These results were then compared to the literature vales for the truxene-cored molecules. By comparing the both the film and solution photophysical properties, it was possible to identify the some of the key molecular properties for a good organic laser material. Upon comparison the lasing performance of the truxene-cored molecules was found to be better than that of the benzene-cored molecules. The only major difference between the two molecules in terms of their photophysical properties was found to be the film PLQY, which was much higher for the truxene-cored molecules than the benzene-cored molecules. This suggests that the extra size and the side chains attached to the truxene core help to reduce the number of non-radiative decay pathways and thus reduce the lasing threshold.

8.1 Future design of organic semiconductor laser materials

This study has set out to understand the photophysical properties of a family of oligofluorene molecules with the aim of identifying which photophysical and structural properties are key to lasing. This found that, as the molecular length is increased, the properties improve, but the emission is self-trapped to ~5 repeat units. When comparing these results to star-shaped oligofluorene molecules it is apparent that the star-shaped molecules present many photophysical advantages over linear oligofluorene molecules, with higher PLQYs and molar extinction coefficients. They also present larger absorption and emission transition dipole moments, suggesting

that they interact more strongly with the radiation. The laser results also showed that, by progressing to a two dimensional star-shaped architecture, a significant reduction in both the ASE and lasing threshold can be achieved.

If we compare the two star-shaped molecules there is a clear case that the truxene-cored molecules are better, because they have much higher PLQYs in both film and solution. This is a result of the much more rigid core with side groups attached which isolate the core from solvent and other molecules when in film and solution, thus reducing the number of non-radiative pathways available to the molecule. This improvement is clearly shown in the laser results where both the ASE and lasing thresholds are much lower in the truxene-cored molecules when compared against the benzene-cored molecule. This implies that for designing future lasing molecules it is important to use a highly emissive chromophore for the arms. This could be a single oligomeric material such as BBEH-PPV[9] or a fluorene co-polymer such as F8BT, with the BT unit located close to the centre of the arm. These arms should then be attached to a large rigid core, with side chains attached to isolate the core and the molecule and prevent π-stacking.

The study presented in this thesis covers a lot of the basic understanding of the photophysical and structural properties, and analyses how they relate to lasing for these oligofluorene molecules. However, in order to progress this work and to improve understanding, experiments need to be performed which investigate the role that excited state absorption and singlet-singlet annihilation has on the lasing performance. Moreover, further work needs to be performed on reducing the number of triplets within the system to progress towards either CW or electrically pumped lasing; this would involve a systematic look at materials which are capable of scavenging the triplets from the molecules. If this extra work were to build upon these findings then a good description of the photophysical and structural properties of lasing molecules can be obtained, and that further progress in organic semiconductor lasers can be made from this.

8.2 Summary

In summary this work has set about studying the photophysical properties of a family of fluorene molecules to understand the nature of their photophysical transitions. These have then been used to study key material characteristics for organic semiconductor lasers and have shown that it is beneficial to move from one dimensional linear molecule into two dimensional star-shaped molecules. These show improved photophysical characteristics and lower lasing thresholds achieved by doing this.

8.3 References

1 Shkunov, M. N., Osterbacka, R., Fujii, A., Yoshino, K. & Vardeny, Z. V. Laser action in polydialkylfluorene films: Influence of low-temperature thermal treatment. *Appl. Phys. Lett.* **74**, 1648-1650 (1999).

2 Heliotis, G. *et al.* Blue, surface-emitting, distributed feedback polyfluorene lasers. *Appl. Phys. Lett.* **83**, 2118-2120 (2003).

3 Heliotis, G. *et al.* Emission Characteristics and Performance Comparison of Polyfluorene Lasers with One- and Two-Dimensional Distributed Feedback. *Adv. Funct. Mater.* **14**, 91-97, doi:10.1002/adfm.200305504 (2004).

4 Lai, W.-Y. *et al.* Enhanced Solid-State Luminescence and Low-Threshold Lasing from Starburst Macromolecular Materials. *Adv. Mater.* **21**, 355-360 (2009).

5 Xia, R. D., Lai, W. Y., Levermore, P. A., Huang, W. & Bradley, D. D. C. Low-Threshold Distributed-Feedback Lasers Based on Pyrene-Cored Starburst Molecules with 1,3,6,8-Attached Oligo(9,9-Dialkylfluorene) Arms. *Adv. Funct. Mater.* **19**, 2844-2850, doi:10.1002/adfm.200900503 (2009).

6 Burn, P., Lo, S. C. & Samuel, I. The Development of Light-Emitting Dendrimers for Displays. *Adv. Mater.* **19**, 1675-1688, doi:10.1002/adma.200601592 (2007).

7 Kanibolotsky, A. L., Perepichka, I. F. & Skabara, P. J. Star-shaped pi-conjugated oligomers and their applications in organic electronics and photonics. *Chem. Soc. Rev.* **39**, 2695-2728, doi:10.1039/b918154g (2010).

8 Lo, S.-C. & Burn, P. L. Development of Dendrimers: Macromolecules for Use in Organic Light-Emitting Diodes and Solar Cells. *Chem. Rev.* **107**, 1097-1116, doi:10.1021/cr050136l (2007).

9 Rose, A., Zhu, Z., Madigan, C. F., Swager, T. M. & Bulovic, V. Sensitivity gains in chemosensing by lasing action in organic polymers. *Nature* **434**, 876-879, doi:http://www.nature.com/nature/journal/v434/n7035/suppinfo/nature03438_S1.html (2005).

A

List of Publications arising from this work

- SCHUMACHER, S., RUSECKAS, A., MONTGOMERY, N. A., SKABARA, P. J., KANIBOLOTSKY, A. L., PATERSON, M. J., GALBRAITH, I., TURNBULL, G. A. & SAMUEL, I. D. W. 2009. Effect of exciton self-trapping and molecular conformation on photophysical properties of oligofluorenes. *Journal of Chemical Physics,* 131**,** 154906.

- MONTGOMERY, N. A., DENIS, J.-C., SCHUMACHER, S., RUSECKAS, A., SKABARA, P. J., KANIBOLOTSKY, A., PATERSON, M. J., GALBRAITH, I., TURNBULL, G. A. & SAMUEL, I. D. W. 2011. Optical Excitations in Star-Shaped Fluorene Molecules. *The Journal of Physical Chemistry A,* 115**,** 2913-2919

- MONTGOMERY, N. A., HEDLEY, G. J., RUSECKAS, A., DENIS, J.-C., SCHUMACHER, S., KANIBOLOTSKY, A. L., SKABARA, P. J., GALBRAITH, I., TURNBULL, G. A. & SAMUEL, I. D. W. 2012. Dynamics of fluorescence depolarisation in star-shaped oligofluorene-truxene molecules. *Physical Chemistry Chemical Physics,* 14**,** 9176-9184.

- TSIMINIS, G., MONTGOMERY, N. A., KANIBOLOTSKY, A. L., RUSECKAS, A., PEREPICHKA, I. F., SKABARA, P. J., TURNBULL, G. A. & SAMUEL, I. D. W. 2012. Laser characteristics of a family of benzene-cored star-shaped oligofluorenes. *Semiconductor Science and Technology,* 27**,** 094005.

- LIU, N., RUSECKAS, A., MONTGOMERY, N. A., SAMUEL, I. D. W. & TURNBULL, G. A. 2009. Semiconducting polymer waveguides for end-fired ultra-fast optical amplifiers. *Optics Express,* 17**,** 21452-21458.